ANALYSIS OF STEEL SILO STRUCTURES

ON DISCRETE SUPPORTS

By

Hongyu Li

A thesis submitted in fulfilment of the requirements
for the degree of Doctor of Philosophy

Department of Civil Engineering & Building Science
The University of Edinburgh
Edinburgh, Scotland, UK
September 1994

ABSTRACT

The objective of this thesis is to broaden current knowledge of the strength and buckling/collapse of shells, with special reference to steel silo structures on discrete supports, and thus to provide design guidance of practical value for future silo design and construction and to develop new research aspects for further investigation.

A linear elastic solution of the cylindrical shell bending equations is presented for local loadings, with special attention to local longitudinal distributed loadings. Algebraic expressions for the displacements and stresses induced by a rectangular patch of longitudinal load on a simply supported cylindrical shell are derived using double Fourier series. The solution of this problem is general, and therefore can be applied to cylindrical shells under local loadings in any direction and with different boundary conditions.

Linear elastic analyses of discretely supported perfect cylinders under axial compression are presented using the finite element method. The pre-buckling meridional membrane stress distribution above the support centreline is examined in detail, and is followed by investigations of the linear bifurcation behaviour of the cylinders. The effects on the stress distribution and the buckling strength of different loading patterns and different geometric configurations are extensively examined.

Geometrically nonlinear elastic buckling analyses are also performed using large deflection theory. Both perfect and imperfect cylinders are studied with various geometric configurations and under different loading conditions. The nonlinear elastic buckling behaviour, the buckling strength and the buckling configuration are thoroughly investigated for discretely supported cylinders.

Further studies extend the work into the plastic range. Discretely supported cylinders obeying the von Mises yield criterion are analysed. Limit analyses of perfect cylinders are first conducted using small deflection theory. Geometrically nonlinear elastic-plastic collapse analyses of both perfect and imperfect cylinders are performed next. Studies of different loading conditions and parametric studies of varying geometries and material strengths are presented in both types of analysis. The nonlinear elastic-plastic behaviour of discretely supported cylinders is thus explored.

A complete silo which consists of a cylindrical shell, a conical roof hopper and a conical discharge hopper is briefly examined, with the aim of exploring the applicability of the established cylinder model in the elastic buckling analysis of silo structures.

Finally, the conclusions drawn from this research are summarised and recommendations are also made for further research on locally supported shells.

ACKNOWLEDGEMENTS

I am indebted to my supervisor, Professor J.M. Rotter, for his encouragement, help and guidance in carrying out this research and in producing this thesis.

I would like to thank all those who have helped me in various ways during my PhD studies, particularly the former and present members of the Silo Research Group in the Department of Civil Engineering, University of Edinburgh.

I would like to express my special thanks to my parents, my sisters and friends for their love, care and support during the last three years.

Finally, financial support from the ORS Award and the Faculty of Science & Engineering Postgraduate Scholarship, University of Edinburgh, the Edinburgh University Crisis/Hardship Fund, the Great Britain-China Educational Trust Fund and the Henry Lester Trust Ltd. Fund is greatly acknowledged.

H.Y. LI

DECLARATION

This thesis, entitled Analysis of Steel Silo Structures on Discrete Supports, is submitted for the Degree of Doctor of Philosophy, in the Department of Civil Engineering, at the University of Edinburgh, Scotland, UK.

The research, on which this thesis is based was carried out between February 1991 and May 1994 under the supervision of Professor J.M. Rotter. It is solely the work of the author except where otherwise acknowledged in the text and has not formed the basis of a submission for any other degree.

Two supporting papers which are based on the work described in this thesis have been presented in:

1. Rotter, J.M. and Teng, J.G. and Li, H.Y. (1991), "Buckling in Thin Elastic Cylinders on Column Supports", in Buckling of Shell Structures, on Land, in the Sea and in the Air, edt. J.F. Jullien, Elsevier Applied Science, London and New York.

2. Rotter, J.M., Greiner, R., Guggenberger, W., Li, H.Y., and She, K.M. (1993), "Proposed Design Rule for Buckling Strength Assessment of Cylindrical Shells under Local Axial Loads", Submission to ECCS TWG8.4 Buckling of Shells, Edinburgh Meeting, September 1993.

Signed .....

Date 28th October 1994

CONTENTS

NOTATIONS

The symbols listed below are those that appear in this thesis. They are of either general interest or particular specification. Only one meaning is assigned to each symbol unless otherwise defined in the text where it occurs.

Symbols	Meaning
a, R	radius of cylindrical shell
b	co-ordinate x of centre of loading surface
b_1	half-length of loading surface in circumferential direction
b_2	half-length of loading surface in longitudinal direction
D	$Et^3 / 12(1 - \nu^2)$
d	width of support
E	Young's modulus
H	height of cylinder
l	length of cylindrical shell
M_x, M_ϕ	bending moments in shell wall per unit length of axial section and a section perpendicular to the axis of a cylindrical shell, respectively
$M_{x\phi}$	twisting moment in shell wall per unit length of an axial section of a cylindrical shell
m, n	integer numbers
N_x, N_ϕ, $N_{x\phi}$	membrane forces in shell wall per unit length of axial section and a section perpendicular to the axis of a cylindrical shell
n	number of supports
P_L	limit load
P_x	equally distributed longitudinal load in a rectangle.
P_-	statically admissible load parameter
P_+	kinematically admissible load parameter
p	internal pressure
p*	dimensionless internal pressure parameter ($pR/t\ \sigma_{cl}$)
p_l	uniformly distributed line load
p_v	uniformly distributed wall friction load
t	wall thickness of shell
u, v, w	components of displacements in the x, y, and z directions respectively
X, Y, Z	components of the intensity of the external load on a shell parallel to x, y, and z axes, respectively
x, y, z	global co-ordinates

x, ϕ, z		cylindrical co-ordinates
Z		vertical distance from the bottom edge of cylinder
Z_c		critical position of the imperfection
Z_0		distance from the centre of an imperfection to the bottom edge of cylinder
α		l / a
β_1		b_1 / a
β_2		b_2 / a
δ		imperfection amplitude
δ_0		characteristic amplitude of a local imperfection
$\varepsilon_x, \varepsilon_\phi$		unit elongations in x and ϕ directions
$\gamma_{x\phi}$		shear strain in cylindrical co-ordinates
θ_1		half angle of conical roof
θ_2		half angle of conical hopper
χ_x, χ_ϕ		changes of curvature of a cylindrical shell in axial plane and in a plane perpendicular to the axis, respectively
$\chi_{x\phi}$		change of curvature in cylindrical co-ordinates
ν		Poisson's ratio
λ		$n\pi a / l$
	or	buckling half wave length
σ_{cl}		classical elastic critical stress of a cylinder under uniform axial compression
σ_m		mean meridional membrane stress above support
$\sigma_{m\phi}$		meridional membrane stress
σ_y		yield stress in tension or compression.

CHAPTER 1

INTRODUCTION

1.1 STEEL SILOS

Containers for the storage of bulk solids are usually called bins, bunkers, silos or tanks. While there is no generally accepted definition for each of these terms, shallow containers for coal, coke, ore, crushed stone, gravel, etc. are often called bins or bunkers, and tall containers for materials such as grain and cement are usually called silos. In this thesis, silo is an inclusive term for all steel structures for the storage of bulk solids.

Steel silos differ principally from their concrete counterparts in that they are much lighter structures, quick to erect and dismantle, carrying their loads by different structural mechanisms, deforming readily and reversibly when subject to unsymmetrical loads, and placing smaller loads on their foundations. Thus steel silos are widely used for short and long term storage of large quantities of bulk solids and have been built increasingly in recent years in many industries including mining, chemical, electric power generation, agriculture and food processing.

Steel silos in common use are usually circular in cross section, and may be ground-supported (Fig. 1-1a) or elevated. Typical elevated silos generally consist of a conical roof, a cylindrical shell and a conical hopper (Fig. 1-2) and may be supported on a load-bearing skirt (Fig. 1-2a) or on discrete supports. The junction between the vertical wall and the hopper is termed the transition. A stiff ring is usually provided at the transition. Typical forms of the transition junction are shown in Figure 1-3. In practice, there are many forms of support, which locally contact the shell, and which may be described as discrete supports. Columns of various widths have been widely used as supports and these may terminate below the transition junction (Fig. 1-2b), extend to the eaves (Fig. 1-2c) or engage into the shell for a short distance (Fig. 1-2d). In this thesis, the term 'discretely supported silo' is used to mean that the silo cylinder is directly supported on local supports of a defined width.

Elevated silos have the advantage that the bulk solid can be discharged by gravity flow. The pattern of flow depends on the shape of the silo, the roughness of its interior surfaces, and the properties of the stored material. Several patterns of flow are possible during emptying (Fig. 1.4). A silo which consists of a vertical cylinder with smooth walls and a steep smooth-walled hopper is likely to develop mass flow (Fig. 1-4a). This is a first-in, first-out flow pattern. By

contrast, one with a shallow rough-walled hopper is likely to develop funnel flow (Fig. 1-4b), or pipe flow (Fig. 1-4c), which is generally a last-in, first-out flow sequence. An expanded flow silo (Fig. 1-4d) is a funnel-flow silo with a small mass flow hopper which can obviate the disadvantages of the funnel-flow silo. This type of silo is useful for the storage of large quantities of nondegrading solids such as mineral ores.

Steel silos are generally very light and thin structures for their size. The radius-to-thickness ratio of the cylinder R/t is generally in the range 200-3000. Squat silos with a height-to-radius ratio H/R less than 2 are being built increasingly, as they have a large ratio of stored volume to structural construction cost.

1.2 LOADS ON SILO WALLS

The walls of silos are subjected to both normal pressures and vertical frictional shears or tractions which come from the stored material inside the silo and vary all over the wall. The magnitude and distribution of these pressures may be symmetric or non-symmetric and depend on whether the silo is being filled or discharged. Geometric imperfections in the silo wall, which are caused inevitably during its fabrication and by the flexibility of the wall, may also strongly affect the pressures on the walls.

In simple terms, it is to be expected that normal pressures on the cylindrical wall will give rise to circumferential (or hoop) tensions, and that frictional tractions will cause cumulative axial (or vertical) compressive stresses in the silo wall. In practice, the real loading is very complex: different load cases may give rise to different stress patterns in the shell.

A strenuous effort has been put into exploring the pressures on silo walls from bulk solids over the last two or three decades. The simplest useful theory for predicting the pressures on the vertical walls of a silo is probably that of Janssen [1895] (Fig. 1-1b). It is widely accepted that pressures close to Janssen values are exerted on the walls of a silo when it is first filled. Much larger pressures have frequently been observed during discharge. These high pressures, termed over-pressures or flow pressures (or sometimes 'switch' pressures) (Fig. 1-5), can be two to four times as large as the initial pressures, even in silos with a concentric discharge arrangement. Further, many tests have shown that large peak pressures can occur in either the cylinder or the hopper. Many empirical approximations and several theories have been developed to predict the magnitudes of flow pressures. The differences between these theories are also reflected in silo design standards, where considerable differences exist between different national and international codes.

Practical steel silo designs in different countries are usually very similar even though there is a wide discrepancy between the flow pressures defined by different codes. This fact has caused some confusion amongst designers. The reason is that normal wall pressures do not control the design of most cylindrical walls. Instead, the vertical forces in the wall induced by friction control the design, and these do not vary markedly from filling to discharge. In addition, for hoppers the initial filling condition is generally critical, so the flow condition may affect the design only slightly.

Almost all the theories and empirical approximations for predicting pressures on silo walls assume a perfect silo geometry with homogeneous isotropic stored solid behaviour. They consequently predict wall pressures which do not vary around the circumference at a given height. The cylindrical silo structure is well suited to carrying symmetrical pressures of this kind. By contrast, many experiments on full scale silos have shown that unsymmetrical patches of local high pressure occur on the wall during flow (Fig. 1-6), which can give rise to the commonest failure mode of silos in service - buckling. Unfortunately no current silo pressure theories deal with randomly-occurring unsymmetrical pressures and there is insufficient experimental data to define these patches with certainty at present.

Apart from the pressures arising from bulk solids storage and discharge, some other loading conditions are also of importance in the design of steel silos. These include seismic loads from earthquake [Rotter and Hull, 1985, 1989], differential thermal expansion between the silo wall and the stored bulk solids [Anderson, 1966], swelling of the stored bulk solid [Rotter, 1983b], differential thermal expansion and differential settlements in column supports [Gorenc et al, 1986], wind loads [Kwok, 1985] and local discrete support forces [Teng and Rotter, 1990, 1991] in elevated silos.

In elevated silos on discrete supports [Teng and Rotter, 1990, 1991; Guggenberger, 1991], the local vertical forces of the supports must be distributed into the shell, and give rise to very high stresses adjacent to the support terminations. It is this critical feature which discretely supported silos possess that makes the analysis and understanding of this type of silo not only more complex and difficult but also more challenging and necessary. The problem has received very little attention to date.

1.3 FAILURE MODES IN STEEL SILOS

Silos are subjected to many different loading conditions, so that many different modes of failure are possible. Nevertheless, the critical stress conditions in the wall generally lead ultimately to one of only a few modes of failure. These may be simply listed as:

For the cylindrical shell

- bursting
- buckling under axial (vertical) compression
- buckling under circumferential (hoop) compression
- buckling under membrane shear
- local collapse near the support of the silo

For the conical hopper

- collapse or rupture in the hopper body
- plastic collapse or rupture of the hopper/ring junction

For the transition ring

- buckling of the transition ring
- plastic collapse of the transition ring

1.3.1 Failure Modes in the Cylindrical Shell

The bulk solid applies both internal pressure and a downward frictional drag on the silo wall [Janssen, 1895] (Fig. 1-1b). Theoretical studies of flow pressures in silos suggest that the occurrence of very high 'switch' pressures on limited zones of the wall should cause the bursting failure of the cylindrical shell of many silos. However, very few bursting failures occur in steel silos in service. There are several reasons for this: usually the steel of which a silo is made is ductile. It can locally bulge outwards without failure. Further, the solid stored in a silo has a high stiffness, and can sometimes dissipate the local high internal pressure when yielding occurs. In addition, the design thickness for the wall is chiefly governed by its buckling strength under axial compression. Therefore, high local internal pressures are not a serious design concern in many silos, but do have a marked influence on the buckling strength under axial compression for quite different reasons.

However, there are some special circumstances in which bursting failures are to be expected and have been observed in the field. These are swelling of the stored solid [Rotter,1986d], and a sudden decrease in the ambient temperature which cools a steel silo but not its contents [Anderson, 1986; Manbeck et al, 1985]. Silos in which circumferential and vertical loads are

carried by different mechanisms (e.g. vertically stiffened circumferentially corrugated cylinders) may also sometimes fail by bursting.

The commonest failure mode of silos in service is probably buckling under axial or vertical compression. Under axisymmetric filling conditions, this is usually the controlling design consideration for most of the silo wall. Under other loading conditions, higher axial compressions may develop over limited parts of the wall. In particular, eccentric discharge, eccentric filling, earthquake loading on squat silos, and forces from discrete supports in elevated silos are all potential causes of buckling failure.

The buckling strengths of silo walls are normally related to the classical elastic critical stress [ECCS, 1987]. Measured buckling strengths in the laboratory are, however, extremely variable (Fig. 1-7). Many factors affect the buckling strength under vertical compressive loads. They include the amplitudes of the wall's initial geometric imperfections, the magnitude of normal pressures on the silo wall, the elastic properties of the stored material, the type of joints used, the use of ring or vertical stiffeners and the boundary conditions at the base detail.

Only a few studies have investigated the buckling strength under locally raised stresses which are introduced by the discrete supports in elevated silos [Peter,1974; Teng and Rotter, 1990, 1991; Guggenberger, 1991, 1992; Rotter and She, 1993], patch loads and eccentric discharge [Jumikis et al, 1986; Fitz-Henry, 1986; Rotter, 1985] and even fewer studies have addressed the question of imperfection-sensitivity under local high stresses, so that much further work in this area is needed.

Silos may buckle under external pressure occasionally. Two conditions cause most of these failures: rapid withdrawal of the contents with inadequate venting or rapid cooling, and severe windstorms when the silo is empty. Squat ground-supported structures are particularly susceptible to wind buckling because the wall construction is lighter and the diameter is larger than for elevated storages. Squat ground-supported silo structures are also susceptible to being torn from their foundations in windstorms.

In practice, silos can be of uniform or variable wall thickness; they can be stiffened or unstiffened. They can also stand isolated or in a group, and their roofs can be fixed or free to displace radially. Each of these factors has a strong influence on the buckling strength under external pressure or wind.

Silos which are subject to unbalanced horizontal shears from eccentric filling (Fig. 1-8a), eccentric cleanout (Fig. 1-8b), earthquake or mechanical handling equipment carry these loads

principally in membrane shear. A number of failures due to buckling in shear have been reported, but the design of shells against this mode of failure has always been difficult because buckling predictions are not yet available for cylinders with appropriate stress distributions.

A local plastic stability collapse can also occur in axially compressed cylindrical walls just near the base of a silo, or at rings and changes of plate thickness when the internal pressure is high. This mode of failure has commonly known as 'elephant's foot' buckling (Fig. 1-9), in which an axisymmetric outward bulge occurs around a significant part of the shell [Rotter, 1985, 1990].

1.3.2 Failure Modes in the Conical Hopper

The conical hopper on a silo is used to allow gravity discharge. The hopper and its supporting ring are susceptible to a number of failure modes.

Conical hoppers on elevated silos are generally in a state of biaxial membrane tension as a result of the applied internal pressure and the frictional drag on the wall (Fig. 1-10). The most severe loading condition for the body of the hopper is usually initial filling [Rotter, 1986b]. Stresses in the hopper body follow the predictions of the membrane theory of shells closely, but the location of the most highly stressed point varies according to the relative sizes of the hopper and surmounting cylinder. Welded hoppers may fail by formation of a plastic collapse mechanism (Fig. 1-11) [Teng and Rotter, 1989a], whilst bolted hoppers are likely to rupture down a meridional seam under the circumferential stresses [Rotter, 1990a]. In silos with a large hopper beneath a small cylinder, these potential failures occur in quite different locations [Rotter, 1986b, 1990a].

From the global equilibrium at the hopper/cylinder junction (Fig. 1-12), it is certain that a ring at the junction is subject to high circumferential compressive stresses arising from the hopper meridional tension. When a large heavy ring is used, the high meridional tensile stresses at the top of the hopper may lead to failure of the hopper by rupture at the transition junction. This is the commonest failure mode for hoppers.

In addition, it has been noted that very high bending stresses develop at the transition junction [Gaylord and Gaylord, 1984; Rotter, 1985d]. Thus fatigue failure may occur and should be considered carefully if the silo is subject to the filling and discharge cycle more often than daily [Trahair et al, 1983].

1.3.3 Failure Modes in the Transition Ring

Failure modes of the transition ring involve the hopper, cylinder and skirt either by plastic collapse or by buckling. Even under axisymmetric loading conditions, the transition ring may fail by elastic or plastic buckling or by plastic collapse of the junction. A buckling failure of the ring incurs a periodic rotational deformation about the attached point (Fig. 1-13a), whilst plastic collapse of the junction causes large radial inward deformations (Fig. 1-13b).

It seems that additional circumferential bending and warping stresses in quite complex patterns arise in the rings of discretely supported silos (Fig. 1-14), where the ring is required to fulfil the role of a bowgirder beam flange spanning between supports [Rotter, 1984; 1985d]. In large silos, either multiple rings or a beam section in the style of that indicated in Fig. 1-15d is often designed, but lighter silos are usually built either with terminating engaged discrete supports (Fig. 1-15b) or supports extending to the eaves (Fig. 1-15c). These four structural types shown in Fig. 1-15 behave in quite different ways and are not simple to analyse.

The majority of researchers have demonstrated through their studies on ring buckling that in-plane buckling of the ring is almost always prevented by the hopper, but Greiner [1991] has suggested that there are some special geometries where in-plane buckling can occur. In addition, out-of-plane buckling into a mode involving many circumferential waves is a potential mode of failure and has been studied for both uniformly and discretely supported configurations. Buckling is however a problem only when thin annular plate rings are used.

1.4 STRUCTURAL ANALYSIS AND DESIGN OF STEEL SILOS

Numerous steel silos have been built for a wide variety of industrial applications, but there are no specific codes of practice in the world for the structural design of large steel silos, although a few design guides are available [Ketchum, 1909; Lambert, 1968; Wozniak, 1979; Trahair et al, 1983; Gaylord and Gaylord, 1984; Rotter, 1985d, 1990]. Limited structural design advice for small steel silos is given in the British draft code [BMHB, 1987] and a Japanese code for aluminium silos was produced recently [JIS, 1989]. For silo designers, the basic understandings required are in the definition of loads to be used in design, in the stress analysis of these shell structures, and in recognising the many potential failure modes.

As mentioned above, the patterns of loading on silos containing bulk solids are complex and sometimes unpredictable, with significant interactions between the structure and its contained solid. Silos must sustain the internal pressure and the downward frictional traction exerted on the wall caused by the stored bulk solid. The failure modes vary from elastic buckling at very

low stresses with acute imperfection-sensitivity to plastic collapse with post-collapse stiffening where the failure load is not easily clarified. Rival predictions of pressures on silo walls in several design codes and existing theories vary by as much as a factor of 4. Reliable appropriate values are often difficult to choose.

Knowledge of the structural behaviour of steel silos has advanced rapidly in recent decades. The membrane and bending theories of shells have wide applications to silo and tank structures which are of circular planform, determining the linear behaviour and stresses in steel cylinders and hoppers [Rotter, 1985a, 1985b].

These theories are described extensively by Timoshenko and Woinowsky-Krieger [1956], Novozhilov [1959], Flügge, [1973], Seide [1975], Gould [1977], and Calladine [1983], as well as in many other texts.

The membrane theory of shells is based on the assumption that there are no bending moments or transverse shears on a shell element. Thus there are only three stress resultants on an element and three equations of equilibrium for the element. The stress distribution in the shell can then be determined by considering equilibrium alone.

Membrane theory often provides an accurate picture of the stress state in the silo, and is a good basis for the design of silo structures, except in regions adjacent to boundaries, junctions, stiffeners, supports and load concentrations, where bending stresses and transverse shears develop in addition to the membrane stress resultants. Such bending in silos and hoppers is usually localised and is sometimes called an edge effect. The bending theory for silos can be used to evaluate these effects. It is relatively simple for a circular cylindrical shell loaded symmetrically with respect to its axis.

A linear elastic analysis of the structure can provide both membrane stresses and bending stresses and is therefore a useful step in understanding the structural behaviour. However, thin shell structures such as silos can undergo large deflections and significant stress redistributions as plasticity develops. To give a precise indication of when these will occur is beyond the scope of a linear stress analysis. A nonlinear analysis is therefore required to obtain an accurate determination of the failure load of the structure.

A number of classical theories for thin shells of revolution have been developed since the beginning of this century. These involve classical linear bifurcation analysis, nonlinear elastic buckling analysis, small deflection limit analysis, nonlinear elastic-plastic collapse analysis and plastic buckling analysis. However, applications of these theories to silo structures have been

rather few. The elastic buckling of cylinders under axial compression is probably the most significantly and intensively researched subject in silos.

Recent structural analyses [Trahair et al, 1983; Gaylord and Gaylord, 1984; Rotter, 1985d, 1990; Rotter et al, 1991; Teng and Rotter, 1989,1990, 1991; Guggenberger, 1991; Rotter and She 1993] have paid special attention to the buckling and collapse behaviour of silo structures and have provided significant guides in design, but lack of knowledge has still left many problems unsolved. It is already known that for discretely supported silos, local supports give rise to high local stresses in the silo wall adjacent to the support terminations which can lead to buckling failure of the shell at a load much lower than a uniformly supported shell. Discretely supported silo structures have been receiving more attention in recent years. It is believed that more research studies of these structures will bring about better design guidance for practical design use.

1.5 BUCKLING FAILURES IN CYLINDRICAL SILO WALLS

Many possible failure modes of silos have been discussed above. However, the evidence from field observations shows that the commonest failure mode for silos is buckling of the cylindrical wall under axial compression (both local and axisymmetric).

Classical theoretical analysis has been able to predict the buckling strength of unstiffened unpressurized uniformly supported perfect cylinders under axisymmetric axial compression. However, real silos in service contain significant geometric imperfections and are subject to complex loadings. Asymptotic analyses [following Koiter, 1945] and nonlinear analyses [Yamaki, 1984; Rotter and Teng, 1989] have shown that the strength is very sensitive to the amplitudes of initial wall imperfections (Fig. 1-16), which are in turn dependent on the quality of fabrication. Both experiments and analyses reveal that the size and shape of the most detrimental imperfection is probably that of a depression which extends around a significant part of the circumference of the shell at a given height but covers only over a short height [Ding et al, 1992]. These imperfections can be represented as axisymmetric.

The normal pressure exerted by the bulk solid on a silo wall is another factor which influences the strength for buckling under axial compression. The strength of a cylindrical shell increases significantly when it is internally pressurized [Rotter and Teng, 1989] (Fig. 1-17). But the magnitude of the increase in strength is still uncertain.

The silo is not a pressure vessel, but is filled with a bulk solid with finite shear strength. As a result, the solid restrains the silo wall against buckling, and may cause a stable post-buckling response in a shell which would otherwise have had an unstable response. Thus, the stiffness of the solid is also important, but this depends on both the stress in the solid, and its stress history.

A number of common loading conditions in a silo lead to much higher local axial compressive stresses than would arise from the frictional drag alone in the wall. Amongst them is eccentric filling or eccentric clean-out of squat silos (Fig. 1-8a, 1-8b) [Rotter, 1983; Gaylord and Gaylord, 1984]. Experiments on eccentric filling [Eccleston, 1987] showed that two buckle types occur, one running into another. The first is called an 'elephant's foot' buckle at the base (Fig. 1-9), which can become quite stable because the compressive stresses in the wall are redistributed back into the solid as buckling progresses. The second is a membrane shear buckle, since the shell wall is also placed in membrane shear when eccentric filling occurs.

The quasi-static response of squat silos under earthquake loading has a close similarity to the response under eccentric filling, and failures by buckling under axial compression and in membrane shear may also be expected [Rotter and Hull, 1985].

It is more interesting and challenging that during eccentric discharge (Fig. 1-8c), thin-walled steel silos respond quite differently from reinforced concrete silos in which failures are caused by circumferential bending in the reinforced walls. Numerous experiments have shown that there are at least three distinct buckling failure patterns associated with eccentric discharge in steel silos, and that many silo geometries can successfully support eccentric discharge without distress. The buckling modes are demonstrably elastic, as the initial shape of the silo is restored after removal of the solid. In addition, the commonest failure pattern is likely to occur away from the base, close to but above the effective transition (the effective transition is the lowest point on a funnel-flowing silo wall at which moving solid touches the wall).

As noted above, silo structures are also susceptible to buckling failure under severe wind loads when empty and to being torn from their foundations in windstorms. In particular, light-gauge stiffened squat ground-supported structures are the most susceptible to wind buckling. Both buckling and foundation failures are sensitive to the external wind pressure distribution on the walls.

Because information on buckling states under non-uniform axial compression is very scarce, almost all design recommendations relate to conditions of uniform compression. These recommendations are clearly applicable to ground-supported silo structures, but they give no

advice at all on the design of silo walls for locally increased axial compression. In particular, in elevated silos on discrete supports, the local vertical forces of the discrete supports must be distributed into the shell and give rise to local high axial compressive stresses (Fig. 1-18), which may induce the buckling failure of the wall [Teng and Rotter 1990, 1991]. Information on the buckling behaviour of discretely supported silos is extremely rare, and no study appears to have addressed the question of the imperfection-sensitivity of silos on discrete supports until the studies of which this thesis represents a part. Similar work is being undertaken simultaneously at the Technical University of Graz, Austria.

1.6 STRATEGY FOR ATTACKING THE STABILITY PROBLEM

1.6.1 Introduction

It is evident that many fundamental theories have been developed and a great deal of research effort invested on thin shell structures since the beginning of this century. However, very little attention has been paid to practical silo structures, and especially those on discrete supports, which are widely used as storage containers in the chemical process, mining, agricultural, food processing and transportation industries. Many disastrous structural failures of silos have occurred throughout the world [Ravenet, 1976; Jenkyn and Goodwill, 1987]. New research and development in this field is urgently needed.

Current knowledge on the stability of discretely supported silos is still almost entirely confined to the linear bifurcation of perfect cylinders. Only limited non-linear elastic analyses of imperfect cylinders have been carried out because of the enormous amount of work involved. Very little investigation has been made of the structural behaviour in the plastic region [Guggenberger, 1991]. Because current understanding of discretely supported cylinders is both inadequate and fragmentary, no current theory is able to provide adequate advice for practical design.

Both theoretical studies and practical experience have revealed that many factors have a substantial influence on the stability (buckling or collapse) of silo structures. Amongst them, the shell geometry and boundary conditions, the amplitude and profile of imperfection, and the loading pattern are the most important. The discrete supports widely used for large elevated silo structures induce high local stresses adjacent to the support terminations, leading to potential local buckling failures of the shell at a total load much lower than that for a uniformly supported shell. Local loads introduce more complexity and difficulties for new research in this field.

The work of this thesis is mainly focused on the elastic and plastic stability of cylindrical shells under local loading, with special reference to for discretely supported silo structures. Intensive systematic studies are conducted on a few aspects: the formal solution of the shell equations under local loadings; numerical analysis of cylindrical shells under local loading; linear stress and bifurcation analyses; nonlinear elastic buckling analyses, and both limit and elastic-plastic geometrically nonlinear analyses of cylindrical shells on discrete supports. Finally, the complete form of a silo (a cylindrical shell together with a roof and a bottom conical hopper) is examined to investigate the applicability of the simpler modelling using a cylinder instead of a silo, and to gain a more realistic insight into the behaviour of silo structures.

It should be noted that most of the work described in this thesis was undertaken using finite element analyses. However, early analyses of the problem showed that the buckling mode is very local and sensitive to the stress distribution adjacent to the support. As a result, an analytical solution for the stress distribution near the support was developed. This is the first known solution of the shell bending equations for a distributed patch of load in meridional direction. Although the solution is very involved, it gives some insight into the controlling parameters of the problem, and indicates the scale of complexity which would be involved if analytical solutions of the nonlinear behaviour were attempted.

The remaining studies in this thesis all exploit numerical finite element analysis. Only the isolated silo of circular planform is considered. Its finite element modelling is individually described in the relevant chapters.

With regard to the loads on silo walls from bulk solids, which have been briefly described above and will be extensively discussed in Chapter 2, several simplified loading cases are chosen to apply to the structural model. The corresponding strength obtained under each of these loading cases is usually represented in this thesis by the dimensionless mean stress above the support at buckling or collapse.

1.6.2 Simplified Loading Cases

In previous investigations of cylindrical silo shells carried out by other researchers [Rotter, 1982, 1983, 1985, 1990; Teng and Rotter, 1989, 1990, 1991, Rotter and She, 1993], a uniformly distributed axisymmetric downward meridional traction has usually been assumed to model the frictional force imposed on the silo wall by the stored bulk solids. Many research results have been obtained on the basis of this type of loading pattern. Such a loading case is also involved in the analyses carried out in this thesis and is referred to as wall frictional load. Moreover, in this thesis, other two loading cases have been extensively used: one is a uniform vertical line load around the lower edge of the cylinder, referred to as the hopper load. The

other is a uniform vertical line load around the upper edge of the cylinder, and referred to as the roof load. The reasons why these three loading cases are important are to be found in the patterns of real silo loads:

According to Janssen's theory [1895], the pressures on the vertical walls of silos (Fig. 1-19a) change their magnitude according to the height of the cylinder, measured in terms of $\frac{H}{Z_0} = \frac{2H\mu k}{R}$ (where H is the cylinder height, Z_0 is the depth below the effective surface, μ is the coefficient of wall friction, and k is the ratio of horizontal to vertical stress in the stored solid). Thus, it can be seen that the pressure distribution on the wall depends not just on $\frac{H}{R}$, but also μ and k which are bulk solids properties (Fig. 1-19b).

(a) If the silo is fairly tall, a lot of the weight of the stored solids is transmitted through wall friction. In this circumstance, the pressure distribution on the wall involves much of the wall under uniform pressure, so there is also almost uniform wall friction (Fig. 1-19c). Therefore, the uniform wall friction is an extreme load case for the silo.

(b) If μk is small or $\frac{H}{R}$ is small, only a small amount of the weight is transmitted through wall friction, whilst most of the weight of the solids in the silo rests on the hopper. Thus the real loading is very like the hopper load case. This is a second extreme load case.

Accordingly, it can be seen that all symmetrical bulk solids loading cases lie somewhere between the hopper load case and the uniform wall friction case (all others are typically close to combinations of these two).

(c) Since tests in the laboratory are almost always arranged with loading at the top edge, the roof load case is really a modelling of the loading occurring in a laboratory experiment.

The axial stress distributions for uniformly supported cylinders under the three loading conditions are shown in Fig. 1-20. It is evident that these three loading cases can induce different patterns of stress distribution in the cylindrical shells of silos.

As the bulk solid applies internal pressure on the silo wall in addition to a downward frictional drag, a combined loading pattern is represented as a uniform roof load applied on the upper boundary of a cylinder together with an internal pressure uniformly distributed on the cylinder wall in the nonlinear elastic buckling analysis conducted in Chapter 6.

In Chapter 8, the study focuses on a complete discretely supported silo, instead of the reduced problem of a simple cylindrical shell. The three loading patterns, namely roof load, wall friction load, and hopper load, are again examined to investigate the buckling behaviour of a whole silo structure under axial compression.

All the above loading cases involve considerable simplification of the real external loadings imposed on the silo walls. The latter are rather complex, so that any chosen real loading pattern restricts the generality of the solution. Instead the simpler loading cases are most helpful in exploring the extremes of possible loading patterns and thus encompass all loadings on practical silo structures in service.

1.6.3 Characterisation of Strength

To make the results immediately usable and comprehensible, the axial load applied to the silo wall at failure is characterised by the dimensionless mean vertical membrane stress immediately above the support in all the analyses of the discretely supported silos. This dimensionless stress is found as the mean meridional membrane stress σ_m divided by the classical elastic critical stress for uniform axial compression σ_{cl} or alternatively divided by the yield stress σ_y for the analyses in the plastic region.

When a cylinder is subjected to a uniformly distributed downward load p_v on the wall (ie. the wall friction per unit wall area), the mean meridional membrane stress σ_m above each support is given by

$$\sigma_m = \frac{2\pi R H p_v}{n d t} = \frac{2\pi}{n}\frac{R}{t}\frac{H}{R}\frac{R}{d} p_v \tag{1.1}$$

where R is the radius of the cylinder, H is the height of the cylinder, t is the thickness of the cylinder wall, d is the width of the support, and n is the number of supports.

When the cylinder is subjected to a uniformly distributed downward line load P_l per unit circumference at either the upper or lower edge, the mean meridional membrane stress σ_m above each support is instead in the form

$$\sigma_m = \frac{2\pi R P_l}{n d t} = \frac{2\pi}{n}\frac{R}{t}\frac{R}{d}\frac{P_l}{R} \tag{1.2}$$

The classical elastic critical stress may be expressed as

$$\sigma_{cl} = \frac{1}{[3(1-\nu^2)]^{1/2}}\frac{Et}{R} \tag{1.3}$$

where E is Young's modulus and ν is Poisson's ratio.

For a material with a Poisson's ratio of ν = 0.3, it becomes

$$\sigma_{cl} = 0.605 \frac{Et}{R} \tag{1.4}$$

The dimensionless mean meridional membrane stress above the support is then given by

$$\frac{\sigma_m}{\sigma_{cl}} = \frac{10.39}{n} \frac{R}{d} \frac{H}{R} \left(\frac{R}{t}\right)^2 \frac{p_v}{E} \tag{1.5}$$

or alternatively

$$\frac{\sigma_m}{\sigma_y} = \frac{2\pi}{n} \frac{R}{t} \frac{H}{R} \frac{R}{d} \frac{p_v}{\sigma_y} \tag{1.6}$$

for the case of a uniformly distributed frictional load p_v; and

$$\frac{\sigma_m}{\sigma_{cl}} = \frac{10.39}{n} \frac{R}{d} \frac{R}{t} \frac{P_l}{tE} \tag{1.7}$$

or alternatively

$$\frac{\sigma_m}{\sigma_y} = \frac{2\pi}{n} \frac{R}{t} \frac{R}{d} \frac{P_l}{R\sigma_y} \tag{1.8}$$

for the case of a uniformly distributed line load P_l.

If it is supposed that the total applied load is the same irrespective of whether it is applied to the edge or to the wall, then the relation between the line load (roof load and hopper load) P_l and the frictional load p_v becomes

$$P_l = p_v H \tag{1.9}$$

These above relations define the dimensionless groups of the stability problem studied in this thesis, whether it involves linear or nonlinear elastic buckling or plastic collapse.

In addition, when an internal pressure p is applied to the shell wall in addition to the axial compression, it is denoted as a dimensionless parameter $p^* = \frac{pR}{t\sigma_{cl}}$ throughout the analyses conducted in Chapters 6 and 7, following the formulations of Calladine [1983] and Rotter and Teng [1988].

1.8 CONTENTS OF THE THESIS

The objective of this thesis is to broaden current knowledge of the strength and buckling/collapse of shells, with special reference to steel silo structures on discrete supports. Its conclusions provide design guidance of practical value for future silo design and construction. The material in this thesis is presented in nine chapters together with the references. The work presented in this thesis only relates to isolated silos of circular planform, under axisymmetric loads from the bulk solids contained in the silos and directly supported on rigid discrete supports.

This chapter, Chapter 1, provides a general introduction. The existing knowledge of silo structures has been described in the following categories: loads on silo walls, failure modes in steel silos, structural analysis and design of steel silos and buckling failures in cylindrical silo walls. Then, the strategy for attacking the stability problem in this thesis was introduced, including the simplified loading cases and the characterisation of strength adopted in the studies of this thesis. The contents of the thesis are finally outlined to introduce the range of the work carried out.

Current background knowledge in the field of silo structures is described in Chapter 2, which is entitled Historical Review, and focuses on the aspects to which this thesis is related. These aspects include the loads on silo walls from bulk solids, theory of circular cylindrical shells, structural design of steel silos, and computer programs used in this research. Extensive references to more detailed sources are given.

Chapter 3 briefly describes Rotter and She's recent studies of the nonlinear and stability behaviour of discretely supported thin elastic cylinders. These exploratory investigations of the geometrically nonlinear buckling behaviour, buckling mode and buckling strength for discretely supported perfect and imperfect cylinders provide a conceptual background on which the research of this thesis relates.

In Chapter 4, a linear elastic solution of the cylinderical shell bending equations is presented for local loadings, with special attention to local longitudinal distributed loadings. Algebraic expressions for the displacements and stresses induced by a rectangular patch of longitudinal load on a simply supported cylindrical shell are derived using double Fourier series. The solution of this problem is general and therefore can be applied to cylindrical shells under local loadings in any direction and with different boundary conditions.

Linear elastic analyses of discretely supported perfect cylinders under axial compression are presented in Chapter 5, using the finite element method. The pre-buckling meridional membrane stress distribution above the support centreline is examined in detail, and is followed by investigations of the linear bifurcation behaviour of the cylinders. The effects on the stress distribution and the buckling strength of different loading patterns and different sets of geometric parameters are extensively examined.

Using large deflection theory, Chapter 6 presents geometrically nonlinear elastic buckling analyses of cylinders on discrete supports. Both perfect and imperfect cylinders are examined. Two forms of imperfection are employed. The effect of the loading pattern applied to the shell which has been discussed in Chapter 5 is re-examined to show the comparison between the linear and nonlinear buckling strengths. Axial compression in silo cylinders is almost always accompanied by internal pressure. An internal pressure is next introduced with the axial compression. Under the combination of internal pressure and axial compression, the nonlinear elastic buckling behaviour, the buckling strength and the buckling configuration are thoroughly investigated for discretely supported cylinders.

Chapter 7 extends the work into the plastic range. Discretely supported cylinders obeying the von Mises yield criterion are analysed. Limit analyses of perfect cylinders are first conducted using small deflection theory. Geometrically nonlinear elastic-plastic collapse analyses of both perfect and imperfect cylinders are performed next. Studies of different loading conditions and parametric studies of varying geometries and material strengths are presented in both types of analysis. The nonlinear elastic-plastic collapse behaviour of discretely supported cylinders is thus explored.

A complete silo which consists of a cylindrical shell, a conical roof hopper and a conical discharge hopper is briefly examined in Chapter 8, with the aim of exploring the applicability of the established cylinder model in the elastic buckling analysis of silo structures.

Finally, the conclusions drawn from this research are summarised in Chapter 9. Recommendations are also made for further research on locally supported shells.

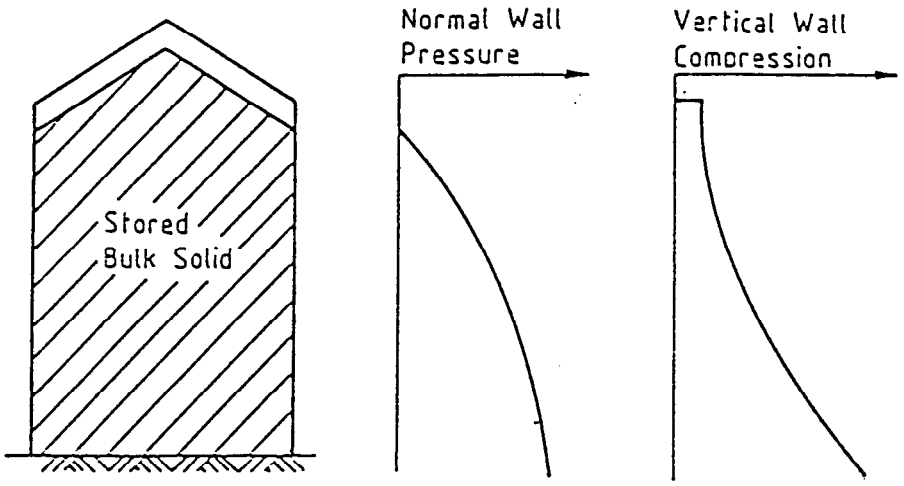

(a) On-Ground Silo (b) Typical Pattern of Wall Forces

Figure 1-1 Silo and Wall Loads

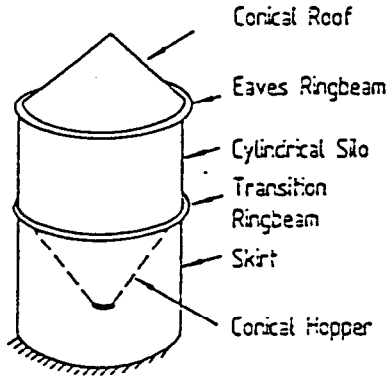

(a) Deep Skirt Silo

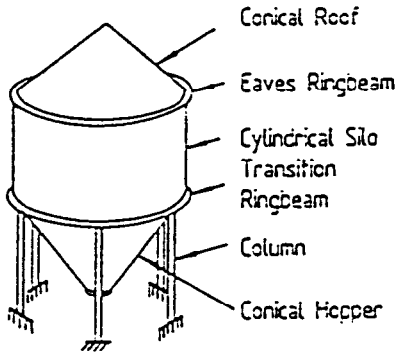

(b) Column-Supported Silo with Columns Terminating at the Transition Ring

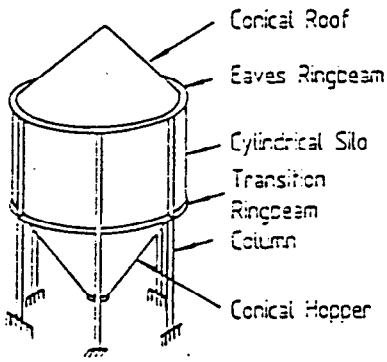

(c) Column-Supported Silo with Columns Extending to the Eaves Ring

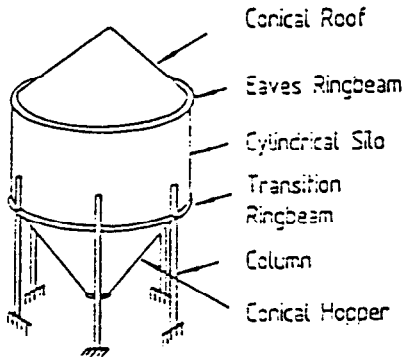

(d) Column-Supported Silo with Engaged Column

Figure 1-2 Support Arrangements of Elevated Silos

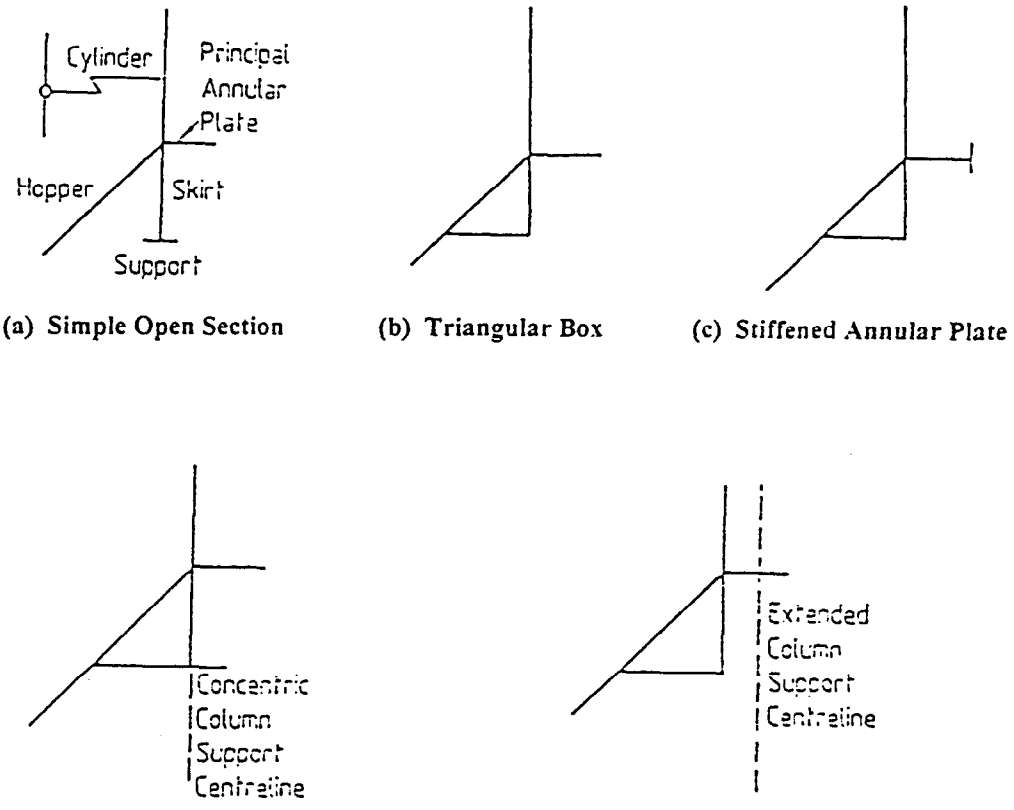

(a) Simple Open Section (b) Triangular Box (c) Stiffened Annular Plate

(d) Column Sopport at Skirt (e) Column Support Extended up Wall

Figure 1-3 Typical Forms of Transition Junction

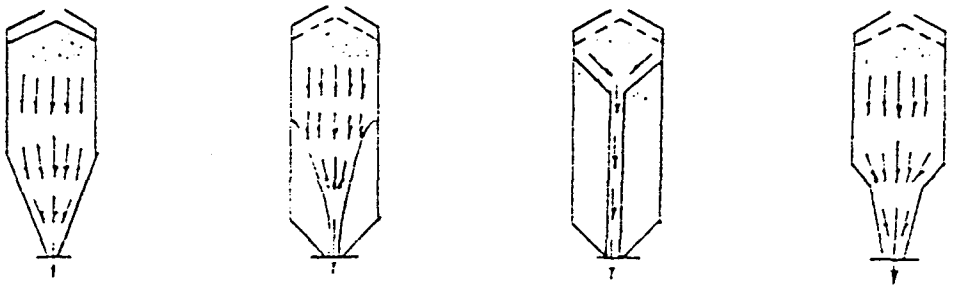

(a) Mass Flow (b) Funnel Flow (c) Pipe Flow (d) Expanded Flow

Figure 1-4 Flow Patterns

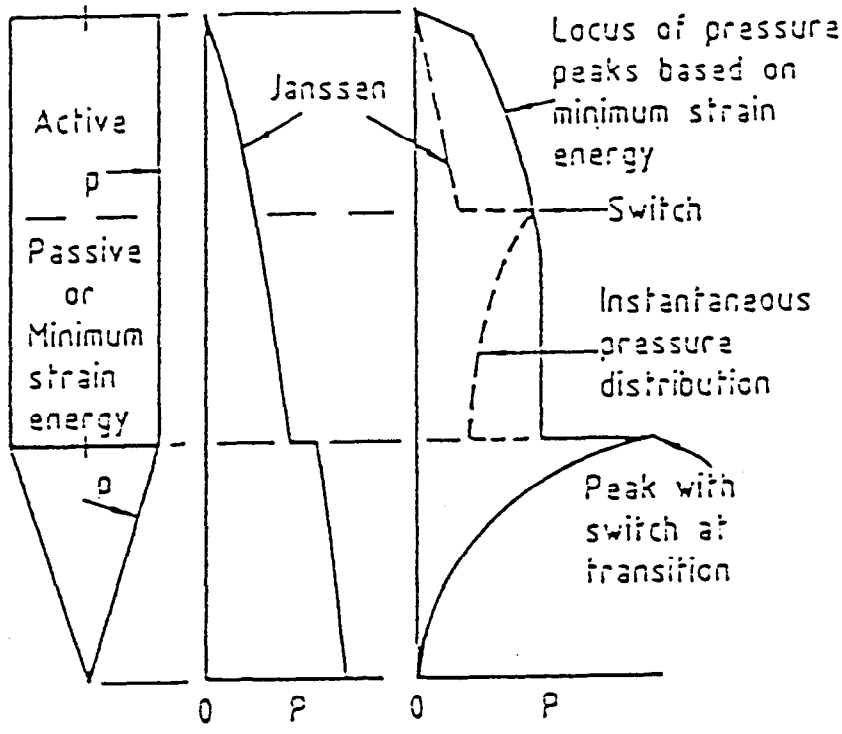

(a) Initial Pressures (b) Flow Pressures

Figure 1-5 Theoretical Pressure Distribution on Silo Walls

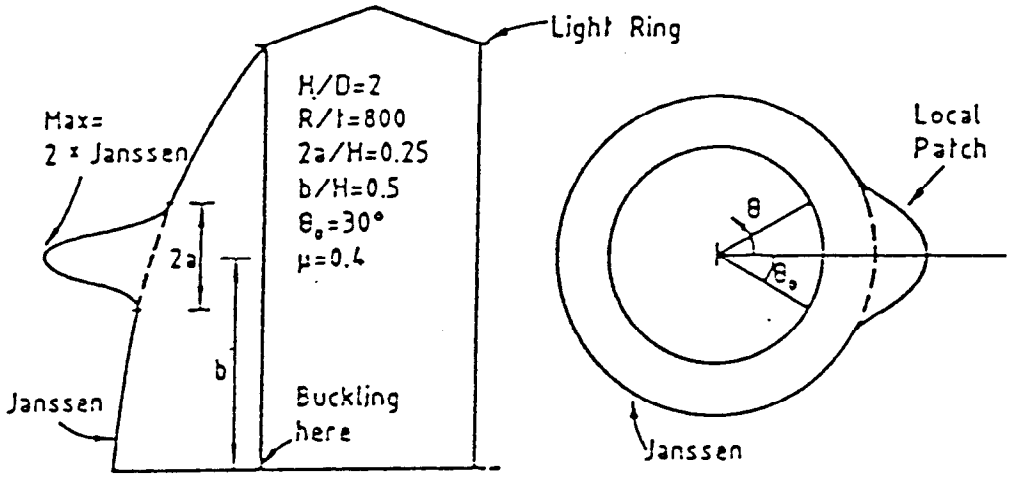

(a) Example Silo

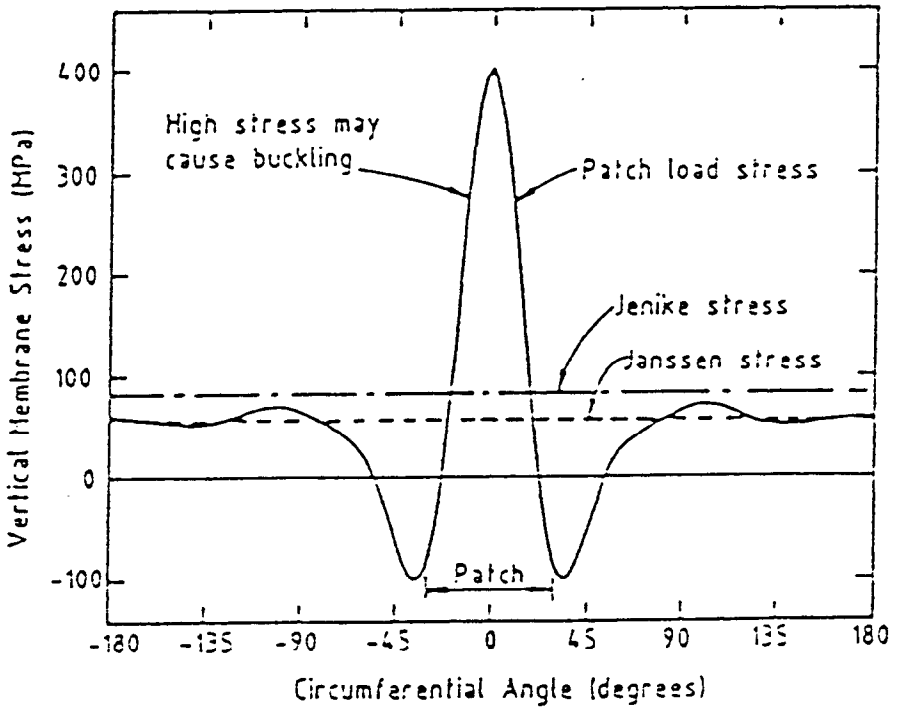

(b) Vertical Wall Stresses near Silo Base

Figure 1-6 Buckling Consequence of a Local Patch of High Pressure

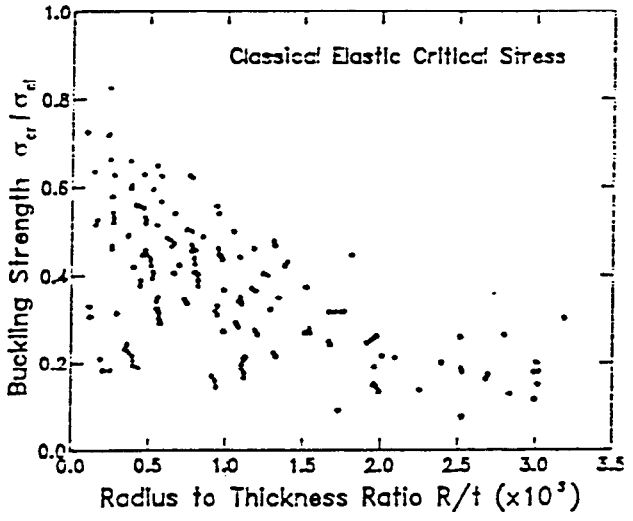

Figure 1-7 Experimental Buckling Strengths under Axial Compression

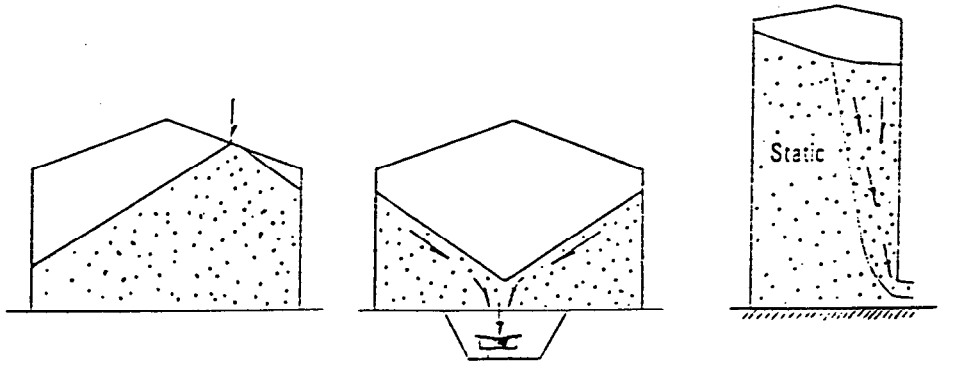

(a) Eccentric Filling (b) Unsymmetrical Cleanout (c) Eccentric Discharge

Figure 1-8 Eccentric Filling and Eccentric Discharge

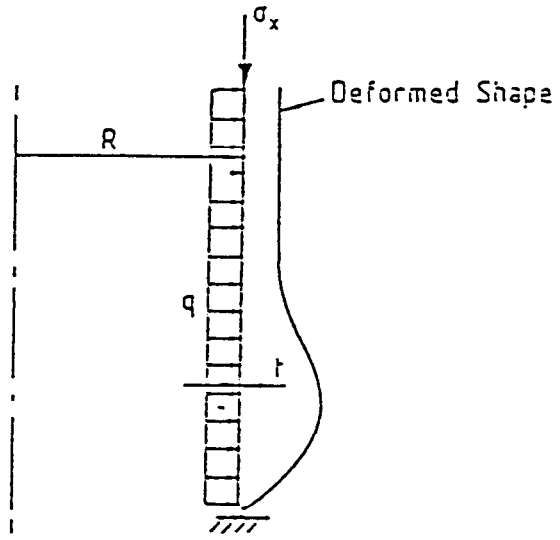

Figure 1-9 Elephant's Foot Buckling Mode

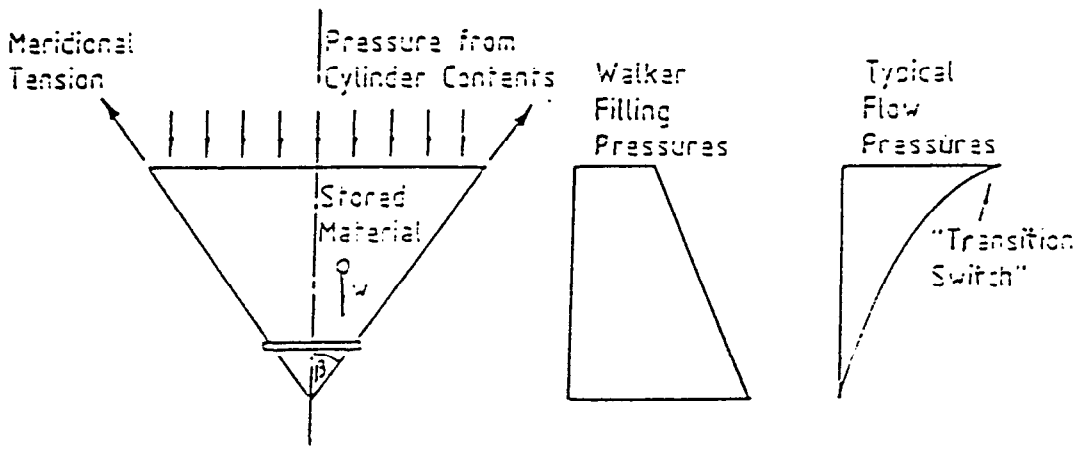

Figure 1-10 Vertical Equilibrium and Pressure in Conical Hopper

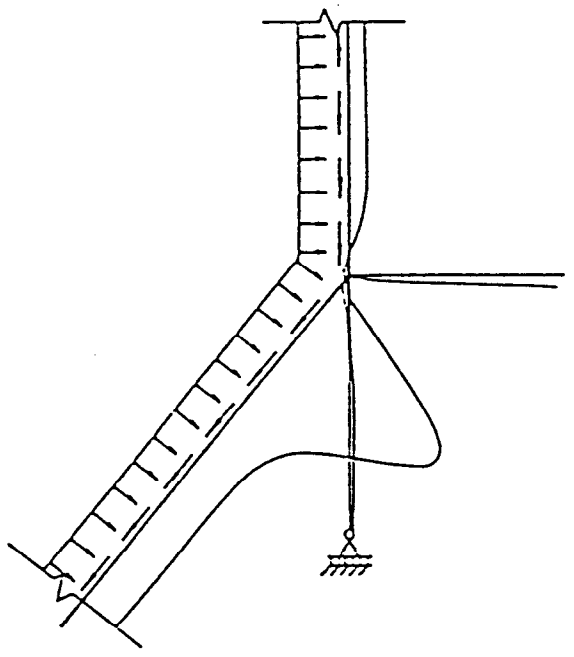

Figure 1-11 Hopper Collapse Mode

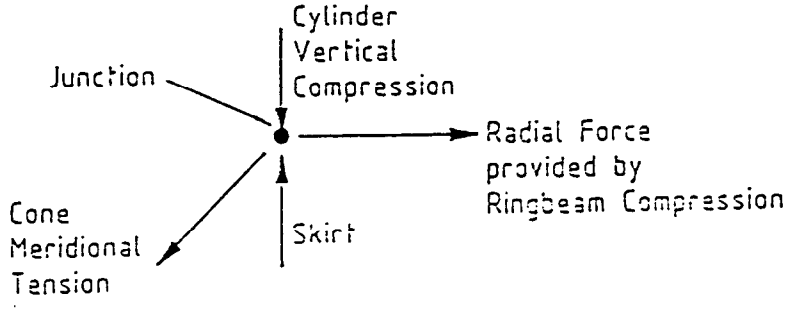

(b) Static Equilibrium at the Junction

Figure 1-12 Equilibrium at the Hopper/Cylinder Junction

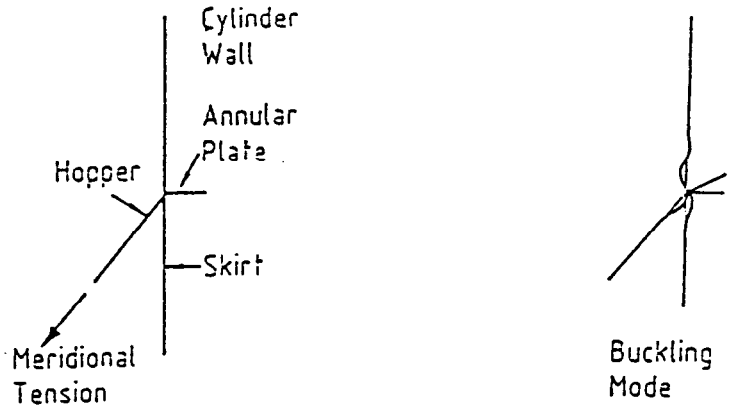

(a) Geometry and Buckling Mode of Ring

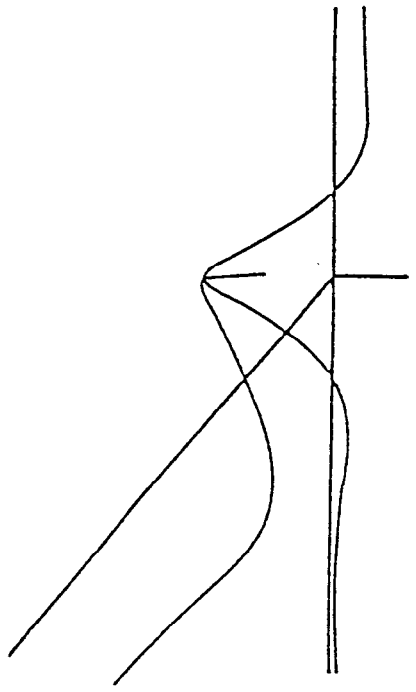

(b) Collapse Mode of Junction

Figure 1-13 Transition Ring Buckling and Collapse

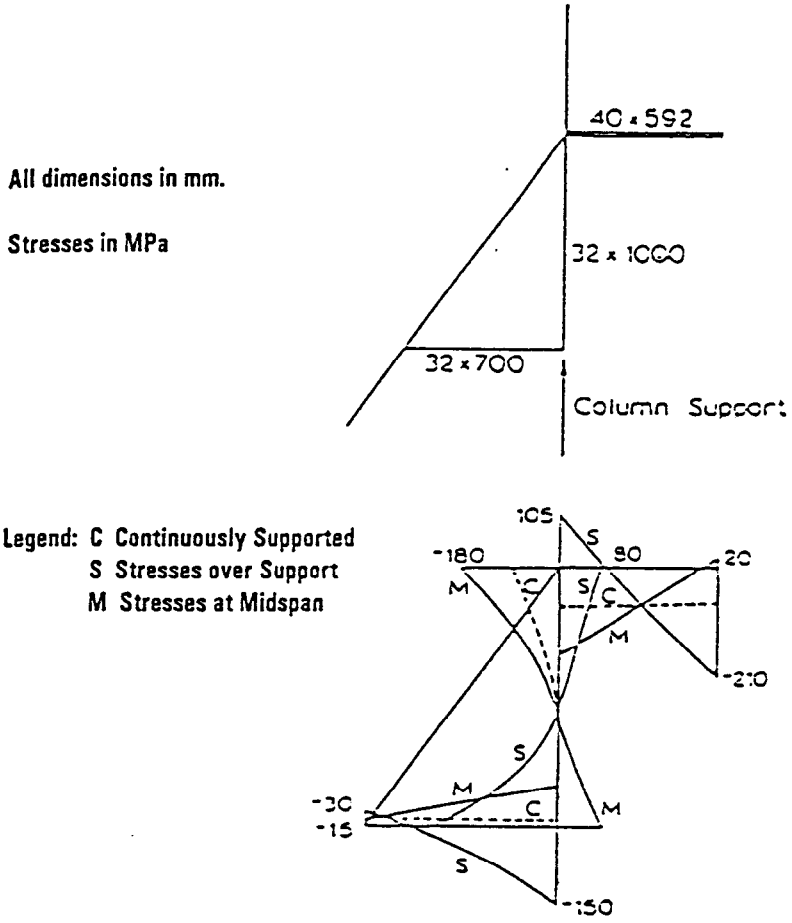

Figure 1-14 Stresses in the Ring of a Column-Supported Silo

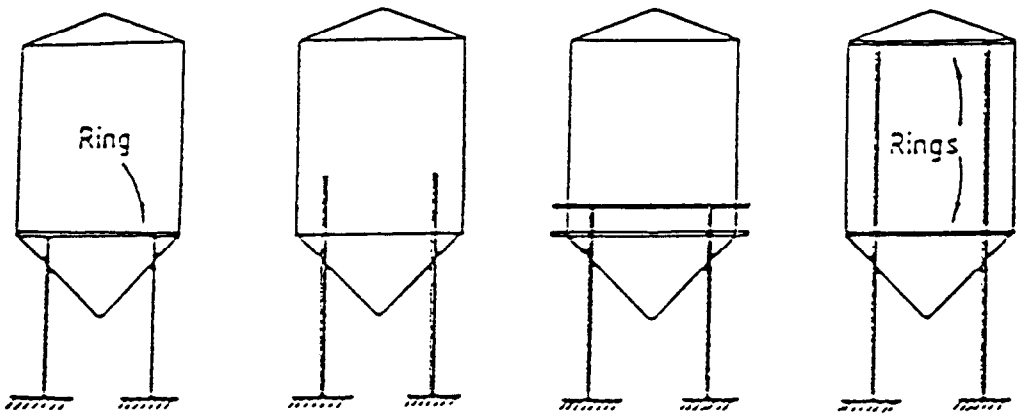

(a) Very Light Bins: Terminating Columns with Ring

(b) Light Bins: Engaged Columns

(c) Medium and Heavy Bins: Columns to Eaves

(d) Medium and Heavy Bins: StrongRingbeam

Figure 1-15 Light Column-Supported Silos

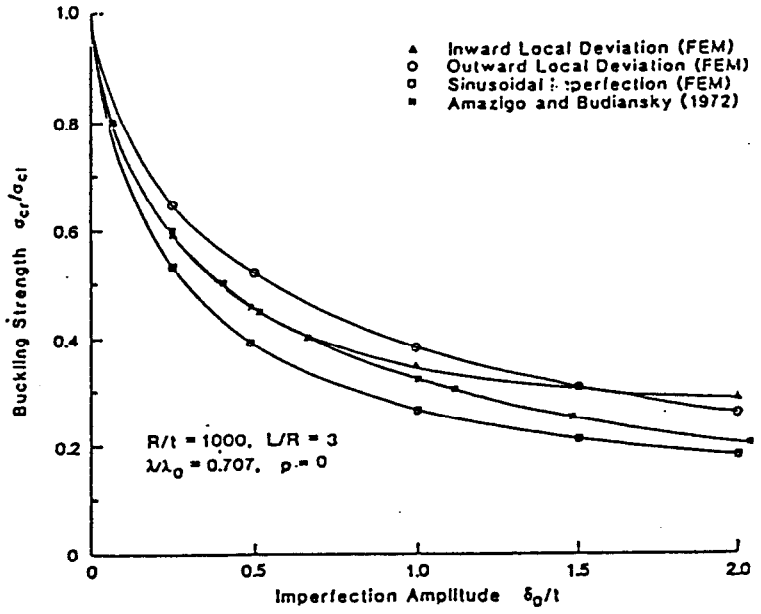

Figure 1-16 Effect of Imperfection Amplitude on Axial Compression Buckling Strength

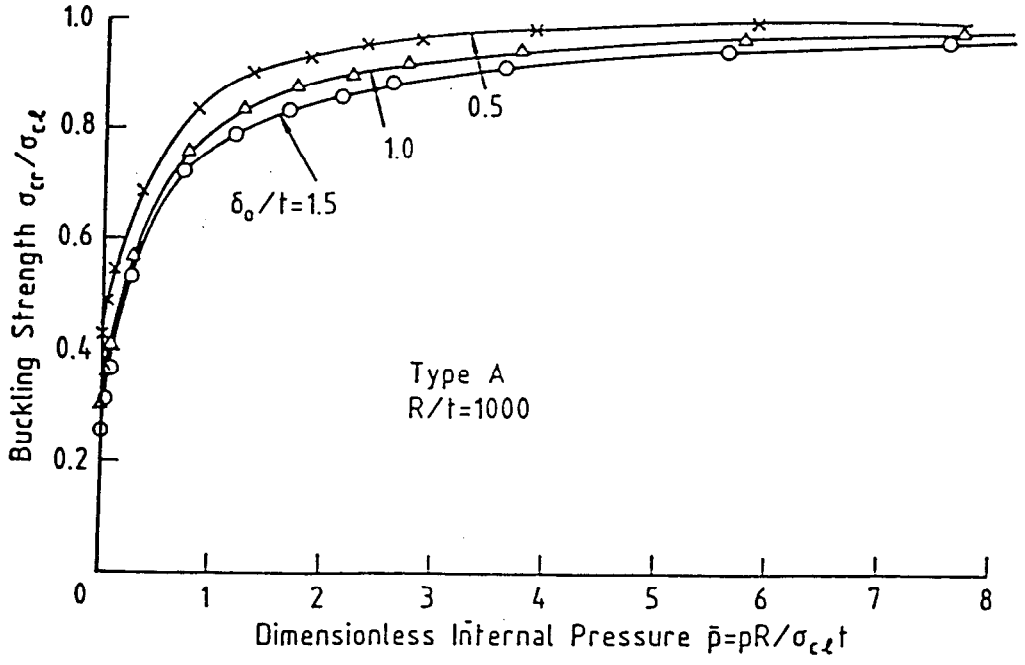

Figure 1-17 Effect of Internal Pressure on Buckling Strengths

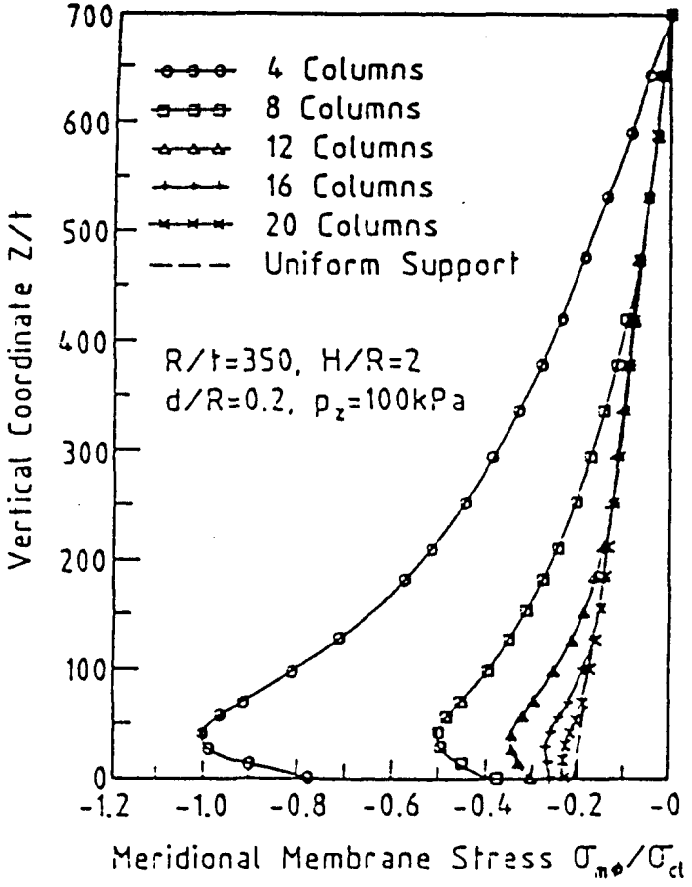

(a) Changes with the number of columns

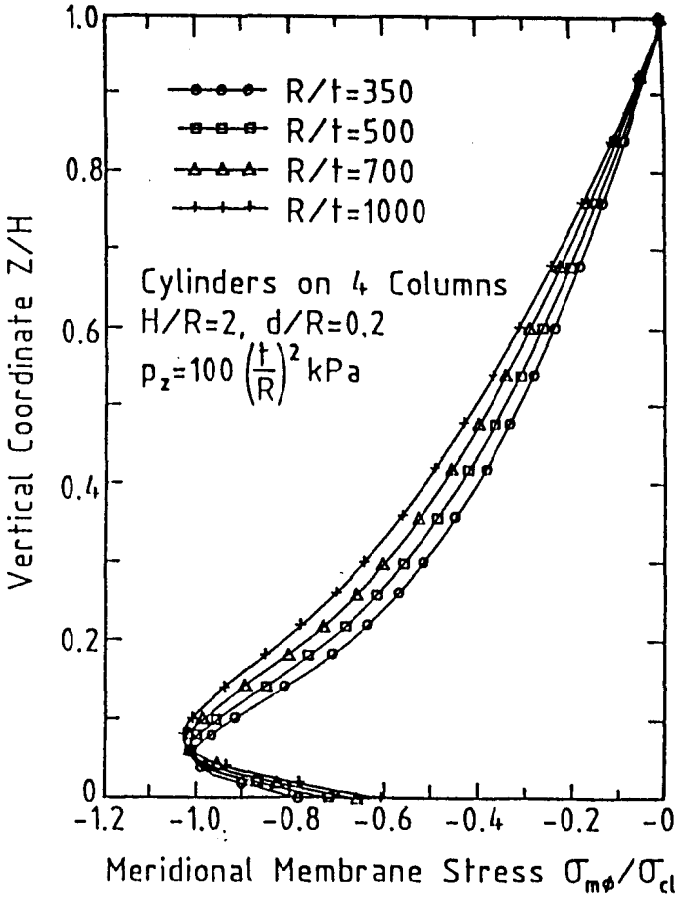

(b) Changes with the thickness of the cylinder

Figure 1-18 Meridional Membrane Stress above Column Centreline (rigid support)

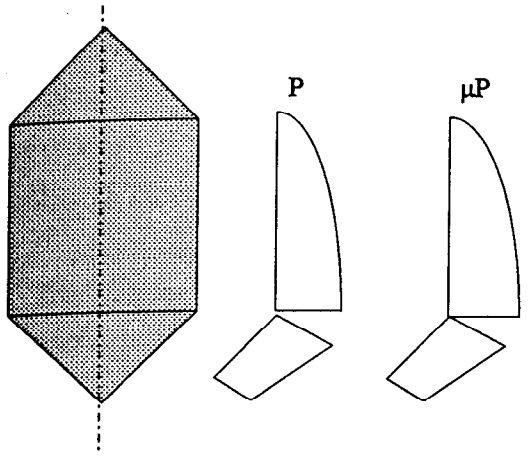

(a) Pressure Distribution on Silo Wall

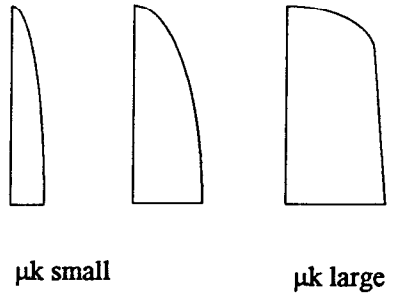

(b) Influence of Bulk Solids Properties

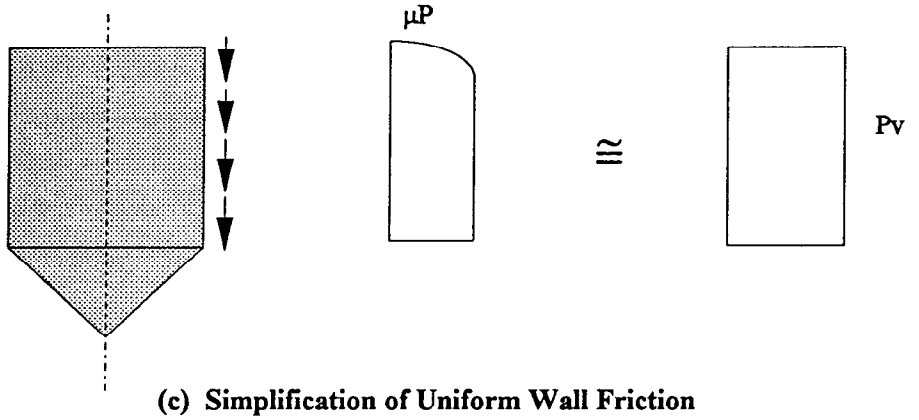

(c) Simplification of Uniform Wall Friction

Figure 1-19 Simplification of Loading on Silo Wall

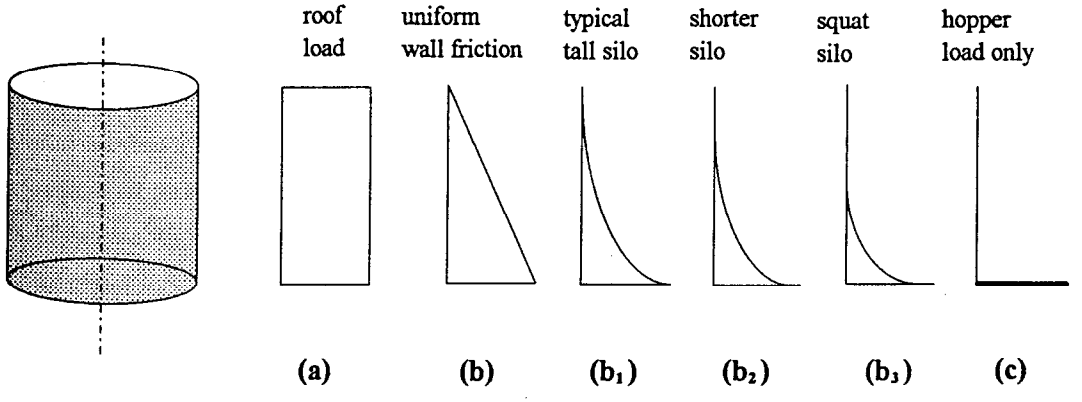

Figure 1-20 Axial Stress Distribution for Uniformly Supported Cylinders under Three Loading Conditions

CHAPTER 2

HISTORICAL REVIEW

2.1 INTRODUCTION

This chapter presents a review of current knowledge of steel silo structures, with special emphasis on the theories for buckling and collapse in circular cylindrical thin-walled silo structures and the existing design criteria used for steel silo structures.

This chapter starts with a description of the existing theories for predicting the loads (wall pressures) on silo walls from the stored bulk solids. Next, a brief review is given of the development of the theories most often used in the research studies of silo structures. Attention is first placed on a few typical theories of circular cylindrical shells, and then turned onto buckling and collapse analyses of circular cylindrical shells with different geometries and boundary conditions and under various loading conditions. Current available criteria for design against many failure modes of silo structures are subsequently discussed. Finally the computer programs which are later used in the studies of this thesis are described.

2.2 LOADS ON SILO WALLS FROM BULK SOLIDS: WALL PRESSURES

2.2.1 Loads in Cylinders after Initial Filling

Early designers of silos for the storage of bulk solids assumed that the stored materials behaved like liquids and designed the silos for equivalent fluid pressures. No frictional forces were considered and the weight of the ensiled material was assumed to rest entirely on the bottom of the silo.

In 1882, Roberts in England made the first tests on models and full-size silos to determine the static horizontal and vertical pressures in silos due to a stored bulk solid [Roberts, 1882]. The results of these tests showed that the pressures attained a sustained maximum value at a depth of stored material equal to about twice the diameter of the silo [Roberts, 1884]. These tests demonstrated that the fluid theory previously used in the analysis of silos is incorrect because some of the weight of the stored materials is transferred to the walls by friction, and the horizontal and vertical pressures in the solid are not equal.

Janssen confirmed Roberts' conclusion and in 1895 published a theory that describes the pressures on the vertical walls of silos (Fig. 1-1b). In this simple theory, the pressures depend on the bulk density of solid, the silo radius, the depth below the effective surface, the coefficient of wall friction and the ratio of horizontal to vertical stress in the stored solid k (Fig. 1-17).

Since that time, the distribution of wall loads (Fig. 1-5a) used in the design of taller silos has most often been based on Janssen's equation [1895]. Other authors [Koenen, 1896; Jaky, 1948; Pieper and Wenzel, 1969; Walker, 1966; Homes, 1972; Walters, 1973; Jenike et al, 1973; Haaker and Scott, 1983; Hartlen et al, 1984; Arnold et al, 1978; Rotter, 1988] modified the lateral pressure ratio k in their studies. According to Jenike et al [1973], k=0.4 gives results that compare favourably with filling pressures determined experimentally with many materials.

Difficulties arise in the application of Janssen's theory to squatter silos, because it does not properly satisfy the top surface boundary condition, which is affected by the conical pile of stored material. Reimbert and Reimbert [1976] produced an alternative solution to Janssen's differential equation which is suitable for squat silos. In this solution, the value of the lateral pressure ratio k varies with depth. Rankine's [1857] and Coulomb's [1776] theories were often proposed for squat silos, but both of these theories only apply to straight walls, not to the curved walls which are commonly used in silos. In more recent work [Ooi and Rotter, 1986, 1987], the limitations of the above approaches have been overcome using the finite element method.

2.2.2 Loads in Hoppers after Initial Filling

In elevated silos, the majority of the total weight of stored bulk solid rests on the hopper. The total load on the hopper is defined by the hopper volume, and the vertical stress in the stored solid at the transition junction (Fig. 1-10). More effort must be put into the definition of the vertical stress in the stored solid at the level of the hopper/cylinder transition junction than that of loading which derives from the stored solid, since the volume of the hopper is known, and the density of the stored material does not change greatly.

The simplest assumption for hopper filling pressures is that of Walker [1966]. In his theory, the stored bulk solid carries no shear stresses, leading to a linear variation of pressure (Fig. 1-10). This is often the worst pressure distribution for steel hoppers [Arnold et al, 1978; Rotter, 1986b]. Whether the pressures can be as high as the predictions of Walker's theory is doubtful, so this pressure distribution may be unduly conservative.

Walker's theory for initial filling is adopted in some codes [Gorenc et al, 1986; BMHB, 1987], but not in others [DIN 1055, 1986; ACI, 1977]. It should be noted that the frictional drag has been omitted in drafting some code rules based on Walker's theory [BMHB, 1987] leading to an unsafe definition, since the hopper is deemed to carry less than the total load acting on it.

2.2.3 Loads in Cylinders during Flow

It was noted as early as 1896 that pressures during discharge may be larger than those after filling. The patterns of flow from silos (Fig. 1-4) are known to affect both the patterns and magnitudes of pressures on silo walls.

The Janssen equations [1895] have long been used as a convenient means for the calculation of normal pressures, vertical pressures and frictional forces on the wall from which the values during flow can be estimated. The design values of loads on the silo wall are thus obtained by using flow load multipliers or overpressure factors applied to the Janssen pressures. This approach has been widely used over many years and was adopted in the ACI 313 [1977] code. Flow load multipliers were also derived from the minimum strain energy theory of Jenike et al [1973] by Arnold et al [1978] and McLean et al [1983]. Alternatively, the flow pressures may be calculated directly from Janssen's equation, but using unrealistic values of the lateral pressure ratio k and wall friction coefficient μ which lead to a close modelling of the expected maximum flow pressures on the vertical walls of the silo [Pieper and Wenzel, 1969]. This approach was used in the DIN 1055 [1964] code, but presents considerable difficulties when applied to both steel and concrete silos because the stress resultants controlling the failure modes are different.

Problems with many silos in service have led to a substantial research effort on silo loads to determine whether existing design procedures are adequate. Under certain conditions, the loads on silo walls can be expected to exceed the predictions of the ACI and DIN codes [Walker, 1966; Jenike et al, 1973; Walters, 1973; Nielsen and Andersen, 1981; McLean et al, 1983; Arnold et al, 1978]. Very much larger flow pressures have been suggested on theoretical grounds by some researchers [Walters, 1973; Van Zanten et al, 1977], but these have not been supported by experimental evidence and have been rejected by code committees as unnecessarily conservative.

2.2.4 Loads in Hoppers during Flow

Flow pressures in a mass flow silo (Fig. 1-4a) are usually well defined and reproducible because the flow channel is well defined and constant [Walker, 1966; Walters, 1973; Horne and Nedderman, 1978; Jenike et al, 1973]. It is widely recognised that the pressure at the outlet decreases during discharge and that a local high pressure ('switch' pressure) develops at

the transition. Most design guides recommended that this 'switch' pressure be considered. The transition 'switch' pressure has been examined both experimentally and theoretically [Walker, 1966; Clague, 1973; Walters, 1973, Jenike et al, 1973; Motzkus, 1974; Moriyama and Jotaki, 1980; Haussler and Eibl, 1984; Rotter, 1986b, 1988]. It has been concluded that the switch pressure only becomes really large when a very steep hopper is used.

The pressures on hopper walls during funnel flow (including pipe flow) (Fig. 1-4b and 1-4c) are more difficult to define. The theoretical equations of Jenike et al [1973], Arnold et al [1978] and Gorenc et al [1986] are often quoted for hopper flow pressures. The above funnel flow theories mostly only apply to tall silos with small hoppers, because the material inside the hopper is ignored. Because of the poor current understanding of funnel flow pressure distributions on hopper walls, Rotter [1988] suggested that all hoppers should be designed for the pressures which are known to occur under mass flow conditions.

Eccentric discharge of the stored material, and dynamic conditions such as rapid filling with powdery solids and impact loads from relatively large lumps, can lead to significant additional loads on the silo structure. Of these, eccentric discharge pressures are probably the most critical and difficult to define. A number of experimental studies have explored the wall pressures occurring during eccentric discharge [Jamieson, 1904; Pieper, 1969; Ravenet, 1976; Nielsen et al, 1979, 1981; Hartlen et al, 1984; Gale et al, 1986] but the results are not entirely consistent. Evidently more work is required to clarify the question of design loads to be used for eccentrically discharged silos.

2.3 THEORY OF CIRCULAR CYLINDRICAL SHELLS

2.3.1 Introduction

Since the thin-walled circular cylindrical shell is very widely used as a structural element in light-weight, it is important to clarify the elastic and plastic stability of circular cylindrical shells under various loading conditions. With the development of aircraft structures, since the beginning of this century, numerous research studies have been carried out on the buckling and collapse of circular cylindrical shells [Donnell, 1933; Flügge, 1932, Timoshenko, 1940; Sanders, 1963; Timoshenko and Gere, 1961; Hodge, 1963; Koiter, 1967; Olszak and Sawczuk, 1967; Save and Massonnet, 1972; Brush and Almroth, 1975; Calladine, 1983; Kollar and Dulacska, 1984; Yamaki, 1984; Esslinger and Geier, 1977; Rotter et al., 1983, 1985, 1989, 1990]. Many review articles on various aspects of shell buckling and collapse have appeared in the literature [Nash, 1960; Budiansky and Hutchinson, 1966; Hutchinson and Koiter, 1970; Sewell, 1972; Budiansky, 1974; Hutchinson, 1974; Sechler, 1974; Tvergaard,

1976; Budiansky and Hutchinson, 1979; Bushnell, 1981b, Babcock, 1983; Simitses, 1986]. A number of symposia have also been held [e.g. Fung and Sechler, 1974; Koiter and Mikhailov, 1980; Thompson and Hunt, 1983; Ramm, 1983].

No attempt is made in this section to give a complete review of the development of analytical theories for circular cylindrical shells, but only those which are closely related to the particular problems tackled in this thesis are briefly discussed. In the first part, several elastic theories for circular cylindrical shells are briefly introduced. Then, buckling and collapse analyses of both axially compressed and axially compressed pressurized cylindrical shells with different boundary conditions are also reviewed. Finally an introduction to the plastic analysis of circular cylindrical shells is given.

2.3.2 Elastic Theories of Cylindrical Shells

In this section, some well-known elastic theories for circular cylindrical shells are briefly described. These are the theories developed by Donnell, Timoshenko, Flügge and Sanders, which have often provided the governing equations for many analyses throughout the historical development of the elastic stability of shells.

Donnell's nonlinear theory for circular cylindrical shells was developed by Donnell in 1933 for application to aircraft structures, in connection with the analysis of torsional buckling of thin-walled tubes [1933]. Owing to its relative simplicity and practical accuracy, this theory has been very widely used for analysing stress distributions, and for both buckling and post-buckling problems, despite criticisms concerning its scope and applicability.

Based upon Donnell's theory, Timoshenko developed his work on shells in the 1940s. In his theory for circular cylindrical shells, Timoshenko modified one of the assumptions on which the Donnell's theory is based and thus extended Donnell's theory. He took into consideration the influence of the axial displacement u and the circumferential displacement v on the curvature changes which were neglected by Donnell. Thus, Timoshenko's theory has a greater range of applicability than Donnell theory, and has therefore been widely used.

Donnell's theory has a shortcoming, commonly described as the shallow shell approximation, in that the bending curvature is assumed to derive only from the normal displacements. Thus, it is not applicable to the analysis of deformations in a cylinder where the magnitude of the in-plane displacement is of the same order as that of the normal displacement. For example, bending deformations of a long cylinder with the circumferential wave number N less than 4 are poorly represented by Donnell's equations. On the other hand, Flügge derived basic equations for the buckling of circular cylindrical shells under typical loading conditions [1932],

without resort to the shallow shell approximation. These equations apply to problems with any buckling configuration, including Euler buckling in long shells under axial compression. However, they are not sufficiently accurate for some purposes because the prebuckling state is assumed to be a membrane stress state, neglecting the effect of bending deformations near boundary conditions or under unsymmetrical loading.

Sanders' theory for finite deformations of thin shells [Sanders, 1963] was first published in 1963. Taking the finite deformations of non-shallow shells with small strains and moderately small rotations into account, Sanders' equations are much more complex than those of Donnell but somewhat simpler than those of the modified Flügge theory. Since its generality makes it directly applicable to non-shallow shells with any geometric configuration, Sanders' theory has been favoured in structural analysis especially using the finite element method.

On the basis of these many elastic theories of Donnell, Timoshenko, Flügge and Sanders, theoretical solutions for many buckling problems have been derived, and the elastic stability characteristics of circular cylindrical shells examined for a wide range of shell geometries and boundary conditions under both fundamental loads such as uniform torsion, pressure and axial compression and combinations of these loads [Yamaki, 1984]. However, relatively few studies have considered non-uniform loading conditions.

2.3.3 Elastic Buckling of Cylindrical Shells under Axial Compression

The buckling of cylindrical shells under axial compression has long been one of the most fascinating problems in the theory of elastic stability, because of the perplexing significant discrepancies between theoretical and experimental results, along with its technical importance in the design of light-weight structures. A brief description is given here of the developments of elastic buckling analysis which are particularly useful in relation to silo structures.

The first theoretical solutions for the buckling strength of cylinders under axial compression were presented by Lorenz [1908], Timoshenko [1910] and Southwell [1914]. These earliest solutions were restricted to typical perfect cylinders with simple boundary conditions and assumed a uniform membrane stress state prior to buckling. The buckling stress derived on the basis of the assumptions of simple end supports, perfect shell geometry, elastic material behaviour and a uniform membrane prebuckling stress distribution is commonly referred to as the 'classical elastic axial buckling stress', σ_{cl}, which is expressed in Equation (1.3) of Chapter 1.

In spite of its limitations, the classical elastic buckling stress is useful in providing a very simple upper bound to the buckling stress for an axially loaded cylinder and is therefore commonly used as the reference value for buckling calculations.

Early test results [Robertson, 1929; Flugge, 1932; Wilson and Newmark, 1933; Lundquist, 1933] indicated that practical cylinders buckle at loads well below the classical buckling stress (Fig. 1-7). Buckling loads as small as 30% of the classical value are common. This large discrepancy between the theoretical and experimental results led to extensive studies and a major research effort since the 1930s on (a) the effects of boundary conditions; (b) the effects of prebuckling deformations; and (c) the effects of initial imperfections. These studies continue up to the present time.

The effects of various boundary conditions were first studied by Ohira [1961, 1963], Hoff [1965], Hoff and Rehfield [1965], Hoff and Soong [1965] and Thielmann and Esslinger [1964]. Solutions of a precise nature were obtained on the basis of the Donnell basic equations using the membrane stress assumption. It was found that the critical compressive load reduces to almost one half of the classical value when both edges of the shell are free to displace circumferentially during buckling. However, in practical structures and in experiments, the shell edges are usually connected to relatively stiff end plates and considerable bending deformations are likely to occur near the loaded edges when compressed in the axial direction. Under similar relaxed boundary conditions where the edges are simply supported and are not constrained in the circumferential direction during buckling, the study conducted by Stein [1964] showed that the critical stress may be reduced to less than half the classical value. Further studies [Hoff, 1965; Hoff and Rehfield, 1965] revealed that this reduction was mainly due to the special boundary conditions, which could be obtained through analyses by neglecting the prebuckling edge rotations. Later, taking the effect of prebuckling deformations into consideration, studies carried out by Fischer [1963, 1965], Almroth [1966], Gorman and Evan-Iwanowski [1970] and Yamaki and Kodama [1972, 1973] showed that, for shells of medium length, consideration of the prebuckling edge rotations generally leads to between 8 and 15% reduction in the critical stress from those previously obtained, while it leads to a slight increase in the critical stress under the special relaxed boundary conditions described above. In these studies, only a symmetric buckling mode with respect to the central section of the shell was considered and the calculations on the basis of Donnell and Flügge theories were confined to relatively long shells.

A variety of research studies have been conducted on the effect of initial imperfections on the buckling strength of cylinders under axial compression. Two methods have mainly been used. One is to directly analyse the nonlinear post-buckling behaviour of cylindrical shells with

specified initial deflection. However, due to an excessive complexity in this approach, solutions of only an approximate nature were obtained [Donnell and Wan, 1950; Loo, 1954]. The other method is to apply an asymptotic analysis based upon the general theory of the initial post-buckling behaviour as developed by Koiter [1945]. With this method, Budiansky, Hutchinson and others performed many studies on the initial post-buckling behaviour and the critical load degradation due to imperfections, usually in the shape of the relevant buckling mode, for a variety of shell structures including cylindrical shells [Budiansky, 1969; Budiansky and Amazigo, 1968; Hutchinson and Amazigo, 1967; Hutchinson, 1968]. In these studies, the linear prebuckling state was assumed for simplicity. Taking the effect of nonlinear prebuckling deflections into account, similar analyses were also performed for stiffened cylindrical shells under compression [Hutchinson and Frauenthal, 1969; Cohen, 1971]. On the other hand, by assuming a variety of axisymmetric initial imperfections, a series of studies have clarified the imperfection sensitivity of cylindrical shells under compression [Koiter, 1963; Tennyson and Muggeridge, 1969; Arbocz and Babcock, 1969; Hutchinson et al., 1971; Amazigo and Budiansky, 1972; Budiansky and Hutchinson, 1972; Pedersen, 1973; Arbocz and Sechler, 1974; Arbocz, 1974, 1982, 1983; Sheinman and Simitses, 1977; Yamaki, 1977, 1984; Rotter, 1985; Rotter and Teng, 1989; Teng and Rotter, 1989, 1990; Guggenberger, 1991,1992; Rotter and She, 1993].

More importantly, experimental techniques to measure the shape of geometric imperfections in the shell surface were developed by Arbocz and others [Arbocz, 1974, 1982, 1983; Arbocz and Babcock, 1969; Arbocz and Sechler, 1974], and these measured imperfections were then introduced into shell analyses to predict the strength of cylinders with known imperfections. Singer [1980] also developed vibration techniques to make an experimental evaluation of the boundary conditions, so that both of these former uncertainties could be properly assessed. The ensuing analyses have generally indicated that measured boundary conditions and geometric imperfections lead to accurate predictions of experimental strength, but some anomalous tests still occasionally occur [e.g. Blachut and Galletly, 1994], suggesting that there may be other unknown quantities which need further investigation.

The aforestated studies on the buckling of circular cylindrical shells under axial compression have revealed that the close agreement between theoretical and experimental results may exist when the effect of imperfections and the boundary conditions are taken into consideration. The strengths are acutely sensitive to the amplitude of the initial imperfection in the shell surface. The shape of the initial imperfection is important in assessing the buckling strength: in particular, axisymmetric imperfections which often occur in silos, appear to be very detrimental. The buckling modes are relatively local and are directly associated with a critical imperfection. Although many researchers have explored the problem, the results obtained are

difficult to generalize, since they are very dependent on the shell geometry and boundary conditions, the shape of imperfection, the shell theory used, and the approximations made.

All the above theories for circular cylindrical shells have been comprehensively applied in the analysis of silo structures under uniform compression. However, many silo structures in service are elevated or subjected to non-uniform compression. It is therefore of practical importance to clarify the elastic stability of locally supported circular cylindrical shells. Current information on the behaviour of discretely supported silos is scarce. Some studies [Ory et al, 1958; Gould et al, 1976; Rotter, 1982, 1985; Bodarski et al, 1984; Ory and Reimerdes, 1987; Samuelson, 1987, Teng and Rotter, 1990, 1991] have investigated linear prebuckling stress distributions and the linear bifurcation in discretely supported silos, but none appears to have investigated the nonlinear buckling behaviour until recent research studies being carried on by the Silos Research Group in the Department of Civil Engineering, University of Edinburgh.

Despite extensive research efforts on shell buckling over the last few decades, only a few studies [Abir and Nardo, 1958; Bijlaard and Gallagher, 1959; Hoff et al., 1964; Johns, 1966; and Libai and Durban, 1973, 1977] have examined the buckling behaviour of cylindrical shells under axial loads which vary in any pattern around the circumference. A simple general conclusion from this work on perfect shells might be that buckling occurs under a circumferentially non-uniform distribution of axial stress when the maximum stress is similar to the classical elastic critical value for uniform axial compression. Libai and Durban [1973, 1977] gave simple expressions which describe the increase in buckling stress above this simple rule, but the strength gains are generally small. All the above authors only dealt with perfect shells, even though shell buckling under axial compression is normally acutely imperfection-sensitive. The loading and boundary conditions considered by them did not involve discrete local support forces in the shell.

Initial exploratory investigations of the buckling behaviour of perfect and imperfect steel cylinders on discrete supports were made by Rotter and Teng [1990, 1991]. Their studies were restricted to a single shell geometry with several different numbers of column supports and the supports were modelled to terminate at the lower edge of the shell (Fig. 2-1a), forcing a uniform displacement to the lower edge (rigid support). An axisymmetric geometric imperfection was introduced for the imperfect shell to simulate a local weld depression (Fig. 2-1b).

Their studies of perfect cylinders showed that very high local compressive membrane stresses can develop in the vicinity of the column support but decay rapidly from this point (Fig. 1-18).

The region of high vertical compressive stress is quite limited, and the stress changes markedly within an area comparable in size with typical buckles. The buckling deformations occur above the column support in the zone of rapidly varying stress. Thus, any factors which change the rate of stress dispersal in the cylinder (support width, radius-to-thickness ratio, ring stiffeners, and support rigidity) lead to significantly changed buckling strengths. In their studies, the shell buckling strength was defined in terms of the mean membrane stress above each support. It was found that the normalised buckling strength is almost invariant with the number of supports, provided that the shell is supported on a small number of supports of practical width. It was similarly found to be invariant with the height of the shell unless it falls below a certain value. Therefore, in most practical silo structures, both the number of supports and the cylinder height are not important factors in influencing the buckling strength.

Rotter and Teng's studies of column-supported imperfect cylinders showed that a deep imperfection induces much larger local compressive circumferential stresses (Fig. 2-2b) than occur in perfect cylinders (Fig. 2-2a). These high compressive stresses can significantly reduce the buckling strength. The buckling mode and strength of an imperfect cylinder were also found to be sensitive to the boundary condition used at the bottom edge of the cylinder. The removal of rotational and/or horizontal translational restraints at the bottom edge can reduce the buckling strength of the cylinder very markedly. In particular, the buckling modes were also found to change radically when translational restraints are absent. However, all the above conclusions were derived from linear bifurcation studies, so careful checking of these findings is needed using nonlinear analysis.

Most of Rotter and Teng's studies were of linear bifurcation buckling in perfect cylinders with the variations of support width, radius-to-thickness ratio, cylinder height, boundary conditions, number of discrete supports and some imperfections etc. Bifurcation studies may give a useful indication of the character of the phenomena, but they often do not define the strength accurately, especially for imperfect shells. The restriction of most of their study to bifurcation was a consequence of the computing package LUSAS which they were using.

The nonlinear response of discretely supported silo structures was not extensively explored until the two theoretical studies recently undertaken by Guggenberger [1991, 1992] and Rotter and She [1993], using large displacement theory and the finite element method. The finite element program ABAQUS was employed in both studies to undertake nonlinear calculations from which bifurcation points could be found. Guggenberger [1991, 1992] performed the analyses of the buckling of cylindrical shells under local axial loads. The nonlinear axial buckling behaviour was examined for both unstiffened and stiffened circular cylindrical shells with various local support constructions. The effects of geometric nonlinearity, elastic-plastic

material nonlinearity and initial geometric imperfections on the buckling behaviour and the buckling strength of the shells were explored (Fig. 2-4). Rotter and She [1993] performed fundamental studies of the geometrically nonlinear behaviour and stability of discretely supported thin elastic cylinders. The nonlinear bifurcation phenomena in both perfect and imperfect cylinders were explored. The effects of the cylinder geometric parameters and initial geometric imperfections on the nonlinear behaviour and the buckling strength were investigated.

Both studies assumed that the cylinder is locally supported on an integer number of equally spaced supports of finite width situated at the lower edge of the shell; the lower edge is effectively restrained against normal and circumferential deformations; and the cylinder is subjected to axial compression only. However, there are slightly different assumptions used in the two studies concerning loading, support boundary conditions and the assumed geometric imperfections. In Guggenberger's studies, two different loading conditions were used for different calculations: a) symmetry at the half height of the cylinder; b) uniform applied loading at the upper edge. The support was assumed to apply a uniform stress to the lower edge of the cylinder (flexible support). A local imperfection of bi-cubic form was adopted, which is not very different from the buckling mode (Fig. 2-3). In addition, local rings and meridional stiffeners were adopted to model the practical stiffened silo structures. In Rotter and She's studies, only a uniform shear pressure on the whole surface of the shell was analysed. The support was assumed to apply a uniform displacement to the lower edge of the cylinder (rigid support) (Fig. 2-1a). A local axisymmetric imperfection (Fig. 2-1b) was adopted in line with the previous research on uniformly compressed cylinders and imperfection measurements from full scale silo structures [Rotter and Teng, 1989; Teng and Rotter, 1989; Teng, 1990]. Rotter and She's work promotes Teng and Rotter's studies into geometrically nonlinear analyses and fundamentally assist the research undertaken in this thesis. Their work is briefly described in the next chapter - Chapter 3.

It has been clarified [Rotter et al, 1993] (Fig. 2-5) that the differences in assumptions between Guggenberger's studies and Rotter and She's studies do not make for marked differences in the calculated strengths because the buckle is quite locally situated a little above the support. The greatest discrepancies appear to arise from the choice of flexible or rigid modelling of the support.

These studies of Rotter and Teng, Guggenberger and Rotter and She represent a first step towards a better understanding of the complicated buckling problem in practical discretely supported silos. The objective of this thesis is to present further studies on the structural stability of discretely supported silos.

2.3.4 Elastic Buckling and Plastic Collapse of Cylindrical Shells under Internal Pressure and Axial Compression

Although axial compression is one of the most basic and common loading conditions, it is not unusual for a cylindrical structure to be subjected to the combined action of both axial compression and internal pressurization. For example, the aforestated silos in service are subjected to internal pressure from stored materials, together with axial compression from the frictional drag of stored materials on the walls.

The buckling of circular cylindrical shells under combined internal pressure and axial load has been studied by many researchers. Initially, approximate solutions based on the membrane prebuckling assumption were obtained by Lei and Cheng [1969] and Zyczkowski and Bucko [1971]. Taking the effect of prebuckling bending deformations into consideration, more accurate solutions were obtained by Fischer [1963, 1965] and Almroth [1966] under various boundary conditions, assuming a symmetric buckling mode with respect to the mid-section of the shell. The effect of axisymmetric initial imperfections on the buckling strength under combined loads was approximately analysed by Hutchinson [1965] while more accurate solutions were obtained by Esslinger and Geier [1977], Tennyson et al. [1978, 1979], Kodama and Yamaki [1983], and Rotter and Teng [1989, 1992]. Experimental studies were conducted by Weingarten and Seide [1965], Weingarten et al. [1965] (Fig. 2-6), and Saal et al. [1979] to examine and to improve available design formulas and by Tennyson et al. [1978, 1979] to check the validity of their theoretical analyses.

Through these studies, it has been repeatedly shown that, when an axially compressed cylinder is internally pressurized, the tensile circumferential membrane stress reduces the deleterious effects of the imperfections, and buckling axial load increases. At very low internal pressures, the cylindrical shell fails near an imperfection by elastic buckling in a mode similar to that for unpressurized cylinders [Rotter and Teng, 1989]. At high internal pressures, the buckling mode becomes axisymmetric [Fung and Sechler, 1957; Harris et al, 1957; Weingarten et al, 1965; Rotter and Teng, 1989]. The changing buckling mode reflects the declining imperfection-sensitivity of the buckling load.

In thin steel cylinders ($R/t > 250$), the buckling collapse stress for axial compression is usually low compared with the yield stress, so elastic investigations are directly relevant. However, once the internal pressure becomes significant, high bending as well as membrane stresses arise near the base of the cylinder, and local yielding may then occur. This failure mode is commonly known as 'elephant's foot' buckling (Fig. 1-9). First yield in a thin cylinder occurs in the zone of local bending adjacent to a boundary support, change in wall thickness, stiffener, or other local disturbance. The strength appears to be less sensitive to random imperfections

but dependent on the form of local stress raisers [Esslinger and Geier, 1977]. The collapse modes of many silos that have failed in service show that this zone is critical in design.

The nonlinear elastic behaviour of internally pressurized axially loaded thin perfect cylinders near a boundary was explored by Rotter [1983]. A first yield criterion was devised to provide a lower bound to the strengths of perfect cylinders failing in this mode. His further studies [Rotter, 1990] of the geometrically nonlinear elastic-plastic collapse and instability of these cylinders revealed that the collapse load is typically 10-20% higher than first-yield conditions, except for thin cylinders without internal pressurization, when elastic buckling is predicted. The transition from elastic buckling to elastic-plastic collapse occurs at similar levels of circumferential stress (approximately $pR/t = \sigma_y/2$) for different yield stresses (he studied yield stresses of 250 MPa and 350 MPa). The importance of elastic-plastic collapse as a failure mode is therefore not dependent on the steel grade used. He also developed a simple empirical design rule to predict the strengths of simply supported cylinders under high internal pressure and low axial loads, such as are encountered in large tanks and in squat silos. All the elastic buckling and elastic-plastic collapse analyses carried out by Rotter [1983, 1990] are confined to uniformly compressed and uniformly supported cylinders with clamped or simply-supported boundary conditions.

For elevated silos on discrete supports, current knowledge of elastic buckling is rather limited and fragmentary. The field of plastic collapse analysis remains completely unexplored so far. However, such topics as the elastic buckling, yielding, and plastic behaviour are of great practical importance for design, and they are not studied only for theoretical interest.

2.3.5 Plastic Analysis of Circular Cylindrical Shells

The classical approach to structural analysis was based upon the assumption that the stresses in the structure are within the elastic limit of the material used and that the deflections are small. The approach has been widely used for many purposes. However, it is evident that any structure can be made to fall down (collapse) by applying loading of a sufficient magnitude. The purpose of collapse or limit analysis is to find that magnitude. It requires a knowledge of what happens at collapse and how structures behave when the stresses in the material exceed the elastic limit. This philosophy is embodied in the plastic methods of analysis and design.

The foundations of the theory of plasticity were laid by Tresca [1898] and von Mises [1913]. The plastic behaviour of plates and shells received serious attention after the publication of Hopkins and Prager's [1953] paper on plates and Drucker's [1954] work on cylindrical shells. The increasing use of plastic design and the present trend towards applying its methods to structures indicates that the basic advantages of plastic analysis are more and more appreciated

by engineers: accurate estimate of the collapse load, simplicity of application, and economy of design. Plastic methods for steel and concrete plate and shell structures have been developed by many authors since the 1950s [Hill, 1950; Prager, 1959; Hodge, 1963; Save and Massonnet, 1972; Moy, 1981; Save, 1985].

For relatively complex structures such as plates and shells, the emphasis of plastic analysis is usually on the direct determination of the limit state in which the plastic deformation in the plastic zones is no longer contained by the adjacent non-plastic zones and the deformations of the structure become unbounded. The intensity of loading for this limit state is called the limit load P_L. Limit analysis is concerned with evaluating these limit states. In many problems, it is difficult to find the exact limit load, but there are two theorems of limit analysis [Hill, 1951] which provide a means of identifying a lower bound and an upper bounds on P_L.

Theorem 1 - Statical (or lower bound) theorem: The limit load P_L is the largest of all possible loads P_- corresponding to statically admissible stress fields.

Theorem 2 - Kinematical (or upper bound) theorem: The limit load P_L is the smallest of all possible loads P_+ corresponding to kinematically admissible mechanisms.

It follows from the two theorems of limit analysis that the exact limit load is the only load for which a statically and kinematically admissible solution can be found. The calculation of the exact value of the limit load is called a complete solution.

Both of the fundamental theorems were introduced by Gvozdev [1960], Hill [1951], and Prager [1955, 1958] for the case of a rigid-perfectly plastic body, and by Drucker, Prager, and Greenberg [1952] for elastic-perfectly plastic materials. Both idealizations are appropriate and absolutely identical for the purposes of limit analysis [Prager, 1958].

Limit analysis of a rigid-perfectly plastic continuum is based on the following three concepts: (1) a yield condition and related flow rule; (2) a statically admissible stress field; and (3) a kinematically admissible flow mechanism. The yield condition of von Mises for a shell that has rotational symmetry in shape and loading was derived independently by Ilyushin [1956] and Hodge [1961]. The corresponding Tresca condition was derived by Onat and Prager [1954]. Both conditions are nonlinear, so their application is difficult. One method of tackling the problem is to simplify the yield condition. If this is done, the theorems of limit analysis provide a means of bounding the error introduced. The other approximation is to replace the uniform shell by an idealised sandwich shell with the same plastic resistance to pure tension or pure bending. One such approximation was proposed by Drucker and Shield [1959]. They

ignored the circumferential bending moment and retained the meridional bending moment in rotationally symmetric shells to satisfy the boundary conditions, but neglected any interaction between the longitudinal moment and the direct stresses. The resulting yield condition corresponding to this approximation is termed as the one-moment limited-interaction surface. An improved approximation, proposed by Hodge [1960], took all interactions between forces in the two principal directions and between moments in the two principal directions into account, but neglected all interactions between forces and moments. This is referred to as the two-moment limited interaction yield surface. A further improved approximation was presented by Flügge and Nakamura [1965]. However, both the one-moment limited interaction and the two-moment limited interaction curves are identical for cylindrical shells subjected to rotationally symmetric loads, because the circumferential bending moment disappears as a reaction (a stress resultant which does not contribute to the dissipation of energy in the process of irreversible deformation) [Save and Massonet, 1972].

Drucker [1954] was the first to derive a simple approximate yield surface for a circular cylindrical shell in stress resultant space. He considered a cylindrical shell under axisymmetric loads without axial forces and solved the problem of a cylinder of infinite length loaded by a ring of force and by a band of uniform pressure using the limited interaction yield locus and the exact Tresca yield condition. This work was extended by Hodge [1954] and Onat [1955] to include axial force. Based on the linearized (sandwich) Tresca yield surface and the limited interaction yield surface, further studies were conducted for shells under external pressure and/or axial force [e.g. Paul and Hodge, 1958; Drucker and Shield, 1959; Ball and Lee, 1963]. Some detailed solutions have been given with a Tresca and a von Mises material respectively [e.g. Hodge and Panarelli, 1962; Hodge, 1963; Save and Massonnet, 1972]. Sawczuk and Hodge [1960] made a comparison of the yield conditions for cylindrical shells.

It should be noted that all the limit loads obtained above are based on the rigid-perfectly plastic material idealisation. However, real shells are neither rigid nor perfectly plastic but elastic-plastic work-hardening. When circular cylindrical shells are subjected to both internal pressure and axial loads, the outward radial deflection provides a lever arm for the compressive axial force, introducing supplementary bending moments. These second order effects occur in the elastic-plastic range and are likely to decrease the load required to cause unrestrained plastic flow, if we neglect the counteracting influence of work-hardening. To include those second order effects, the equilibrium equations must be written for the deformed state: thus the theorems of limit analysis no longer apply. Hodge [1956] and Paul and Hodge [1958] demonstrated in examples that a load as high as 98% of the limit load could be attained for some loading configurations and structural geometries without the maximum elastic-plastic deflection exceeding five times the maximum elastic deflection. Hodge and Nardo [1958]

found that working hardening seems to have a very small effect on the load-carrying capacity for thick cylinders under external uniform pressure, but in any case it should increase the strength with respect to theoretical predictions based on perfect plasticity. Also, the use of a linearized yield condition 'inscribed' to the exact Tresca condition and in turn to the more realistic von Mises condition, should also result in collapse predictions on the safe side.

In the studies described in this thesis, the loading applied to the cylindrical shell (local meridional load at the edge) induces only a small amount of primary bending in the structure. Moreover, the silo structures being investigated are relatively thin. As a result, the limit analyses described above have only limited relevance to the real collapse strength. Nevertheless, finite element based limit analyses are described in the early part of Chapter 7, and these show how the primary bending action in the shell affects the limit load.

2.3.6 Conclusions

In this section, a brief outline of elastic buckling and plastic collapse theories for circular cylindrical shells has been given. Although numerous theoretical solutions are available for tackling many shell problems, they are generally limited to very simple geometries, loading and boundary conditions and might not be directly of use in the design of steel silo structures. Nevertheless, these classical solutions are informative for structural engineers to understand the buckling and collapse behaviour of more complicated shell configurations, and are fundamental to all further work.

As a result of the development of computers and computer analyses of structures since the 1960s, more accurate analyses of the buckling and collapse behaviour of practical structures have become possible. As a result, attention has increasingly turned onto developing the computer analysis of structures rather than the development of classical solutions.

2.4 STRUCTURAL DESIGN OF STEEL SILOS

A large number of steel silos have been built for a huge variety of industrial applications, but there are no codes of practice or standard specification in the world for the structural design of large steel silos, although a few design guides are available [Ketchum, 1909; Lambert, 1968; Wozniak, 1979; Trahair et al, 1983; Gaylord and Gaylord, 1984; Rotter, 1985d, 1990; Rotter et al, 1993]. Limited structural design advice for small steel silos is given in the British draft code [BMHB, 1987] and a Japanese code for aluminium silos was produced recently [JIS, 1989].

As stated in Chapter 1, the basic understandings required for silo designers are in the definition of loads to be used in design, in the stress analysis of these shell structures, and in quantitatively predicting the many potential failure modes. The following discussion is concerned with current design information with reference to the problem studied in this thesis.

Design procedures for the prevention of buckling under axial compression were first developed from the strengths of unstiffened unpressurized uniformly compressed cylinders under axial compression. A relatively wide range of empirical design equations of this sort have been in common use in the design of steel silos. Two approaches were used in developing design rules [Rotter, 1985a]: the first was simply to draw a lower bound curve on all available reliable test results; the second attempted to use an equation relating the strength to an imperfection amplitude, and thus to categorize the test results into groups of specimens of different quality. Empirical relationships were then proposed for the maximum level of imperfection to be expected in a shell of given quality.

An early lower bound equation proposed by Donnell [1933] is still quite widely used in the USA even though it was based on limited early data and suffers the disadvantage of predicting zero strength for $R/t > 2450$. A proposal by Weingarten et al [1965a] was derived from a large data base gathered chiefly for aerospace applications with a higher quality of construction, but it has been widely used in civil engineering.

In the AWWA [1979] standard, the Boardman equation for the buckling stress of a shell in membrane compression was adopted, with a limit (15,000 psi) placed on the allowable compressive stress. This is based on quite old data [Wilson and Newmark, 1933; Wilson, 1937; Wilson and Olson, 1941], but does relate to civil engineering welded and rivetted construction at R/t ratios up to 1000. An equation was also proposed by Steinhardt and Schultz [1971], based on a very complete set of data ($70 < R/t < 2800$). This provides a 90 percentile lower bound on experimental results.

Amongst the design guides, Wozniak [1979], API 620 [1978], Johnston [1976], Trahair et al. [1983] and Gaylord and Gaylord [1984] refer to the AWWA (Boardman) equation. Trahair et al. [1983] restrict the use of this equation to $R/t < 1030$ and use the test results of Weingarten et al. [1965a] at higher radius to thickness ratios. Gaylord and Gaylord [1984] also quote Steinhardt and Schultz [1971] and the early ECCS [1977] code.

In the second approach [Rotter, 1985a], the strength was directly related to a defined level of imperfection. Design recommendations in this group include those of Hoff and Soong [1967], ESDU [1974], Odland [1978], the ECCS [1984, 1988], Rotter [1985a, 1990] and Rotter and

Teng [1989, 1990]. Of these, the ECCS [1988] code does not strictly relate strength to imperfection, but provides a limit on measurable inward imperfection over a length roughly equal to the axisymmetric buckling mode wavelength which was the basis of Koiter's equation [1945], and describes a simple measurement technique for imperfections in prototype structures. In addition, the strengthening effect of internal pressurization is included in more recent design guides [ESDU, 1974; Trahair et al, 1983; ECCS, 1984; Gaylord and Gaylord 1984; API, 1988, Rotter, 1985, 1990].

The design equations in this second group are less frequently quoted for silo design. Guidance was provided by the British Farm Silo Code [BS5061, 1974] that the buckling strength of axially compressed cylinders should be assessed using the ESDU [1974] recommendation. Rotter [1985a] suggested the use of an equation modified from that of Odland [1978] to match the soundly based Steinhardt and Schultz [1971] equation. This has the advantage that the large data base of the latter's work can be used with a clear definition of the corresponding assumed imperfections of the type given in Koiter's strength-imperfection relationship.

For locally supported silos, the existing literature [Rotter and Teng, 1990, 1991; Rotter et al. 1991] on theoretical studies of the buckling of discretely supported cylinders are so few as to provide wholly inadequate advice and no general understanding for designers. Experiments on the buckling of discretely supported cylinder [Rotter and She, 1994] have only been performed at the time of writing of this thesis and remain unpublished. However, a high incidence of failures in discretely supported silos, together with a relentless trend towards the construction of larger elevated silos is making strong demands for more research work to expand the knowledge of structural behaviour, techniques of strength prediction and design requirements for locally supported silos.

2.5 COMPUTER PROGRAMS USED IN SILO STRUCTURE ANALYSIS

2.5.1 Introduction

The circular cylindrical shell constitutes a fundamental element in light-weight structures and the realistic determination of its stability has been a critical problem for the design and development of these structures. Thus, many studies have been conducted on this subject since the basic equations were established by Flügge and Donnell in the 1930s. In the early stages of the development, only rough approximate solutions were obtained owing to the excessive complexity of the problems. Accurate analyses became possible only after the advent of the high-speed digital computer in the 1960s. Following the rapid spreading of computers, the finite element, finite difference and numerical integration techniques underwent vigorous

development. In particular, the finite element method is now very widely used for its flexibility. Many computer programs have been developed and effectively applied to shell structure analyses. Numerical formulations for different types of analysis have been developed: those of special interest here may be summarized as (a) linear stress analysis, (b) linear bifurcation analysis, (c) elastic large deflection analysis, (d) elastic-plastic small deflection analysis and (e) elastic-plastic large deflection analysis. Very few programs [e.g. Bishara et al., 1977; Chandrangsu and Bishara, 1978; Eibl and Haussler, 1984; Askari and Elwi, 1988] have been developed specifically for the analysis of silo structures. These were all developed to study the loads applied to silo walls by the bulk solids, and were not at all concerned with the stresses in the structure. In particular, buckling and collapse analyses of the shell wall were untouched.

In this section, only a brief description of finite element computer programs which mainly undertake the calculation of silo structures in this thesis is given. They are FELASH program suite and ABAQUS program package.

2.5.2 The FELASH Suite of Computer Programs

A suite of finite element computer programs named FELASH (Finite ELement analysis for Axisymmetric SHells) has been developed by Rotter and his co-workers for stress, buckling and collapse analysis of axisymmetric shells with special applications to storage structures like silos and tanks [Rotter, 1989]. The FELASH suite consists of many finite element programs of which some important ones are the pre-processor PASHA, the post-processor SUMP, and LEASH, NEPAC, NEPAS etc. It has been widely applied to the analysis of steel silo structures [Rotter, 1981, 1982, 1983a, 1983c, 1984, 1986a, 1987a; Jumikis and Rotter, 1983, 1986; Rotter and Jumikis, 1985; Sharma et al., 1987; Teng and Rotter, 1989].

The FELASH suite is able to create an efficient and accurate finite element model for analyses. With powerful pre- and post-processors incorporating special features pertinent to silo structures, this program suite has many advantages. They are that all the programs included in the suite are free of 'black box' routines, a clear understanding of all the working features of the program can be maintained, and control is kept over the evolution of the program to suit new types of problem.

Program PASHA (Pre-processor for Axisymmetric SHell Analysis) is used to prepare the input data file for any of the FELASH finite element programs of structural analysis. All information is given through interactive interrogation. The program can automatically generate many loading conditions pertinent to silo structures such as wind loading, loadings from stored bulk solids, eccentric discharge and local discrete supports.

Program LEASH (Linear Elastic Analysis for Stresses using Harmonics) performs linear elastic stress analysis on axisymmetric shells under non-symmetric loads [Rotter, 1987a]. The shell theory of Sanders [Budiansky and Sanders, 1963] is used. The non-symmetric loads, deformations and stresses are all expanded in harmonic series and each harmonic is analysed separately. The results from each harmonic are summed up to provide the complete solution.

Program SUMP (SUMmation and Plotting of stresses, reactions and deformations) is the post-processor for the FELASH program suite. It sums harmonic series and interactively plots the deformations, stresses and buckling modes.

2.5.3 ABAQUS Finite Element Package

ABAQUS, developed and supported by Hibbitt, Karlsson & Sorensen, Inc. (HKS) [1992], is a general purpose finite element analysis program package. It is designed specially to serve advanced structural analysis needs. The most challenging of these applications involves large models with highly nonlinear response.

The theoretical formulation of ABAQUS is based on the finite element stiffness method. The aspects of the problem that are particularly well addressed with ABAQUS are the great variety of geometry modelling, kinematics, material modelling, boundary and loading conditions, and analyses. In the aspect of geometry modelling, the models can include structures and continua. One-, two- and three-dimensional continuum models are provided, as well as beams and shells. The beam and shell elements are based on modern discrete Kirchhoff or shear flexible methods. Shell elements are provided for heat transfer, as well as for stress analysis. Except for some special purpose elements, all of the elements in ABAQUS are formulated to provide accurate modelling for arbitrary magnitudes of displacements, rotations and strains. In material modelling, models are provided for metals, rubber, plastics, composites, concrete, sand, clay and crushable foam. The material response can be highly nonlinear. Very general elastic, elastic-plastic and elastic-viscoplastic models are provided. Boundary conditions can include prescribed kinematic conditions (single point and multi-point constraints) and prescribed foundation conditions. Loading conditions can include point forces, described loads and thermal loading. Follower force effects (for example, pressure, centrifugal and Coriolis forces, fluid drag and buoyancy) are included where appropriate.

Primarily using implicit integration for time (or load) stepping with automatic choice of the time (or load) increments, ABAQUS provides both static and dynamic, linear and nonlinear stress analyses; eigen-value buckling analysis; nonlinear elastic and plastic stability analyses; transient and steady-state heat transfer analysis; etc. In nonlinear problems, the challenge is always to provide a convergent solution at minimum cost. This is addressed in ABAQUS by

automatic control of time (or load) stepping which is provided for all analysis procedures. Provided that the user defines a 'step' (a portion of the analysis history) and certain tolerance or error measures, then ABAQUS can automatically select the increments to model the step. This approach is highly effective for nonlinear problems, because the model's response may change drastically during an analysis step. Automatic control allows nonlinear problems to be run with confidence without extensive experience with the problem. For nonlinear static stress/displacement analysis, ABAQUS offers two approaches. One is for cases when a prescribed history of loading must be followed. The alternative is an arc-length (modified Riks) method, which is provided for unstable static problems such as post-collapse or post-buckling cases.

The finite element program ABAQUS is used in this thesis to undertake the studies of the stability of steel silo structures on discrete supports. Analyses of several types are performed for discretely supported thin cylindrical shells: linear stress analysis, linear bifurcation analysis, geometrically nonlinear elastic buckling analysis, limit analysis and geometrically nonlinear elastic-plastic analysis. The eigenvalue extraction method is used in the linear bifurcation analysis. The modified Riks method is adopted in all the nonlinear analyses. The definitions of geometry modelling, kinematics, material modelling, and boundary and loading conditions are specified in detail for each analysis, which is presented in the corresponding chapter of this thesis.

2.6 SUMMARY

A brief review has been presented of the existing knowledge revelant to the theories of thin cylindrical shells and the structural analysis and design of steel silo structures. Current knowledge of the pressures on silo walls from the stored bulk solids was initially discussed. A brief description of the development of the theories of buckling and collapse of thin-walled circular cylindrical shell structures was followed by a short summary of the current design criteria used for steel silo structures. Extensive references to more detailed sources have been given.

From the above general review, it is known that cylindrical silos in service are mainly subjected to internal pressure from stored materials together with axial compression from the frictional drag of stored materials on the walls and from roof loads. The governing failure mode of silos is frequently buckling under axial compression. Under axisymmetric filling conditions, this is usually the controlling design consideration for most of the silo wall. Under other loading conditions such as eccentric filling, eccentric discharge and discrete support forces in elevated silos etc, higher axial compressions may develop over limited parts of the wall and quite possibly lead to the buckling failure of the structure. The internal pressure can significantly enhance the buckling strength, but high internal pressures lead to severe local bending near the base. Local yielding, alternatively known as 'elephant's foot' buckling, then might happen prior to a buckling failure. The buckling strength of a thin cylindrical shell is notoriously sensitive to the magnitude of the geometric imperfections in the wall, but the imperfection-sensitivity is much reduced when the cylinder is internally pressurized.

It is evident that the classical theories of thin shell structures have undergone vigorous development over the second half of this century. Many rigorous theoretical solutions as well as reliable experimental information are now available for the buckling and collapse of shells with simple geometries, loading and boundary conditions, which now provide a basic viewpoint for understanding the shell buckling and collapse problems. The finite element method plays an important role in computing analysis. Numerous computer programs have been developed for various engineering applications.

However, those classical shell theories have mostly relied on for the analysis and design of silo structures. Modern powerful numerical methods have generally made little impact on silo designers. There are very few computer programs written specifically for silos, except for those which are only concerned with the calculation of stresses in the bulk solids, the pressures on the silo wall and sometimes the wall/bulk solid interaction. General shell analysis programs are seldom employed to study buckling and collapse problems in silos. In addition, a shortage

of sufficient experimental information on silo buckling and collapse may be another reason for slow development of silo design codes.

It is the complexity of the silo geometry and loading patterns which has been making the subject of solving the buckling and collapse problems more challenging and a great effort on it more worthwhile and valuable. This thesis is intended to attack some of these problems to broaden current understanding in the fields of elastic and plastic stability of shell structures, with special attention to discretely supported silo structures.

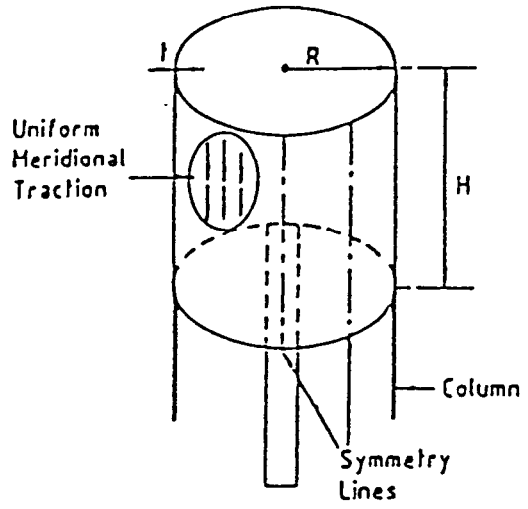

(a) Column-Supported Cylinder Model

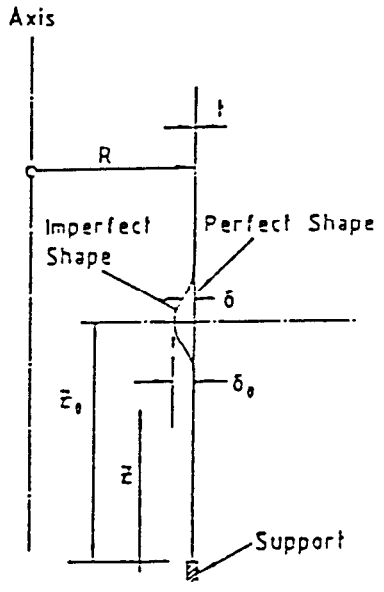

(b) Imperfection Model

Figure 2-1

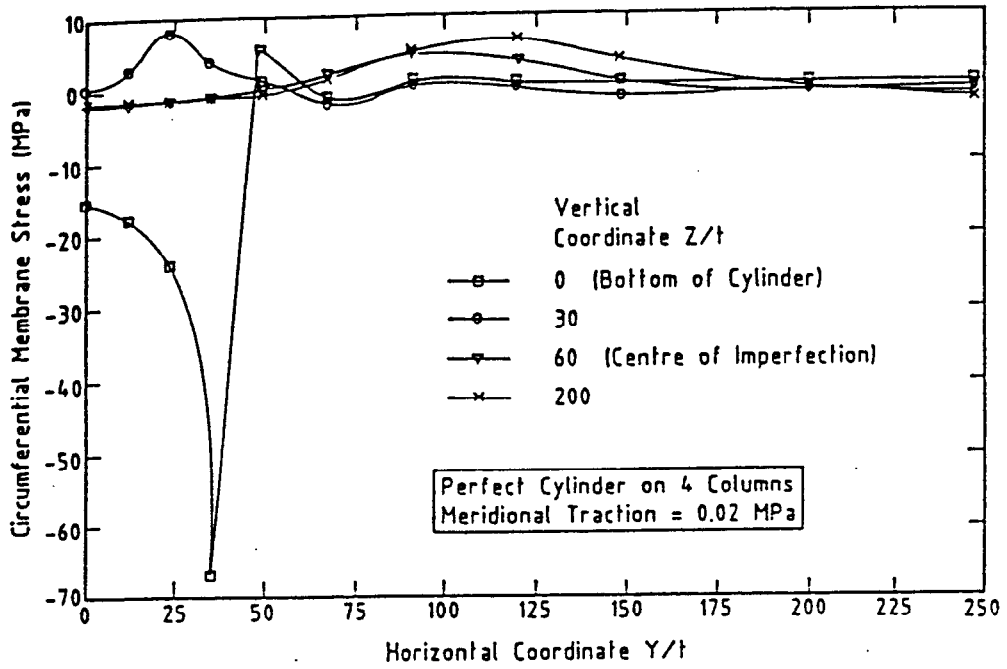

(a) **Perfect Cylinder (rigid support)**

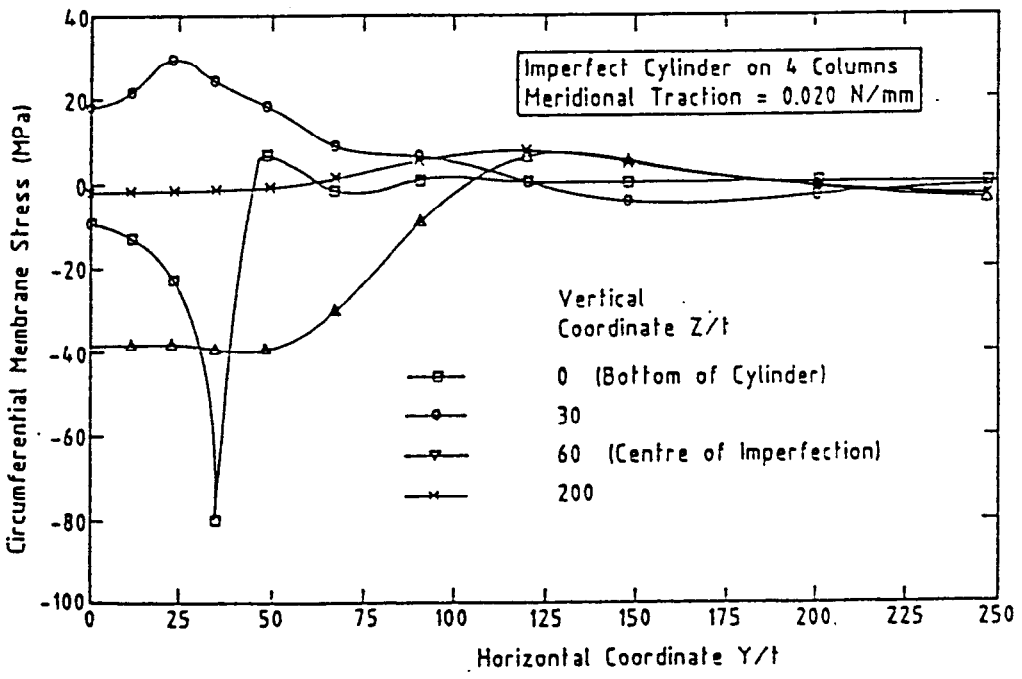

(b) **Imperfect Cylinder (rigid support)**

Figure 2-2 Circumferential Variations of Circumferential Membrane Stresses

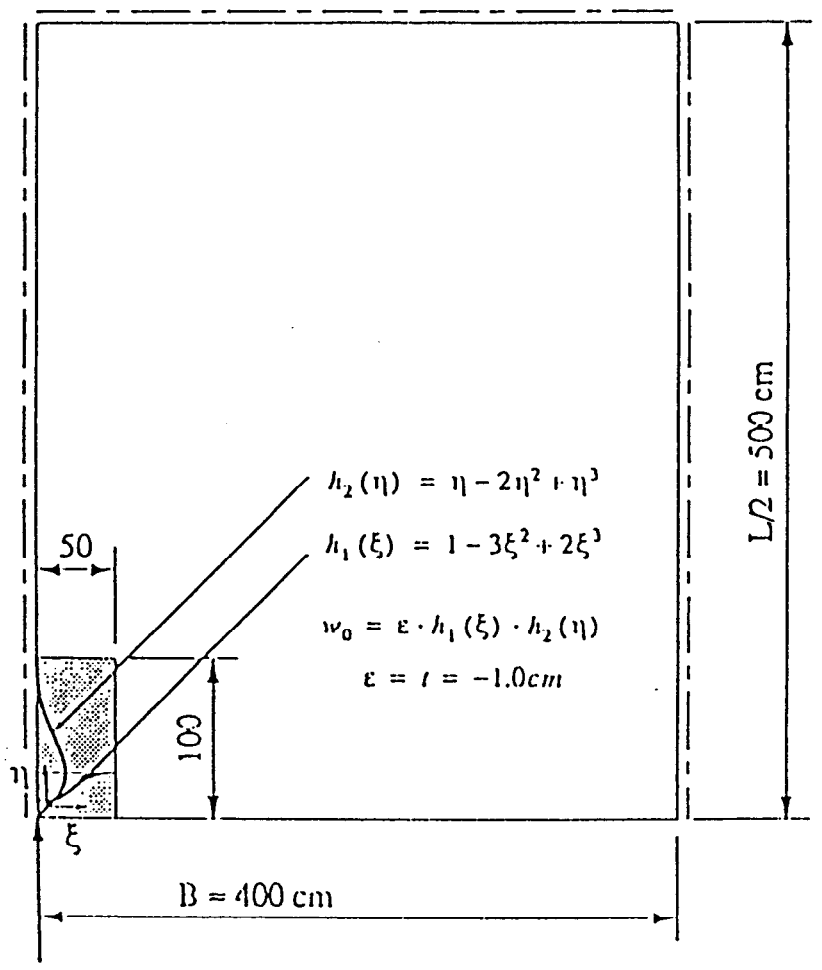

Figure 2-3 Shape of Local Geometrical Imperfection

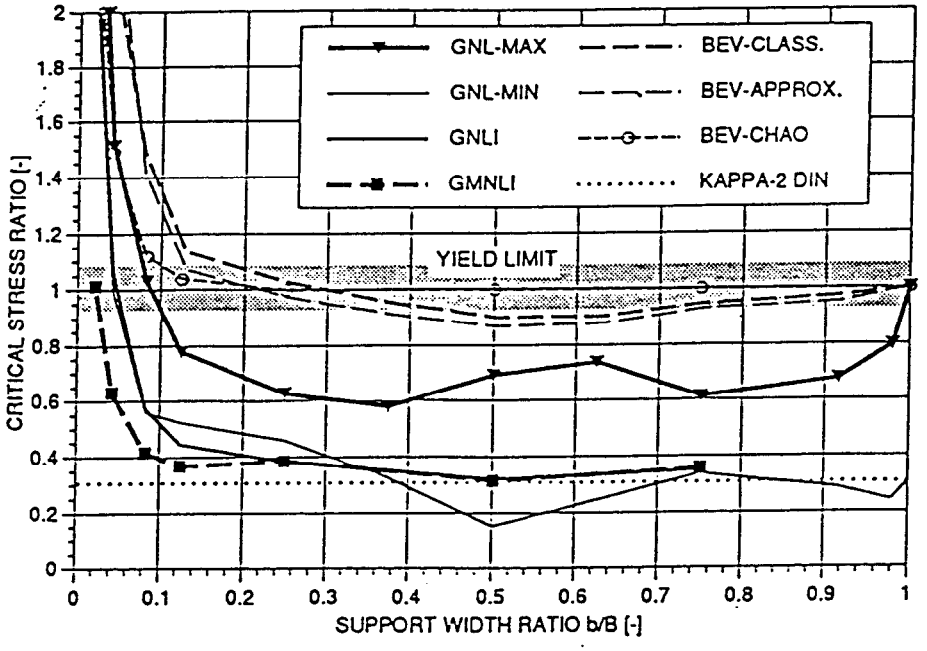

Figure 2-4 Eigenvalue Buckling Stresses and Imperfect/Elastoplastic Buckling Stresses for Variable Support Widths

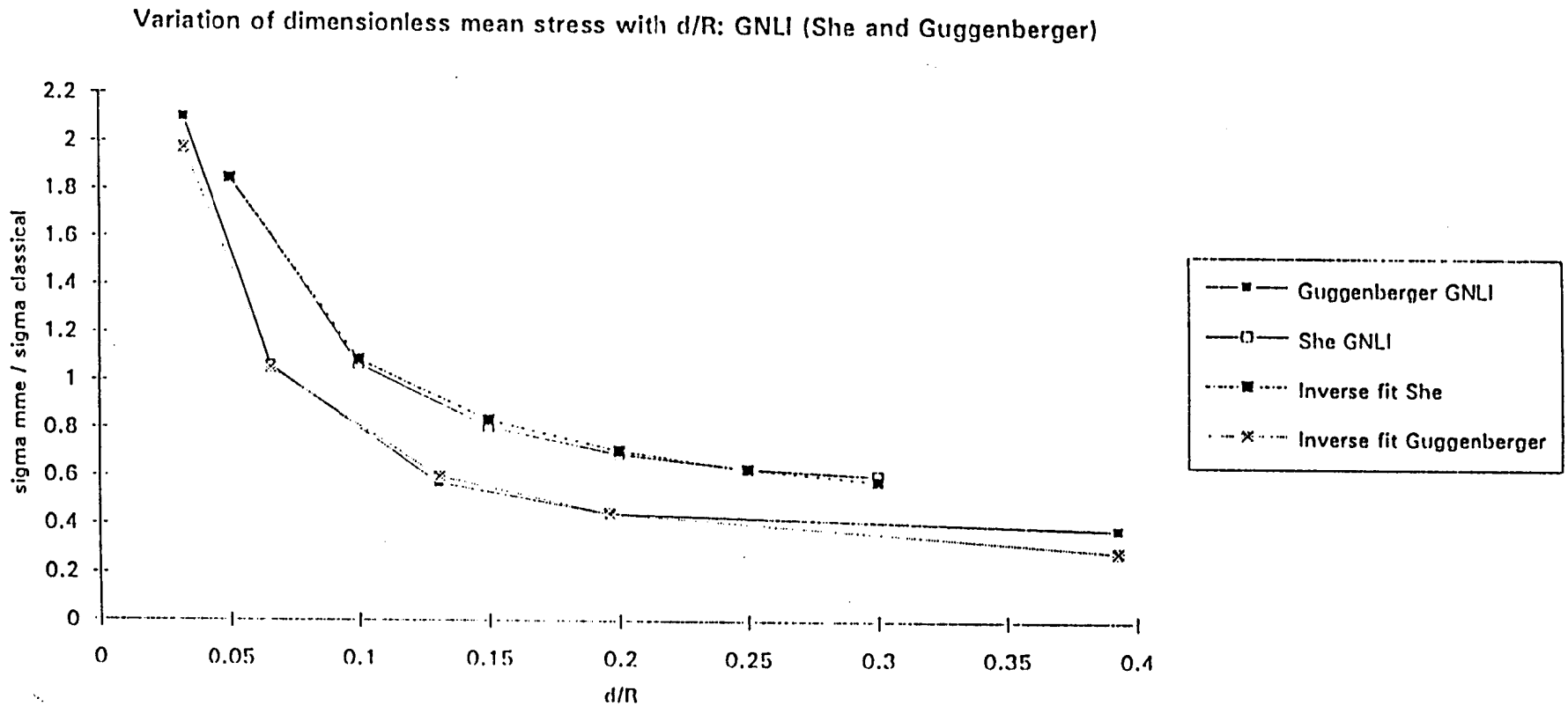

Figure 2-5 Strength Variation with Support-Width

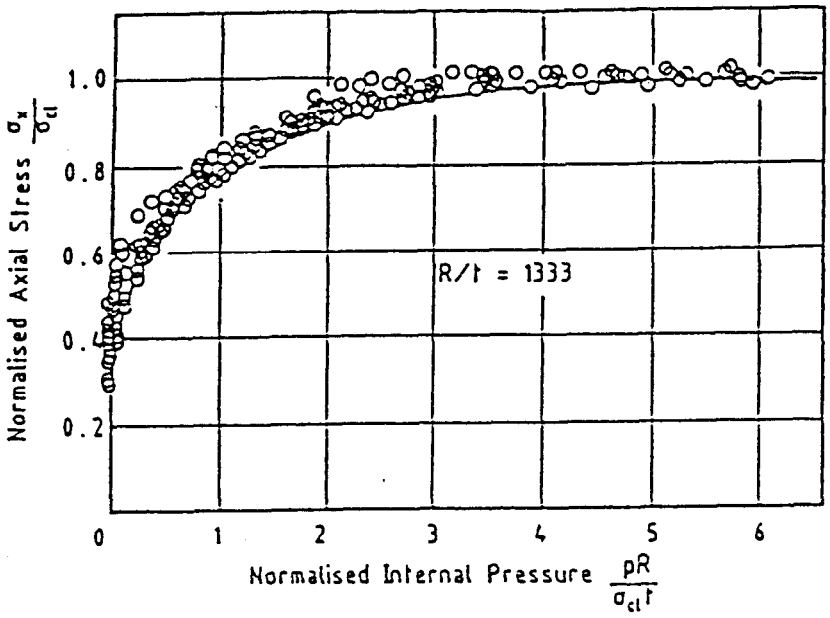

Figure 2-6 Elastic Buckling of Internally Pressurized Cylinders

CHAPTER 3

NONLINEAR ELASTIC BEHAVIOUR AND BUCKLING IN DISCRETELY SUPPORTED CYLINDERS

3.1 INTRODUCTION

From the previous introduction and historical review described in Chapters 1 and 2, it is evident that the governing failure mode of a metal silo is frequently buckling under axial compression. The practical problem of buckling in a discretely supported steel silo has many features, which cannot be addressed all at once. A large deflection analysis is needed to give an accurate prediction of the buckling or collapse load. Local plasticity, geometric imperfections and interactions between the cylinder, the transition ring and other shell segments must also be included.

These factors make the number of variables in the problem vary large, so no comprehensive understanding can be gained without some simplifying assumptions. Usually, the study starts by modelling the elevated silo structure as an isolated elastic structure, resting on equally spaced supports of uniform width placed at the lower edge of the cylindrical shell. Some investigations [Teng and Rotter, 1991, 1992; Guggenberger, 1991,1992; Ramm and Buechter, 1991; Rotter and She, 1993] were concerned with such a structural model.

Among them, Rotter and She's recent studies [1993] dealt with the nonlinear behaviour and stability of discretely supported thin elastic unpressurised cylinders, using the finite element method. In their studies, the nonlinear response, bifurcation behaviour and post-buckling response of the cylinders were extensively explored. The effects of variations in geometry and initial geometric imperfections on the buckling strength of the cylinder were thoroughly examined. It was hoped that the essential features of the real structures were captured through these simplified investigations, and that the buckling strength predictions were transformable into rules which could be used to design structures.

This chapter presents the essential nonlinear features of elastic cylinders discretely supported at the lower edge which have been explored recently [Rotter and She, 1993]. The work done by Rotter and She is described since it forms the background to some of the work of this thesis. The following summary of the study by Rotter and She is the candidate's own summary and

critical review. This thesis represents both a major extension of their work and some investigations into the validity of their assumptions.

3.2 FINITE ELEMENT MODELLING

The study of the elastic buckling behaviour of discretely supported isolated cylinders was undertaken using the ABAQUS finite element program. Nonlinear analyses were performed with the modified Riks method.

An elastic isotropic cylinder of radius R, wall thickness t and height H was assumed to be directly supported on n equally spaced discrete supports of finite width along the lower edge, as shown in Fig. 2-1a. The cylinder was subjected only to symmetrical vertical load. The geometric symmetry of the cylinder and the loading condition permits the computational model to be restricted to only 1/(2n) of the whole circumference provided that the cylinder is only supported on a small number of fairly narrow supports (typically 4, 6, 8 or 12) [Teng and Rotter, 1990,1991; Rotter and She, 1993]. For the case when the cylinder rests on four discrete supports, only one eighth of the cylinder is modelled (Fig. 2-1a). Both the upper and lower edges were restrained against radial and circumferential displacements. The parts of the lower edge in contact with the supports were completely restrained against any displacement or rotation, modelling the support as ideal rigid.

The geometry of a perfect discretely supported cylinder was characterised in a dimensionless manner by four non-dimensional parameters: the radius-to-thickness ratio R/t, the height-to-radius ratio H/R, the support-width-to-radius ratio d/R and the number of supports n.

The imperfection-sensitivity of the buckling strength was investigated using a local axisymmetric inward imperfection, which was designed to represent a local weld depression which commonly occurs in a metal silo. The form of this imperfection is the Type A shape (Fig. 2-1b) used in previous studies [Rotter and Teng, 1989; Rotter and Zhang, 1990; Teng and Rotter, 1990, 1992]. The shape of this local imperfection was defined by Rotter and Teng [1989] as

$$\delta = \delta_0 \, e^{-\pi z/\lambda} \, [\, \sin(\pi z/\lambda) + \cos(\pi z/\lambda) \,] \tag{3.1}$$

$$z = |Z - Z_0| \tag{3.2}$$

where δ is the local amplitude of the imperfection at height Z above the bottom edge. λ is the linear elastic meridional bending half wavelength of the cylinder ($\cong 2.44\,(Rt)^{1/2}$). δ_0 is the imperfection amplitude at the centre of the imperfection. Z_0 is the distance from the centre of

the imperfection to the bottom edge of the cylinder. Such an imperfection was introduced into an initially unstressed perfect cylinder and in the inward radial direction.

In the studies of imperfect cylinders, two further parameters were used to define the local imperfection: the ratio of the imperfection amplitude δ_0 to the cylinder thickness t, and the ratio of the distance Z_0 to the cylinder thickness t.

The cylinders were assumed to be linear and isotropic and made of steel with Young's modulus $E = 2\times10^5$ MPa and Poisson's ratio $\nu = 0.3$. The results obtained can be applied to other materials, though small errors are present if Poisson's ratio is very different from $\nu = 0.3$.

In Rotter and She's studies, a uniformly distributed axial force p_v was assumed to model the wall friction load component imposed by the stored bulk solids on the silo wall. The forces carried by the supports were represented in terms of the mean meridional membrane stress above each support. The mean meridional membrane stress above the support $\sigma_{m\phi}$ was normalised by the classical elastic critical stress for a cylinder under uniform axial compression σ_{cl}. The conditions at buckling of the cylinder were presented in terms of the normalised mean meridional membrane stress above the support, ie. σ_m/σ_{cl} . The relationship between this parameter and the applied loading has been given in Chapter 1. It is

$$\frac{\sigma_m}{\sigma_{cl}} = \frac{10.39}{n}\frac{R}{d}\frac{H}{R}\left(\frac{R}{t}\right)^2\frac{p_v}{E}$$

for a Poisson's ratio of $\nu = 0.3$.

3.3 TYPICAL BEHAVIOUR OF A DISCRETELY SUPPORTED CYLINDER

3.3.1 A Perfect Cylinder

The elastic pre-buckling stress distribution in discretely supported perfect cylinders was previously investigated by Teng and Rotter [1990, 1991], as shown in Figs 1-18 and 2-2. It was recognized that very high local compressive membrane stresses can develop in the vicinity of the support but decay rapidly from this point.

Rotter and She paid attention to the detailed form of the stress distribution at the bottom edge of the cylinder and its influence on the buckling strength. The geometry of an example cylinder was defined as R/t=350, H/R=2.0, d/R=0.2 and n=4. Two forms of finite element mesh model were used with the same number of elements: one with elements of equal size covering twice

the support width, the other with smaller elements near the support edge. The stress distributions near the bottom edge are shown in Fig. 3-1 for both meshes. It is evident that the second mesh produces a much smoother transition from the highly stressed region above the support to the stress-free part of the bottom edge. However, the buckling strength, or the mean meridional membrane stress above the support at buckling, obtained by using these two different mesh arrangements, remains virtually the same. This indicates that a local inaccuracy in stress distribution near the support edge has little effect on the elastic buckling strength of the shell. This simple conclusion, which is valid for elastic cylinders, led to some difficulties when elastic-plastic limit calculations were performed as part of this thesis. The sensitivity of these plastic calculations to mesh form is described in Chapter 7.

The linear bifurcation of discretely supported perfect cylinders was previously investigated by Teng and Rotter [1990, 1991]. The nonlinear behaviour of these cylinders was studied by Rotter and She [1993]. A typical nonlinear load-displacement curve is shown in Fig. 3-2. The axial displacements of a node at the top edge of the cylinder above the support centreline are very small until the load has reached the bifurcation point. Large displacements follow and a single buckle occurs a moderate distance above the support if there is only a single bifurcation point on the curve. The radial displacements of a point near the centre of the buckle are shown in Fig. 3-3. Again, the initial displacements are small, followed by large radial displacements after the bifurcation point. The buckling mode of the example cylinder is shown in Fig. 3-4. It was found that the buckle is very local above the support, in the zone of high and rapidly varying stresses. The local nature of the buckle corresponds to the rapidly changing stress in the cylinder. Therefore, it is clear that the locally higher stress above the support is very important and critical to the formation of the buckle and can strongly influence the buckling strength of the cylinder. By comparing the nonlinear bifurcation load with the linear bifurcation load previously obtained by Teng and Rotter [1990], it was found that the nonlinear strength is typically lower than the linear bifurcation stress by about 40%. This clearly shows the importance of large displacement effects on the buckling strength of the shell.

3.3.2 An Imperfect Cylinder

The effect of geometrical imperfections in practical silo structures is well-known. They can significantly reduce the buckling strength of the shell. In Rotter and She's studies, an inward imperfect cylinder (Fig. 3-5) was investigated with the same values of the geometric parameters R/t, H/R d/R and n as defined above for the example cylinder and with the imperfect geometric parameters δ_0/t and Z_0/t chosen as 1.0 and 60, respectively. The corresponding nonlinear load-displacement curve is shown by Curve 6 of Fig. 3-9 for this discretely supported imperfect cylinder. No bifurcation point can be observed on this curve.

This characteristic of the buckling behaviour corresponds to the chosen amplitude of the imperfection $\delta_0 = t$.

If the buckling strength of the imperfect cylinder is measured in terms of the maximum dimensionless mean meridional membrane stress above the support, the weakening effect of the introduced imperfection can be clearly seen by comparing the buckling strength with that obtained for the example perfect cylinder (Fig. 3-2). It has previously been shown [Rotter and Teng, 1989] that the inward imperfection gives rise to compressive circumferential membrane stresses near the centre of the imperfection and tensile circumferential membrane stresses above and below the centre, as shown in Fig. 2-2b. According to an idea proposed by Calladine [1983], in an axially compressed cylinder, a compressive circumferential membrane stress in the buckle area helps to promote buckling, whilst a tensile circumferential stress helps to resist buckling. Thus, it may be supposed that buckling will occur in an imperfect cylinder at the point where detrimental compressive stresses in both the meridional and circumferential directions co-exist. For this cylinder with an inward axisymmetric imperfection (Fig. 3-5), the buckle area occurs around the centre of the imperfection, and the buckling strength becomes lower than that of the perfect cylinder by 42%.

In the next section, parametric studies conducted by Rotter and She of the effects of changes in the geometry of the cylinder are described.

3.4 PARAMETRIC STUDIES

3.4.1 Variation with Wall Thickness t

The effect of the wall thickness on the buckling strength was examined for both perfect and imperfect cylinders with a range of R/t varying from 350 to 950. Other geometric parameters remain unchanged, defined by n=4, d/R=0.2, H/R=2, δ_0/t=1 and Z_0/t=60. The variation of the elastic buckling strength with R/t is relatively small for both perfect and imperfect cylinders as shown in Fig. 3-6. Nevertheless, Teng and Rotter [1992] found a significant decrease in the buckling strength as the wall thickness became smaller. Their observation was obtained from linear bifurcation analysis, which can provide misleading results for a problem of this kind.

3.4.2 Variation with Cylinder Height H/R

Since the buckling deformations are found to be localised near the support, the height of the cylinder is not an important parameter unless it falls below a certain value. Short cylinders are strongly affected by the proximity of the upper boundary condition, and if the upper boundary is held circular, significant increases in the buckling strength are found. For most practical silo

geometries of reasonable height, the dimensionless mean buckling stress above the support may be considered to be independent of the shell height.

3.4.3 Variation with Number of Supports n

Figure 3-7 shows the variation of the buckling strength with the number of the supports. Where the cylindrical shell is supported on a small number of columns of practical width, the buckling strength, as characterised here, is almost constant regardless of the number of supports. This means that there is little interaction between adjacent supports. Therefore, only a single buckle is formed above each support, as shown in Fig. 3-4 (n=4). When the supports become very numerous ($n \geq 16$), the buckling mode begins to display interaction between adjacent buckling locations: thus the buckling strength experiences an increase there. The following decrease in the buckling strength is accompanied by several changes in the buckling mode from a single buckle, to several buckles, to stacked rows of buckles and finally to the ring buckle mode. However, the effect is not dramatically deleterious, and supports so numerous that this becomes significant are very rare. Thus, it is easiest to ignore the effect and treat the mean stress above each support as independent of the number of supports, n.

3.4.4 Variation with Width of the Supports d/R

A range of the support-width-to-radius ratio d/R varying from 0.05 to 0.3 was examined. The relationship between the normalised mean stress above the support at buckling and the varying ratio d/R is shown in Fig. 3-8. With d/R decreasing from 0.3 to 0.15, there is only a small change in the buckling strength. Further decrease in d/R results in a sharp increase in the buckling strength. The same observation was obtained in Teng and Rotter's linear bifurcation analyses of discretely supported perfect cylinders.

As the support width becomes smaller, the buckle size reduces and the distance between the centre of the buckle and the top of the support shortens. This distance is about equal to the buckling half wave length λ ($=2.44\,(Rt)^{1/2}$) for d/R=0.15. For d/R=0.05, the distance becomes even smaller and the buckling deformation becomes extremely localised. This indicates that the buckling strength may be strongly affected by the support width only if the centre of the buckle is within a distance of the buckling half wave length from the support. This fact was not recognised by Rotter and She [1993].

3.4.5 Variation with Imperfection Amplitude δ_0/t

A range of dimensionless imperfection amplitudes δ_0/t was studied varying from 0.05 to 2.0. The corresponding load-displacement response curves are shown in Fig 3-9. The buckling strength reduces as the imperfection amplitude increases. However, the post-buckling response

becomes progressively more ductile (Figs 3-9 and 3-10) so that the strength is insensitive to the imperfection amplitude once this amplitude exceeds about $\delta_0/t = 1$.

3.4.6 Variation with Imperfection Position Z_0

An inward axisymmetric imperfection was placed at a variety of different heights above the support. Figure 3-11 shows the buckling strength as function of Z_0 for R/t of 350, 650 and 950, and demonstrates that the critical position Z_c corresponding to the largest reduction in the buckling strength is approximately proportional to $(R/t)^{7/8}(R/t)^{1/2}$. This means that for the same support width, the critical position of the weld depression imperfection is related to the radius-to-thickness ratio, R/t, and the buckling half wave length λ. It is also clear that the critical position is lower in thin cylinders than in thick cylinders, and that the buckling strength is not very sensitive to the position of the imperfection if Z_0 varies slightly in the vicinity of the critical value Z_c.

3.5 CONCLUSIONS

Nonlinear analyses of discretely supported elastic cylinders were performed by Rotter and She [1993], using the finite element method. Both perfect and imperfect cylinders of a constant height-to-radius ratio were studied. The effects of the cylinder geometric parameters and simple imperfections on the buckling behaviour and the buckling strength were examined.

It was recognized that the buckling phenomenon is very local above the support. It occurs in a region of rapidly changing stresses above the support. This illustrates the fact that the stresses just above the support are very important. Therefore, it is appropriate that the buckling strength should be characterised in the manner first proposed by Teng and Rotter [1990] as the ratio of the mean meridional membrane stress above the support to the classical elastic critical stress for a uniformly supported cylindrical shell.

The buckling deformations were found to be localised near the support, so that the height of the cylinder is not an important parameter unless it falls below a certain value. Where the cylinder is supported on a small number of supports of practical width, the dimensionless buckling stress is almost constant regardless of the number of supports. Thus, for most practical discretely supported silo structures, the dimensionless mean buckling stress above each support may be considered to be independent of both the shell height and the number of supports. It was also found that the change of wall thickness brings about little change in this dimensionless buckling strength. However, the parameter which most strongly affects the buckling strength is

the width of the support. Wider supports lead to higher buckling loads but buckling occurs at a lower mean meridional membrane stress immediately above the support.

A geometric imperfection results in a significant reduction in the buckling strength. The position of the imperfection affects the level of the buckling strength reduction. For a constant number of supports, the critical position, corresponding to the largest loss of the buckling strength, depends on the support width and the cylinder wall thickness. The imperfection amplitude naturally influences the buckling strength. However, no further reduction in the buckling strength occurs if the imperfection amplitude exceeds a certain level. With a local axisymmetric inward imperfection of amplitude $\delta_0/t = 1$ placed at the critical height Z_c, the buckling strength of this imperfect cylinder is reduced to about half that of a perfect cylinder.

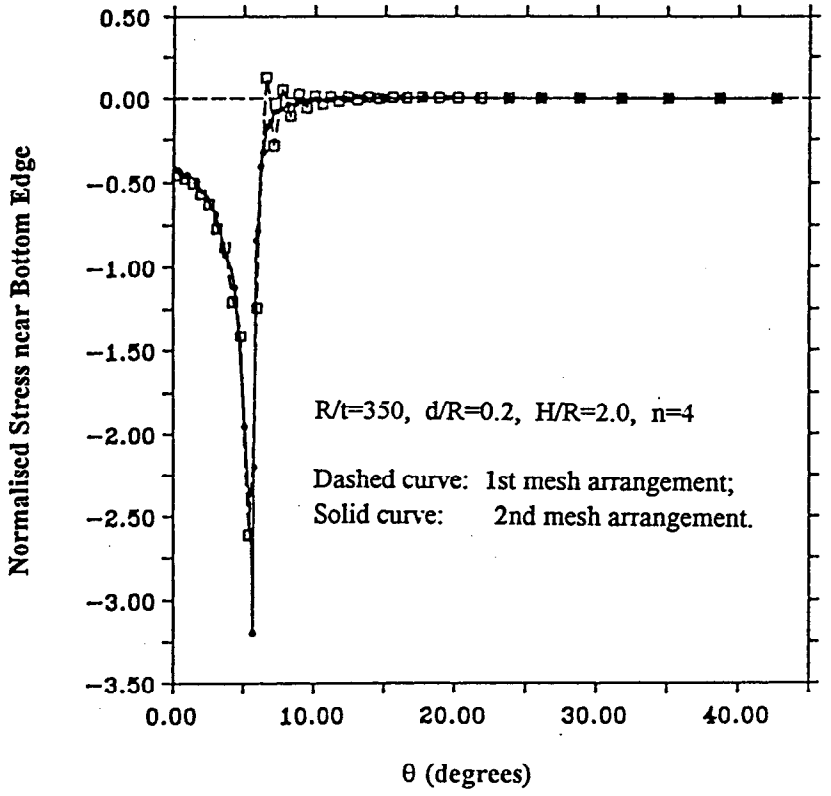

Figure 3-1 Meridional Stress Distribution near the Lower Edge of the Cylinder for Different Mesh Arrangements

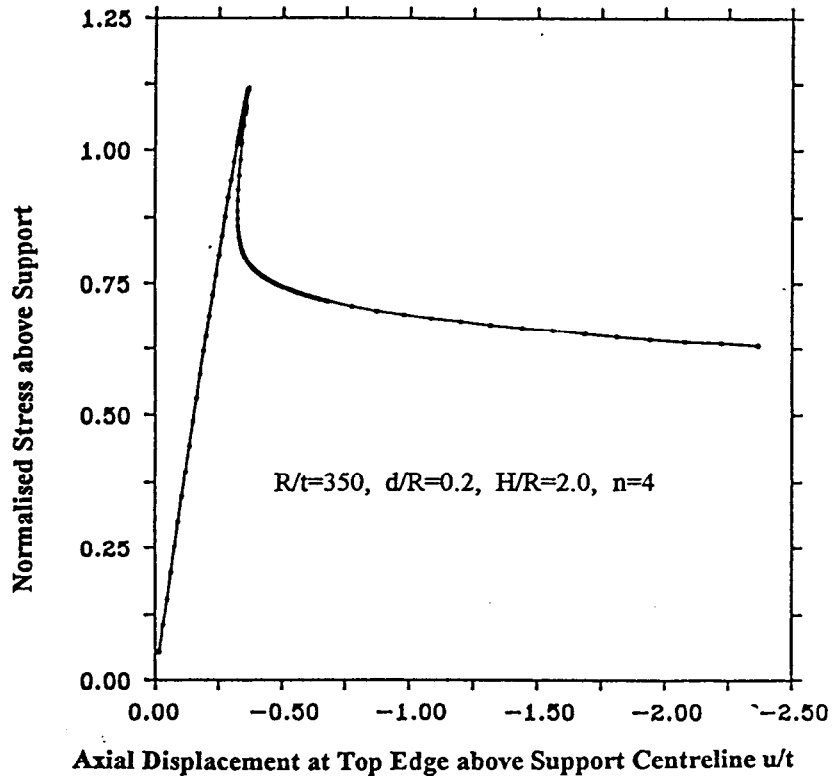

Figure 3-2 Load-Deflection Curve for a Perfect Cylinder under Axial Compression

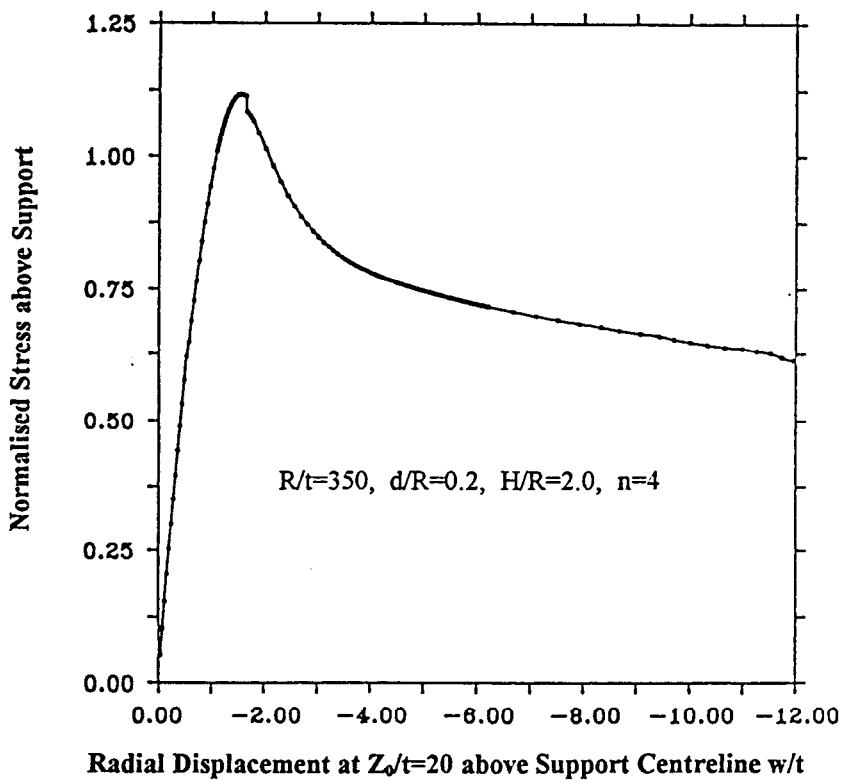

Figure 3-3 Load-Deflection Curve for a Perfect Cylinder under Axial Compression

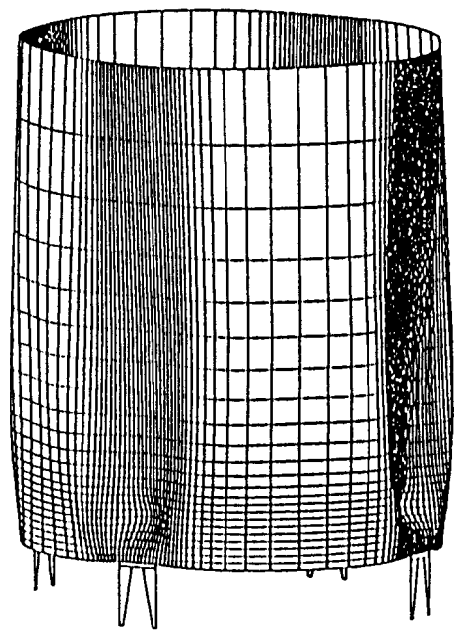

Discretely Supported Perfect Cylinder (n=4, R/t=350, d/R=0.2, H/R=0.2)

Figure 3-4 Buckling Mode for a Perfect Cylinder under Axial Compression

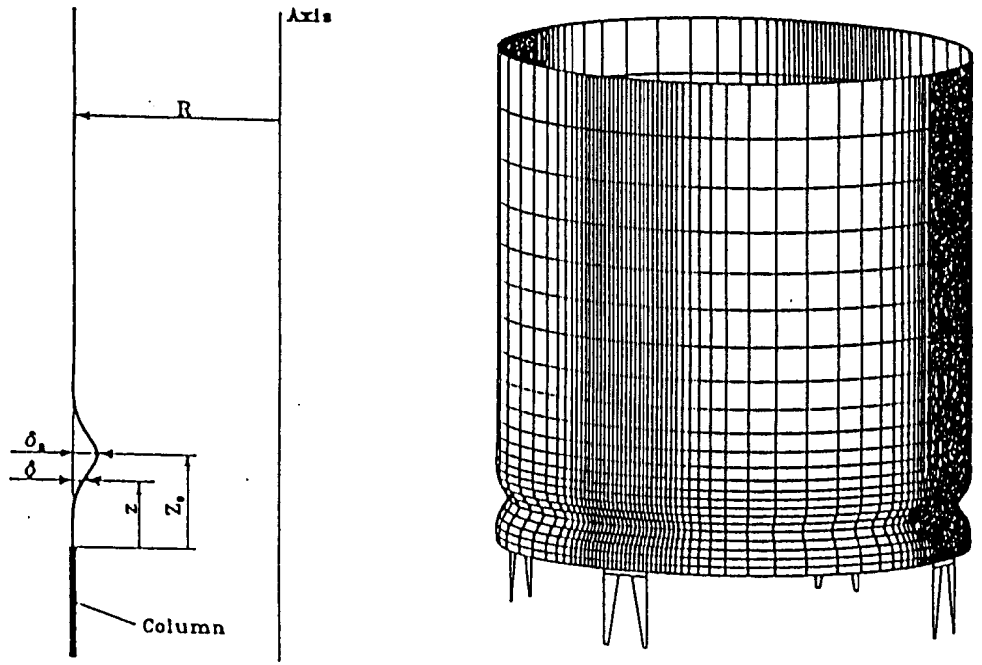

(n=4, R/t=350, d/R=0.2, H/R=0.2)

Figure 3-5 Discretely Supported Imperfect Cylinder Model

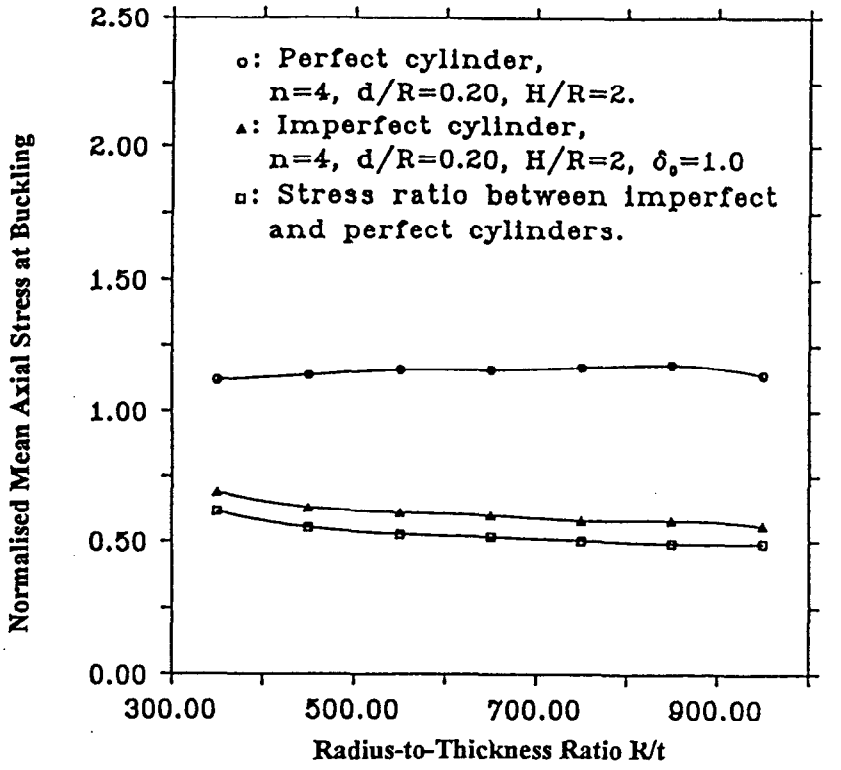

Figure 3-6 Buckling Strength of Axially Compressed Perfect and Imperfect Cylinders at Different Ratios of R/t

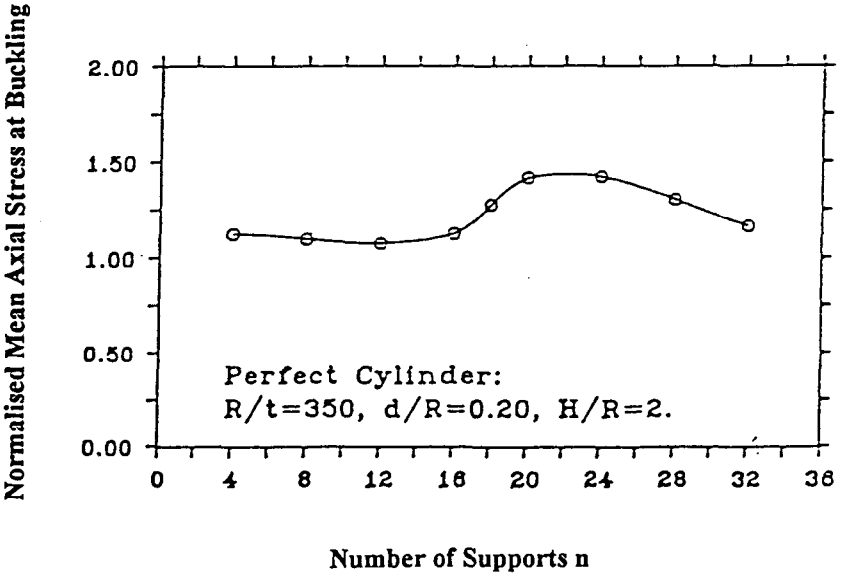

Figure 3-7 Buckling Strength of Axially Compressed Perfect and Imperfect Cylinders on Different Number of Supports n

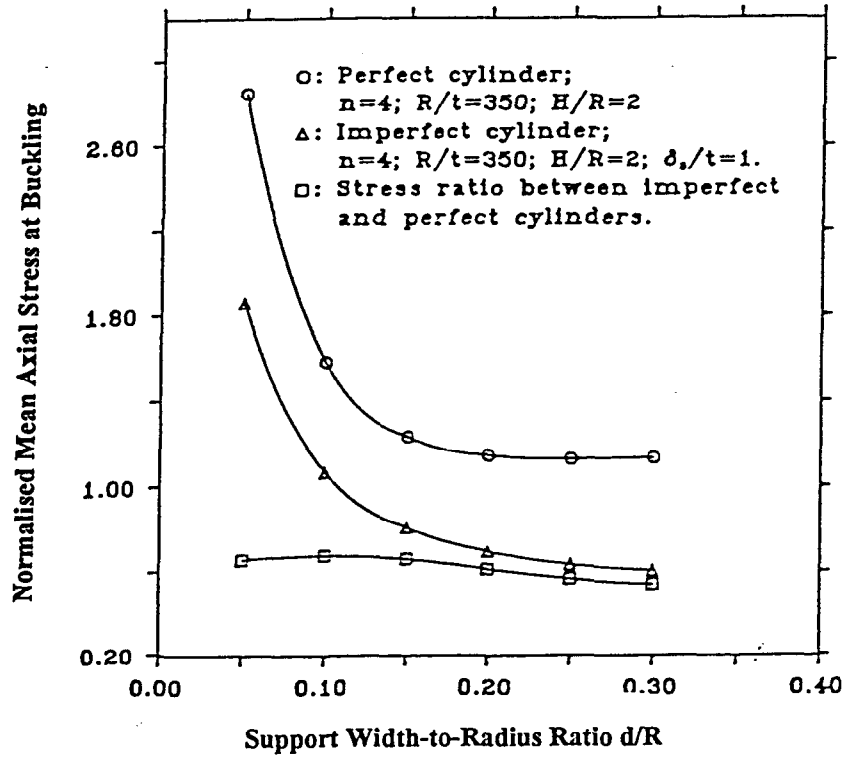

Figure 3-8 Buckling Strength of Axially Compressed Perfect and Imperfect Cylinders at Different Ratios of d/R

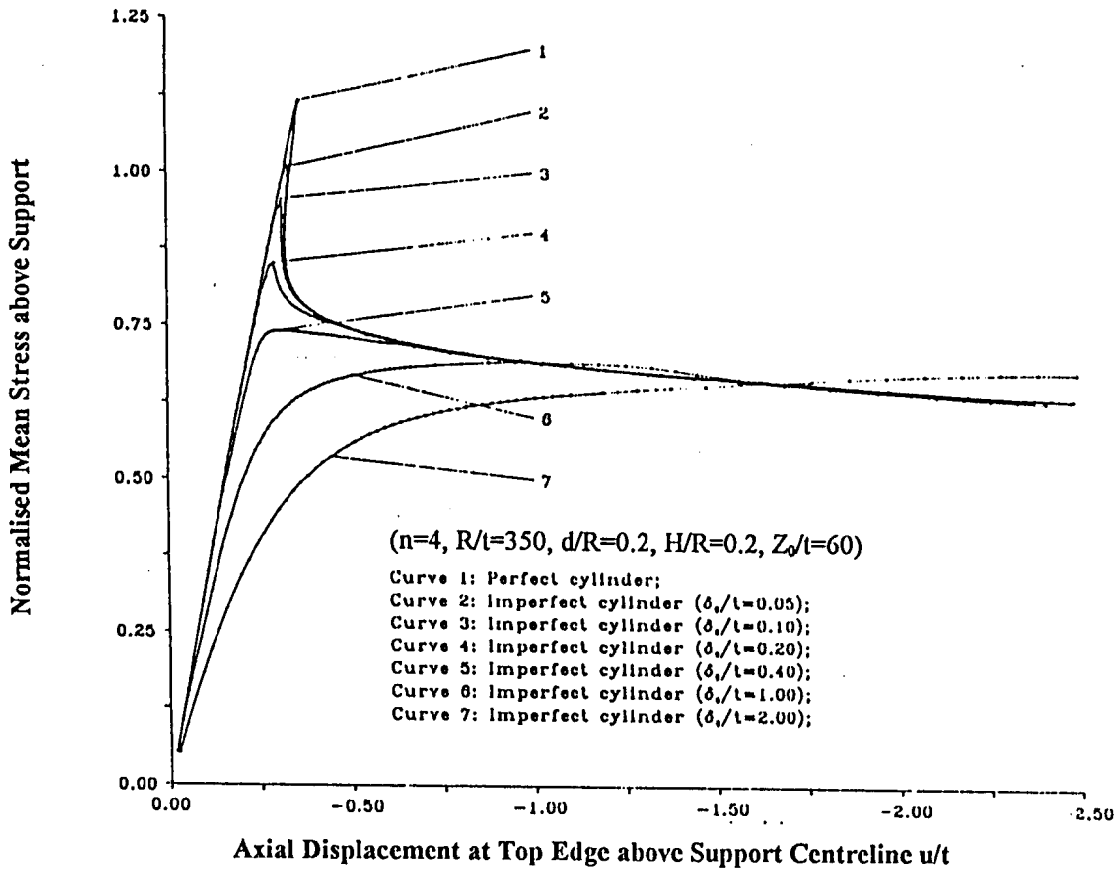

Figure 3-9 Load-Deflection Curves for Axially Compressed Imperfect Cylinders with Different Amplitudes of Imperfection δ_0/t

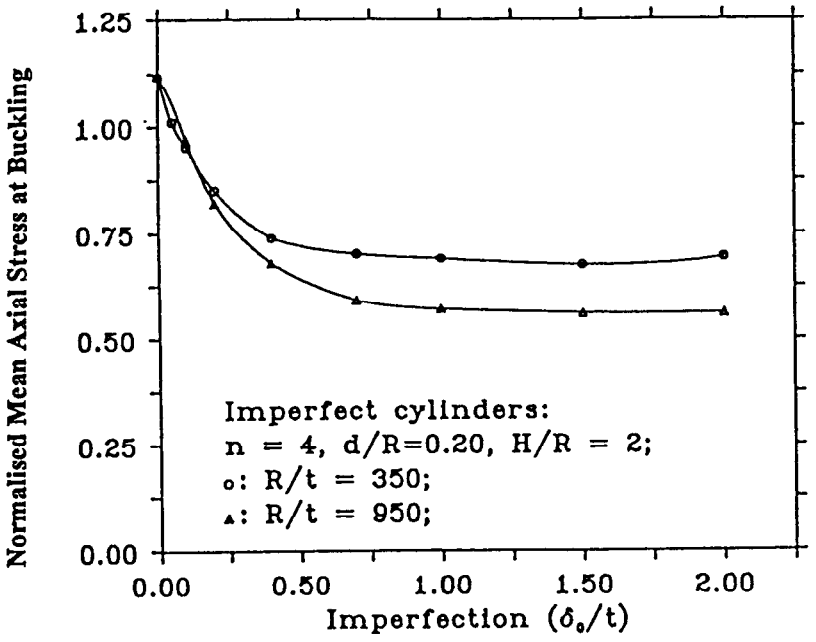

Figure 3-10 Buckling Strength of Axially Compressed Imperfect Cylinders at Different Amplitudes of Imperfection δ_0

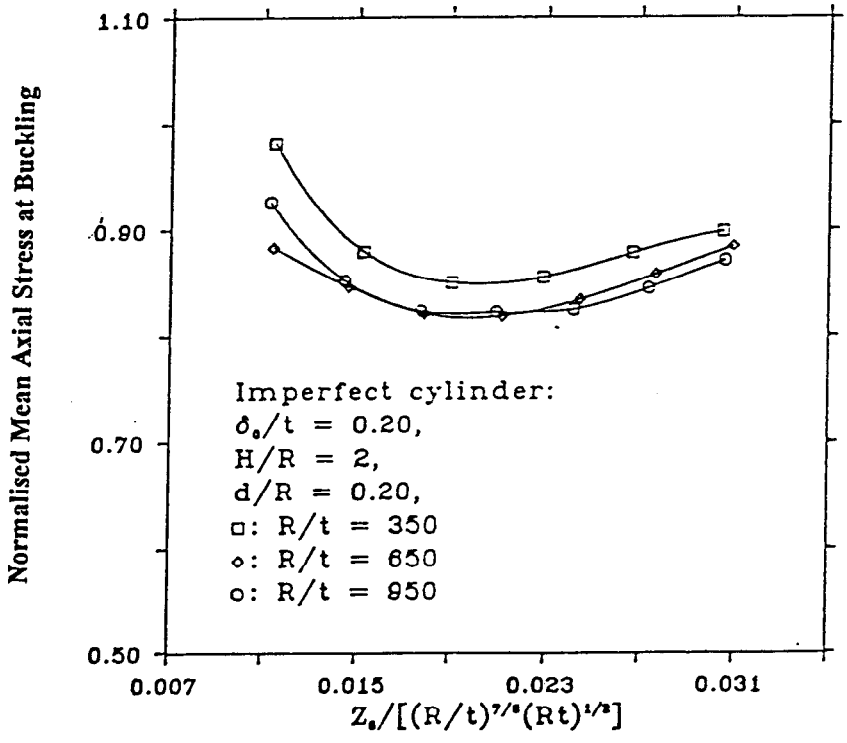

Figure 3-11 Buckling Strength of Axially Compressed Cylinders with an Axisymmetric Imperfection Localised at Different Positions Z_0

CHAPTER 4

ALGEBRAIC ANALYSIS OF ELASTIC CIRCULAR CYLINDRICAL SHELLS UNDER LOCAL LOADINGS

4.1 INTRODUCTION

The formal algebraic analysis of the stresses and displacements in elastic circular cylindrical shell structures has been carried on for many years. Several studies have developed mathematical foundations for calculating the displacements and stresses induced in cylindrical shells by local loadings, mainly focussing on the analysis of practical pressure vessels. However, these analyses have beeen almost exclusively concerned only with loads normal to the shell surface. In this chapter, an algebraic analysis is developed for more general local loads, and fully solved for local loads parallel to the cylinder axis, a problem which does not appear to have been solved before.

A silo structure generally consists of a cylindrical shell together with a conical roof and a bottom discharge hopper. The emphasis of research has usually been on the main part of a silo - the circular cylindrical shell, since many disastrous structural failures of silos occur in the cylindrical shell. In practice, the cylindrical shell has to sustain all the possible external loads applied to a silo in service. As has been discussed in Chapter 1, many different loading conditions are likely to occur. Among them, local loadings may arise from eccentric filling or discharge and attachments such as the local discrete supports and lugs, leading to local high stresses which cannot be neglected in design. The objective of this chapter is to examine the stresses caused by local loads on a cylindrical shells.

The first important studies were undertaken by Bijlaard [1954, 1955]. He solved the Donnell shell equations to find the displacements, and the membrane and bending stresses induced by both radial and circumferential loads and external moments (represented by non-uniform radial loads) in horizontal axis cylindrical pressure vessels which were simply supported at both ends. He used a double Fourier series technique. Longitudinal or axial loading was excluded in his studies. However, in an elevated silo, the discrete supports locally affixed to the shell wall transmit large longitudinal or axial loads to the shell, inducing high stresses near the attached areas. Therefore, the pattern of stresses caused by local axial loads in cylindrical shells needs investigation.

This chapter describes the algebraic analysis of cylindrical shells under longitudinal local loadings and uses a double Fourier series technique. General formulas for the displacements induced by local loads are derived. The boundary conditions are taken as simply supported at both ends. The corresponding expressions for stress resultants (resultant forces and bending and twisting moments) are obtained from the constitutive relations.

4.2 GENERAL THEORY OF CYLINDRICAL SHELLS

A circular cylindrical shell of radius a and length l and the global axis system are shown in Fig. 4-1. The x axis is along a generatrix of the cylinder, y or the angle ϕ varies around the circumference, and z is normal to middle surface, inward positive. The displacements in the x, ϕ and z directions are denoted by u, v, and w respectively. To establish the general differential equations for the displacements u, v, and w which define the deformation of the cylindrical shell, an element is cut out from the cylindrical shell (Fig. 4-1) by two adjacent axial sections and by two adjacent sections perpendicular to the axis of the cylinder. External forces X, Y, and Z per unit surface in the x, ϕ and z directions respectively are applied on the element. Three differential equilibrium equations can be derived under thin-shell theory by considering the equilibrium of the element under the external forces X, Y, and Z, which are written as following

$$\frac{\partial N_x}{\partial x} + \frac{\partial N_{\phi x}}{a\,\partial \phi} + X = 0$$

$$\frac{\partial N_\phi}{a\,\partial \phi} + \frac{\partial N_{x\phi}}{\partial x} - \frac{1}{a}\frac{\partial M_\phi}{a\,\partial \phi} + \frac{1}{a}\frac{\partial M_{x\phi}}{\partial x} + Y = 0 \qquad (4.1)$$

$$\frac{1}{a}N_\phi + \frac{\partial^2 M_x}{\partial x^2} - 2\frac{\partial^2 M_{x\phi}}{a\,\partial x \partial \phi} + \frac{\partial^2 M_\phi}{a^2\,\partial \phi^2} + Z = 0$$

in which N_x, N_ϕ and $N_{\phi x}$ are membrane forces and M_x, M_ϕ are bending moments and $M_{\phi x}$ twisting moment in shell wall per unit length of axial section and a section perpendicular to the axis of a cylindrical shell, respectively.

For a circular cylindrical shell, the strain-displacement (kinematic) equations may be found

$$\left.\begin{aligned} &\varepsilon_x = \frac{\partial u}{\partial x}, \quad \varepsilon_\phi = \frac{\partial v}{a\partial \phi} - \frac{w}{a}, \quad \gamma_{x\phi} = \frac{\partial u}{a\,\partial \phi} + \frac{\partial v}{\partial x} \\ &\chi_x = \frac{\partial^2 w}{\partial x^2}, \quad \chi_\phi = \frac{1}{a^2}\left(\frac{\partial v}{\partial \phi} + \frac{\partial^2 w}{\partial \phi^2}\right), \quad \chi_{x\phi} = \frac{1}{a}\left(\frac{\partial v}{\partial x} + \frac{\partial^2 w}{\partial x \partial \phi}\right) \end{aligned}\right\} \qquad (4.2)$$

in which ε_x, ε_ϕ are unit elongations in x and ϕ directions, $\gamma_{x\phi}$ is shear and χ_x, χ_ϕ are changes of curvature of a cylindrical shell in axial plane and in a plane perpendicular to the axis respectively, $\chi_{x\phi}$ is change of curvature.

The stress-strain relations (constitutive equations) may also be obtained as

$$
\begin{aligned}
N_x &= \frac{Et}{1-\nu^2}(\varepsilon_x + \nu\varepsilon_\phi) \\
N_\phi &= \frac{Et}{1-\nu^2}(\varepsilon_\phi + \nu\varepsilon_x) \\
N_{x\phi} &= N_{\phi x} = \frac{Et}{2(1+\nu)}\gamma_{x\phi} \\
M_x &= -D(\chi_x + \nu\chi_\phi) \\
M_\phi &= -D(\chi_\phi + \nu\chi_x] \\
M_{x\phi} &= -M_{\phi x} = D(1-\nu)\chi_{x\phi}
\end{aligned}
\tag{4.3}
$$

in which E is Young's modulus, ν is Poisson's ratio and the stress bending rigidity D is given by $D=ET^3/[12(1-\nu^2)]$.

By substituting the constitutive equations and kinematic equations into the set of equilibrium equations, a set of three partial differential equations is obtained for a cylindrical shell element under thin-shell theory [Timoshenko, 1936, 1940; Rekach, 1978], for general loadings represented by longitudinal load X, circumferential load Y and radial load Z per unit surface.

$$
\begin{aligned}
&\frac{\partial^2 u}{\partial x^2} + \frac{1-\nu}{2a^2}\frac{\partial^2 u}{\partial \phi^2} + \frac{1+\nu}{2a}\frac{\partial^2 v}{\partial x \partial \phi} - \frac{\nu}{a}\frac{\partial w}{\partial x} = -\frac{1-\nu^2}{Et}X \\
&\frac{1+\nu}{2a}\frac{\partial^2 u}{\partial x \partial \phi} + \frac{1-\nu}{2}\frac{\partial^2 v}{\partial x^2} + \frac{1}{a^2}\frac{\partial^2 v}{\partial \phi^2} - \frac{1}{a^2}\frac{\partial w}{\partial \phi} + \frac{t^2}{12a^2}\left(\frac{\partial^3 w}{\partial x^2 \partial \phi} + \frac{\partial^3 w}{a^2 \partial \phi^3}\right) + \\
&\frac{t^2}{12a^2}\left[(1-\nu)\frac{\partial^2 v}{\partial x^2} + \frac{1}{a^2}\frac{\partial^2 v}{\partial \phi^2}\right] = -\frac{1-\nu^2}{Et}Y \\
&\nu\frac{\partial u}{\partial x} + \frac{\partial v}{a\partial \phi} - \frac{w}{a} - \frac{at^2}{12}\nabla^4 w - \frac{t^2}{12}\left(\frac{2-\nu}{a}\frac{\partial^3 v}{\partial x^2 \partial \phi} + \frac{\partial^3 v}{a^3 \partial \phi^3}\right) = -\frac{(1-\nu^2)a}{Et}Z
\end{aligned}
\tag{4.4}
$$

These simultaneous partial differential equations can be transformed to give a single partial differential equation in w, which can be solved directly, and two others which define the diaplacement fields for u and v.

$$
\begin{aligned}
a\nabla^4 u = {} & \nu\frac{\partial^3 w}{\partial x^3} - \frac{1}{a^2}\frac{\partial^3 w}{\partial x \partial \phi^2} + \frac{t^2}{12a^2}\frac{1+\nu}{1-\nu}\left(\frac{\partial^5 w}{\partial x^3 \partial \phi^2} + \frac{1}{a^2}\frac{\partial^5 w}{\partial x \partial \phi^4}\right) - \frac{a(1-\nu^2)}{Et}\frac{\partial^2 X}{\partial x^2} - \frac{2(1+\nu)}{Eta} \\
& \frac{\partial^2 X}{\partial \phi^2} + \frac{(1+\nu)^2}{Et}\frac{\partial^2 Y}{\partial x \partial \phi}
\end{aligned}
\tag{4.5}
$$

$$a\nabla^4 v = \frac{1}{a^3}\frac{\partial^3 w}{\partial \phi^3} + \frac{2+\nu}{a}\frac{\partial^3 w}{\partial x^2 \partial \phi} - \frac{t^2}{12a^2}\left[\frac{2a}{1-\nu}\frac{\partial^5 w}{\partial x^4 \partial \phi} + \frac{3-\nu}{a(1-\nu)}\frac{\partial^5 w}{\partial x^2 \partial \phi^3} + \frac{1}{a^3}\frac{\partial^5 w}{\partial \phi^5}\right] + \frac{(1+\nu)^2}{Et}$$
$$\frac{\partial^2 X}{\partial x \partial \phi} - \frac{2(1+\nu)a}{Et}\frac{\partial^2 Y}{\partial x^2} - \frac{1-\nu^2}{Eta}\frac{\partial^2 Y}{\partial \phi^2} \qquad (4.6)$$

$$\nabla^8 w + \frac{12(1-\nu^2)}{a^2 t^2}\frac{\partial^4 w}{\partial x^4} + \frac{1}{a^2}\left[\frac{2}{a^6}\frac{\partial^6 w}{\partial \phi^6} + \frac{6+\nu-\nu^2}{a^2}\frac{\partial^6 w}{\partial x^4 \partial \phi^2} + \frac{7+\nu}{a^4}\frac{\partial^6 w}{\partial x^2 \partial \phi^4}\right] = \frac{1}{D}\nabla^4 Z - \frac{1}{aD}\left(\nu\frac{\partial^3 X}{\partial x^3} - \frac{1}{a^2}\frac{\partial^3 X}{\partial x \partial \phi^2}\right) - \frac{(1+\nu)^2}{Eta^3}\left[(2-\nu)\frac{\partial^5 X}{\partial x^3 \partial \phi^2} + \frac{1}{a^2}\frac{\partial^5 X}{\partial x \partial \phi^4}\right] - \frac{1}{a^2 D}\left[(2+\nu)\frac{\partial^3 Y}{\partial x^2 \partial \phi} + \frac{1}{a^2}\frac{\partial^3 Y}{\partial \phi^3}\right] \qquad (4.7)$$

For a cylindrical shell subject to external loadings in the axial x, circumferential y and radial z directions, the relevant deformations u, v, and w in the three directions can be obtained from the above equations. From the displacement fields all other effects can be found, including the stresses arising in the shell.

4.3 ANALYSIS FOR LONGITUDINAL LOAD DISTRIBUTION

4.3.1 The Differential Equations of Equilibrium

As solutions already exist for the simpler cases of radial and circumferential loadings (Y and Z) [Bijlaard, 1954, 1955], the following analysis is concerned only with local longitudinal loads. Other loads may be added to those of this analysis by superposition.

A cylinder (Fig. 4-1) of radius a and length l is subjected to a rectangular patch $2b_1 \times 2b_2$ of load located at a distance b from the origin end. The circumferential coordinate is arranged to have its origin at the centre of the loaded patch. For this loading case, Y = Z = 0 in the above differential equations (4.4), (4.5), (4.6) and (4.7), so the differential equations of equilibrium become

$$\frac{\partial^2 u}{\partial x^2} + \frac{1-\nu}{2a^2}\frac{\partial^2 u}{\partial \phi^2} + \frac{1+\nu}{2a}\frac{\partial^2 v}{\partial x \partial \phi} - \frac{\nu}{a}\frac{\partial w}{\partial x} = -\frac{1-\nu^2}{Et}X$$

$$\frac{1+\nu}{2a}\frac{\partial^2 u}{\partial x \partial \phi} + \frac{1-\nu}{2}\frac{\partial^2 v}{\partial x^2} + \frac{1}{a^2}\frac{\partial^2 v}{\partial \phi^2} - \frac{1}{a^2}\frac{\partial w}{\partial \phi} + \frac{t^2}{12a^2}\left(\frac{\partial^3 w}{\partial x^2 \partial \phi} + \frac{\partial^3 w}{a^2 \partial \phi^3}\right) + \frac{t^2}{12a^2}\left[(1-\nu)\frac{\partial^2 v}{\partial x^2} + \frac{1}{a^2}\frac{\partial^2 v}{\partial \phi^2}\right] = 0 \qquad (4.8)$$

$$\nu\frac{\partial u}{\partial x} + \frac{\partial v}{a\partial \phi} - \frac{w}{a} - \frac{at^2}{12}\nabla^4 w - \frac{t^2}{12}\left(\frac{2-\nu}{a}\frac{\partial^3 v}{\partial x^2 \partial \phi} + \frac{\partial^3 v}{a^3 \partial \phi^3}\right) = 0$$

$$a\nabla^4 u = \nu \frac{\partial^3 w}{\partial x^3} - \frac{1}{a^2}\frac{\partial^3 w}{\partial x \partial \phi^2} + \frac{t^2}{12a^2}\frac{1+\nu}{1-\nu}\left(\frac{\partial^5 w}{\partial x^3 \partial \phi^2} + \frac{1}{a^2}\frac{\partial^5 w}{\partial x \partial \phi^4}\right) - \frac{a(1-\nu^2)}{Et}\frac{\partial^2 X}{\partial x^2} - \frac{2(1+\nu)}{Eta}\frac{\partial^2 X}{\partial \phi^2} \tag{4.9}$$

$$a\nabla^4 v = \frac{1}{a^3}\frac{\partial^3 w}{\partial \phi^3} + \frac{2+\nu}{a}\frac{\partial^3 w}{\partial x^2 \partial \phi} - \frac{t^2}{12a^2}\left[\frac{2a}{1-\nu}\frac{\partial^5 w}{\partial x^4 \partial \phi} + \frac{3-\nu}{a(1-\nu)}\frac{\partial^5 w}{\partial x^2 \partial \phi^3} + \frac{1}{a^3}\frac{\partial^5 w}{\partial \phi^5}\right] + \frac{(1+\nu)^2}{Et}\frac{\partial^2 X}{\partial x \partial \phi} \tag{4.10}$$

$$\nabla^8 w + \frac{12(1-\nu^2)}{a^2 t^2}\frac{\partial^4 w}{\partial x^4} + \frac{1}{a^2}\left[\frac{2}{a^6}\frac{\partial^6 w}{\partial \phi^6} + \frac{6+\nu-\nu^2}{a^2}\frac{\partial^6 w}{\partial x^4 \partial \phi^2} + \frac{7+\nu}{a^4}\frac{\partial^6 w}{\partial x^2 \partial \phi^4}\right] = -\frac{1}{aD}\left(\nu\frac{\partial^3 X}{\partial x^3} - \frac{1}{a^2}\frac{\partial^3 X}{\partial x \partial \phi^2}\right) - \frac{(1+\nu)^2}{Eta^3}\left[(2-\nu)\frac{\partial^5 X}{\partial x^3 \partial \phi^2} + \frac{1}{a^2}\frac{\partial^5 X}{\partial x \partial \phi^4}\right] \tag{4.11}$$

4.3.2 General Case: Expressions for Displacements u, v and w

Since Equation (4.11) contains only even derivatives of w and X with respect to the circumferential coordinate ϕ, this equation can be solved by developing both the radial deflection w and the external longitudinal load X as double Fourier series in x and ϕ, and using only symmetrical terms in ϕ:

$$w = \Sigma_m \Sigma_n \cos m\phi \; f_{mn}\left(\frac{\lambda}{a}x\right) \qquad (m = 0, 1, 2, \ldots\infty;\; n = 1, 2, \ldots\infty) \tag{4.12}$$

$$X = \Sigma_m \Sigma_n \cos m\phi \; X_{mn}\left(\frac{\lambda}{a}x\right) \qquad (m = 0, 1, 2, \ldots\infty;\; n = 1, 2, \ldots\infty) \tag{4.13}$$

where $\lambda = n\pi a/l$.

Introducing these expressions into Equation (4.11), the eighth order partial differential equation reduces to a eighth order ordinary differential equation:

$$\Sigma_m \Sigma_n \left\{\left[\frac{d^8}{dx^8} - 4\frac{m^2}{a^2}\frac{d^6}{dx^6} + 6\frac{m^4}{a^4}\frac{d^4}{dx^4} + \frac{12(1-\nu^2)}{a^2 t^2}\frac{d^4}{dx^4} - \frac{m^2(6+\nu-\nu^2)}{a^4}\frac{d^4}{dx^4} - 4\frac{m^6}{a^6}\frac{d^2}{dx^2} + \frac{m^4(7+\nu)}{a^6}\frac{d^2}{dx^2} + \frac{m^6(m^2-2)}{a^8}\right] f_{mn}\left(\frac{\lambda}{a}x\right) + \left[\frac{\nu}{aD}\frac{d^3}{dx^3} - \frac{m^2(1+\nu)^2(2-\nu)}{Eta^3}\frac{d^3}{dx^3} + \frac{m^2}{a^3 D}\frac{d}{dx} + \frac{m^4(1+\nu)^2}{Eta^5}\frac{d}{dx}\right] X_{mn}\left(\frac{\lambda}{a}x\right)\right\} \cos m\phi = 0 \tag{4.14}$$

Since Equation (4.14) is true for all ϕ, the expression inside the braces must vanish for any m, so that for any value of m Equation (4.14) reduces to

$$\frac{d^8 f_{mn}}{dx^8} - 4\frac{m^2}{\lambda^2}\frac{d^6 f_{mn}}{dx^6} + \frac{1}{\lambda^4}\left[6m^4 + \frac{12a^2(1-\nu^2)}{t^2} - m^2(6+\nu-\nu^2)\right]\frac{d^4 f_{mn}}{dx^4} + m^4\frac{-4m^2+7+\nu}{\lambda^6}\frac{d^2 f_{mn}}{dx^2} + \frac{m^6(m^2-2)}{\lambda^8} f_{mn} = \frac{a^4}{\lambda^5}\left[-\frac{\nu}{D} + \frac{m^2(1+\nu)^2(2-\nu)}{Eta^2}\right]\frac{d^3 X_{mn}}{dx^3} - \frac{a^4 m^2}{\lambda^7}\left[\frac{\nu}{D} + \frac{m^2(1+\nu)^2}{Eta^2}\right]\frac{dX_{mn}}{dx} \tag{4.15}$$

The general solution of the above equation for a given value m may be assumed in the form

$$f_{mn}(\frac{\lambda}{a}x) = \bar{f}_{mn}(\frac{\lambda}{a}x) + f^{0}_{mn}(\frac{\lambda}{a}x) \tag{4.16}$$

where $\bar{f}_{mn}(\frac{\lambda}{a}x)$ = general solution to the homogeneous equation (4.15), ie.

$$\frac{d^8 f_{mn}}{dx^8} - 4\frac{m^2}{\lambda^2}\frac{d^6 f_{mn}}{dx^6} + \frac{1}{\lambda^4}[6m^4 + \frac{12a^2(1-\nu^2)}{t^2} - m^2(6+\nu-\nu^2)]\frac{d^4 f_{mn}}{dx^4} + m^4\frac{-4m^2+7+\nu}{\lambda^6}$$
$$\frac{d^2 f_{mn}}{dx^2} + \frac{m^6(m^2-2)}{\lambda^8} f_{mn} = 0$$

$f^{0}_{mn}(\frac{\lambda}{a}x)$ = partial solution to the inhomogeneous equation (4.15).

Homogeneous solution in w

The general solution to the homogeneous equation (4.15) can be found by assuming

$$\bar{f}_{mn}(\frac{\lambda}{a}x) = \Sigma C_T e^{T(\frac{\lambda}{a}x)} \tag{4.17}$$

Substituting (4.17) into (4.15) leads to the conditions under which Equation (4.17) represents a solution. The problem then reduces to that of solving the eighth-order characteristic equation.

$$T^8 - 4\frac{m^2}{\lambda^2}T^6 + \frac{1}{\lambda^4}[6m^4 + \frac{12a^2(1-\nu^2)}{t^2} - m^2(6+\nu-\nu^2)]T^4 + m^4\frac{-4m^2+7+\nu}{\lambda^6}T^2 +$$
$$\frac{m^6(m^2-2)}{\lambda^8} = 0 \tag{4.18}$$

in which the values of T satisfying Equation (4.18) produce potential homogeneous solution functions in Equation (4.17).

In general, the eight roots of Equation (4.15) are in complementary pairs and differ only in sign. For the cases of m≠1 (the case of m=1 is a special case and will be discussed in Section 4.3.3), these eight roots are in the form

$$T_1 = \delta_1 + i\mu_1, \quad T_3 = -\delta_1 - i\mu_1, \quad T_5 = \delta_2 + i\mu_2, \quad T_7 = -\delta_2 - i\mu_2$$
$$T_2 = \delta_1 - i\mu_1, \quad T_4 = -\delta_1 + i\mu_1, \quad T_6 = \delta_2 - i\mu_2, \quad T_8 = -\delta_2 + i\mu_2 \tag{4.19}$$

It should be noted that Eq. (4.19) is a general representation of a solution form of Eq. (4.18). Thus δ_1 , δ_2 and μ_1 , μ_2 should be regarded as general coefficients of real and imaginary parts of the roots of Eq. (4.18). They do not represent any particular values.

Adopting Eq. (4.19) as the solution, the general solution for $\bar{f}_{mn}(\frac{\lambda}{a}x)$ may be expanded as

$$\bar{f}_{mn}(\frac{\lambda}{a}x) = e^{\delta_1(\frac{\lambda}{a}x)}(C_1\cos\mu_1\frac{\lambda}{a}x + C_2\sin\mu_1\frac{\lambda}{a}x) + e^{-\delta_1(\frac{\lambda}{a}x)}(C_3\cos\mu_1\frac{\lambda}{a}x + C_4\sin\mu_1\frac{\lambda}{a}x) + e^{\delta_2(\frac{\lambda}{a}x)}(C_5\cos\mu_2\frac{\lambda}{a}x + C_6\sin\mu_2\frac{\lambda}{a}x) + e^{-\delta_2(\frac{\lambda}{a}x)}(C_7\cos\mu_2\frac{\lambda}{a}x + C_8\sin\mu_2\frac{\lambda}{a}x) \quad (4.20)$$

in which C_i are real arbitrary constants (8 constants are required for each term of the double Fourier series).

The arbitrary constants in Eq. (4.17) must be found from eight boundary conditions at the two ends of the cylinder (x = 0 and x = l). This matter will be pursued further after the inhomogeneous solution has been discussed.

Inhomogeneous solution in w

To solve the inhomogeneous part of Eq. (4.15), a partial solution $f^0_{mn}(\frac{\lambda}{a}x)$ will be sought in the form

$$f^0_{mn}(\frac{\lambda}{a}x) = w_{mn}\cos(\frac{\lambda}{a}x) \quad (4.21)$$

To represent a rectangular patch of loading at some point within the length of the cylinder (0 < b-b_2, b+b_2 < l), the loading must be represented as

$$X_{mn}(\frac{\lambda}{a}x) = X_{mn}\sin(\frac{\lambda}{a}x) \quad (4.22)$$

in which X_{mn} = load coefficient for the mn th term of the solution, and it will be recalled that $\lambda = n\pi a/l$.

The expressions of the load coefficient X_{mn} depend on the pattern of load chosen. The derivation of the expressions for load coefficient X_{mn} are described in Section 4.3.6.

Insertion of Eqs (4.21) and (4.22) into Eq. (4.15) yields

$$[\{\frac{1}{a^8}(\lambda^2+m^2)^4+\frac{12(1-\nu^2)}{a^2t^2}(\frac{\lambda}{a})^4+\frac{1}{a^2}[-2\frac{m^6}{a^6}-\frac{m^2(6+\nu-\nu^2)}{a^2}(\frac{\lambda}{a})^4-\frac{m^4(7+\nu)}{a^4}(\frac{\lambda}{a})^2]\}$$

$$w_{mn}+\{\frac{1}{aD}[-\nu(\frac{\lambda}{a})^3+\frac{m^2}{a^2}\frac{\lambda}{a}]+\frac{(1+\nu)^2}{Eta^3}[(2-\nu)m^2(\frac{\lambda}{a})^3+\frac{m^4}{a^2}\frac{\lambda}{a}]\}X_{mn}]\cos(\frac{\lambda}{a}x)=0 \quad (4.23)$$

Since Eq. (4.23) must be satisfied for all values of x, the expression within the outer square brackets must be zero for all values of λ (ie. n), from which

$$w_{mn}=\frac{\{a^4\lambda(\nu\lambda^2-m^2)-\frac{a^2m^2t^2(1+\nu)\lambda}{12(1-\nu)}[(2-\nu)\lambda^2+m^2]\}X_{mn}}{D\{(\lambda^2+m^2)^4+\frac{12a^2(1-\nu^2)}{t^2}\lambda^4-m^2[2m^4+(6+\nu-\nu^2)\lambda^4+(7+\nu)m^2\lambda^2]\}} \quad (4.24)$$

Substituting the solutions for $f^{-}_{mn}(\frac{\lambda}{a}x)$ and $f^{o}_{mn}(\frac{\lambda}{a}x)$ in Eq. (4.12), the general expression for displacement w is found as

$$\begin{aligned} w &= \Sigma_m\Sigma_n\cos m\phi\, f_{mn}(\frac{\lambda}{a}x) \\ &= \Sigma_m\Sigma_n[e^{\delta_1}(\frac{\lambda}{a}x)(C_1\cos\mu_1\frac{\lambda}{a}x+C_2\sin\mu_1\frac{\lambda}{a}x)+e^{-\delta_1}(\frac{\lambda}{a}x)(C_3\cos\mu_1\frac{\lambda}{a}x+ \\ &\quad C_4\sin\mu_1\frac{\lambda}{a}x)+e^{\delta_2}(\frac{\lambda}{a}x)(C_5\cos\mu_2\frac{\lambda}{a}x+C_6\sin\mu_2\frac{\lambda}{a}x)+e^{-\delta_2}(\frac{\lambda}{a}x)(C_7\cos\mu_2\frac{\lambda}{a}x+ \\ &\quad C_8\sin\mu_2\frac{\lambda}{a}x)+w_{mn}\cos(\frac{\lambda}{a}x)]\cos m\phi \qquad (m=0,1,2,....\infty;\ n=1,2,....\infty) \end{aligned} \quad (4.25)$$

Displacements u and v

The other displacements, u and v, which satisfy Eqs (4.9) and (4.10) respectively, can also be solved by being developed into double Fourier series. Again, the symmetry of the axis system with respect to the position of the load determines that the displacements u and v must be represented in the forms:

$$u=\Sigma_m\Sigma_n\cos m\phi\, u_{mn}(\frac{\lambda}{a}x) \qquad (m=0,1,2,....\infty;\ n=1,2,....\infty) \quad (4.26)$$

$$v=\Sigma_m\Sigma_n\sin m\phi\, v_{mn}(\frac{\lambda}{a}x) \qquad (m=0,1,2,....\infty;\ n=1,2,....\infty) \quad (4.27)$$

Longitudinal displacement u

For the longitudinal displacement u, insertion of Eqs (4.26), (4.12), (4.16), (4.13) and (4.22) into Eq. (4.9) gives

$$\Sigma_m\Sigma_n\left[\frac{d^4}{dx^4} - \frac{2m^2}{a^2}\frac{d^2}{dx^2} + \frac{m^4}{a^4}\right] u_{mn}\left(\frac{\lambda}{a}x\right)\cos m\phi = \Sigma_m\Sigma_n\left\{\left[\left(\frac{\nu}{a} - \frac{m^2t^2}{12a^3}\frac{1+\nu}{1-\nu}\right)\frac{d^3}{dx^3} + \left(\frac{m^2}{a^3} + \frac{m^4t^2}{12a^5}\right.\right.\right.$$
$$\left.\left.\left.\frac{1+\nu}{1-\nu}\right)\frac{d}{dx}\right]\left[\bar{f}_{mn}\left(\frac{\lambda}{a}x\right) + f^0_{mn}\left(\frac{\lambda}{a}x\right)\right] - \left[\frac{1-\nu^2}{Et}\frac{d^2}{dx^2} - \frac{2m^2(1+\nu)}{Eta^2}\right] X_{mn}\left(\frac{\lambda}{a}x\right)\right\}\cos m\phi$$
$$(m = 0, 1, 2,....\infty;\ n = 1, 2,....\infty) \qquad (4.28)$$

Since the harmonics are orthogonal, this equation must be separately satisfied for each values of m, leading to

$$\left[\frac{d^4}{dx^4} - \frac{2m^2}{a^2}\frac{d^2}{dx^2} + \frac{m^4}{a^4}\right] u_{mn}\left(\frac{\lambda}{a}x\right) = \left[\left(\frac{\nu}{a} - \frac{m^2t^2}{12a^3}\frac{1+\nu}{1-\nu}\right)\frac{d^3}{dx^3} + \left(\frac{m^2}{a^3} + \frac{m^4t^2}{12a^5}\frac{1+\nu}{1-\nu}\right)\frac{d}{dx}\right]$$
$$\left[\bar{f}_{mn}\left(\frac{\lambda}{a}x\right) + f^0_{mn}\left(\frac{\lambda}{a}x\right)\right] - \left[\frac{1-\nu^2}{Et}\frac{d^2}{dx^2} - \frac{2m^2(1+\nu)}{Eta^2}\right] X_{mn}\left(\frac{\lambda}{a}x\right) \qquad (4.29)$$

The longitudinal displacement u can also be divided into components satisfying the homogeneous and inhomogeneous parts of Eq. (4.29).

$$u_{mn}\left(\frac{\lambda}{a}x\right) = \bar{u}_{mn}\left(\frac{\lambda}{a}x\right) + u^0_{mn}\left(\frac{\lambda}{a}x\right) \qquad (4.30)$$

where $\bar{u}_{mn}\left(\frac{\lambda}{a}x\right)$ = general solution to Equation (4.26).

$u^0_{mn}\left(\frac{\lambda}{a}x\right)$ = partial solution to Equation (4.26).

Homogeneous solution in u

Substituting Eq. (4.30) into Eq. (4.29), the following equation is chosen to solve $\bar{u}_{mn}\left(\frac{\lambda}{a}x\right)$

$$\left[\frac{d^4}{dx^4} - \frac{2m^2}{a^2}\frac{d^2}{dx^2} + \frac{m^4}{a^4}\right]\bar{u}_{mn}\left(\frac{\lambda}{a}x\right) = \left[\left(\frac{\nu}{a} - \frac{m^2t^2}{12a^3}\frac{1+\nu}{1-\nu}\right)\frac{d^3}{dx^3} + \left(\frac{m^2}{a^3} + \frac{m^4t^2}{12a^5}\frac{1+\nu}{1-\nu}\right)\frac{d}{dx}\right]\bar{f}_{mn}\left(\frac{\lambda}{a}x\right) \qquad (4.31)$$

In a similar manner to the solution for $\bar{f}_{mn}\left(\frac{\lambda}{a}x\right)$ in Eq. (4.20), the solution to Eq. (4.31) may be assumed to be

$$\bar{u}_{mn}\left(\frac{\lambda}{a}x\right) = e^{\delta_1\left(\frac{\lambda}{a}x\right)}\left(P_1\cos\mu_1\frac{\lambda}{a}x + P_2\sin\mu_1\frac{\lambda}{a}x\right) + e^{-\delta_1\left(\frac{\lambda}{a}x\right)}\left(P_3\cos\mu_1\frac{\lambda}{a}x + P_4\right.$$
$$\left.\sin\mu_1\frac{\lambda}{a}x\right) + e^{\delta_2\left(\frac{\lambda}{a}x\right)}\left(P_5\cos\mu_2\frac{\lambda}{a}x + P_6\sin\mu_2\frac{\lambda}{a}x\right) + e^{-\delta_2\left(\frac{\lambda}{a}x\right)}\left(P_7\cos\mu_2\frac{\lambda}{a}x\right.$$
$$\left. + P_8\sin\mu_2\frac{\lambda}{a}x\right) \qquad (4.32)$$

in which P_i are real arbitrary constants in terms of C_i in Eq. (4.20).

The relationships between P_i and C_i can be established by substituting Eqs (4.32) and (4.20) into Eq. (4.31) and equating coefficients of like terms which involve the multiplication of the relevant exponential and trigonometric functions on the both sides of the equation, respectively. This produces a set of 8 simultaneous equations relating P_i and C_i:

$$P_1 4\delta_1\mu_1 [-\lambda^2(\delta_1^2-\mu_1^2)+m^2] + P_2[\lambda^2(\delta_1^4+\mu_1^4-6\delta_1^2\mu_1^2) - 2m^2(\delta_1^2-\mu_1^2) + \frac{m^4}{\lambda^2}] =$$
$$C_1\mu_1[-(\nu-\frac{m^2t^2}{12a^2}\frac{1+\nu}{1-\nu})\lambda(3\delta_1^2-\mu_1^2) - \frac{m^2}{\lambda}(1+\frac{m^2t^2}{12a^2}\frac{1+\nu}{1-\nu})] + C_2\delta_1[(\nu-\frac{m^2t^2}{12a^2}\frac{1+\nu}{1-\nu})\lambda$$
$$(\delta_1^2-3\mu_1^2) + \frac{m^2}{\lambda}(1+\frac{m^2t^2}{12a^2}\frac{1+\nu}{1-\nu})],$$

$$P_1[\lambda^2(\delta_1^4+\mu_1^4-6\delta_1^2\mu_1^2) - 2m^2(\delta_1^2-\mu_1^2) + \frac{m^4}{\lambda^2}] + P_2 4\delta_1\mu_1[\lambda^2(\delta_1^2-\mu_1^2) - m^2] =$$
$$C_1\delta_1[(\nu-\frac{m^2t^2}{12a^2}\frac{1+\nu}{1-\nu})\lambda(\delta_1^2-3\mu_1^2) + \frac{m^2}{\lambda}(1+\frac{m^2t^2}{12a^2}\frac{1+\nu}{1-\nu})] + C_2\mu_1[(\nu-\frac{m^2t^2}{12a^2}\frac{1+\nu}{1-\nu})\lambda$$
$$(3\delta_1^2-\mu_1^2) + \frac{m^2}{\lambda}(1+\frac{m^2t^2}{12a^2}\frac{1+\nu}{1-\nu})],$$

$$P_3 4\delta_1\mu_1[\lambda^2(\delta_1^2-\mu_1^2)-m^2] + P_4[\lambda^2(\delta_1^4+\mu_1^4-6\delta_1^2\mu_1^2) - 2m^2(\delta_1^2-\mu_1^2) + \frac{m^4}{\lambda^2}] =$$
$$C_3\mu_1[-(\nu-\frac{m^2t^2}{12a^2}\frac{1+\nu}{1-\nu})\lambda(3\delta_1^2-\mu_1^2) - \frac{m^2}{\lambda}(1+\frac{m^2t^2}{12a^2}\frac{1+\nu}{1-\nu})] + C_4\delta_1[-(\nu-\frac{m^2t^2}{12a^2}\frac{1+\nu}{1-\nu})\lambda$$
$$(\delta_1^2-3\mu_1^2) - \frac{m^2}{\lambda}(1+\frac{m^2t^2}{12a^2}\frac{1+\nu}{1-\nu})],$$

$$P_3[\lambda^2(\delta_1^4+\mu_1^4-6\delta_1^2\mu_1^2) - 2m^2(\delta_1^2-\mu_1^2) + \frac{m^4}{\lambda^2}] + P_4 4\delta_1\mu_1[-\lambda^2(\delta_1^2-\mu_1^2)+m^2] =$$
$$C_3\delta_1[-(\nu-\frac{m^2t^2}{12a^2}\frac{1+\nu}{1-\nu})\lambda(\delta_1^2-3\mu_1^2) - \frac{m^2}{\lambda}(1+\frac{m^2t^2}{12a^2}\frac{1+\nu}{1-\nu})] + C_4\mu_1[(\nu-\frac{m^2t^2}{12a^2}\frac{1+\nu}{1-\nu})\lambda$$
$$(3\delta_1^2-\mu_1^2) + \frac{m^2}{\lambda}(1+\frac{m^2t^2}{12a^2}\frac{1+\nu}{1-\nu})],$$

$$P_5 4\delta_2\mu_2[-\lambda^2(\delta_2^2-\mu_2^2)+m^2] + P_6[\lambda^2(\delta_2^4+\mu_2^4-6\delta_2^2\mu_2^2) - 2m^2(\delta_2^2-\mu_2^2) + \frac{m^4}{\lambda^2}] =$$
$$C_5\mu_2[-(\nu-\frac{m^2t^2}{12a^2}\frac{1+\nu}{1-\nu})\lambda(3\delta_2^2-\mu_2^2) - \frac{m^2}{\lambda}(1+\frac{m^2t^2}{12a^2}\frac{1+\nu}{1-\nu})] + C_6\delta_2[(\nu-\frac{m^2t^2}{12a^2}\frac{1+\nu}{1-\nu})\lambda$$
$$(\delta_2^2-3\mu_2^2) + \frac{m^2}{\lambda}(1+\frac{m^2t^2}{12a^2}\frac{1+\nu}{1-\nu})],$$

$$P_5[\lambda^2(\delta_2^4+\mu_2^4-6\delta_2^2\mu_2^2) - 2m^2(\delta_2^2-\mu_2^2) + \frac{m^4}{\lambda^2}] + P_6 4\delta_2\mu_2[\lambda^2(\delta_2^2-\mu_2^2) - m^2] =$$
$$C_5\delta_2[(\nu-\frac{m^2t^2}{12a^2}\frac{1+\nu}{1-\nu})\lambda(\delta_2^2-3\mu_2^2) + \frac{m^2}{\lambda}(1+\frac{m^2t^2}{12a^2}\frac{1+\nu}{1-\nu})] + C_6\mu_2[(\nu-\frac{m^2t^2}{12a^2}\frac{1+\nu}{1-\nu})\lambda$$
$$(3\delta_2^2-\mu_2^2) + \frac{m^2}{\lambda}(1+\frac{m^2t^2}{12a^2}\frac{1+\nu}{1-\nu})],$$

$$P_7 4\delta_2\mu_2[\lambda^2(\delta_2^2-\mu_2^2)-m^2] + P_8[\lambda^2(\delta_2^4+\mu_2^4-6\delta_2^2\mu_2^2) - 2m^2(\delta_2^2-\mu_2^2) + \frac{m^4}{\lambda^2}] =$$

$$C_7\mu_2[-(\nu-\frac{m^2t^2}{12a^2}\frac{1+\nu}{1-\nu})\lambda(3\delta_2^2-\mu_2^2)-\frac{m^2}{\lambda}(1+\frac{m^2t^2}{12a^2}\frac{1+\nu}{1-\nu})]+C_8\delta_2[-(\nu-\frac{m^2t^2}{12a^2}\frac{1+\nu}{1-\nu})\lambda$$
$$(\delta_2^2-3\mu_2^2)-\frac{m^2}{\lambda}(1+\frac{m^2t^2}{12a^2}\frac{1+\nu}{1-\nu})],$$

$$P_7[\lambda^2(\delta_2^4+\mu_2^4-6\delta_2^2\mu_2^2)-2m^2(\delta_2^2-\mu_2^2)+\frac{m^4}{\lambda^2}]+P_8 4\delta_2\mu_2[-\lambda^2(\delta_2^2-\mu_2^2)+m^2]=$$
$$C_7\delta_2[-(\nu-\frac{m^2t^2}{12a^2}\frac{1+\nu}{1-\nu})\lambda(\delta_2^2-3\mu_2^2)-\frac{m^2}{\lambda}(1+\frac{m^2t^2}{12a^2}\frac{1+\nu}{1-\nu})]+C_8\mu_2[(\nu-\frac{m^2t^2}{12a^2}\frac{1+\nu}{1-\nu})\lambda$$
$$(3\delta_2^2-\mu_2^2)+\frac{m^2}{\lambda}(1+\frac{m^2t^2}{12a^2}\frac{1+\nu}{1-\nu})].$$

(4.33)

The solution of these simultaneous equations may be presented by the following. First, the following terms are defined.

$$a_{11}=4\delta_1\mu_1[-\lambda^2(\delta_1^2-\mu_1^2)+m^2],$$
$$a_{12}=\lambda^2(\delta_1^4+\mu_1^4-6\delta_1^2\mu_1^2)-2m^2(\delta_1^2-\mu_1^2)+\frac{m^4}{\lambda^2},$$
$$a_{21}=a_{12},\quad a_{22}=-a_{11},$$
$$a_{31}=-a_{11},\quad a_{32}=a_{12},$$
$$a_{41}=a_{12},\quad a_{42}=a_{11},$$
$$a_{51}=4\delta_2\mu_2[-\lambda^2(\delta_2^2-\mu_2^2)+m^2]$$
$$a_{52}=\lambda^2(\delta_2^4+\mu_2^4-6\delta_2^2\mu_2^2)-2m^2(\delta_2^2-\mu_2^2)+\frac{m^4}{\lambda^2}$$
$$a_{61}=a_{52},\quad a_{62}=-a_{51},$$
$$a_{71}=-a_{51},\quad a_{72}=a_{52},$$
$$a_{81}=a_{52},\quad a_{82}=a_{51},$$

(4.34)

and

$$b_{11}=-(\nu-\frac{m^2t^2}{12a^2}\frac{1+\nu}{1-\nu})\lambda(3\delta_1^2-\mu_1^2)-\frac{m^2}{\lambda}(1+\frac{m^2t^2}{12a^2}\frac{1+\nu}{1-\nu})$$
$$b_{12}=(\nu-\frac{m^2t^2}{12a^2}\frac{1+\nu}{1-\nu})\lambda(\delta_1^2-3\mu_1^2)+\frac{m^2}{\lambda}(1+\frac{m^2t^2}{12a^2}\frac{1+\nu}{1-\nu})$$
$$b_{21}=b_{12},\quad b_{22}=-b_{11},$$
$$b_{31}=b_{11},\quad b_{32}=-b_{12},$$
$$b_{41}=-b_{12},\quad b_{42}=-b_{11},$$
$$b_{51}=-(\nu-\frac{m^2t^2}{12a^2}\frac{1+\nu}{1-\nu})\lambda(3\delta_2^2-\mu_2^2)-\frac{m^2}{\lambda}(1+\frac{m^2t^2}{12a^2}\frac{1+\nu}{1-\nu})$$
$$b_{52}=(\nu-\frac{m^2t^2}{12a^2}\frac{1+\nu}{1-\nu})\lambda(\delta_2^2-3\mu_2^2)+\frac{m^2}{\lambda}(1+\frac{m^2t^2}{12a^2}\frac{1+\nu}{1-\nu})$$
$$b_{61}=b_{52},\quad b_{62}=-b_{51},$$
$$b_{71}=b_{51},\quad b_{72}=-b_{52},$$
$$b_{81}=-b_{52},\quad b_{82}=-b_{51}.$$

(4.35)

Introducing the above a_{ij} and b_{ij} into Eq. (4.33) and solving the set of equations, the real constants P_i are then found as

$$P_1 = C_1 \frac{a_{22}\mu_1 b_{11} - a_{12}\delta_1 b_{21}}{a_{11}a_{22} - a_{12}a_{21}} + C_2 \frac{a_{22}\delta_1 b_{12} - a_{12}\mu_1 b_{22}}{a_{11}a_{22} - a_{12}a_{21}}$$

$$P_2 = C_1 \frac{a_{11}\delta_1 b_{21} - a_{21}\mu_1 b_{11}}{a_{11}a_{22} - a_{12}a_{21}} + C_2 \frac{a_{11}\mu_1 b_{22} - a_{21}\delta_1 b_{12}}{a_{11}a_{22} - a_{12}a_{21}}$$

$$P_3 = C_3 \frac{a_{42}\mu_1 b_{31} - a_{32}\delta_1 b_{41}}{a_{31}a_{42} - a_{32}a_{41}} + C_4 \frac{a_{42}\delta_1 b_{32} - a_{32}\mu_1 b_{42}}{a_{31}a_{42} - a_{32}a_{41}}$$

$$P_4 = C_3 \frac{a_{31}\delta_1 b_{41} - a_{41}\mu_1 b_{31}}{a_{31}a_{42} - a_{32}a_{41}} + C_4 \frac{a_{31}\mu_1 b_{42} - a_{41}\delta_1 b_{32}}{a_{31}a_{42} - a_{32}a_{41}}$$

$$P_5 = C_5 \frac{a_{62}\mu_2 b_{51} - a_{52}\delta_2 b_{61}}{a_{51}a_{62} - a_{52}a_{61}} + C_6 \frac{a_{62}\delta_2 b_{52} - a_{52}\mu_2 b_{62}}{a_{51}a_{62} - a_{52}a_{61}}$$

$$P_6 = C_5 \frac{a_{51}\delta_2 b_{61} - a_{61}\mu_2 b_{51}}{a_{51}a_{62} - a_{52}a_{61}} + C_6 \frac{a_{51}\mu_2 b_{62} - a_{61}\delta_2 b_{52}}{a_{51}a_{62} - a_{52}a_{61}}$$

$$P_7 = C_7 \frac{a_{82}\mu_2 b_{71} - a_{72}\delta_2 b_{81}}{a_{71}a_{82} - a_{72}a_{81}} + C_8 \frac{a_{82}\delta_2 b_{72} - a_{72}\mu_2 b_{82}}{a_{71}a_{82} - a_{72}a_{81}}$$

$$P_8 = C_7 \frac{a_{71}\delta_2 b_{81} - a_{81}\mu_2 b_{71}}{a_{71}a_{82} - a_{72}a_{81}} + C_8 \frac{a_{71}\mu_2 b_{82} - a_{81}\delta_2 b_{72}}{a_{71}a_{82} - a_{72}a_{81}} \tag{4.36}$$

Inhomogeneous solution in u

To find a partial solution to Eq. (4.29), $u^0_{mn}(\frac{\lambda}{a}x)$, the following equation is considered

$$\left[\frac{d^4}{dx^4} - \frac{2m^2}{a^2}\frac{d^2}{dx^2} + \frac{m^4}{a^4}\right] u^0_{mn}\left(\frac{\lambda}{a}x\right) = \left[\left(\frac{\nu}{a} - \frac{m^2t^2}{12a^3}\frac{1+\nu}{1-\nu}\right)\frac{d^3}{dx^3} + \left(\frac{m^2}{a^3} + \frac{m^4t^2}{12a^5}\frac{1+\nu}{1-\nu}\right)\frac{d}{dx}\right] f^0_{mn}\left(\frac{\lambda}{a}x\right) - \left[\frac{1-\nu^2}{Et}\frac{d^2}{dx^2} - \frac{2m^2(1+\nu)}{Eta^2}\right] X_{mn}\left(\frac{\lambda}{a}x\right) \tag{4.37}$$

Taking the solution of Eq. (4.37) to be

$$u^0_{mn}\left(\frac{\lambda}{a}x\right) = u_{mn}\sin\left(\frac{\lambda}{a}x\right) \tag{4.38}$$

and substituting it into Equation (4.37), the expression for the terms u_{mn} in terms of w_{mn} and X_{mn} are found as

$$u_{mn} = \frac{\lambda}{(m^2+\lambda^2)^2}\left[\nu\lambda^2 - m^2 - \frac{m^2t^2}{12a^2}\frac{1+\nu}{1-\nu}(m^2+\lambda^2)\right] w_{mn} + \frac{a^2}{(m^2+\lambda^2)^2}\frac{1+\nu}{Et}\left[\lambda^2(1-\nu) + 2m^2\right] X_{mn} \tag{4.39}$$

Thus, the final form of the longitudinal displacement u is gived by

$$\begin{aligned} u &= \Sigma_m\Sigma_n \cos m\phi \; u_{mn}\left(\frac{\lambda}{a}x\right) \\ &= \Sigma_m\Sigma_n\left[e^{\delta_1}\left(\frac{\lambda}{a}x\right)\left(P_1\cos\mu_1\frac{\lambda}{a}x + P_2\sin\mu_1\frac{\lambda}{a}x\right) + e^{-\delta_1}\left(\frac{\lambda}{a}x\right)\left(P_3\cos\mu_1\frac{\lambda}{a}x + P_4\right.\right. \\ &\quad \left.\sin\mu_1\frac{\lambda}{a}x\right) + e^{\delta_2}\left(\frac{\lambda}{a}x\right)\left(P_5\cos\mu_2\frac{\lambda}{a}x + P_6\sin\mu_2\frac{\lambda}{a}x\right) + e^{-\delta_2}\left(\frac{\lambda}{a}x\right)\left(P_7\cos\mu_2\frac{\lambda}{a}x\right. \\ &\quad \left.\left. + P_8\sin\mu_2\frac{\lambda}{a}x\right) + u_{mn}\sin\left(\frac{\lambda}{a}x\right)\right]\cos(m\phi) \quad (m = 0, 1, 2,....\infty;\ n = 1, 2,....\infty) \end{aligned} \tag{4.40}$$

Circumferential displacement v

The circumferential displacement v is found from Eq. (4.10) by dividing it again into homogeneous and inhomogeneous parts as

$$v_{mn}\left(\frac{\lambda}{a}x\right) = \bar{v}_{mn}\left(\frac{\lambda}{a}x\right) + v^0_{mn}\left(\frac{\lambda}{a}x\right) \tag{4.41}$$

Substituting the corresponding Eqs (4.27), (4.41), (4.12), (4.17) and (4.13) into Eq. (4.10) results in

$$\left[\frac{d^4}{dx^4} - \frac{2m^2}{a^2}\frac{d^2}{dx^2} + \frac{m^4}{a^4}\right]\left[\bar{v}_{mn}\left(\frac{\lambda}{a}x\right) + v^0_{mn}\left(\frac{\lambda}{a}x\right)\right] = \left[\frac{m^3}{a^4} - \frac{m(2+\nu)}{a^2}\frac{d^2}{dx^2} + \frac{t^2}{12a^2}\left(\frac{2m}{1-\nu}\frac{d^4}{dx^4}\right.\right.$$
$$\left.\left. - \frac{m^3}{a^2}\frac{3-\nu}{1-\nu}\frac{d^2}{dx^2} + \frac{m^5}{a^4}\right)\right]\left[\bar{f}_{mn}\left(\frac{\lambda}{a}x\right) + f^0_{mn}\left(\frac{\lambda}{a}x\right)\right] - \frac{m(1+\nu)^2}{Eta}\frac{d}{dx}X_{mn}\left(\frac{\lambda}{a}x\right) \tag{4.42}$$

Homogeneous solution in v

To solve $\bar{v}_{mn}\left(\frac{\lambda}{a}x\right)$ by means of $\bar{f}_{mn}\left(\frac{\lambda}{a}x\right)$, the following equation from Eq. (4.42) is considered

$$\left[\frac{d^4}{dx^4} - \frac{2m^2}{a^2}\frac{d^2}{dx^2} + \frac{m^4}{a^4}\right]\bar{v}_{mn}\left(\frac{\lambda}{a}x\right) = \left[\frac{m^3}{a^4} - \frac{m(2+\nu)}{a^2}\frac{d^2}{dx^2} + \frac{t^2}{12a^2}\left(\frac{2m}{1-\nu}\frac{d^4}{dx^4} - \frac{m^3}{a^2}\frac{3-\nu}{1-\nu}\frac{d^2}{dx^2}\right.\right.$$
$$\left.\left. + \frac{m^5}{a^4}\right)\right]\bar{f}_{mn}\left(\frac{\lambda}{a}x\right) \tag{4.43}$$

Hence, the corresponding expression for $\bar{v}_{mn}\left(\frac{\lambda}{a}x\right)$ can be represented by

$$\bar{v}_{mn}\left(\frac{\lambda}{a}x\right) = e^{\delta_1\left(\frac{\lambda}{a}x\right)}\left(Q_1\cos\mu_1\frac{\lambda}{a}x + Q_2\sin\mu_1\frac{\lambda}{a}x\right) + e^{-\delta_1\left(\frac{\lambda}{a}x\right)}\left(Q_3\cos\mu_1\frac{\lambda}{a}x + Q_4\sin\mu_1\frac{\lambda}{a}x\right) + e^{\delta_2\left(\frac{\lambda}{a}x\right)}\left(Q_5\cos\mu_2\frac{\lambda}{a}x + Q_6\sin\mu_2\frac{\lambda}{a}x\right) + e^{-\delta_2\left(\frac{\lambda}{a}x\right)}\left(Q_7\cos\mu_2\frac{\lambda}{a}x + Q_8\sin\mu_2\frac{\lambda}{a}x\right) \tag{4.44}$$

where Q_i are real constants and are related to the real constants C_i of Eq. (4.20).

Taking the same procedure as that for investigating P_i, the relations between Q_i and C_i can be found as:

$$Q_1 = C_1\frac{a_{22}d_{11} - a_{12}d_{21}}{a_{11}a_{22} - a_{12}a_{21}} + C_2\frac{a_{22}d_{12} - a_{12}d_{22}}{a_{11}a_{22} - a_{12}a_{21}}$$

$$Q_2 = C_1\frac{a_{11}d_{21} - a_{21}d_{11}}{a_{11}a_{22} - a_{12}a_{21}} + C_2\frac{a_{11}d_{22} - a_{21}d_{12}}{a_{11}a_{22} - a_{12}a_{21}}$$

$$Q_3 = C_3\frac{a_{42}d_{31} - a_{32}d_{41}}{a_{31}a_{42} - a_{32}a_{41}} + C_4\frac{a_{42}d_{32} - a_{32}d_{42}}{a_{31}a_{42} - a_{32}a_{41}}$$

$$Q_4 = C_3\frac{a_{31}d_{41} - a_{41}d_{31}}{a_{31}a_{42} - a_{32}a_{41}} + C_4\frac{a_{31}d_{42} - a_{41}d_{32}}{a_{31}a_{42} - a_{32}a_{41}}$$

$$Q_5 = C_5\frac{a_{62}d_{51} - a_{52}d_{61}}{a_{51}a_{62} - a_{52}a_{61}} + C_6\frac{a_{62}d_{52} - a_{52}d_{62}}{a_{51}a_{62} - a_{52}a_{61}}$$

$$Q_6 = C_5\frac{a_{51}d_{61} - a_{61}d_{51}}{a_{51}a_{62} - a_{52}a_{61}} + C_6\frac{a_{51}d_{62} - a_{61}d_{52}}{a_{51}a_{62} - a_{52}a_{61}}$$

$$Q_7 = C_7\frac{a_{82}d_{71} - a_{72}d_{81}}{a_{71}a_{82} - a_{72}a_{81}} + C_8\frac{a_{82}d_{72} - a_{72}d_{82}}{a_{71}a_{82} - a_{72}a_{81}}$$

$$Q_8 = C_7\frac{a_{71}d_{81} - a_{81}d_{71}}{a_{71}a_{82} - a_{72}a_{81}} + C_8\frac{a_{71}d_{82} - a_{81}d_{72}}{a_{71}a_{82} - a_{72}a_{81}} \tag{4.45}$$

in which

a_{ij} (i = 1, 2, ... ,8; j = 1,2) are shown in Eq. (4.34), and

$$d_{11} = -\frac{mt^2\lambda^2}{6a^2(1-\nu)}4\delta_1\mu_1(\delta_1^2 - \mu_1^2) + 2\delta_1\mu_1\left[m(2+\nu) + \frac{m^3t^2}{12a^2}\frac{3-\nu}{1-\nu}\right]$$

$$d_{12} = \frac{mt^2\lambda^2}{6a^2(1-\nu)}(\delta_1^4 + \mu_1^4 - 6\delta_1^2\mu_1^2) - (\delta_1^2 - \mu_1^2)\left[m(2+\nu) + \frac{m^3t^2}{12a^2}\frac{3-\nu}{1-\nu}\right] + \frac{m^3}{\lambda^2}\left(1 + \frac{m^2t^2}{12a^2}\right)$$

$$d_{21} = d_{12}\,,\quad d_{22} = -d_{11}\,,$$

$$d_{31} = -d_{11}\,,\quad d_{32} = d_{12}\,,$$

$$d_{41} = d_{12}\ ,\ d_{42} = d_{11}\ ,$$

$$d_{51} = -\frac{mt^2\lambda^2}{6a^2(1-\nu)} 4\delta_2\mu_2(\delta_2^2 - \mu_2^2) + 2\delta_2\mu_2[m(2+\nu) + \frac{m^3t^2}{12a^2}\frac{3-\nu}{1-\nu}]$$

$$d_{52} = \frac{mt^2\lambda^2}{6a^2(1-\nu)}(\delta_2^4 + \mu_2^4 - 6\delta_2^2\mu_2^2) - (\delta_2^2 - \mu_2^2)[m(2+\nu) + \frac{m^3t^2}{12a^2}\frac{3-\nu}{1-\nu}] + \frac{m^3}{\lambda^2}(1 + \frac{m^2t^2}{12a^2})$$

$$d_{61} = d_{52}\ ,\ d_{62} = -d_{51}\ ,$$

$$d_{71} = -d_{51}\ ,\ d_{72} = d_{52}\ ,$$

$$d_{81} = d_{52}\ ,\ d_{82} = d_{51}\ .$$

(4.46)

Inhomogeneous solution in v

The inhomogeneous or partial solution for the function $v^0_{mn}(\frac{\lambda}{a}x)$ is sought in the form

$$v^0_{mn}(\frac{\lambda}{a}x) = v_{mn}\cos(\frac{\lambda}{a}x) \tag{4.47}$$

and determined from the following equation which is associated with Eq. (4.42)

$$[\frac{d^4}{dx^4} - \frac{2m^2}{a^2}\frac{d^2}{dx^2} + \frac{m^4}{a^4}]\, v^0_{mn}(\frac{\lambda}{a}x) = [\frac{m^3}{a^4} - \frac{m(2+\nu)}{a^2}\frac{d^2}{dx^2} + \frac{t^2}{12a^2}(\frac{2m}{1-\nu}\frac{d^4}{dx^4} - \frac{m^3}{a^2}\frac{3-\nu}{1-\nu}\frac{d^2}{dx^2} + \frac{m^5}{a^4})]\, f^0_{mn}(\frac{\lambda}{a}x) - \frac{m(1+\nu)^2}{Eta}\frac{d}{dx}X_{mn}(\frac{\lambda}{a}x)$$

(4.48)

Insertion of Eq (4.47), (4.21) and (4.22) into Eq. (4.48) leads to the expression of v_{mn} in terms of w_{mn} and X_{mn} as

$$v_{mn} = \frac{1}{(m^2+\lambda^2)^2}\{\frac{t^2}{12a^2}\frac{2m}{1-\nu}\lambda^4 + [m(2+\nu) + \frac{m^3t^2}{12a^2}\frac{3-\nu}{1-\nu}]\lambda^2 + m^3(1 + \frac{m^2t^2}{12a^2})\}\, w_{mn} - \frac{1}{(m^2+\lambda^2)^2}\frac{m\lambda a^2(1+\nu)^2}{Et}X_{mn}$$

(4.49)

The general expression for displacement v is then given by

$$v = \Sigma_m\Sigma_n \sin m\phi\ v_{mn}(\frac{\lambda}{a}x)$$

$$= \Sigma_m\Sigma_n [e^{\delta_1}(\frac{\lambda}{a}x)(Q_1\cos\mu_1\frac{\lambda}{a}x + Q_2\sin\mu_1\frac{\lambda}{a}x) + e^{-\delta_1}(\frac{\lambda}{a}x)(Q_3\cos\mu_1\frac{\lambda}{a}x + Q_4 \sin\mu_1\frac{\lambda}{a}x) + e^{\delta_2}(\frac{\lambda}{a}x)(Q_5\cos\mu_2\frac{\lambda}{a}x + Q_6\sin\mu_2\frac{\lambda}{a}x) + e^{-\delta_2}(\frac{\lambda}{a}x)(Q_7\cos\mu_2\frac{\lambda}{a}x + Q_8\sin\mu_2\frac{\lambda}{a}x) + v_{mn}\cos(\frac{\lambda}{a}x)]\sin m\phi \qquad (m = 0, 1, 2, \ldots\infty;\ n = 1, 2, \ldots\infty)$$

(4.50)

The three equations (4.25), (4.40) and (4.50) represent expressions of the three displacements u, v and w of the cylinder under a patch of longitudinal load. It should be noted that these expressions are only suitable for the general case of $m \neq 1$ where m is the circumferential harmonic number. Taking m = 1 as a special case, expressions for the displacements u, v and w are derived in the following section.

4.3.3 Special Case for Harmonic m=1

When m=1, the eight roots of Eq. (4.18) are found to be in a different form from that defined in Eq. (4.19) for the general case of $m \neq 1$. They are instead

$$\begin{aligned} T_1 &= \delta_1 + i\mu_1, \quad & T_3 &= -\delta_1 - i\mu_1, \quad & T_5 &= \delta_2, \quad & T_7 &= i\mu_2, \\ T_2 &= \delta_1 - i\mu_1, \quad & T_4 &= -\delta_1 + i\mu_1, \quad & T_6 &= -\delta_2, \quad & T_8 &= -i\mu_2. \end{aligned} \tag{4.51}$$

Similar to Eq. (4.19), δ_1, δ_2 and μ_1, μ_2 of Eq. (4.51) are general coefficients of real and imaginary parts of the roots of Eq. (4.18) instead of ones with particular values.

Accordingly, the expression for the general solution to the homogeneous equation (4.15), $\bar{f}_{mn}(\frac{\lambda}{a}x)$, differs from that presented in Eq. (4.20). Instead, it is given by

$$\begin{aligned} \bar{f}_{mn}(\tfrac{\lambda}{a}x) = {} & e^{\delta_1(\frac{\lambda}{a}x)}(C_1\cos\mu_1\tfrac{\lambda}{a}x + C_2\sin\mu_1\tfrac{\lambda}{a}x) + e^{-\delta_1(\frac{\lambda}{a}x)}(C_3\cos\mu_1\tfrac{\lambda}{a}x + \\ & C_4\sin\mu_1\tfrac{\lambda}{a}x) + C_5 e^{\delta_2(\frac{\lambda}{a}x)} + C_6 e^{-\delta_2(\frac{\lambda}{a}x)} + C_7\cos\mu_2\tfrac{\lambda}{a}x + C_8\sin\mu_2\tfrac{\lambda}{a}x \end{aligned} \tag{4.52}$$

in which C_i are real arbitrary constants in respect to the eight roots in Eq. (4.51).

Substitution of Eqs (4.52) and (4.21) in Eq. (4.12) yields the general expression for the displacement w

$$\begin{aligned} w = {} & \Sigma_n [\, e^{\delta_1(\frac{\lambda}{a}x)}(C_1\cos\mu_1\tfrac{\lambda}{a}x + C_2\sin\mu_1\tfrac{\lambda}{a}x) + e^{-\delta_1(\frac{\lambda}{a}x)}(C_3\cos\mu_1\tfrac{\lambda}{a}x + C_4\sin\mu_1\tfrac{\lambda}{a}x) \\ & + C_5 e^{\delta_2(\frac{\lambda}{a}x)} + C_6 e^{-\delta_2(\frac{\lambda}{a}x)} + C_7\cos\mu_2\tfrac{\lambda}{a}x + C_8\sin\mu_2\tfrac{\lambda}{a}x + w_{mn}\cos(\tfrac{\lambda}{a}x)\,]\cos m\phi \\ & (m = 1;\ n = 1, 2, \ldots\infty) \end{aligned} \tag{4.53}$$

For the longitudinal displacement u, because the function $\bar{u}_{mn}(\frac{\lambda}{a}x)$ is defined in Eq. (4.31) to be associated with $\bar{f}_{mn}(\frac{\lambda}{a}x)$, it becomes

$$\bar{u}_{mn}(\frac{\lambda}{a}x) = e^{\delta_1(\frac{\lambda}{a}x)}(P_1\cos\mu_1\frac{\lambda}{a}x + P_2\sin\mu_1\frac{\lambda}{a}x) + e^{-\delta_1(\frac{\lambda}{a}x)}(P_3\cos\mu_1\frac{\lambda}{a}x + P_4 \sin\mu_1\frac{\lambda}{a}x) + P_5 e^{\delta_2(\frac{\lambda}{a}x)} + P_6 e^{-\delta_2(\frac{\lambda}{a}x)} + P_7\cos\mu_2\frac{\lambda}{a}x + P_8\sin\mu_2\frac{\lambda}{a}x \tag{4.54}$$

in which P_i are real constants and related to the arbitrary constants C_i in Eq. (4.52).

Taking the same procedure as before, the relationships between P_i and C_i can be found as

$$P_1 = C_1\frac{a_{22}\mu_1 b_{11} - a_{12}\delta_1 b_{21}}{a_{11}a_{22} - a_{12}a_{21}} + C_2\frac{a_{22}\delta_1 b_{12} - a_{12}\mu_1 b_{22}}{a_{11}a_{22} - a_{12}a_{21}}$$

$$P_2 = C_1\frac{a_{11}\delta_1 b_{21} - a_{21}\mu_1 b_{11}}{a_{11}a_{22} - a_{12}a_{21}} + C_2\frac{a_{11}\mu_1 b_{22} - a_{21}\delta_1 b_{12}}{a_{11}a_{22} - a_{12}a_{21}}$$

$$P_3 = C_3\frac{a_{42}\mu_1 b_{31} - a_{32}\delta_1 b_{41}}{a_{31}a_{42} - a_{32}a_{41}} + C_4\frac{a_{42}\delta_1 b_{32} - a_{32}\mu_1 b_{42}}{a_{31}a_{42} - a_{32}a_{41}}$$

$$P_4 = C_3\frac{a_{31}\delta_1 b_{41} - a_{41}\mu_1 b_{31}}{a_{31}a_{42} - a_{32}a_{41}} + C_4\frac{a_{31}\mu_1 b_{42} - a_{41}\delta_1 b_{32}}{a_{31}a_{42} - a_{32}a_{41}}$$

$$P_5 = C_5\frac{\delta_2 b_{51}}{a_{51}}, \qquad P_6 = C_6\frac{\delta_2 b_{61}}{a_{61}}$$

$$P_7 = C_8\frac{\mu_2 b_{71}}{a_{71}}, \qquad P_8 = C_7\frac{\mu_2 b_{81}}{a_{81}}$$

(4.55)

in which

$$a_{11} = 4\delta_1\mu_1[-\lambda^2(\delta_1^2 - \mu_1^2) + m^2],$$
$$a_{12} = \lambda^2(\delta_1^4 + \mu_1^4 - 6\delta_1^2\mu_1^2) - 2m^2(\delta_1^2 - \mu_1^2) + \frac{m^4}{\lambda^2},$$
$$a_{21} = a_{12}, \quad a_{22} = -a_{11},$$
$$a_{31} = -a_{11}, \quad a_{32} = a_{12},$$
$$a_{41} = a_{12}, \quad a_{42} = a_{11},$$
$$a_{51} = \lambda^2\delta_2^4 - 2m^2\delta_2^2 + \frac{m^4}{\lambda^2},$$
$$a_{61} = a_{51},$$
$$a_{71} = \lambda^2\mu_2^4 + 2m^2\mu_2^2 + \frac{m^4}{\lambda^2},$$
$$a_{81} = a_{71}.$$

(4.56)

and

$$b_{11} = -(\nu - \frac{m^2t^2}{12a^2}\frac{1+\nu}{1-\nu})\lambda(3\delta_1^2 - \mu_1^2) - \frac{m^2}{\lambda}(1 + \frac{m^2t^2}{12a^2}\frac{1+\nu}{1-\nu}),$$
$$b_{12} = (\nu - \frac{m^2t^2}{12a^2}\frac{1+\nu}{1-\nu})\lambda(\delta_1^2 - 3\mu_1^2) + \frac{m^2}{\lambda}(1 + \frac{m^2t^2}{12a^2}\frac{1+\nu}{1-\nu}),$$

$$
\begin{aligned}
b_{21} &= b_{12}\,, \quad b_{22} = -b_{11}\,,\\
b_{31} &= b_{11}\,, \quad b_{32} = -b_{12}\,,\\
b_{41} &= -b_{12}\,, \quad b_{42} = -b_{11}\,,\\
b_{51} &= \lambda\delta_2^2\,(\nu - \frac{m^2t^2}{12a^2}\,\frac{1+\nu}{1-\nu}) + \frac{m^2}{\lambda}(1 + \frac{m^2t^2}{12a^2}\,\frac{1+\nu}{1-\nu})\,,\\
b_{61} &= -b_{51}\,,\\
b_{71} &= -\lambda\,\mu_2^2\,(\nu - \frac{m^2t^2}{12a^2}\,\frac{1+\nu}{1-\nu})) + \frac{m^2}{\lambda}(1 + \frac{m^2t^2}{12a^2}\,\frac{1+\nu}{1-\nu})\,,\\
b_{81} &= -b_{71}\,.
\end{aligned}
\tag{4.57}
$$

The expression for the longitudinal displacement u can therefore be written as

$$
\begin{aligned}
u = \Sigma_n [\, & e^{\delta_1(\frac{\lambda}{a}x)}(P_1 \cos\mu_1\tfrac{\lambda}{a}x + P_2 \sin\mu_1\tfrac{\lambda}{a}x) + e^{-\delta_1(\frac{\lambda}{a}x)}(P_3\cos\mu_1\tfrac{\lambda}{a}x + P_4\sin\mu_1\tfrac{\lambda}{a}x) +\\
& P_5 e^{\delta_2(\frac{\lambda}{a}x)} + P_6 e^{-\delta_2(\frac{\lambda}{a}x)} + P_7\cos\mu_2\tfrac{\lambda}{a}x + P_8\sin\mu_2\tfrac{\lambda}{a}x + u_{mn}\sin(\tfrac{\lambda}{a}x)\,]\cos(m\phi)\\
& (m = 1;\ n = 1, 2, \ldots\ldots\infty)
\end{aligned}
\tag{4.58}
$$

and similarly the circumferential displacement v can be found by solving Eq. (4.43) to give

$$
\begin{aligned}
\bar{v}_{mn}(\tfrac{\lambda}{a}x) = {} & e^{\delta_1(\frac{\lambda}{a}x)}(Q_1\cos\mu_1\tfrac{\lambda}{a}x + Q_2\sin\mu_1\tfrac{\lambda}{a}x) + e^{-\delta_1(\frac{\lambda}{a}x)}(Q_3\cos\mu_1\tfrac{\lambda}{a}x + Q_4\\
& \sin\mu_1\tfrac{\lambda}{a}x) + Q_5 e^{\delta_2(\frac{\lambda}{a}x)} + Q_6 e^{-\delta_2(\frac{\lambda}{a}x)} + Q_7\cos\mu_2\tfrac{\lambda}{a}x + Q_8\sin\mu_2\tfrac{\lambda}{a}x
\end{aligned}
\tag{4.59}
$$

in which Q_i are real constants and are related to the C_i of Eq. (4.52).

The relations between Q_i and C_i can be found by solving Eq. (4.43) after inserting Eqs (4.59) and (4.52) into it, yielding

$$
\begin{aligned}
Q_1 &= C_1\,\frac{a_{22}d_{11} - a_{12}d_{21}}{a_{11}a_{22} - a_{12}a_{21}} + C_2\,\frac{a_{22}d_{12} - a_{12}d_{22}}{a_{11}a_{22} - a_{12}a_{21}}\\
Q_2 &= C_1\,\frac{a_{11}d_{21} - a_{21}d_{11}}{a_{11}a_{22} - a_{12}a_{21}} + C_2\,\frac{a_{11}d_{22} - a_{21}d_{12}}{a_{11}a_{22} - a_{12}a_{21}}\\
Q_3 &= C_3\,\frac{a_{42}d_{31} - a_{32}d_{41}}{a_{31}a_{42} - a_{32}a_{41}} + C_4\,\frac{a_{42}d_{32} - a_{32}d_{42}}{a_{31}a_{42} - a_{32}a_{41}}\\
Q_4 &= C_3\,\frac{a_{31}d_{41} - a_{41}d_{31}}{a_{31}a_{42} - a_{32}a_{41}} + C_4\,\frac{a_{31}d_{42} - a_{41}d_{32}}{a_{31}a_{42} - a_{32}a_{41}}
\end{aligned}
$$

$$Q_5 = C_5 \frac{d_{51}}{a_{51}}, \qquad Q_6 = C_6 \frac{d_{61}}{a_{61}}$$

$$Q_7 = C_7 \frac{d_{71}}{a_{71}}, \qquad Q_8 = C_8 \frac{d_{81}}{a_{81}} \tag{4.60}$$

in which

$$d_{11} = -\frac{mt^2\lambda^2}{6a^2(1-\nu)} 4\delta_1\mu_1(\delta_1^2 - \mu_1^2) + 2\delta_1\mu_1[m(2+\nu) + \frac{m^3t^2}{12a^2}\frac{3-\nu}{1-\nu}],$$

$$d_{12} = \frac{mt^2\lambda^2}{6a^2(1-\nu)}(\delta_1^4 + \mu_1^4 - 6\delta_1^2\mu_1^2) - (\delta_1^2 - \mu_1^2)[m(2+\nu) + \frac{m^3t^2}{12a^2}\frac{3-\nu}{1-\nu}] + \frac{m^3}{\lambda^2}(1 + \frac{m^2t^2}{12a^2}),$$

$$d_{21} = d_{12}, \quad d_{22} = -d_{11},$$

$$d_{31} = -d_{11}, \quad d_{32} = d_{12},$$

$$d_{41} = d_{12}, \quad d_{42} = d_{11},$$

$$d_{51} = \frac{mt^2\lambda^2}{6a^2(1-\nu)}\delta_2^4 - [m(2+\nu) + \frac{m^3t^2}{12a^2}\frac{3-\nu}{1-\nu}]\delta_2^2 + \frac{m^3}{\lambda^2}(1 + \frac{m^2t^2}{12a^2}),$$

$$d_{61} = d_{51},$$

$$d_{71} = \frac{mt^2\lambda^2}{6a^2(1-\nu)}\mu_2^4 + [m(2+\nu) + \frac{m^3t^2}{12a^2}\frac{3-\nu}{1-\nu}]\mu_2^2 + \frac{m^3}{\lambda^2}(1 + \frac{m^2t^2}{12a^2}),$$

$$d_{81} = d_{71}.$$

(4.61)

Thus, in the special case of m=1 , the circumferential displacement v may be expressed as

$$v = \Sigma_n [e^{\delta_1}(\frac{\lambda}{a}x)(Q_1 \cos\mu_1\frac{\lambda}{a}x + Q_2 \sin\mu_1\frac{\lambda}{a}x) + e^{-\delta_1}(\frac{\lambda}{a}x)(Q_3 \cos\mu_1\frac{\lambda}{a}x + Q_4 \sin\mu_1\frac{\lambda}{a}x)$$
$$+ Q_5 e^{\delta_2}(\frac{\lambda}{a}x) + Q_6 e^{-\delta_2}(\frac{\lambda}{a}x) + Q_7 \cos\mu_2\frac{\lambda}{a}x + Q_8 \sin\mu_2\frac{\lambda}{a}x + v_{mn}\cos(\frac{\lambda}{a}x)] \sin m\phi$$
$$(m = 1; n = 1, 2, \ldots\infty) \tag{4.62}$$

4.3.4 General Case of Expressions of Stress Resultants

The expression for the three displacements u, v and w presented in the preceding sections all contain eight arbitrary constants regardless of whether m=1 or m≠1. These arbitrary constants must be determined from eight edge conditions at the two ends of the cylindrical shell. This means that the three displacements u, v and w must satisfy the relevant eight edge conditions. When the eight arbitrary constants have been found, the three displacements are completely defined. The stresses in the cylindrical shell may then be calculated from the derived displacements.

According to thin-shell theory [Timoshenko, 1940, 1959], the relevant membrane and shear forces and bending and twisting moments may be derived from the displacements u, v and w using Eqs (4.2) and (4.3) as

$$
\begin{aligned}
N_x &= \frac{Et}{1-\nu^2}\left[\frac{\partial u}{\partial x} + \frac{\nu}{a}\left(\frac{\partial v}{\partial \phi} - w\right)\right] \\
N_\phi &= \frac{Et}{1-\nu^2}\left[\frac{1}{a}\left(\frac{\partial v}{\partial \phi} - w\right) + \nu\frac{\partial u}{\partial x}\right)\right] \\
N_{x\phi} &= \frac{Et}{2(1+\nu)}\left(\frac{\partial u}{a\partial \phi} + \frac{\partial v}{\partial x}\right) \\
M_x &= -D\left[\frac{\partial^2 w}{\partial x^2} + \frac{\nu}{a^2}\left(\frac{\partial v}{\partial \phi} + \frac{\partial^2 w}{\partial \phi^2}\right)\right] \\
M_\phi &= -D\left[\frac{1}{a^2}\left(\frac{\partial v}{\partial \phi} + \frac{\partial^2 w}{\partial \phi^2}\right) + \nu\frac{\partial^2 w}{\partial x^2}\right] \\
M_{x\phi} &= D(1-\nu)\frac{1}{a}\left(\frac{\partial v}{\partial x} + \frac{\partial^2 w}{\partial x \partial \phi}\right)
\end{aligned}
\tag{4.63}
$$

To find the stresses in a cylindrical shell caused by a longitudinal patch load as shown in Fig. 4-1, appropriate boundary conditions must first be defined.

Assuming that both ends of the shell are simply supported, the boundary conditions are given by

$$
\begin{aligned}
&\text{when } x = 0, \quad w = v = u = M_x = 0, \text{ and} \\
&\text{when } x = l, \quad w = v = N_x = M_x = 0.
\end{aligned}
\tag{4.64}
$$

Introducing the above boundary conditions into the expressions for displacements leads to a set of eight equations. Solving the set of equations then yields the eight arbitrary constants. Since different values of m result in different expressions for displacements, the general case of m ≠1 is considered here first.

For the conditions of w = 0 at x = 0 and x=l respectively, the boundary conditions inserted into Eq. (4.25) yield the two conditions relating to w

$$C_1 + C_3 + C_5 + C_7 = -w_{mn} \tag{4.65}$$

$$C_1 e^{\delta_1(\frac{\lambda}{a}1)}\cos\mu_1\frac{\lambda}{a}1 + C_2 e^{\delta_1(\frac{\lambda}{a}1)}\sin\mu_1\frac{\lambda}{a}1 + C_3 e^{-\delta_1(\frac{\lambda}{a}1)}\cos\mu_1\frac{\lambda}{a}1 + C_4 e^{-\delta_1(\frac{\lambda}{a}1)}\sin\mu_1\frac{\lambda}{a}1$$
$$+ C_5 e^{\delta_2(\frac{\lambda}{a}1)}\cos\mu_2\frac{\lambda}{a}1 + C_6 e^{\delta_2(\frac{\lambda}{a}1)}\sin\mu_2\frac{\lambda}{a}1 + C_7 e^{-\delta_2(\frac{\lambda}{a}1)}\cos\mu_2\frac{\lambda}{a}1 + C_8 e^{-\delta_2(\frac{\lambda}{a}1)}$$
$$\sin\mu_2\frac{\lambda}{a}1 = -w_{mn}\cos\frac{\lambda}{a}1 \tag{4.66}$$

and for v = 0 at x = 0, l; Eq. (4.50) gives two further conditions

$$Q_1 + Q_3 + Q_5 + Q_7 = -v_{mn} \tag{4.67}$$

$$Q_1 e^{\delta_1(\frac{\lambda}{a}1)}\cos\mu_1\frac{\lambda}{a}1 + Q_2 e^{\delta_1(\frac{\lambda}{a}1)}\sin\mu_1\frac{\lambda}{a}1 + Q_3 e^{-\delta_1(\frac{\lambda}{a}1)}\cos\mu_1\frac{\lambda}{a}1 + Q_4 e^{-\delta_1(\frac{\lambda}{a}1)}\sin\mu_1\frac{\lambda}{a}1$$
$$+ Q_5 e^{\delta_2(\frac{\lambda}{a}1)}\cos\mu_2\frac{\lambda}{a}1 + Q_6 e^{\delta_2(\frac{\lambda}{a}1)}\sin\mu_2\frac{\lambda}{a}1 + Q_7 e^{-\delta_2(\frac{\lambda}{a}1)}\cos\mu_2\frac{\lambda}{a}1 + Q_8 e^{-\delta_2(\frac{\lambda}{a}1)}$$
$$\sin\mu_2\frac{\lambda}{a}1 = -v_{mn}\cos\frac{\lambda}{a}1 \tag{4.68}$$

Making use of Eq. (4.45), Q_i is replaced by C_i in the above equations as follows

$$C_1\frac{a_{22}d_{11} - a_{12}d_{21}}{a_{11}a_{22} - a_{12}a_{21}} + C_2\frac{a_{22}d_{12} - a_{12}d_{22}}{a_{11}a_{22} - a_{12}a_{21}} + C_3\frac{a_{42}d_{31} - a_{32}d_{41}}{a_{31}a_{42} - a_{32}a_{41}} + C_4$$
$$\frac{a_{42}d_{32} - a_{32}d_{42}}{a_{31}a_{42} - a_{32}a_{41}} + C_5\frac{a_{62}d_{51} - a_{52}d_{61}}{a_{51}a_{62} - a_{52}a_{61}} + C_6\frac{a_{62}d_{52} - a_{52}d_{62}}{a_{51}a_{62} - a_{52}a_{61}} + C_7$$
$$\frac{a_{82}d_{71} - a_{72}d_{81}}{a_{71}a_{82} - a_{72}a_{81}} + C_8\frac{a_{82}d_{72} - a_{72}d_{82}}{a_{71}a_{82} - a_{72}a_{81}} = -v_{mn} \tag{4.69}$$

$$C_1 e^{\delta_1(\frac{\lambda}{a}1)}\left[\frac{a_{22}d_{11} - a_{12}d_{21}}{a_{11}a_{22} - a_{12}a_{21}}\cos\mu_1\frac{\lambda}{a}1 + \frac{a_{11}d_{21} - a_{21}d_{11}}{a_{11}a_{22} - a_{12}a_{21}}\sin\mu_1\frac{\lambda}{a}1\right] + C_2 e^{\delta_1(\frac{\lambda}{a}1)}$$
$$\left[\frac{a_{22}d_{12} - a_{12}d_{22}}{a_{11}a_{22} - a_{12}a_{21}}\cos\mu_1\frac{\lambda}{a}1 + \frac{a_{11}d_{22} - a_{21}d_{12}}{a_{11}a_{22} - a_{12}a_{21}}\sin\mu_1\frac{\lambda}{a}1\right] + C_3 e^{-\delta_1(\frac{\lambda}{a}1)}$$
$$\left[\frac{a_{42}d_{31} - a_{32}d_{41}}{a_{31}a_{42} - a_{32}a_{41}}\cos\mu_1\frac{\lambda}{a}1 + \frac{a_{31}d_{41} - a_{41}d_{31}}{a_{31}a_{42} - a_{32}a_{41}}\sin\mu_1\frac{\lambda}{a}1\right] + C_4 e^{-\delta_1(\frac{\lambda}{a}1)}$$
$$\left[\frac{a_{42}d_{32} - a_{32}d_{42}}{a_{31}a_{42} - a_{32}a_{41}}\cos\mu_1\frac{\lambda}{a}1 + \frac{a_{31}d_{42} - a_{41}d_{32}}{a_{31}a_{42} - a_{32}a_{41}}\sin\mu_1\frac{\lambda}{a}1\right] + C_5 e^{\delta_2(\frac{\lambda}{a}1)}$$
$$\left[\frac{a_{62}d_{51} - a_{52}d_{61}}{a_{51}a_{62} - a_{52}a_{61}}\cos\mu_2\frac{\lambda}{a}1 + \frac{a_{51}d_{61} - a_{61}d_{51}}{a_{51}a_{62} - a_{52}a_{61}}\sin\mu_2\frac{\lambda}{a}1\right] + C_6 e^{\delta_2(\frac{\lambda}{a}1)}$$
$$\left[\frac{a_{62}d_{52} - a_{52}d_{62}}{a_{51}a_{62} - a_{52}a_{61}}\cos\mu_2\frac{\lambda}{a}1 + \frac{a_{51}d_{62} - a_{61}d_{52}}{a_{51}a_{62} - a_{52}a_{61}}\sin\mu_2\frac{\lambda}{a}1\right] + C_7 e^{-\delta_2(\frac{\lambda}{a}1)}$$
$$\left[\frac{a_{82}d_{71} - a_{72}d_{81}}{a_{71}a_{82} - a_{72}a_{81}}\cos\mu_2\frac{\lambda}{a}1 + \frac{a_{71}d_{81} - a_{81}d_{71}}{a_{71}a_{82} - a_{72}a_{81}}\sin\mu_2\frac{\lambda}{a}1\right] + Q_8 e^{-\delta_2(\frac{\lambda}{a}1)}$$

$$\left[\frac{a_{82}d_{72} - a_{72}d_{82}}{a_{71}a_{82} - a_{72}a_{81}}\cos\mu_2\frac{\lambda}{a}1 + \frac{a_{71}d_{82} - a_{81}d_{72}}{a_{71}a_{82} - a_{72}a_{81}}\sin\mu_2\frac{\lambda}{a}1\right] = -v_{mn}\cos\frac{\lambda}{a}1 \tag{4.70}$$

The boundary condition u = 0 at x = 0 used in Eq. (4.40) produces the single condition

$$P_1 + P_3 + P_5 + P_7 = 0 \tag{4.71}$$

Again using Eq. (4.36) to replace P_i with C_i in Equation (4.71) gives

$$\begin{aligned}
&C_1\frac{a_{22}\mu_1b_{11} - a_{12}\delta_1b_{21}}{a_{11}a_{22} - a_{12}a_{21}} + C_2\frac{a_{22}\delta_1b_{12} - a_{12}\mu_1b_{22}}{a_{11}a_{22} - a_{12}a_{21}} + C_3\frac{a_{42}\mu_1b_{31} - a_{32}\delta_1b_{41}}{a_{31}a_{42} - a_{32}a_{41}} + C_4\\
&\frac{a_{42}\delta_1b_{32} - a_{32}\mu_1b_{42}}{a_{31}a_{42} - a_{32}a_{41}} + C_5\frac{a_{62}\mu_2b_{51} - a_{52}\delta_2b_{61}}{a_{51}a_{62} - a_{52}a_{61}} + C_6\frac{a_{62}\delta_2b_{52} - a_{52}\mu_2b_{62}}{a_{51}a_{62} - a_{52}a_{61}} + C_7\\
&\frac{a_{82}\mu_2b_{71} - a_{72}\delta_2b_{81}}{a_{71}a_{82} - a_{72}a_{81}} + C_8\frac{a_{82}\delta_2b_{72} - a_{72}\mu_2b_{82}}{a_{71}a_{82} - a_{72}a_{81}} = 0
\end{aligned} \tag{4.72}$$

The second boundary condition relating to the axial direction is $N_x = 0$ at x = 1. Here N_x is given by Eq. (4.63), thus implying $\frac{\partial u}{\partial x} = 0$. Applying this condition into Eq. (4.40) yields

$$\begin{aligned}
&P_1e^{\delta_1(\frac{\lambda}{a}1)}(\delta_1\cos\mu_1\frac{\lambda}{a}1 - \mu_1\sin\mu_1\frac{\lambda}{a}1) + P_2e^{\delta_1(\frac{\lambda}{a}1)}(\delta_1\sin\mu_1\frac{\lambda}{a}1 + \mu_1\cos\mu_1\frac{\lambda}{a}1) + P_3\\
&e^{-\delta_1(\frac{\lambda}{a}1)}(-\delta_1\cos\mu_1\frac{\lambda}{a}1 - \mu_1\sin\mu_1\frac{\lambda}{a}1) + P_4e^{-\delta_1(\frac{\lambda}{a}1)}(-\delta_1\sin\mu_1\frac{\lambda}{a}1 + \mu_1\cos\mu_1\frac{\lambda}{a}1)\\
&+ P_5e^{\delta_2(\frac{\lambda}{a}1)}(\delta_2\cos\mu_2\frac{\lambda}{a}1 - \mu_2\sin\mu_2\frac{\lambda}{a}1) + P_6e^{\delta_2(\frac{\lambda}{a}1)}(\delta_2\sin\mu_2\frac{\lambda}{a}1 + \mu_2\cos\mu_2\frac{\lambda}{a}1)\\
&+ P_7e^{-\delta_2(\frac{\lambda}{a}1)}(-\delta_2\cos\mu_2\frac{\lambda}{a}1 - \mu_2\sin\mu_2\frac{\lambda}{a}1) + P_8e^{-\delta_2(\frac{\lambda}{a}1)}(-\delta_2\sin\mu_2\frac{\lambda}{a}1 + \mu_2\cos\mu_2\frac{\lambda}{a}1)\\
&= -u_{mn}\cos\frac{\lambda}{a}1
\end{aligned} \tag{4.73}$$

After substitution of C_i for P_i using Eq. (4.36), the condition becomes

$$\begin{aligned}
&C_1e^{\delta_1(\frac{\lambda}{a}1)}\left[\frac{a_{22}\mu_1b_{11} - a_{12}\delta_1b_{21}}{a_{11}a_{22} - a_{12}a_{21}}(\delta_1\cos\mu_1\frac{\lambda}{a}1 - \mu_1\sin\mu_1\frac{\lambda}{a}1) + \frac{a_{11}\delta_1b_{21} - a_{21}\mu_1b_{11}}{a_{11}a_{22} - a_{12}a_{21}}(\delta_1\sin\mu_1\frac{\lambda}{a}1\right.\\
&\left. + \mu_1\cos\mu_1\frac{\lambda}{a}1)\right] + C_2e^{\delta_1(\frac{\lambda}{a}1)}\left[\frac{a_{22}\delta_1b_{12} - a_{12}\mu_1b_{22}}{a_{11}a_{22} - a_{12}a_{21}}(\delta_1\cos\mu_1\frac{\lambda}{a}1 - \mu_1\sin\mu_1\frac{\lambda}{a}1) +\right.\\
&\left.\frac{a_{11}\mu_1b_{22} - a_{21}\delta_1b_{12}}{a_{11}a_{22} - a_{12}a_{21}}(\delta_1\sin\mu_1\frac{\lambda}{a}1 + \mu_1\cos\mu_1\frac{\lambda}{a}1)\right] + C_3e^{-\delta_1(\frac{\lambda}{a}1)}\left[\frac{a_{42}\mu_1b_{31} - a_{32}\delta_1b_{41}}{a_{31}a_{42} - a_{32}a_{41}}\right.\\
&\left.(-\delta_1\cos\mu_1\frac{\lambda}{a}1 - \mu_1\sin\mu_1\frac{\lambda}{a}1) + \frac{a_{31}\delta_1b_{41} - a_{41}\mu_1b_{31}}{a_{31}a_{42} - a_{32}a_{41}}(-\delta_1\sin\mu_1\frac{\lambda}{a}1 + \mu_1\cos\mu_1\frac{\lambda}{a}1)\right] +\\
&C_4e^{-\delta_1(\frac{\lambda}{a}1)}\left[\frac{a_{42}\delta_1b_{32} - a_{32}\mu_1b_{42}}{a_{31}a_{42} - a_{32}a_{41}}(-\delta_1\cos\mu_1\frac{\lambda}{a}1 - \mu_1\sin\mu_1\frac{\lambda}{a}1) + \frac{a_{31}\mu_1b_{42} - a_{41}\delta_1b_{32}}{a_{31}a_{42} - a_{32}a_{41}}\right.\\
&\left.(-\delta_1\sin\mu_1\frac{\lambda}{a}1 + \mu_1\cos\mu_1\frac{\lambda}{a}1)\right] + C_5e^{\delta_2(\frac{\lambda}{a}1)}\left[\frac{a_{62}\mu_2b_{51} - a_{52}\delta_2b_{61}}{a_{51}a_{62} - a_{52}a_{61}}(\delta_2\cos\mu_2\frac{\lambda}{a}1\right.\\
&\left. - \mu_2\sin\mu_2\frac{\lambda}{a}1) + \frac{a_{51}\mu_2b_{61} - a_{61}\delta_2b_{51}}{a_{51}a_{62} - a_{52}a_{61}}(\delta_2\sin\mu_2\frac{\lambda}{a}1 + \mu_2\cos\mu_2\frac{\lambda}{a}1)\right] +
\end{aligned}$$

$$C_6 e^{\delta_2(\frac{\lambda}{a}1)}\left[\frac{a_{62}\delta_2 b_{52} - a_{52}\mu_2 b_{62}}{a_{51}a_{62} - a_{52}a_{61}}\left(\delta_2 \cos \mu_2\frac{\lambda}{a}1 - \mu_2 \sin \mu_2\frac{\lambda}{a}1\right) + \frac{a_{51}\mu_2 b_{62} - a_{61}\delta_2 b_{52}}{a_{51}a_{62} - a_{52}a_{61}}\right.$$
$$\left.\left(\delta_2 \sin \mu_2\frac{\lambda}{a}1 + \mu_2 \cos \mu_2\frac{\lambda}{a}1\right)\right] + C_7 e^{-\delta_2(\frac{\lambda}{a}1)}\left[\frac{a_{82}\mu_2 b_{71} - a_{72}\delta_2 b_{81}}{a_{71}a_{82} - a_{72}a_{81}}\left(-\delta_2 \cos \mu_2\frac{\lambda}{a}1 -\right.\right.$$
$$\left.\left.\mu_2 \sin \mu_2\frac{\lambda}{a}1\right) + \frac{a_{71}\delta_2 b_{81} - a_{81}\mu_2 b_{71}}{a_{71}a_{82} - a_{72}a_{81}}\left(-\delta_2 \sin \mu_2\frac{\lambda}{a}1 + \mu_2 \cos \mu_2\frac{\lambda}{a}1\right)\right] +$$
$$C_8 e^{-\delta_2(\frac{\lambda}{a}1)}\left[\frac{a_{82}\delta_2 b_{72} - a_{72}\mu_2 b_{82}}{a_{71}a_{82} - a_{72}a_{81}}\left(-\delta_2 \cos \mu_2\frac{\lambda}{a}1 - \mu_2 \sin \mu_2\frac{\lambda}{a}1\right) + \frac{a_{71}\mu_2 b_{82} - a_{81}\delta_2 b_{72}}{a_{71}a_{82} - a_{72}a_{81}}\right.$$
$$\left.\left(-\delta_2 \sin \mu_2\frac{\lambda}{a}1 + \mu_2 \cos \mu_2\frac{\lambda}{a}1\right)\right] = -u_{mn}\cos\frac{\lambda}{a}1 \tag{4.74}$$

The final two boundary conditions are for longitudinal bending at the ends, and require $M_x = 0$ at $x = 0, 1$. The moment M_x is given by Eq. (4.63), which can be converted to $\frac{\partial^2 w}{\partial x^2} = 0$ at $x = 0$ and $x = 1$. The following equations are then obtained from Eq. (4.25).

$$(\delta_1^2 - \mu_1^2)(C_1 + C_3) + 2\delta_1\mu_1(C_2 - C_4) + (\delta_2^2 - \mu_2^2)(C_5 + C_7) + 2\delta_2\mu_2(C_6 - C_8) = w_{mn} \tag{4.75}$$

and

$$C_1 e^{\delta_1(\frac{\lambda}{a}1)}\left[(\delta_1^2 - \mu_1^2)\cos\mu_1\frac{\lambda}{a}1 - 2\delta_1\mu_1 \sin\mu_1\frac{\lambda}{a}1\right] + C_2 e^{\delta_1(\frac{\lambda}{a}1)}\left[(\delta_1^2 - \mu_1^2)\sin\mu_1\frac{\lambda}{a}1 +\right.$$
$$\left.2\delta_1\mu_1 \cos\mu_1\frac{\lambda}{a}1\right] + C_3 e^{-\delta_1(\frac{\lambda}{a}1)}\left[(\delta_1^2 - \mu_1^2)\cos\mu_1\frac{\lambda}{a}1 + 2\delta_1\mu_1 \sin\mu_1\frac{\lambda}{a}1\right] + C_4 e^{-\delta_1(\frac{\lambda}{a}1)}$$
$$\left[(\delta_1^2 - \mu_1^2)\sin\mu_1\frac{\lambda}{a}1 - 2\delta_1\mu_1 \cos\mu_1\frac{\lambda}{a}1\right] + C_5 e^{\delta_2(\frac{\lambda}{a}1)}\left[(\delta_2^2 - \mu_2^2)\cos\mu_2\frac{\lambda}{a}1 - 2\delta_2\mu_2\right.$$
$$\left.\sin\mu_2\frac{\lambda}{a}1\right] + C_6 e^{\delta_2(\frac{\lambda}{a}1)}\left[(\delta_2^2 - \mu_2^2)\sin\mu_2\frac{\lambda}{a}1 + 2\delta_2\mu_2 \cos\mu_2\frac{\lambda}{a}1\right] + C_7 e^{-\delta_2(\frac{\lambda}{a}1)}$$
$$\left[(\delta_2^2 - \mu_2^2)\cos\mu_2\frac{\lambda}{a}1 + 2\delta_2\mu_2 \sin\mu_2\frac{\lambda}{a}1\right] + C_8 e^{-\delta_2(\frac{\lambda}{a}1)}\left[(\delta_2^2 - \mu_2^2)\sin\mu_2\frac{\lambda}{a}1 -\right.$$
$$\left.2\delta_2\mu_2 \cos\mu_2\frac{\lambda}{a}1\right] = w_{mn}\cos\frac{\lambda}{a}1 \tag{4.76}$$

The eight real constants C_i can be found by solving the eight equations (4.65), (4.66), (4.68), (4.70), (4.72), (4.74), (4.75), and (4.76). The constants P_i and Q_i, which have been expressed in terms of C_i, can then be found from C_i using Eqs (4.36) and (4.45).

The real constants C_i, P_i and Q_i have now been determined. This indicates that the associated displacements of the cylindrical shell under these boundary conditions are completely known.

Stress Resultants

The stress resultants are represented by Eqs. (4.63) and can be computed using the following expressions

$$N_x = \frac{Et}{1-\nu^2} \Sigma_m \Sigma_n \frac{\lambda}{a} \{ e^{\delta_1}(\frac{\lambda}{a}x)[P_1(\delta_1 \cos \mu_1 \frac{\lambda}{a}x - \mu_1 \sin \mu_1 \frac{\lambda}{a}x) + P_2(\delta_1 \sin \mu_1 \frac{\lambda}{a}x + \mu_1 \cos \mu_1 \frac{\lambda}{a}x)] + e^{-\delta_1}(\frac{\lambda}{a}x)[P_3(-\delta_1 \cos \mu_1 \frac{\lambda}{a}x - \mu_1 \sin \mu_1 \frac{\lambda}{a}x) + P_4(-\delta_1 \sin \mu_1 \frac{\lambda}{a}x + \mu_1 \cos \mu_1 \frac{\lambda}{a}x)] + e^{\delta_2}(\frac{\lambda}{a}x)[P_5(\delta_2 \cos \mu_2 \frac{\lambda}{a}x - \mu_2 \sin \mu_2 \frac{\lambda}{a}x) + P_6(\delta_2 \sin \mu_2 \frac{\lambda}{a}x + \mu_2 \cos \mu_2 \frac{\lambda}{a}x)] + e^{-\delta_2}(\frac{\lambda}{a}x)[P_7(-\delta_2 \cos \mu_2 \frac{\lambda}{a}x - \mu_2 \sin \mu_2 \frac{\lambda}{a}x) + P_8(-\delta_2 \sin \mu_2 \frac{\lambda}{a}x + \mu_2 \cos \mu_2 \frac{\lambda}{a}x)] + u_{mn} \cos(\frac{\lambda}{a}x) + \frac{\nu}{\lambda} m [e^{\delta_1}(\frac{\lambda}{a}x)(Q_1 \cos \mu_1 \frac{\lambda}{a}x + Q_2 \sin \mu_1 \frac{\lambda}{a}x) + e^{-\delta_1}(\frac{\lambda}{a}x)(Q_3 \cos \mu_1 \frac{\lambda}{a}x + Q_4 \sin \mu_1 \frac{\lambda}{a}x) + e^{\delta_2}(\frac{\lambda}{a}x)(Q_5 \cos \mu_2 \frac{\lambda}{a}x + Q_6 \sin \mu_2 \frac{\lambda}{a}x) + e^{-\delta_2}(\frac{\lambda}{a}x)(Q_7 \cos \mu_2 \frac{\lambda}{a}x + Q_8 \sin \mu_2 \frac{\lambda}{a}x) + v_{mn} \cos(\frac{\lambda}{a}x)] - \frac{\nu}{\lambda}[e^{\delta_1}(\frac{\lambda}{a}x)(C_1 \cos \mu_1 \frac{\lambda}{a}x + C_2 \sin \mu_1 \frac{\lambda}{a}x) + e^{-\delta_1}(\frac{\lambda}{a}x)(C_3 \cos \mu_1 \frac{\lambda}{a}x + C_4 \sin \mu_1 \frac{\lambda}{a}x) + e^{\delta_2}(\frac{\lambda}{a}x)(C_5 \cos \mu_2 \frac{\lambda}{a}x + C_6 \sin \mu_2 \frac{\lambda}{a}x) + e^{-\delta_2}(\frac{\lambda}{a}x)(C_7 \cos \mu_2 \frac{\lambda}{a}x + C_8 \sin \mu_2 \frac{\lambda}{a}x) + w_{mn} \cos(\frac{\lambda}{a}x)] \} \cos m\phi. \quad (4.77)$$

$$N_\phi = \frac{Et}{1-\nu^2} \Sigma_m \Sigma_n \frac{\nu\lambda}{a} \{ \frac{m}{\nu\lambda}[e^{\delta_1}(\frac{\lambda}{a}x)(Q_1 \cos \mu_1 \frac{\lambda}{a}x + Q_2 \sin \mu_1 \frac{\lambda}{a}x) + e^{-\delta_1}(\frac{\lambda}{a}x)(Q_3 \cos \mu_1 \frac{\lambda}{a}x + Q_4 \sin \mu_1 \frac{\lambda}{a}x) + e^{\delta_2}(\frac{\lambda}{a}x)(Q_5 \cos \mu_2 \frac{\lambda}{a}x + Q_6 \sin \mu_2 \frac{\lambda}{a}x) + e^{-\delta_2}(\frac{\lambda}{a}x)(Q_7 \cos \mu_2 \frac{\lambda}{a}x + Q_8 \sin \mu_2 \frac{\lambda}{a}x) + v_{mn} \cos(\frac{\lambda}{a}x)] - \frac{1}{\nu\lambda}[e^{\delta_1}(\frac{\lambda}{a}x)(C_1 \cos \mu_1 \frac{\lambda}{a}x + C_2 \sin \mu_1 \frac{\lambda}{a}x) + e^{-\delta_1}(\frac{\lambda}{a}x)(C_3 \cos \mu_1 \frac{\lambda}{a}x + C_4 \sin \mu_1 \frac{\lambda}{a}x) + e^{\delta_2}(\frac{\lambda}{a}x)(C_5 \cos \mu_2 \frac{\lambda}{a}x + Q_6 \sin \mu_2 \frac{\lambda}{a}x) + e^{-\delta_2}(\frac{\lambda}{a}x)(Q_7 \cos \mu_2 \frac{\lambda}{a}x + Q_8 \sin \mu_2 \frac{\lambda}{a}x) + w_{mn} \cos(\frac{\lambda}{a}x)] + e^{\delta_1}(\frac{\lambda}{a}x)[P_1(\delta_1 \cos \mu_1 \frac{\lambda}{a}x - \mu_1 \sin \mu_1 \frac{\lambda}{a}x) + P_2(\delta_1 \sin \mu_1 \frac{\lambda}{a}x + \mu_1 \cos \mu_1 \frac{\lambda}{a}x)] + e^{-\delta_1}(\frac{\lambda}{a}x)[P_3(-\delta_1 \cos \mu_1 \frac{\lambda}{a}x - \mu_1 \sin \mu_1 \frac{\lambda}{a}x) + P_4(-\delta_1 \sin \mu_1 \frac{\lambda}{a}x + \mu_1 \cos \mu_1 \frac{\lambda}{a}x)] + e^{\delta_2}(\frac{\lambda}{a}x)[P_5(\delta_2 \cos \mu_2 \frac{\lambda}{a}x - \mu_2 \sin \mu_2 \frac{\lambda}{a}x) + P_6(\delta_2 \sin \mu_2 \frac{\lambda}{a}x + \mu_2 \cos \mu_2 \frac{\lambda}{a}x)] + e^{-\delta_2}(\frac{\lambda}{a}x)[P_7(-\delta_2 \cos \mu_2 \frac{\lambda}{a}x - \mu_2 \sin \mu_2 \frac{\lambda}{a}x) + P_8(-\delta_2 \sin \mu_2 \frac{\lambda}{a}x + \mu_2 \cos \mu_2 \frac{\lambda}{a}x)] + u_{mn} \cos(\frac{\lambda}{a}x) \} \cos m\phi. \quad (4.78)$$

$$M_x = (-D)\Sigma_m\Sigma_n \frac{\lambda^2}{a^2}\{ e^{\delta_1}(\frac{\lambda}{a}x)\{ C_1[(\delta_1^2-\mu_1^2)\cos\mu_1\frac{\lambda}{a}x - 2\delta_1\mu_1\sin\mu_1\frac{\lambda}{a}x] + C_2[(\delta_1^2-\mu_1^2)\sin\mu_1\frac{\lambda}{a}x + 2\delta_1\mu_1\cos\mu_1\frac{\lambda}{a}x]\} + e^{-\delta_1}(\frac{\lambda}{a}x)\{ C_3[(\delta_1^2-\mu_1^2)\cos\mu_1\frac{\lambda}{a}x + 2\delta_1\mu_1\sin\mu_1\frac{\lambda}{a}x] + C_4[(\delta_1^2-\mu_1^2)\sin\mu_1\frac{\lambda}{a}x - 2\delta_1\mu_1\cos\mu_1\frac{\lambda}{a}x]\} + e^{\delta_2}(\frac{\lambda}{a}x)\{ C_5[(\delta_2^2-\mu_2^2)\cos\mu_2\frac{\lambda}{a}x - 2\delta_2\mu_2\sin\mu_2\frac{\lambda}{a}x] + C_6[(\delta_2^2-\mu_2^2)\sin\mu_2\frac{\lambda}{a}x + 2\delta_2\mu_2\cos\mu_2\frac{\lambda}{a}x]\} + e^{-\delta_2}(\frac{\lambda}{a}x)\{C_7[(\delta_2^2-\mu_2^2)\cos\mu_2\frac{\lambda}{a}x + 2\delta_2\mu_2\sin\mu_2\frac{\lambda}{a}x] + C_8[(\delta_2^2-\mu_2^2)\sin\mu_2\frac{\lambda}{a}x - 2\delta_2\mu_2\cos\mu_2\frac{\lambda}{a}x]\} - w_{mn}\cos(\frac{\lambda}{a}x) + \frac{\nu m}{\lambda^2}[e^{\delta_1}(\frac{\lambda}{a}x)(Q_1\cos\mu_1\frac{\lambda}{a}x + Q_2\sin\mu_1\frac{\lambda}{a}x) + e^{-\delta_1}(\frac{\lambda}{a}x)(Q_3\cos\mu_1\frac{\lambda}{a}x + Q_4\sin\mu_1\frac{\lambda}{a}x) + e^{\delta_2}(\frac{\lambda}{a}x)(Q_5\cos\mu_2\frac{\lambda}{a}x + Q_6\sin\mu_2\frac{\lambda}{a}x) + e^{-\delta_2}(\frac{\lambda}{a}x)(Q_7\cos\mu_2\frac{\lambda}{a}x + Q_8\sin\mu_2\frac{\lambda}{a}x) + v_{mn}\cos(\frac{\lambda}{a}x)] - \frac{\nu m^2}{\lambda^2}[e^{\delta_1}(\frac{\lambda}{a}x)(C_1\cos\mu_1\frac{\lambda}{a}x + C_2\sin\mu_1\frac{\lambda}{a}x) + e^{-\delta_1}(\frac{\lambda}{a}x)(C_3\cos\mu_1\frac{\lambda}{a}x + C_4\sin\mu_1\frac{\lambda}{a}x) + e^{\delta_2}(\frac{\lambda}{a}x)(C_5\cos\mu_2\frac{\lambda}{a}x + C_6\sin\mu_2\frac{\lambda}{a}x) + e^{-\delta_2}(\frac{\lambda}{a}x)(C_7\cos\mu_2\frac{\lambda}{a}x + C_8\sin\mu_2\frac{\lambda}{a}x) + w_{mn}\cos(\frac{\lambda}{a}x)]\}\cos m\phi. \quad (4.79)$$

$$M_\phi = (-D)\Sigma_m\Sigma_n \frac{\nu\lambda^2}{a^2}\{ \frac{m}{\nu\lambda^2}[e^{\delta_1}(\frac{\lambda}{a}x)(Q_1\cos\mu_1\frac{\lambda}{a}x + Q_2\sin\mu_1\frac{\lambda}{a}x) + e^{-\delta_1}(\frac{\lambda}{a}x)(Q_3\cos\mu_1\frac{\lambda}{a}x + Q_4\sin\mu_1\frac{\lambda}{a}x) + e^{\delta_2}(\frac{\lambda}{a}x)(Q_5\cos\mu_2\frac{\lambda}{a}x + Q_6\sin\mu_2\frac{\lambda}{a}x) + e^{-\delta_2}(\frac{\lambda}{a}x)(Q_7\cos\mu_2\frac{\lambda}{a}x + Q_8\sin\mu_2\frac{\lambda}{a}x) + v_{mn}\cos(\frac{\lambda}{a}x)] - \frac{m^2}{\nu\lambda^2}[e^{\delta_1}(\frac{\lambda}{a}x)(C_1\cos\mu_1\frac{\lambda}{a}x + C_2\sin\mu_1\frac{\lambda}{a}x) + e^{-\delta_1}(\frac{\lambda}{a}x)(C_3\cos\mu_1\frac{\lambda}{a}x + C_4\sin\mu_1\frac{\lambda}{a}x) + e^{\delta_2}(\frac{\lambda}{a}x)(C_5\cos\mu_2\frac{\lambda}{a}x + C_6\sin\mu_2\frac{\lambda}{a}x) + e^{-\delta_2}(\frac{\lambda}{a}x)(C_7\cos\mu_2\frac{\lambda}{a}x + C_8\sin\mu_2\frac{\lambda}{a}x) + w_{mn}\cos(\frac{\lambda}{a}x)] + e^{\delta_1}(\frac{\lambda}{a}x)\{ C_1[(\delta_1^2-\mu_1^2)\cos\mu_1\frac{\lambda}{a}x - 2\delta_1\mu_1\sin\mu_1\frac{\lambda}{a}x] + C_2[(\delta_1^2-\mu_1^2)\sin\mu_1\frac{\lambda}{a}x + 2\delta_1\mu_1\cos\mu_1\frac{\lambda}{a}x]\} + e^{-\delta_1}(\frac{\lambda}{a}x)\{ C_3[(\delta_1^2-\mu_1^2)\cos\mu_1\frac{\lambda}{a}x + 2\delta_1\mu_1\sin\mu_1\frac{\lambda}{a}x] + C_4[(\delta_1^2-\mu_1^2)\sin\mu_1\frac{\lambda}{a}x - 2\delta_1\mu_1\cos\mu_1\frac{\lambda}{a}x]\} + e^{\delta_2}(\frac{\lambda}{a}x)\{ C_5[(\delta_2^2-\mu_2^2)\cos\mu_2\frac{\lambda}{a}x - 2\delta_2\mu_2\sin\mu_2\frac{\lambda}{a}x] + C_6[(\delta_2^2-\mu_2^2)\sin\mu_2\frac{\lambda}{a}x + 2\delta_2\mu_2\cos\mu_2\frac{\lambda}{a}x]\} + e^{-\delta_2}(\frac{\lambda}{a}x)\{ C_7[(\delta_2^2-\mu_2^2)\cos\mu_2\frac{\lambda}{a}x + 2\delta_2\mu_2\sin\mu_2\frac{\lambda}{a}x] + C_8[(\delta_2^2-\mu_2^2)\sin\mu_2\frac{\lambda}{a}x - 2\delta_2\mu_2\cos\mu_2\frac{\lambda}{a}x]\} - w_{mn}\cos(\frac{\lambda}{a}x)\}\cos m\phi.$$

(4.80)

$$N_{x\phi} = \frac{Et}{2(1+\nu)}\Sigma_m\Sigma_n \frac{\lambda}{a}\{ -\frac{m}{\lambda}[e^{\delta_1}(\frac{\lambda}{a}x)(P_1\cos\mu_1\frac{\lambda}{a}x + P_2\sin\mu_1\frac{\lambda}{a}x) + e^{-\delta_1}(\frac{\lambda}{a}x)(P_3\cos\mu_1\frac{\lambda}{a}x + P_4\sin\mu_1\frac{\lambda}{a}x) + e^{\delta_2}(\frac{\lambda}{a}x)(P_5\cos\mu_2\frac{\lambda}{a}x + P_6\sin\mu_2\frac{\lambda}{a}x) + e^{-\delta_2}(\frac{\lambda}{a}x)$$

$$(P_7 \cos \mu_2 \frac{\lambda}{a} x + P_8 \sin \mu_2 \frac{\lambda}{a} x) + u_{mn} \sin (\frac{\lambda}{a} x)] + e^{\delta_1 (\frac{\lambda}{a} x)} [Q_1 (\delta_1 \cos \mu_1 \frac{\lambda}{a} x -$$

$$\mu_1 \sin \mu_1 \frac{\lambda}{a} x) + Q_2 (\delta_1 \sin \mu_1 \frac{\lambda}{a} x + \mu_1 \cos \mu_1 \frac{\lambda}{a} x)] + e^{-\delta_1 (\frac{\lambda}{a} x)} [Q_3 (- \delta_1 \cos \mu_1 \frac{\lambda}{a} x -$$

$$\mu_1 \sin \mu_1 \frac{\lambda}{a} x) + Q_4 (- \delta_1 \sin \mu_1 \frac{\lambda}{a} x + \mu_1 \cos \mu_1 \frac{\lambda}{a} x)] + e^{\delta_2 (\frac{\lambda}{a} x)} [Q_5 (\delta_2 \cos \mu_2 \frac{\lambda}{a} x -$$

$$\mu_2 \sin \mu_2 \frac{\lambda}{a} x) + Q_6 (\delta_2 \sin \mu_2 \frac{\lambda}{a} x + \mu_2 \cos \mu_2 \frac{\lambda}{a} x)] + e^{-\delta_2 (\frac{\lambda}{a} x)} [Q_7 (- \delta_2 \cos \mu_2 \frac{\lambda}{a} x -$$

$$\mu_2 \sin \mu_2 \frac{\lambda}{a} x) + Q_8 (- \delta_2 \sin \mu_2 \frac{\lambda}{a} x + \mu_2 \cos \mu_2 \frac{\lambda}{a} x)] - v_{mn} \sin (\frac{\lambda}{a} x) \} \sin m\phi. \tag{4.81}$$

$$M_{x\phi} = D (1 - \nu) \Sigma_m \Sigma_n \frac{\lambda}{a^2} \{ e^{\delta_1 (\frac{\lambda}{a} x)} [Q_1 (\delta_1 \cos \mu_1 \frac{\lambda}{a} x - \mu_1 \sin \mu_1 \frac{\lambda}{a} x) + Q_2 (\delta_1 \sin \mu_1 \frac{\lambda}{a} x +$$

$$\mu_1 \cos \mu_1 \frac{\lambda}{a} x)] + e^{-\delta_1 (\frac{\lambda}{a} x)} [Q_3 (- \delta_1 \cos \mu_1 \frac{\lambda}{a} x - \mu_1 \sin \mu_1 \frac{\lambda}{a} x) + Q_4 (- \delta_1 \sin \mu_1 \frac{\lambda}{a} x$$

$$+ \mu_1 \cos \mu_1 \frac{\lambda}{a} x)] + e^{\delta_2 (\frac{\lambda}{a} x)} [Q_5 (\delta_2 \cos \mu_2 \frac{\lambda}{a} x - \mu_2 \sin \mu_2 \frac{\lambda}{a} x) + Q_6 (\delta_2 \sin \mu_2 \frac{\lambda}{a} x$$

$$+ \mu_2 \cos \mu_2 \frac{\lambda}{a} x)] + e^{-\delta_2 (\frac{\lambda}{a} x)} [Q_7 (- \delta_2 \cos \mu_2 \frac{\lambda}{a} x - \mu_2 \sin \mu_2 \frac{\lambda}{a} x) + Q_8$$

$$(- \delta_2 \sin \mu_2 \frac{\lambda}{a} x + \mu_2 \cos \mu_2 \frac{\lambda}{a} x)] - v_{mn} \sin (\frac{\lambda}{a} x) - m \{ e^{\delta_1 (\frac{\lambda}{a} x)} [C_1 (\delta_1 \cos \mu_1 \frac{\lambda}{a} x -$$

$$\mu_1 \sin \mu_1 \frac{\lambda}{a} x) + C_2 (\delta_1 \sin \mu_1 \frac{\lambda}{a} x + \mu_1 \cos \mu_1 \frac{\lambda}{a} x)] + e^{-\delta_1 (\frac{\lambda}{a} x)} [C_3 (- \delta_1 \cos \mu_1 \frac{\lambda}{a} x -$$

$$\mu_1 \sin \mu_1 \frac{\lambda}{a} x) + C_4 (- \delta_1 \sin \mu_1 \frac{\lambda}{a} x + \mu_1 \cos \mu_1 \frac{\lambda}{a} x)] + e^{\delta_2 (\frac{\lambda}{a} x)} [C_5 (\delta_2 \cos \mu_2 \frac{\lambda}{a} x -$$

$$\mu_2 \sin \mu_2 \frac{\lambda}{a} x) + C_6 (\delta_2 \sin \mu_2 \frac{\lambda}{a} x + \mu_2 \cos \mu_2 \frac{\lambda}{a} x)] + e^{-\delta_2 (\frac{\lambda}{a} x)} [C_7 (- \delta_2 \cos \mu_2 \frac{\lambda}{a} x -$$

$$\mu_2 \sin \mu_2 \frac{\lambda}{a} x) + C_8 (- \delta_2 \sin \mu_2 \frac{\lambda}{a} x + \mu_2 \cos \mu_2 \frac{\lambda}{a} x)] - w_{mn} \sin (\frac{\lambda}{a} x) \} \} \sin m\phi. \tag{4.82}$$

All the above solutions for stress resultants are valid provided $m \neq 1$ ($m = 0, 2, 3, \ldots, \infty$; $n = 1, 2, \ldots, \infty$). The special case of $m = 1$ is considered next.

4.3.5 Special Case of Harmonic m=1: Expressions for Stress Resultants

For the case $m = 1$, the expressions for displacements u, v and w have been given in Equations (4.53), (4.58) and (4.62) respectively in the previous discussion. In order to produce the corresponding relations for the stress resultants, the relevant boundary conditions presented in Eq. (4.63) are introduced into these expressions for the displacements.

For $w = 0$ at $x = 0, l$; Eq. (4.53) gives

$$C_1 + C_3 + C_5 + C_6 + C_7 = - w_{mn} \tag{4.83}$$

$$C_1 e^{\delta_1(\frac{\lambda}{a}1)}\cos\mu_1\frac{\lambda}{a}1 + C_2 e^{\delta_1(\frac{\lambda}{a}1)}\sin\mu_1\frac{\lambda}{a}1 + C_3 e^{-\delta_1(\frac{\lambda}{a}1)}\cos\mu_1\frac{\lambda}{a}1 + C_4 e^{-\delta_1(\frac{\lambda}{a}1)}\sin\mu_1\frac{\lambda}{a}1$$
$$+ C_5 e^{\delta_2(\frac{\lambda}{a}1)} + C_6 e^{-\delta_2(\frac{\lambda}{a}1)} + C_7\cos\mu_2\frac{\lambda}{a}1 + C_8\sin\mu_2\frac{\lambda}{a}1 = -w_{mn}\cos\frac{\lambda}{a}1 \quad (4.84)$$

For v = 0 at x = 0, l, Eq. (4.62) gives

$$Q_1 + Q_3 + Q_5 + Q_6 + Q_7 = -v_{mn} \quad (4.85)$$

$$Q_1 e^{\delta_1(\frac{\lambda}{a}1)}\cos\mu_1\frac{\lambda}{a}1 + Q_2 e^{\delta_1(\frac{\lambda}{a}1)}\sin\mu_1\frac{\lambda}{a}1 + Q_3 e^{-\delta_1(\frac{\lambda}{a}1)}\cos\mu_1\frac{\lambda}{a}1 + Q_4 e^{-\delta_1(\frac{\lambda}{a}1)}\sin\mu_1\frac{\lambda}{a}1$$
$$+ Q_5 e^{\delta_2(\frac{\lambda}{a}1)} + Q_6 e^{-\delta_2(\frac{\lambda}{a}1)} + Q_7\cos\mu_2\frac{\lambda}{a}1 + Q_8\sin\mu_2\frac{\lambda}{a}1 = -v_{mn}\cos\frac{\lambda}{a}1 \quad (4.86)$$

Converting the above equations in Q_i into the corresponding equations in C_i using Eq. (4.60) leads to

$$C_1\frac{a_{22}d_{11} - a_{12}d_{21}}{a_{11}a_{22} - a_{12}a_{21}} + C_2\frac{a_{22}d_{12} - a_{12}d_{22}}{a_{11}a_{22} - a_{12}a_{21}} + C_3\frac{a_{42}d_{31} - a_{32}d_{41}}{a_{31}a_{42} - a_{32}a_{41}} + C_4$$
$$\frac{a_{42}d_{32} - a_{32}d_{42}}{a_{31}a_{42} - a_{32}a_{41}} + C_5\frac{d_{51}}{a_{51}} + C_6\frac{d_{61}}{a_{61}} + C_7\frac{d_{71}}{a_{71}} = -v_{mn} \quad (4.87)$$

$$C_1 e^{\delta_1(\frac{\lambda}{a}1)}\left[\frac{a_{22}d_{11} - a_{12}d_{21}}{a_{11}a_{22} - a_{12}a_{21}}\cos\mu_1\frac{\lambda}{a}1 + \frac{a_{11}d_{21} - a_{21}d_{11}}{a_{11}a_{22} - a_{12}a_{21}}\sin\mu_1\frac{\lambda}{a}1\right] + C_2 e^{\delta_1(\frac{\lambda}{a}1)}$$
$$\left[\frac{a_{22}d_{12} - a_{12}d_{22}}{a_{11}a_{22} - a_{12}a_{21}}\cos\mu_1\frac{\lambda}{a}1 + \frac{a_{11}d_{22} - a_{21}d_{12}}{a_{11}a_{22} - a_{12}a_{21}}\sin\mu_1\frac{\lambda}{a}1\right] + C_3 e^{-\delta_1(\frac{\lambda}{a}1)}$$
$$\left[\frac{a_{42}d_{31} - a_{32}d_{41}}{a_{31}a_{42} - a_{32}a_{41}}\cos\mu_1\frac{\lambda}{a}1 + \frac{a_{31}d_{41} - a_{41}d_{31}}{a_{31}a_{42} - a_{32}a_{41}}\sin\mu_1\frac{\lambda}{a}1\right] + C_4 e^{-\delta_1(\frac{\lambda}{a}1)}$$
$$\left[\frac{a_{42}d_{32} - a_{32}d_{42}}{a_{31}a_{42} - a_{32}a_{41}}\cos\mu_1\frac{\lambda}{a}1 + \frac{a_{31}d_{42} - a_{41}d_{32}}{a_{31}a_{42} - a_{32}a_{41}}\sin\mu_1\frac{\lambda}{a}1\right] + C_5 e^{\delta_2(\frac{\lambda}{a}1)}\frac{d_{51}}{a_{51}}$$
$$+ C_6 e^{-\delta_2(\frac{\lambda}{a}1)}\frac{d_{61}}{a_{61}} + C_7\cos\mu_2\frac{\lambda}{a}1\frac{d_{71}}{a_{71}} + C_8\sin\mu_2\frac{\lambda}{a}1\frac{d_{81}}{a_{81}} = -v_{mn}\cos\frac{\lambda}{a}1 \quad (4.88)$$

For u = 0 at x = 0, Eq.(4.58) gives

$$P_1 + P_3 + P_5 + P_6 + P_7 = 0 \quad (4.89)$$

Again rewriting it after introducing Eq. (4.55)

$$C_1\frac{a_{22}\mu_1 b_{11} - a_{12}\delta_1 b_{21}}{a_{11}a_{22} - a_{12}a_{21}} + C_2\frac{a_{22}\delta_1 b_{12} - a_{12}\mu_1 b_{22}}{a_{11}a_{22} - a_{12}a_{21}} + C_3\frac{a_{42}\mu_1 b_{31} - a_{32}\delta_1 b_{41}}{a_{31}a_{42} - a_{32}a_{41}} + C_4$$
$$\frac{a_{42}\delta_1 b_{32} - a_{32}\mu_1 b_{42}}{a_{31}a_{42} - a_{32}a_{41}} + C_5\frac{\delta_2 b_{51}}{a_{51}} + C_6\frac{\delta_2 b_{61}}{a_{61}} + C_8\frac{\mu_2 b_{71}}{a_{71}} = 0 \quad (4.90)$$

When $x = l$, $N_x = 0$, ie. $\frac{\partial u}{\partial x} = 0$, as before, Eq. (4.58) gives

$$P_1 e^{\delta_1(\frac{\lambda}{a}1)}(\delta_1 \cos \mu_1 \frac{\lambda}{a}1 - \mu_1 \sin \mu_1 \frac{\lambda}{a}1) + P_2 e^{\delta_1(\frac{\lambda}{a}1)}(\delta_1 \sin \mu_1 \frac{\lambda}{a}1 + \mu_1 \cos \mu_1 \frac{\lambda}{a}1) + P_3$$
$$e^{-\delta_1(\frac{\lambda}{a}1)}(-\delta_1 \cos \mu_1 \frac{\lambda}{a}1 - \mu_1 \sin \mu_1 \frac{\lambda}{a}1) + P_4 e^{-\delta_1(\frac{\lambda}{a}1)}(-\delta_1 \sin \mu_1 \frac{\lambda}{a}1 + \mu_1 \cos \mu_1 \frac{\lambda}{a}1)$$
$$+ P_5 \delta_2 e^{\delta_2(\frac{\lambda}{a}1)} - P_6 \delta_2 e^{-\delta_2(\frac{\lambda}{a}1)} - P_7 \mu_2 \sin \mu_2 \frac{\lambda}{a}1 + P_8 \mu_2 \cos \mu_2 \frac{\lambda}{a}1 = -u_{mn} \cos \frac{\lambda}{a}1 \qquad (4.91)$$

and similarly replacing P_i with C_1 using Eq. (4.55) it becomes

$$C_1 e^{\delta_1(\frac{\lambda}{a}1)}[\frac{a_{22}\mu_1 b_{11} - a_{12}\delta_1 b_{21}}{a_{11}a_{22} - a_{12}a_{21}}(\delta_1 \cos \mu_1 \frac{\lambda}{a}1 - \mu_1 \sin \mu_1 \frac{\lambda}{a}1) + \frac{a_{11}\delta_1 b_{21} - a_{21}\mu_1 b_{11}}{a_{11}a_{22} - a_{12}a_{21}}(\delta_1 \sin \mu_1 \frac{\lambda}{a}1$$
$$+ \mu_1 \cos \mu_1 \frac{\lambda}{a}1)] + C_2 e^{\delta_1(\frac{\lambda}{a}1)}[\frac{a_{22}\delta_1 b_{12} - a_{12}\mu_1 b_{22}}{a_{11}a_{22} - a_{12}a_{21}}(\delta_1 \cos \mu_1 \frac{\lambda}{a}1 - \mu_1 \sin \mu_1 \frac{\lambda}{a}1) +$$
$$\frac{a_{11}\mu_1 b_{22} - a_{21}\delta_1 b_{12}}{a_{11}a_{22} - a_{12}a_{21}}(\delta_1 \sin \mu_1 \frac{\lambda}{a}1 + \mu_1 \cos \mu_1 \frac{\lambda}{a}1)] + C_3 e^{-\delta_1(\frac{\lambda}{a}1)}[\frac{a_{42}\mu_1 b_{31} - a_{32}\delta_1 b_{41}}{a_{31}a_{42} - a_{32}a_{41}}$$
$$(-\delta_1 \cos \mu_1 \frac{\lambda}{a}1 - \mu_1 \sin \mu_1 \frac{\lambda}{a}1) + \frac{a_{31}\delta_1 b_{41} - a_{41}\mu_1 b_{31}}{a_{31}a_{42} - a_{32}a_{41}}(-\delta_1 \sin \mu_1 \frac{\lambda}{a}1 + \mu_1 \cos \mu_1 \frac{\lambda}{a}1)] +$$
$$C_4 e^{-\delta_1(\frac{\lambda}{a}1)}[\frac{a_{42}\delta_1 b_{32} - a_{32}\mu_1 b_{42}}{a_{31}a_{42} - a_{32}a_{41}}(-\delta_1 \cos \mu_1 \frac{\lambda}{a}1 - \mu_1 \sin \mu_1 \frac{\lambda}{a}1) + \frac{a_{31}\mu_1 b_{42} - a_{41}\delta_1 b_{32}}{a_{31}a_{42} - a_{32}a_{41}}$$
$$(-\delta_1 \sin \mu_1 \frac{\lambda}{a}1 + \mu_1 \cos \mu_1 \frac{\lambda}{a}1)] + C_5 \delta_2 e^{\delta_2(\frac{\lambda}{a}1)}\frac{\delta_2 b_{51}}{a_{51}} - C_6 \delta_2 e^{-\delta_2(\frac{\lambda}{a}1)}\frac{\delta_2 b_{61}}{a_{61}} +$$
$$C_7 \mu_2 \cos \mu_2 \frac{\lambda}{a}1 \frac{\mu_2 b_{81}}{a_{81}} - C_8 \mu_2 \sin \mu_2 \frac{\lambda}{a}1 = -u_{mn} \cos \frac{\lambda}{a}1 \qquad (4.92)$$

Finally applying $M_x = 0$ (converted into $\frac{\partial^2 w}{\partial x^2} = 0$) at $x = 0$ and $x = l$, Eq. (4.53) gives

$$(\delta_1^2 - \mu_1^2)(C_1 + C_3) + 2\delta_1\mu_1(C_2 - C_4) + \delta_2^2(C_5 + C_6) - \mu_2^2 C_7 = w_{mn} \qquad (4.93)$$

$$C_1 e^{\delta_1(\frac{\lambda}{a}1)}[(\delta_1^2 - \mu_1^2)\cos \mu_1 \frac{\lambda}{a}1 - 2\delta_1\mu_1 \sin \mu_1 \frac{\lambda}{a}1] + C_2 e^{\delta_1(\frac{\lambda}{a}1)}[(\delta_1^2 - \mu_1^2)\sin \mu_1 \frac{\lambda}{a}1 +$$
$$2\delta_1\mu_1 \cos \mu_1 \frac{\lambda}{a}1] + C_3 e^{-\delta_1(\frac{\lambda}{a}1)}[(\delta_1^2 - \mu_1^2)\cos \mu_1 \frac{\lambda}{a}1 + 2\delta_1\mu_1 \sin \mu_1 \frac{\lambda}{a}1] + C_4 e^{-\delta_1(\frac{\lambda}{a}1)}$$
$$[(\delta_1^2 - \mu_1^2)\sin \mu_1 \frac{\lambda}{a}1 - 2\delta_1\mu_1 \cos \mu_1 \frac{\lambda}{a}1] + C_5 \delta_2^2 e^{\delta_2(\frac{\lambda}{a}1)} + C_6 \delta_2^2 e^{-\delta_2(\frac{\lambda}{a}1)} - C_7 \mu_2^2 \cos \mu_2 \frac{\lambda}{a}1$$
$$- C_8 \mu_2^2 \sin \mu_2 \frac{\lambda}{a}1 = w_{mn} \cos \frac{\lambda}{a}1 \qquad (4.94)$$

Solving the eight equations (4.80), (4.81), (4.84), (4.85), (4.87), (4.89), (4.90) and (4.91) gives the corresponding eight real constants C_i as well as P_i and Q_i in the special case of $m = 1$. According to the general formulas (4.63) for stress resultants, the solutions for the stress resultants N_x, N_ϕ, $N_{x\phi}$, M_x, M_ϕ and $M_{x\phi}$ are given by

$$N_x = \frac{Et}{1-\nu^2} \Sigma_n \frac{\lambda}{a} \{ e^{\delta_1 (\frac{\lambda}{a} x)} [P_1 (\delta_1 \cos \mu_1 \frac{\lambda}{a} x - \mu_1 \sin \mu_1 \frac{\lambda}{a} x) + P_2 (\delta_1 \sin \mu_1 \frac{\lambda}{a} x + \mu_1 \cos \mu_1 \frac{\lambda}{a} x)] + e^{-\delta_1 (\frac{\lambda}{a} x)} [P_3 (- \delta_1 \cos \mu_1 \frac{\lambda}{a} x - \mu_1 \sin \mu_1 \frac{\lambda}{a} x) + P_4 (- \delta_1 \sin \mu_1 \frac{\lambda}{a} x + \mu_1 \cos \mu_1 \frac{\lambda}{a} x)] + P_5 \delta_2 e^{\delta_2 (\frac{\lambda}{a} x)} - P_6 \delta_2 e^{-\delta_2 (\frac{\lambda}{a} x)} - P_7 \mu_2 \sin \mu_2 \frac{\lambda}{a} x + P_8 \mu_2 \cos \mu_2 \frac{\lambda}{a} x + u_{mn} \cos (\frac{\lambda}{a} x) + \frac{\nu}{\lambda} m [e^{\delta_1 (\frac{\lambda}{a} x)} (Q_1 \cos \mu_1 \frac{\lambda}{a} x + Q_2 \sin \mu_1 \frac{\lambda}{a} x) + e^{-\delta_1 (\frac{\lambda}{a} x)} (Q_3 \cos \mu_1 \frac{\lambda}{a} x + Q_4 \sin \mu_1 \frac{\lambda}{a} x) + Q_5 e^{\delta_2 (\frac{\lambda}{a} x)} + Q_6 e^{-\delta_2 (\frac{\lambda}{a} x)} + Q_7 \cos \mu_2 \frac{\lambda}{a} x + Q_8 \sin \mu_2 \frac{\lambda}{a} x + v_{mn} \cos (\frac{\lambda}{a} x)] - \frac{\nu}{\lambda} [e^{\delta_1 (\frac{\lambda}{a} x)} (C_1 \cos \mu_1 \frac{\lambda}{a} x + C_2 \sin \mu_1 \frac{\lambda}{a} x) + e^{-\delta_1 (\frac{\lambda}{a} x)} (C_3 \cos \mu_1 \frac{\lambda}{a} x + C_4 \sin \mu_1 \frac{\lambda}{a} x) + C_5 e^{\delta_2 (\frac{\lambda}{a} x)} + C_6 e^{-\delta_2 (\frac{\lambda}{a} x)} + C_7 \cos \mu_2 \frac{\lambda}{a} x + C_8 \sin \mu_2 \frac{\lambda}{a} x + w_{mn} \cos (\frac{\lambda}{a} x)] \} \cos m\phi. \quad (4.95)$$

$$N_\phi = \frac{Et}{1-\nu^2} \Sigma_n \frac{\nu\lambda}{a} \{ \frac{m}{\nu\lambda} [e^{\delta_1 (\frac{\lambda}{a} x)} (Q_1 \cos \mu_1 \frac{\lambda}{a} x + Q_2 \sin \mu_1 \frac{\lambda}{a} x) + e^{-\delta_1 (\frac{\lambda}{a} x)} (Q_3 \cos \mu_1 \frac{\lambda}{a} x + Q_4 \sin \mu_1 \frac{\lambda}{a} x) + Q_5 e^{\delta_2 (\frac{\lambda}{a} x)} + Q_6 e^{-\delta_2 (\frac{\lambda}{a} x)} + Q_7 \cos \mu_2 \frac{\lambda}{a} x + Q_8 \sin \mu_2 \frac{\lambda}{a} x + v_{mn} \cos (\frac{\lambda}{a} x)] - \frac{1}{\nu\lambda} [e^{\delta_1 (\frac{\lambda}{a} x)} (C_1 \cos \mu_1 \frac{\lambda}{a} x + C_2 \sin \mu_1 \frac{\lambda}{a} x) + e^{-\delta_1 (\frac{\lambda}{a} x)} (C_3 \cos \mu_1 \frac{\lambda}{a} x + C_4 \sin \mu_1 \frac{\lambda}{a} x) + C_5 e^{\delta_2 (\frac{\lambda}{a} x)} + C_6 e^{-\delta_2 (\frac{\lambda}{a} x)} + C_7 \cos \mu_2 \frac{\lambda}{a} x + C_8 \sin \mu_2 \frac{\lambda}{a} x + w_{mn} \cos (\frac{\lambda}{a} x)] + e^{\delta_1 (\frac{\lambda}{a} x)} [P_1 (\delta_1 \cos \mu_1 \frac{\lambda}{a} x - \mu_1 \sin \mu_1 \frac{\lambda}{a} x) + P_2 (\delta_1 \sin \mu_1 \frac{\lambda}{a} x + \mu_1 \cos \mu_1 \frac{\lambda}{a} x)] + e^{-\delta_1 (\frac{\lambda}{a} x)} [P_3 (- \delta_1 \cos \mu_1 \frac{\lambda}{a} x - \mu_1 \sin \mu_1 \frac{\lambda}{a} x) + P_4 (- \delta_1 \sin \mu_1 \frac{\lambda}{a} x + \mu_1 \cos \mu_1 \frac{\lambda}{a} x)] + P_5 \delta_2 e^{\delta_2 (\frac{\lambda}{a} x)} - P_6 \delta_2 e^{-\delta_2 (\frac{\lambda}{a} x)} - P_7 \mu_2 \sin \mu_2 \frac{\lambda}{a} x + P_8 \mu_2 \cos \mu_2 \frac{\lambda}{a} 1 + u_{mn} \cos (\frac{\lambda}{a} x) \} \cos m\phi. \quad (4.96)$$

$$M_x = (- D) \Sigma_n \frac{\lambda^2}{a^2} \{ e^{\delta_1 (\frac{\lambda}{a} x)} \{ C_1 [(\delta_1^2 - \mu_1^2) \cos \mu_1 \frac{\lambda}{a} x - 2\delta_1\mu_1 \sin \mu_1 \frac{\lambda}{a} x] + C_2 [(\delta_1^2 - \mu_1^2) \sin \mu_1 \frac{\lambda}{a} x + 2\delta_1\mu_1 \cos \mu_1 \frac{\lambda}{a} x] \} + e^{-\delta_1 (\frac{\lambda}{a} x)} \{ C_3 [(\delta_1^2 - \mu_1^2) \cos \mu_1 \frac{\lambda}{a} x + 2\delta_1\mu_1 \sin \mu_1 \frac{\lambda}{a} x] + C_4 [(\delta_1^2 - \mu_1^2) \sin \mu_1 \frac{\lambda}{a} x - 2\delta_1\mu_1 \cos \mu_1 \frac{\lambda}{a} x] \} + C_5 \delta_2^2 e^{\delta_2 (\frac{\lambda}{a} x)} + C_6 \delta_2^2 e^{\delta_2 (\frac{\lambda}{a} x)} - C_7 \mu_2^2 \cos \mu_2 \frac{\lambda}{a} x - C_8 \mu_2^2 \sin \mu_2 \frac{\lambda}{a} x \} - w_{mn} \cos (\frac{\lambda}{a} x) + \frac{\nu m}{\lambda^2} [e^{\delta_1 (\frac{\lambda}{a} x)} (Q_1 \cos \mu_1 \frac{\lambda}{a} x + Q_2 \sin \mu_1 \frac{\lambda}{a} x) + e^{-\delta_1 (\frac{\lambda}{a} x)} (Q_3 \cos \mu_1 \frac{\lambda}{a} x + Q_4 \sin \mu_1 \frac{\lambda}{a} x) + Q_5 e^{\delta_2 (\frac{\lambda}{a} x)} + Q_6 e^{-\delta_2 (\frac{\lambda}{a} x)} + Q_7 \cos \mu_2 \frac{\lambda}{a} x + Q_8 \sin \mu_2 \frac{\lambda}{a} x + v_{mn} \cos (\frac{\lambda}{a} x)] - \frac{\nu m^2}{\lambda^2} [e^{\delta_1 (\frac{\lambda}{a} x)} (C_1 \cos \mu_1 \frac{\lambda}{a} x + C_2 \sin \mu_1 \frac{\lambda}{a} x) + e^{-\delta_1 (\frac{\lambda}{a} x)} (C_3 \cos \mu_1 \frac{\lambda}{a} x + C_4 \sin \mu_1 \frac{\lambda}{a} x) + C_5 e^{\delta_2 (\frac{\lambda}{a} x)} + C_6 e^{-\delta_2 (\frac{\lambda}{a} x)} + C_7 \cos \mu_2 \frac{\lambda}{a} x + C_8 \sin \mu_2 \frac{\lambda}{a} x + w_{mn}$$

$$\cos\left(\frac{\lambda}{a}x\right)]\Big\}\cos m\phi\,. \tag{4.97}$$

$$M_\phi = (-D)\Sigma_n \frac{\nu\lambda^2}{a^2}\Big\{\frac{m}{\nu\lambda^2}\Big[e^{\delta_1}\left(\frac{\lambda}{a}x\right)\left(Q_1\cos\mu_1\frac{\lambda}{a}x + Q_2\sin\mu_1\frac{\lambda}{a}x\right) + e^{-\delta_1}\left(\frac{\lambda}{a}x\right)\left(Q_3\cos\mu_1\frac{\lambda}{a}x + Q_4\sin\mu_1\frac{\lambda}{a}x\right) + Q_5 e^{\delta_2}\left(\frac{\lambda}{a}x\right) + Q_6 e^{-\delta_2}\left(\frac{\lambda}{a}x\right) + Q_7\cos\mu_2\frac{\lambda}{a}x + Q_8\sin\mu_2\frac{\lambda}{a}x + v_{mn}\cos\left(\frac{\lambda}{a}x\right)\Big] - \frac{m^2}{\nu\lambda^2}\Big[e^{\delta_1}\left(\frac{\lambda}{a}x\right)\left(C_1\cos\mu_1\frac{\lambda}{a}x + C_2\sin\mu_1\frac{\lambda}{a}x\right) + e^{-\delta_1}\left(\frac{\lambda}{a}x\right)\left(C_3\cos\mu_1\frac{\lambda}{a}x + C_4\sin\mu_1\frac{\lambda}{a}x\right) + C_5 e^{\delta_2}\left(\frac{\lambda}{a}x\right) + C_6 e^{-\delta_2}\left(\frac{\lambda}{a}x\right) + C_7\cos\mu_2\frac{\lambda}{a}x + C_8\sin\mu_2\frac{\lambda}{a}x + w_{mn}\cos\left(\frac{\lambda}{a}x\right)\Big] + e^{\delta_1}\left(\frac{\lambda}{a}x\right)\Big\{C_1\Big[(\delta_1^2-\mu_1^2)\cos\mu_1\frac{\lambda}{a}x - 2\delta_1\mu_1\sin\mu_1\frac{\lambda}{a}x\Big] + C_2\Big[(\delta_1^2-\mu_1^2)\sin\mu_1\frac{\lambda}{a}x + 2\delta_1\mu_1\cos\mu_1\frac{\lambda}{a}x\Big]\Big\} + e^{-\delta_1}\left(\frac{\lambda}{a}x\right)\Big\{C_3\Big[(\delta_1^2-\mu_1^2)\cos\mu_1\frac{\lambda}{a}x + 2\delta_1\mu_1\sin\mu_1\frac{\lambda}{a}x\Big] + C_4\Big[(\delta_1^2-\mu_1^2)\sin\mu_1\frac{\lambda}{a}x - 2\delta_1\mu_1\cos\mu_1\frac{\lambda}{a}x\Big]\Big\} + C_5\delta_2^2 e^{\delta_2}\left(\frac{\lambda}{a}x\right) + C_6\delta_2^2 e^{\delta_2}\left(\frac{\lambda}{a}x\right) - C_7\mu_2^2\cos\mu_2\frac{\lambda}{a}x - C_8\mu_2^2\sin\mu_2\frac{\lambda}{a}x - w_{mn}\cos\left(\frac{\lambda}{a}x\right)\Big\}\cos m\phi\,. \tag{4.98}$$

$$N_{x\phi} = \frac{Et}{2(1+\nu)}\Sigma_n\frac{\lambda}{a}\Big\{-\frac{m}{\lambda}\Big[e^{\delta_1}\left(\frac{\lambda}{a}x\right)\left(P_1\cos\mu_1\frac{\lambda}{a}x + P_2\sin\mu_1\frac{\lambda}{a}x\right) + e^{-\delta_1}\left(\frac{\lambda}{a}x\right)\left(P_3\cos\mu_1\frac{\lambda}{a}x + P_4\sin\mu_1\frac{\lambda}{a}x\right) + P_5 e^{\delta_2}\left(\frac{\lambda}{a}x\right) + P_6 e^{-\delta_2}\left(\frac{\lambda}{a}x\right) + P_7\cos\mu_2\frac{\lambda}{a}x + P_8\sin\mu_2\frac{\lambda}{a}x + u_{mn}\sin\left(\frac{\lambda}{a}x\right)\Big] + e^{\delta_1}\left(\frac{\lambda}{a}x\right)\Big[Q_1\left(\delta_1\cos\mu_1\frac{\lambda}{a}x - \mu_1\sin\mu_1\frac{\lambda}{a}x\right) + Q_2\left(\delta_1\sin\mu_1\frac{\lambda}{a}x + \mu_1\cos\mu_1\frac{\lambda}{a}x\right)\Big] + e^{-\delta_1}\left(\frac{\lambda}{a}x\right)\Big[Q_3\left(-\delta_1\cos\mu_1\frac{\lambda}{a}x - \mu_1\sin\mu_1\frac{\lambda}{a}x\right) + Q_4\left(-\delta_1\sin\mu_1\frac{\lambda}{a}x + \mu_1\cos\mu_1\frac{\lambda}{a}x\right)\Big] + Q_5\delta_2 e^{\delta_2}\left(\frac{\lambda}{a}x\right) - Q_6\delta_2 e^{-\delta_2}\left(\frac{\lambda}{a}x\right) - Q_7\mu_2\sin\mu_2\frac{\lambda}{a}x + Q_8\mu_2\cos\mu_2\frac{\lambda}{a}x - v_{mn}\sin\left(\frac{\lambda}{a}x\right)\Big\}\sin m\phi. \tag{4.99}$$

$$M_{x\phi} = D(1-\nu)\Sigma_n\frac{\lambda}{a^2}\Big\{e^{\delta_1}\left(\frac{\lambda}{a}x\right)\Big[Q_1\left(\delta_1\cos\mu_1\frac{\lambda}{a}x - \mu_1\sin\mu_1\frac{\lambda}{a}x\right) + Q_2\left(\delta_1\sin\mu_1\frac{\lambda}{a}x + \mu_1\cos\mu_1\frac{\lambda}{a}x\right)\Big] + e^{-\delta_1}\left(\frac{\lambda}{a}x\right)\Big[Q_3\left(-\delta_1\cos\mu_1\frac{\lambda}{a}x - \mu_1\sin\mu_1\frac{\lambda}{a}x\right) + Q_4\left(-\delta_1\sin\mu_1\frac{\lambda}{a}x + \mu_1\cos\mu_1\frac{\lambda}{a}x\right)\Big] + Q_5\delta_2 e^{\delta_2}\left(\frac{\lambda}{a}x\right) - Q_6\delta_2 e^{-\delta_2}\left(\frac{\lambda}{a}x\right) - Q_7\mu_2\sin\mu_2\frac{\lambda}{a}x + Q_8\mu_2\cos\mu_2\frac{\lambda}{a}x - v_{mn}\sin\left(\frac{\lambda}{a}x\right) - m\Big\{e^{\delta_1}\left(\frac{\lambda}{a}x\right)\Big[C_1\left(\delta_1\cos\mu_1\frac{\lambda}{a}x - \mu_1\sin\mu_1\frac{\lambda}{a}x\right) + C_2\left(\delta_1\sin\mu_1\frac{\lambda}{a}x + \mu_1\cos\mu_1\frac{\lambda}{a}x\right)\Big] + e^{-\delta_1}\left(\frac{\lambda}{a}x\right)\Big[C_3\left(-\delta_1\cos\mu_1\frac{\lambda}{a}x - \mu_1\sin\mu_1\frac{\lambda}{a}x\right) + C_4\left(-\delta_1\sin\mu_1\frac{\lambda}{a}x + \mu_1\cos\mu_1\frac{\lambda}{a}x\right)\Big] + C_5\delta_2 e^{\delta_2}\left(\frac{\lambda}{a}x\right) - C_6\delta_2 e^{-\delta_2}\left(\frac{\lambda}{a}x\right) - C_7\mu_2\sin\mu_2\frac{\lambda}{a}x + C_8\mu_2\cos\mu_2\frac{\lambda}{a}x - w_{mn}\sin\left(\frac{\lambda}{a}x\right)\Big\}\Big\}\sin m\phi. \tag{4.100}$$

where m = 1, and n = 1, 2,...,∞ for Eq. (4.95) to Eq. (4.100).

4.3.6 Expressions of Load Coefficient X_{mn}

In the previous discussion of deformations and stresses of a cylindrical shell under longitudinal local loading, the longitudinal local load X has been described simply in terms of a harmonic coefficient X_{mn}. Here the values of X_{mn} are found to represent a load p_x per unit surface uniformly distributed within a rectangle, bounded by the lines $\phi = \pm \beta_1$ or $y = a\phi = \pm b_1$ and $x = b \pm b_2$, as shown in Fig. 4-1. Such a load X can be described as a double Fourier series in ϕ and x with periods of $2\pi a$ in the circumferential direction and 2l in the longitudinal direction, respectively, according to Eqs (4.13) and (4.22),

$$X = \Sigma_m \Sigma_n X_{mn} \cos m\phi \ \sin \frac{\lambda}{a} x \quad (m = 0, 1, 2, \ldots\infty;\ n = 1, 2, 3, \ldots\infty) \tag{4.101}$$

in which the values of the load coefficients X_{mn} have not yet been established. This section tackles this problem to derive the expressions for load coefficient X_{mn}.

By reference to Bijlaard's investigation of the radial coefficient factor Z_{mn} [1955], the longitudinal load p_x can be similarly taken as a function of ϕ and x, and developed into a Fourier series as follows

$$p_x(x, \phi) = \begin{cases} \dfrac{4\beta_1}{\pi^2} \dfrac{p_x}{n} \Sigma_n \sin\left(\dfrac{n\pi}{\alpha}\beta_2\right) \sin\left(\dfrac{n\pi}{\alpha}\dfrac{b}{a}\right) \cos m\phi \ \sin \dfrac{\lambda}{a} x & (m = 0;\ n = 1, 2, 3, \ldots \infty) \\ \dfrac{8}{\pi^2} \dfrac{p_x}{mn} \Sigma_m \Sigma_n \sin(m\beta_1) \sin\left(\dfrac{n\pi}{\alpha}\beta_2\right) \sin\left(\dfrac{n\pi}{\alpha}\dfrac{b}{a}\right) \cos m\phi \ \sin \dfrac{\lambda}{a} x & (m = 1, 2, 3, \ldots\infty;\ n = 1, 2, 3, \ldots\infty) \end{cases} \tag{4.102}$$

in which $\beta_1 = b_1/a$ and $\beta_2 = b_2/a$.

Observing that $p_x(x, \phi)$ is equal to X which is given by Equation (4.101), the following expressions are obtained for the load coefficient X_{mn}

$$X_{mn} = \frac{4\beta_1}{\pi^2} \frac{p_x}{n} \sin\left(\frac{n\pi}{\alpha}\beta_2\right) \sin\left(\frac{n\pi}{\alpha}\frac{b}{a}\right) \quad (m = 0;\ n = 1, 2, 3, \ldots\infty)$$

$$X_{mn} = \frac{8}{\pi^2} \frac{p_x}{mn} \sin(m\beta_1) \sin\left(\frac{n\pi}{\alpha}\beta_2\right) \sin\left(\frac{n\pi}{\alpha}\frac{b}{a}\right) \quad (m = 1, 2, 3, \ldots\infty;\ n = 1, 2, 3, \ldots\infty) \tag{4.103}$$

For the special case when the centre of the loaded area is at $x = l/2$, $\phi = 0$, these load coefficients reduce to

$$X_{mn} = (-1)^{\frac{n-1}{2}} \frac{4\beta_1}{\pi^2} \frac{p_x}{n} \sin\left(\frac{n\pi}{\alpha}\beta_2\right) \qquad (m = 0;\ n = 1, 3, 5, \ldots\infty)$$

$$X_{mn} = (-1)^{\frac{n-1}{2}} \frac{8}{\pi^2} \frac{p_x}{mn} \sin(m\beta_1) \sin\left(\frac{n\pi}{\alpha}\beta_2\right) \qquad (m = 1, 2, 3, \ldots;\ n = 1, 3, 5, \ldots\infty)$$

$$X_{mn} = 0 \qquad (m = 1, 2, 3, \ldots;\ n = 2, 4, 6, \ldots\infty)$$

(4.104)

For a point load P at $x = l/2$, $\phi = 0$, the relation between the point load P and the distributed traction p_x is

$$\left.\begin{aligned} P &= 4b_1 b_2 p_x = 4a^2\beta_1 \beta_2 p_x \\ \text{or} \qquad p_x &= \frac{P}{4a^2\beta_1 \beta_2} \end{aligned}\right\} \qquad (4.105)$$

so that Eqs (4.104) reduce further to

$$X_{mn} = (-1)^{\frac{n-1}{2}} \frac{P}{\pi a l} \qquad (m = 0;\ n = 1, 3, 5, \ldots\infty)$$

$$X_{mn} = (-1)^{\frac{n-1}{2}} \frac{2P}{\pi a l} \qquad (m = 1, 2, 3, \ldots\infty;\ n = 1, 3, 5, \ldots\infty)$$

$$X_{mn} = 0 \qquad (m = 1, 2, 3, \ldots\infty;\ n = 2, 4, 6, \ldots\infty)$$

(4.106)

Multiple Loaded Patches

If r longitudinal loads are present at the same cross section and at equal distances around the circumference, these are represented as equally distributed loads in rectangles with sides $2b_1$ and $2b_2$, with their centres on a circle where $x = b$. The equations for X_{mn} may be written instead as

$$X_{mn} = r \frac{4\beta_1}{\pi^2} \frac{p_x}{n} \sin\left(\frac{n\pi}{\alpha}\beta_2\right) \sin\left(\frac{n\pi}{\alpha}\frac{b}{a}\right) \qquad (m = 0,\ n = 1, 2, 3, \ldots\infty)$$

$$X_{mn} = r \frac{8}{\pi^2} \frac{p_x}{(rm)n} \sin(rm\beta_1) \sin\left(\frac{n\pi}{\alpha}\beta_2\right) \sin\left(\frac{n\pi}{\alpha}\frac{b}{a}\right) \quad (m = 0, 1, 2, \ldots\infty;\ n = 1, 2, 3, \ldots\infty)$$

(4.107)

For the special case when r longitudinal loads are equally distributed around the circumference at $x = l/2$, Eqs (4.107) reduce to

$$X_{mn} = (-1)^{\frac{n-1}{2}} r \frac{4\beta_1}{\pi^2} \frac{p_x}{n} \sin\left(\frac{n\pi}{\alpha}\beta_2\right) \qquad (m = 0;\ n = 1, 3, 5, \ldots\infty)$$

$$X_{mn} = (-1)^{\frac{n-1}{2}} r \frac{8}{\pi^2} \frac{p_x}{(rm)n} \sin(rm\beta_1) \sin\left(\frac{n\pi}{\alpha}\beta_2\right) \qquad (m = 1, 2, 3, \ldots\infty;\ n = 1, 3, 5, \ldots\infty)$$

$$X_{mn} = 0 \qquad (m = 1, 2, 3,...\infty \ ; n = 2, 4, 6,... \infty) \tag{4.108}$$

For r concentrated loads P equally distributed around a circle at x = l/2, these expressions can be reduced further to

$$\begin{aligned} X_{mn} &= (-1)^{\frac{n-1}{2}} r \frac{P}{\pi a l} && (m = 0; n = 1, 3, 5,... \infty) \\ X_{mn} &= (-1)^{\frac{n-1}{2}} r \frac{2P}{\pi a l} && (m = 1, 2, 3,... \infty ; n = 1, 3, 5,...\infty) \\ X_{mn} &= 0 && (m = 1, 2, 3,... \infty ; n = 2, 4, 6,... \infty) \end{aligned} \tag{4.109}$$

Computational technique

For all the above defined loading cases, the longitudinal load X and the three displacements w, u and v can be redefined by expanding into double Fourier series as follows, instead of Eqs (4.101), (4.12), (4.26) and (4.27),

$$X = \Sigma_m \Sigma_n X_{mn} \sin \frac{\lambda}{a} x \cos (rm)\phi \quad (m = 0, 1, 2,....\infty; n = 1, 2, 3,....\infty) \tag{4.110}$$

$$w = \Sigma_m \Sigma_n f_{mn} (\frac{\lambda}{a} x) \cos (rm)\phi \quad (m = 0, 1, 2,....\infty; n = 1, 2, 3,....\infty) \tag{4.111}$$

$$u = \Sigma_m \Sigma_n u_{mn} (\frac{\lambda}{a} x) \cos (rm)\phi \quad (m = 0, 1, 2,....\infty; n = 1, 2, 3,....\infty) \tag{4.112}$$

$$v = \Sigma_m \Sigma_n v_{mn} (\frac{\lambda}{a} x) \sin (rm)\phi \quad (m = 0, 1, 2,....\infty; n = 1, 2, 3,....\infty) \tag{4.113}$$

Comparison of all the above equations for displacements u, v and w as well as stress resultants shows that if a table of the values of the functions $\bar{f}_{mn} (\frac{\lambda}{a} x)$, $\bar{u}_{mn} (\frac{\lambda}{a} x)$ and $\bar{v}_{mn} (\frac{\lambda}{a} x)$ is found for each harmonic term, solutions for different amplitudes of terms can be easily deduced. Thus many different load cases can easily be solved, once the individual harmonic terms have been found. Multiple load cases can be solved also by substituting rm for m and retaining n in the relevant equations. For the factors of w_{mn}, u_{mn} and v_{mn}, by doing the same substitution of rm for m, the corresponding result must also be multiplied by r.

4.4 COMPUTER EVALUATION FOR A CIRCULAR CYLINDRICAL SHELL

Following the derivation of expressions for the deflections, resultant forces and moments in a circular cylindrical shell caused by longitudinal local loading, these formulas were evaluated numerically.

A Fortran computer program was written, named LECS (Linear Elastic analysis of Cylindrical Shells), with the aim of calculating the relevant displacements and stress resultants induced by local loadings in a simply-supported cylindrical shell. The program includes functions for analysing various loading patterns involving longitudinal, radial and circumferential loads and longitudinal and circumferential moments as well as any combination of these individual loading cases. The computed results from the actions of radial and circumferential loads were compared with both Bijlaard's results and predictions from a FELASH finite element analysis. The comparison demonstrated a good agreement. In this section, it is not intended to present these results for the cases when the shell is subjected to local radial or circumferential loads. The main purpose is to use the above derived expressions to predict the displacements and stresses of a example cylindrical shell which is simply supported at the two ends and subjected to a local longitudinal patch load alone, in view of the fact that a cylindrical silo structure often takes such a loading in service. Finite element calculations using the FELASH program suite (PASHA and LEASH) were also performed for comparisons.

An example cylindrical shell was chosen with a unit thickness t=1, the radius-to-thickness ratio a/t = 500 and the height-to-radius ratio l/a = 2.0. An equally distributed longitudinal load p_x = 0.1 MPa was applied on the surface of the shell wall within a square with sides $2b_1 = 2b_2$ = 0.2a, ie. $\beta_1 = \beta_2 = 0.1$, and with its centre at x = l/4, $\phi = 0$. The material of this elastic cylindrical shell was taken to be steel with a Young's modulus $E = 2 \times 10^5$ and Poisson's ratio υ = 0.3. The total number of double harmonics m and n was taken as 100 respectively in the calculations using both the LECS and LEASH programs. The ends of the cylindrical shell were assumed to be simply supported with the same boundary conditions as expressed previously in Sections 4.3.4 and 4.3.5. The displacements and stress resultants were calculated for this simply-supported cylindrical shell under the local longitudinal load. All membrane forces and moments were those per unit width of shell wall. Tensile forces were considered as positive.

Predictions of the stresses and displacements in this sample cylinder were conducted, using both the LECS program and the LEASH finite element program. For a cylindrical shell subjected to a longitudinal load symmetrically distributed to the generatrix at $\phi = 0$ within a local area, the membrane stress in the axial direction is significant compared with the other

stresses caused by this local load, and the circumferential displacement v is trivially small compared with the displacements in the radial and axial directions. Thus the following comparative studies mainly focused on the longitudinal (axial) membrane force and circumferential bending moment and the axial and radial displacements, which are shown in Fig. 4-2 to Fig. 4-9.

Figures 4-2 and 4-3 give the axial (longitudinal) membrane force N_x caused by the local square load in the shell wall. The former shows the dispersal of the axial membrane force N_x along the generatrix at $\phi = 0$ whilst the latter shows the variations of N_x in the circumferential direction at differing heights. Comparing the results of N_x predicted by LECS and LEASH, it was found that they matched reasonably well both in value and in trend. In general, the LECS results are higher than the LEASH ones. However, it can be observed from Fig. 4-2 that the differences between the two results increases in the region adjacent to the edge of the loaded area (x=200) to the end of the cylinder (x=0). At the end x=0, the LECS value is about 1.7 times as large as the LEASH value. The discrepancy between the results in that region from these two adopted methods may be due to the fact that the loading area is closer to the end (x=0) of the cylinder and the predictions are accordingly influenced by the boundary conditions. It is also possible that some part of the discrepancy is attributable to the differences between the Timoshenko shell theory used in this algebraic analysis and the Sanders shell theory used in the finite element analysis LEASH.

The comparisons of the circumferential bending moment M_y along the generatrix at $\phi = 0$ and at different levels in the cylinder are shown in Figs 4-4 and 4-5 respectively. Similarly the axial displacement u and the radial displacement w are shown in Fig. 4-6 to Fig. 4-9. Again, they also give similar findings to those for the axial membrane force N_x. In summary, the LECS and the LEASH results agreed fairly well, though in general, LECS gives slightly higher values than LEASH does.

It can be concluded from the above comparative studies that the linear elastic solution of the shell bending equations derived using the double Fourier series is applicable to practical design and analysis, and would lead to slightly conservative (higher) results than the finite element method.

4.5 SUMMARY AND CONCLUSIONS

Algebraic expressions for the displacements and stresses in a circular cylindrical shell under local longitudinal loadings have been developed in this chapter. A double Fourier series has been used to express both the local loads applied to the shell and the displacements and stresses induced by the local loads. These expressions for displacements and stresses have been documented for the case of simply supported boundary conditions at both ends of the shell.

The method discussed in this chapter is of a general nature and therefore can be applied to other cases where a circular cylindrical shell is subjected to local loadings in any other direction and may have different boundary conditions.

A computer program has been developed to evaluate the expressions derived in this chapter and the results have been compared with those obtained from finite element analysis. A satisfactory match has been found.

It should be noted that the algebraic method presented in this chapter is only applicable when the local load is be applied away from the ends of the shell. However, present studies for practical elevated silo structures are intended to start from a simple case - the discretely supported cylindrical shell, where local loads from the discrete supports are assumed to be applied immediately at the edge of the shell. To fulfill the main objective of this thesis, the later chapters of the thesis are solely concerned with the analysis of discretely supported cylindrical shells using the finite element method. Although this algebraic analysis has not been used further in this thesis, it provides a useful basis for further studies of cylindrical shell structures.

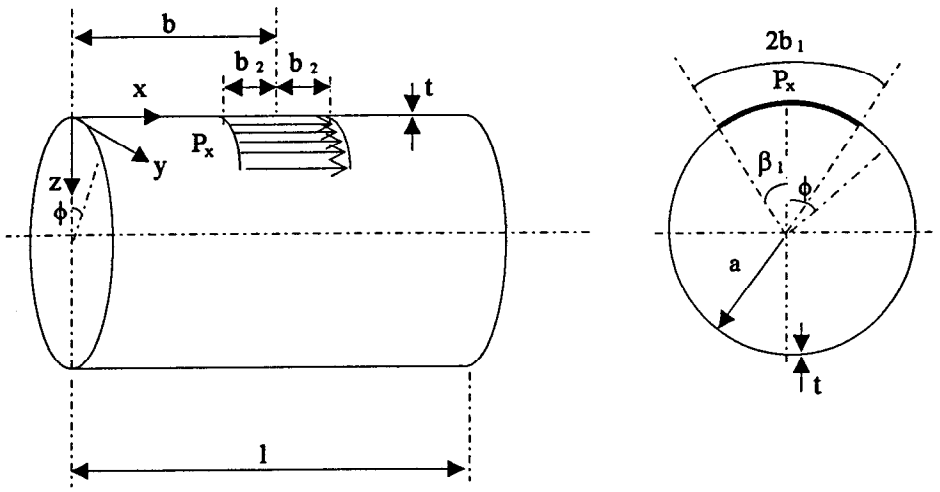

Fiure 4-1 Cylindrical Shell under a Uniformly Distributed Longitudinal Load

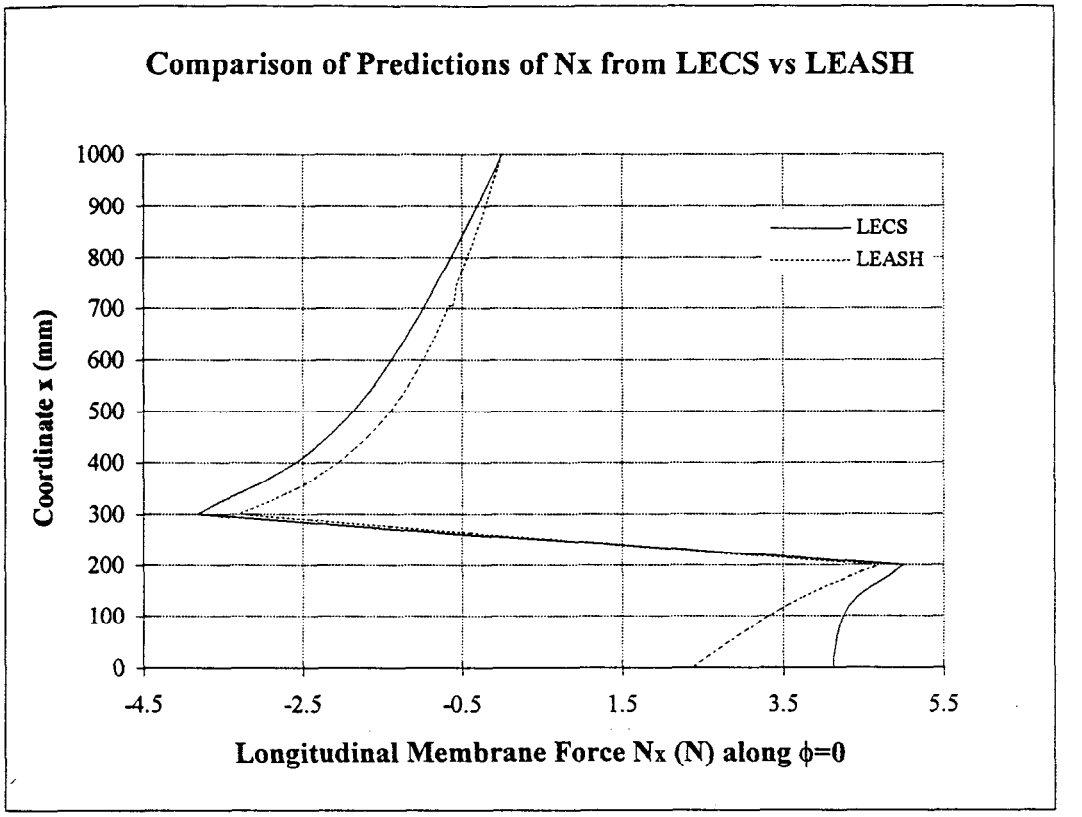
Comparison of Predictions of Nx from LECS vs LEASH
Coordinate x (mm)
1000
900
800
700
600
500
400
300
200
100
0
-4.5
-2.5
-0.5
1.5
3.5
5.5
LECS
LEASH
Longitudinal Membrane Force Nx (N) along ϕ=0

Figure 4-2

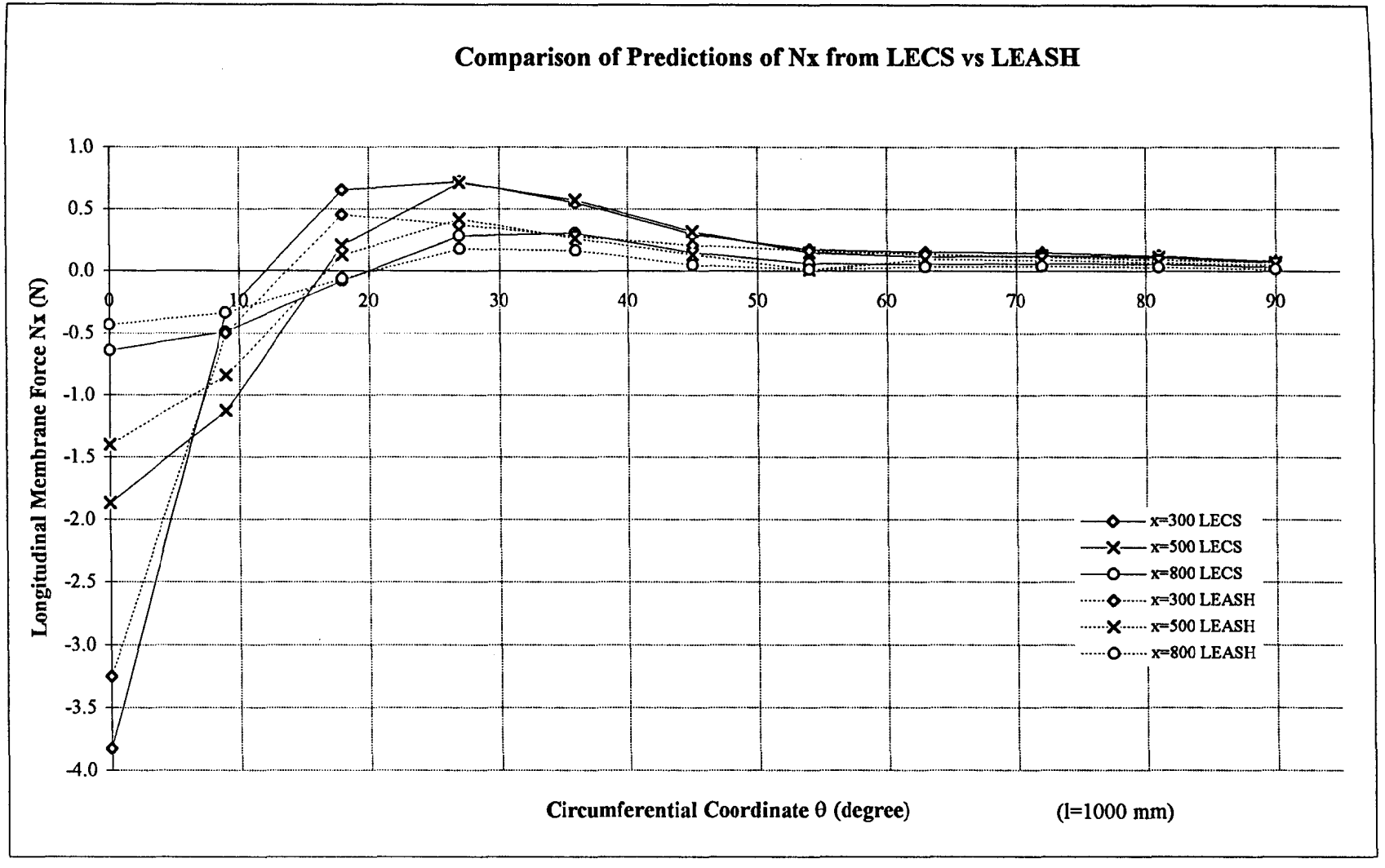
Comparison of Predictions of Nx from LECS vs LEASH
Longitudinal Membrane Force Nx (N)
1.0
0.5
0.0
-0.5
-1.0
-1.5
-2.0
-2.5
-3.0
-3.5
-4.0
0
10
20
30
40
50
60
70
80
90
x=300 LECS
x=500 LECS
x=800 LECS
x=300 LEASH
x=500 LEASH
x=800 LEASH
Circumferential Coordinate θ (degree)
(l=1000 mm)

Figure 4-3

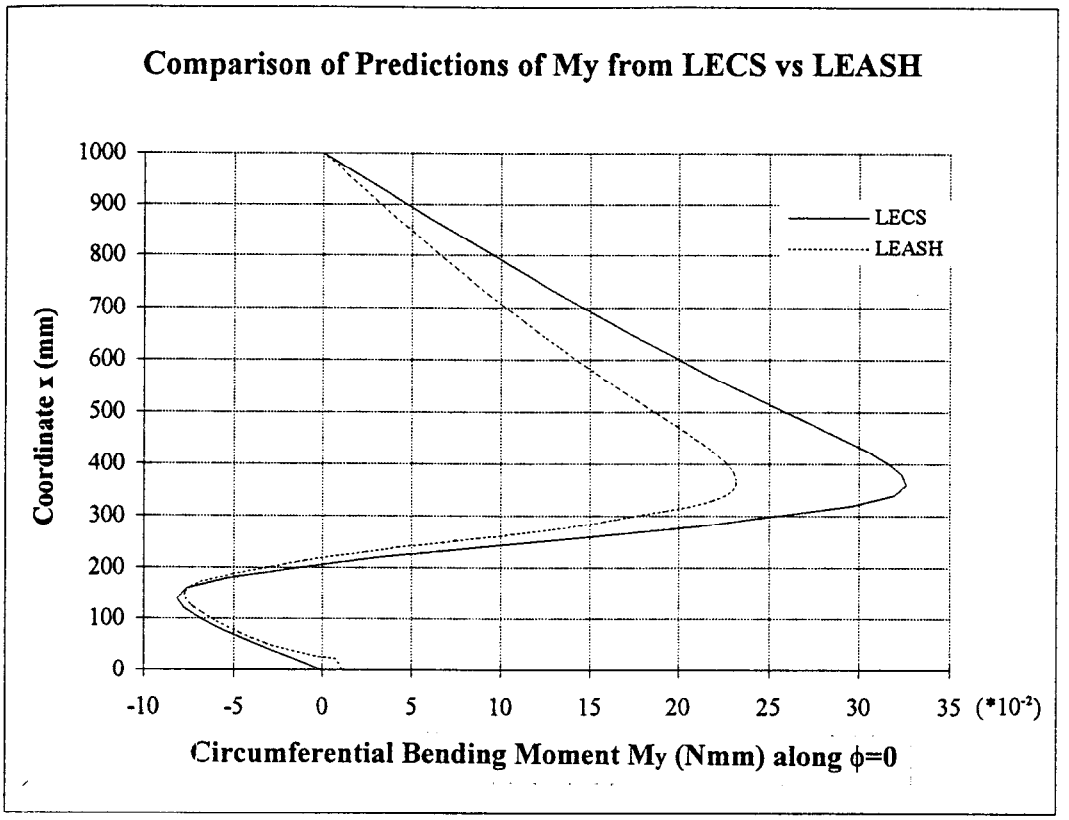
Comparison of Predictions of My from LECS vs LEASH
1000
900
800
700
600
500
400
300
200
100
0
Coordinate x (mm)
LECS
LEASH
-10
-5
0
5
10
15
20
25
30
35
(*10-2)
Circumferential Bending Moment My (Nmm) along ϕ=0

Figure 4-4

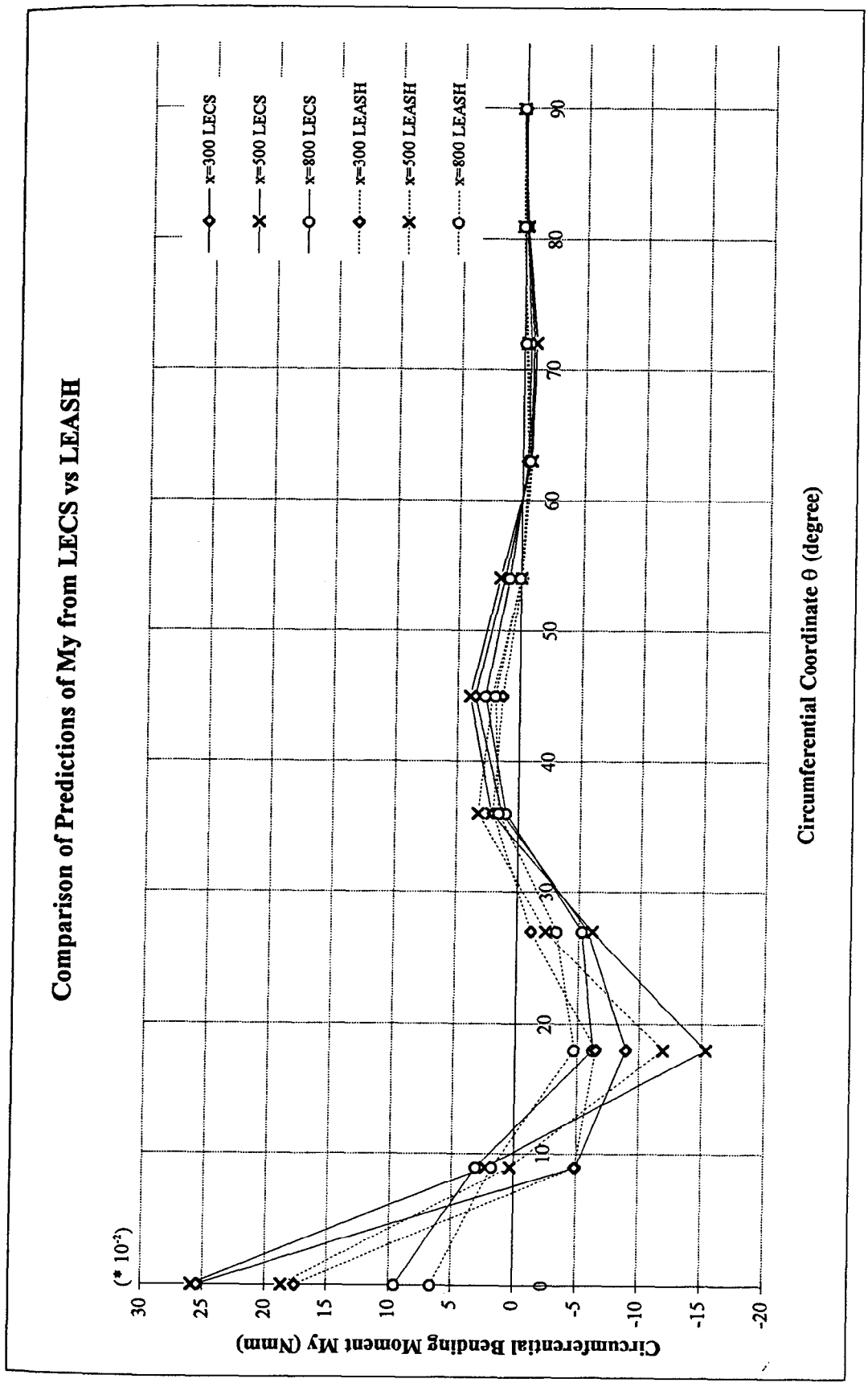
Comparison of Predictions of My from LECS vs LEASH
Circumferential Bending Moment My (Nmm)
(* 10⁻²)
30
25
20
15
10
5
0
-5
-10
-15
-20
0
10
20
30
40
50
60
70
80
90
Circumferential Coordinate θ (degree)
x=300 LECS
x=500 LECS
x=800 LECS
x=300 LEASH
x=500 LEASH
x=800 LEASH

Figure 4-5

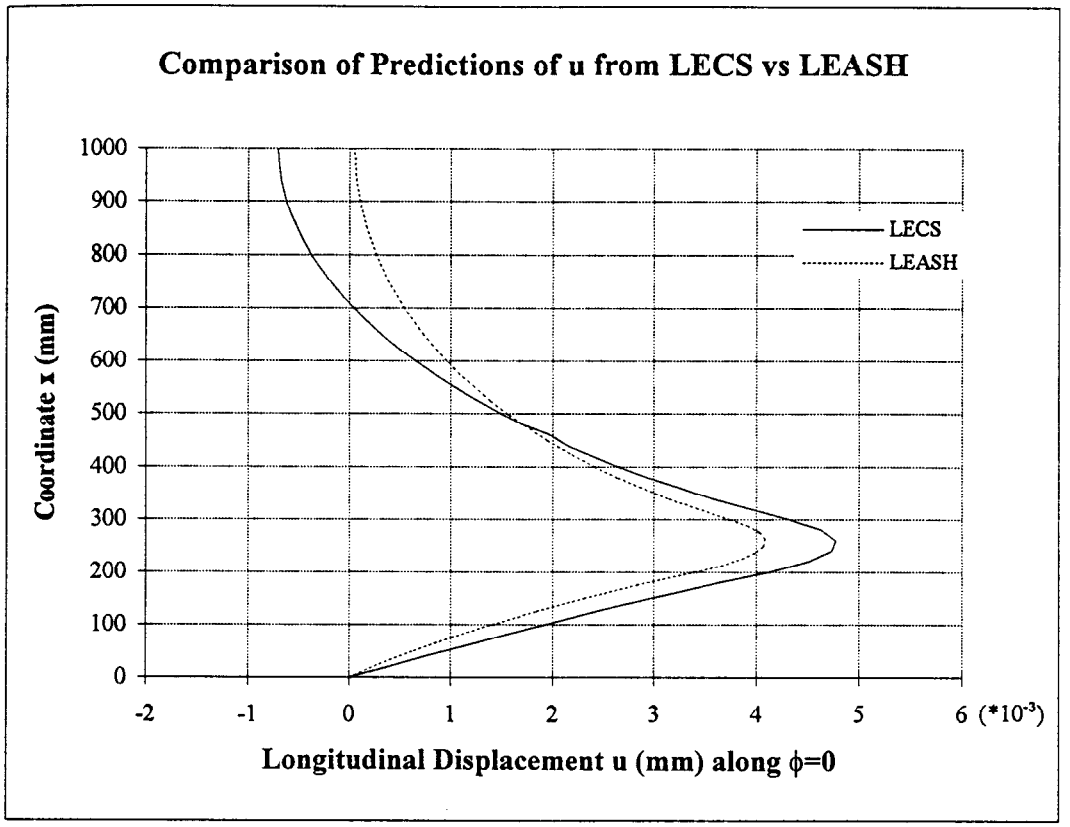
Comparison of Predictions of u from LECS vs LEASH
1000
900
800
700
600
500
400
300
200
100
0
Coordinate x (mm)
LECS
LEASH
-2
-1
0
1
2
3
4
5
6 (*10-3)
Longitudinal Displacement u (mm) along ϕ=0

Figure 4-6

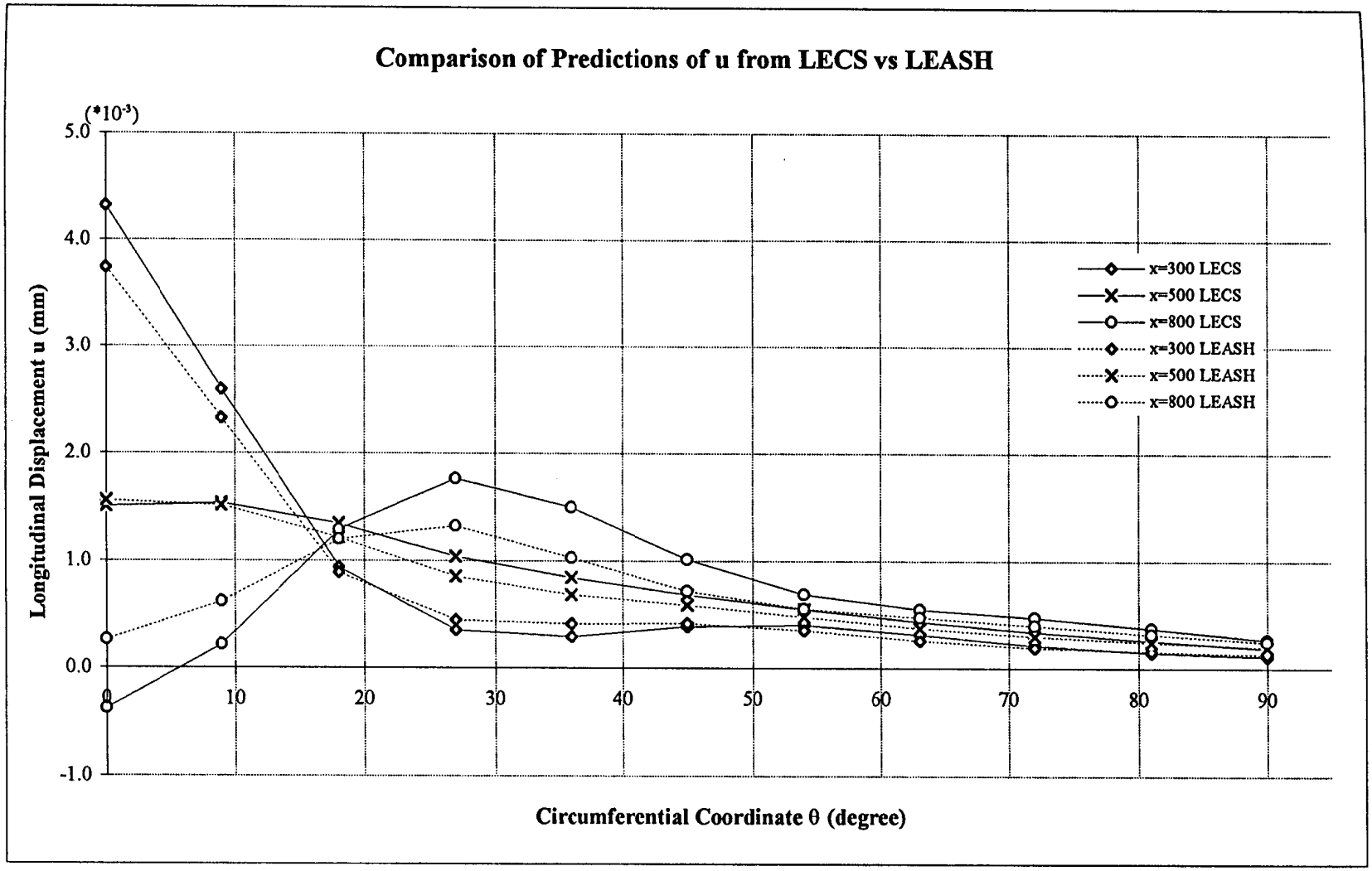
Comparison of Predictions of u from LECS vs LEASH
(*10⁻³)
5.0
4.0
3.0
2.0
1.0
0.0
-1.0
Longitudinal Displacement u (mm)
0
10
20
30
40
50
60
70
80
90
Circumferential Coordinate θ (degree)
x=300 LECS
x=500 LECS
x=800 LECS
x=300 LEASH
x=500 LEASH
x=800 LEASH

Figure 4-7

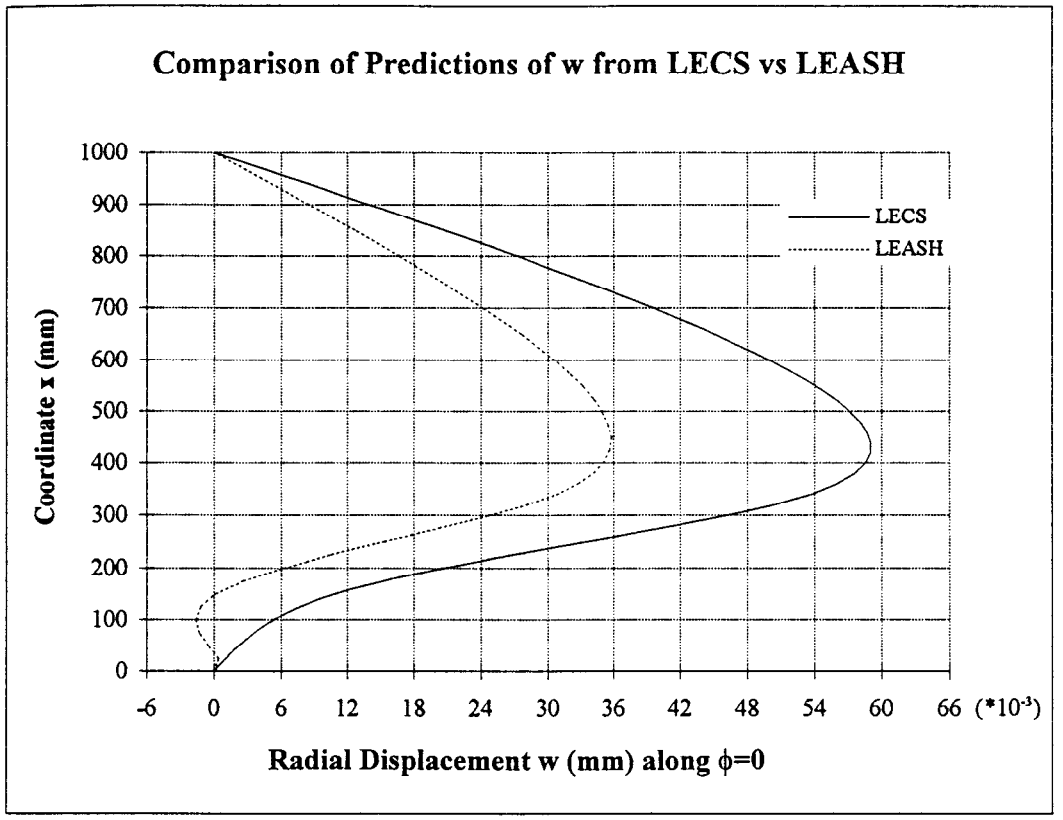
Comparison of Predictions of w from LECS vs LEASH
Coordinate x (mm)
1000
900
800
700
600
500
400
300
200
100
0
-6
0
6
12
18
24
30
36
42
48
54
60
66
(*10-3)
LECS
LEASH
Radial Displacement w (mm) along ϕ=0

Figure 4-8

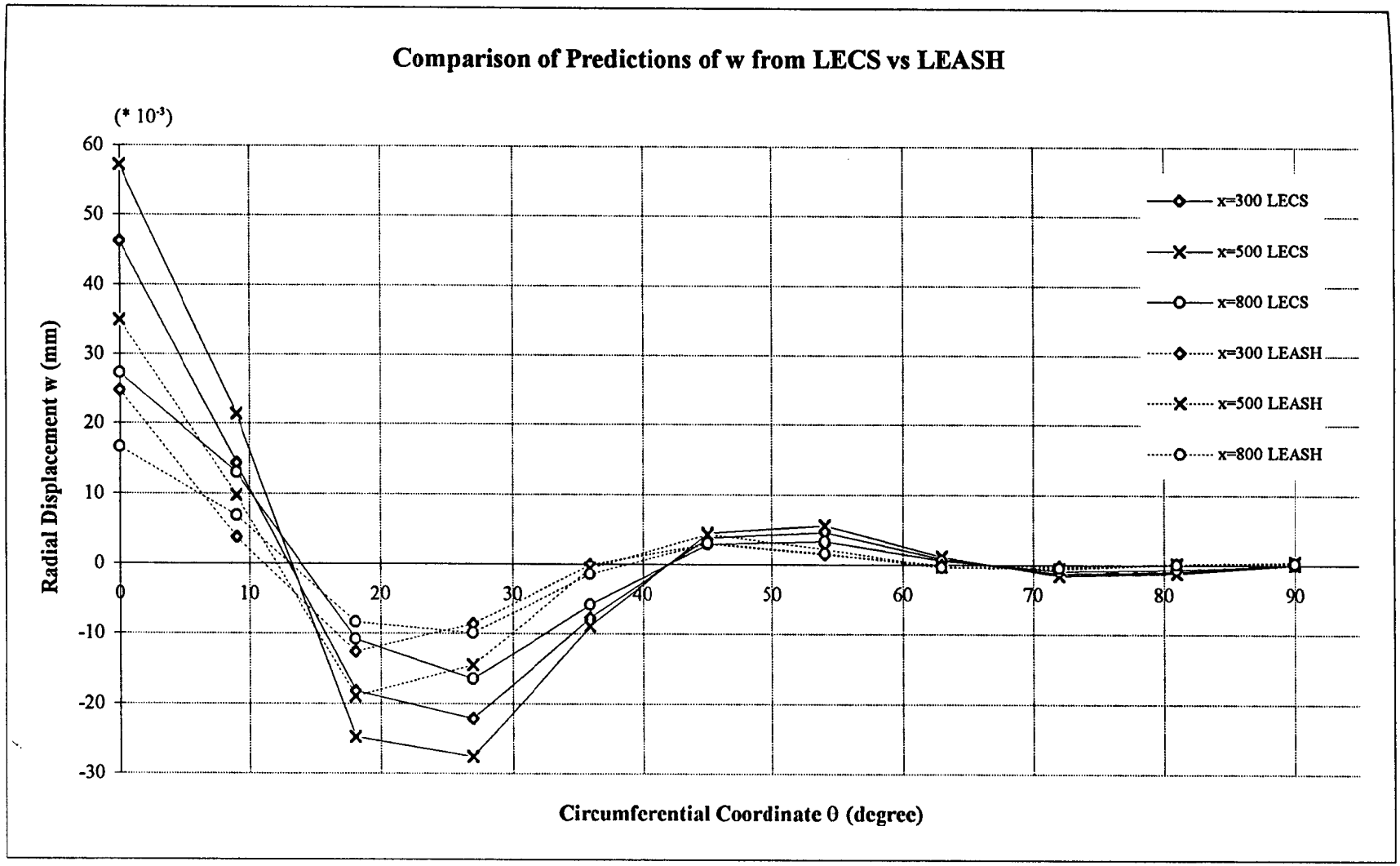
Comparison of Predictions of w from LECS vs LEASH
(* 10-3)
Radial Displacement w (mm)
60
50
40
30
20
10
0
-10
-20
-30
0
10
20
30
40
50
60
70
80
90
Circumferential Coordinate θ (degree)
x=300 LECS
x=500 LECS
x=800 LECS
x=300 LEASH
x=500 LEASH
x=800 LEASH

Figure 4-9

CHAPTER 5

LINEAR ELASTIC STRESS AND BIFURCATION ANALYSES OF DISCRETELY SUPPORTED PERFECT CYLINDERS

5.1 INTRODUCTION

It is widely accepted that the governing loading on the walls of metal silos is usually axial (longitudinal) compression, combined with circumferential tension, caused by the bulk solids stored in silos. Large elevated silo structures are generally supported on a number of discrete supports of finite width. The discrete supports induce high stresses adjacent to the support termination. In particular, very high meridional membrane stresses arise above the support, which can cause buckling of the shell at a load much lower than that for a uniformly supported shell. Most elevated silos are thin shells so that the buckling behaviour is entirely elastic. Practical field observations indicate that the governing failure mode of silos is frequently buckling under axial compression.

Initial exploratory investigations [Teng and Rotter, 1989, 1990, 1991; Rotter et al, 1991; Guggenberger, 1991; Rotter and She, 1993] of the buckling of elevated silos under axial compression have focused on thin-walled cylinders directly supported on discrete supports of finite width. The axial compression from bulk solids has been modelled by a uniformly distributed downward traction on the cylinder wall. Because the loading from the support is intense and local, the stresses decay rapidly away from the support, and when buckling occurs, it is in a regime of very non-uniform stress. Studies of the linear elastic stress distribution and the linear bifurcation mode are therefore very helpful in developing an understanding of the problem.

Linear elastic bifurcation analyses of perfect cylinders are based upon small deflection theory and yield linear buckling loads which usually provide an upper bound to the actual elastic buckling strength. It is therefore difficult to develop design standards from them. However, because of the much quicker computer running time when extracting buckling eigenvalues, linear bifurcation analysis is still of value in providing a starting point for more complex analysis and developing a basic understanding of the structural behaviour of practical silos in an approximate manner.

To broaden current knowledge of the bifurcation behaviour of discretely supported perfect cylinders, this chapter presents linear elastic pre-buckling stress and buckling eigenvalue analyses, with special emphasis on the stress distribution immediately above the support and the bifurcation loads of the cylinder under different loading patterns. The finite element analysis is performed by using the ABAQUS program package. The effects on the buckling strength of many of the governing geometric parameters of the cylinder are also examined.

5.2 FINITE ELEMENT MODELLING

All the numerical calculations of the study described here were performed using the finite element program ABAQUS. The 9-node quadrilateral shell element S9R5 available in ABAQUS was chosen.

The discretely supported cylinder was assumed to have its discrete supports terminating at the lower edge of the cylinder. The supports were assumed to be equally spaced around the circumference of the lower edge. They were modelled as rigid supports, in which all the displacements and rotations of the lower edge in contact with the supports were completely restrained. Apart from the connections with supports, both the lower edge and the upper edge were assumed to be restrained against both radial and circumferential displacements. Three types of axial loading were applied to model extreme cases of practical loadings on the silo walls from the stored bulk solids as shown in Fig. 5-1 . These three are: a) a roof load: uniform applied loading at the upper edge of the cylinder (as in a lab test), b) uniform wall friction: uniform shear pressure on the whole surface of the shell (the most serious case which can arise in a silo structure), and c) a hopper load: uniform applied loading on the lower edge of the cylinder (as from a hopper in a silo). The definitions of the three loading cases were described in Section 1.6.2 of Chapter 1. For the purpose of this analysis, the whole cylinder was divided into 2n symmetric individual sections, exploiting the geometric and loading symmetry. For simplicity, any 1/2n section of the cylinder (Fig. 5-1a) may be modelled for finite element analysis instead of the whole shell, provided that the number of supports n is not very large [Teng and Rotter, 1991; She and Rotter, 1993]. The boundary conditions for the two vertical (meridional) edges of the modelled section are determined by symmetry considerations. Very fine meshes were used for the analyses undertaken in this chapter, especially in the areas near the support, in order to model the local stresses and deformations effectively.

The geometry of the cylinder (Fig. 5-1a) may be defined in terms of the following geometric parameters: the radius-to-thickness ratio R/t, the height-to-radius ratio H/R, the support-width-

to-radius ratio d/R and the number of supports n. Many calculations were performed to examine the effect of these parameters on the stress distribution and the buckling strength.

The cylinders were assumed to be linear and isotropic and made of steel with Young's modulus $E = 2\times10^5$ MPa and Poisson's ratio $\nu = 0.3$. The results obtained can be applied to other materials, though small errors are present if Poisson's ratio is very different.

To illustrate the results in a manner which can be easily assimilated, the meridional membrane stress arising in the cylinder $\sigma_{m\phi}$ is normalised by the classical elastic critical stress for a cylinder under uniform axial compression σ_{cl}. The total load applied to the cylinder at linear bifurcation is presented in terms of the normalised mean meridional membrane stress above each support, ie. σ_m/σ_{cl} . The relationships between this parameter and the applied loadings have been given in Chapter 1.

5.3 PRE-BUCKLING STRESS ANALYSIS

In discretely supported perfect cylinders, linear bifurcation analysis [Teng and Rotter, 1991] has suggested that the buckling behaviour may mostly depend on the meridional membrane stress distribution above the support. For cylinders on rigid supports, the highest meridional membrane stresses occur in a zone slightly above the support termination instead of along the extreme bottom edge, where strong restraints are present. The buckling deformations are localised in the zone with the highest meridional compressive stress. The geometric parameters of R/t, H/R, d/R and n were found to alter the rate of stress dispersal in the cylinder and lead to significant changes in the buckling strength. This knowledge considerably assists the understanding of buckling phenomena of practical silo structures.

The study described in this section is mainly focused on examining the effect of the position of axial loading on the pre-buckling stress distribution (Fig. 5-1a). Only the meridional membrane stress arising above the support centreline is investigated because this dominates the buckling behaviour. For all the cases analysed, the same total axial load was assumed to be applied to the cylinders.

Figure 5-2 shows the vertical variation of the meridional membrane stress above the support centreline in a cylinder on four discrete supports and subjected to the three types of axial compressive loading. The three curves relate to the cases of roof load, wall friction load and hopper load respectively. It can be observed that for the same total load applied, in general, the roof load gives rise to the highest stresses above the support centreline, the hopper load brings

about the lowest and the wall friction load gives an intermediate result. In addition, the highest stresses from the three loading cases are found to occur in the same region ($0 < Z/t < 100$), and in a similar pattern. In this small region, the curve for uniform wall friction appears to be very close to that for roof loading. This indicates that both the roof load and the wall friction may induce nearly the same stress state adjacent to the bottom of the cylinder. However, the hopper load curve is quite distant from other two curves. The reason why the stresses from the hopper load are smaller is that this loading puts large parts of the cylinder into meridional tension. In addition, some of the hopper load is transferred directly into the support from below and never reaches the cylinder, as shown in Fig. 5-1b. Moving upwards into the shell, the meridional membrane stress decreases rapidly within a short distance. The rate of stress decrease is caused by dispersal of the stresses into a larger part of the shell and further up, the rate of stress decrease becomes almost constant. At the upper edge, the wall friction and hopper load curves both reach zero. This is because the wall friction load and the hopper load have no effect on the stress there. By contrast, for the roof load, the stress reaches the value of the load applied at the top edge of the shell.

As the height of the cylinder changes, the meridional membrane stress distribution above the support centreline under these three loading patterns is observed to have the same form as above, except in a very short shell. In a very short cylinder of H/R=0.2, the modified stress dispersal is illustrated in Fig. 5-3. The form of the curves differs very much from the pattern of Fig. 5-2, especially in the area close to the bottom edge of the cylinder. In that area, the three curves show that the stress continues to increase approaching to the bottom edge even though the support is rigid. Because of the short height and the higher stress at the lower edge, the stress reduces throughout the whole height of the shell and is thus more non-uniform.

As the width of the support changes, the stress distribution pattern remains unchanged until the support becomes very narrow or very wide. Normally the support width used in practical silos lies between d/R=0.05 and d/R=0.3. Figures 5-4 and 5-5 show the stress distribution profiles for the cases when a cylinder is supported on 4 very narrow supports with d/R=0.05 and on 4 very wide supports with d/R=0.3. It can be seen that a narrow support induces a very high meridional membrane stress in the cylinder and changes the pattern of stress distribution dramatically. In this case, the maximum stress occurs at the bottom edge rather than at a short distance above the edge as shown in Fig. 5.2. By contrast, a wide support leads to relatively low stresses in the small area above the support. The difference between the maximum stresses due to the roof load and the wall friction increases with an increase in the support width as shown in Figs. 5-2 and 5-5. The distance between the point where the maximum stress occurs and the bottom edge of the cylinder is dependant on the support width. In general, a wider

support yields a higher position for the maximum stress. This also affects the bifurcation buckling modes, illustrated in Figs. 5-10 and 5-11.

The effect of the number of discrete supports on the stress distribution was also investigated. The same conclusions were reached as those of Teng and Rotter [1991]. As shown in Fig. 1-18a of Chapter 1, as the number of supports increases, the peak meridional membrane stress induced in the cylinder declines rapidly in the small region near the bottom edge, and the stresses become more uniform throughout the height of the shell. When there are many supports, the stress distribution profile approaches that formed in a uniformly supported shell.

The effect of the thickness of the cylinder was also studied. The variation of the stress above the support centreline was found to be similar to that obtained by Teng and Rotter [1991] as shown in Fig. 1-18b of Chapter 1. If the same total load is applied to the shell, as the radius-to-thickness ratio R/t varies from 200 to 1000 (R remains constant whilst t varies), the dimensionless meridional membrane stress above the support centreline alters slightly but its distribution retains a similar pattern. For a very thin cylinder (R/t=1000), the highest stress at a short distance above the support increases by around 10% over that for a thick cylinder (R/t=200).

From the results obtained so far, it can be concluded that the type of loading applied to a discretely supported perfect cylinder may alter the stress distribution significantly, and therefore it is expected that it may induce significant changes in the buckling strength of the shell.

5.4 BIFURCATION ANALYSIS

In this section, linear eigenvalue buckling loads were obtained using the ABAQUS program. Only the lowest buckling load (i.e. the first eigenvalue) was calculated. The corresponding buckling modes were also obtained.

5.4.1 Example Study

A perfect cylinder with R/t=500, H/R=2.0, d/R=0.2 and n=4 was initially used as an example. Linear buckling eigenvalue analysis was conducted to examine the buckling behaviour of the cylinder subject to the three axial load cases of Fig. 5-1a. The initial loads, the corresponding buckling eigenvalues, and the dimensionless mean buckling stresses are listed in Table 5-1. It can be seen that, of the three loading cases, the roof load results in the lowest buckling load, which is 1.6% and 25% lower than the ones calculated for the wall friction load case and the

hopper load case respectively. The buckling deformations in the cylinder under the three load cases are found to be in a similar pattern. The buckle occurs in the zone of high and rapidly varying stresses just above the support. The buckling mode in a cylinder subject to a roof load is shown in Fig. 5-6.

The results from the bifurcation analysis are consistent with those from the pre-buckling stress analysis described in Section 5.3. It demonstrates that the magnitude of the buckling load varies with the magnitude of the maximum stress. A higher pre-buckling local stress induces a smaller buckling load. Therefore, it is clear that the locally higher stress above the support is crucial to the formation of the buckle and strongly influences the buckling strength of the cylinder. In the next section, parameters which have been discovered to strongly affect the stress distribution in the critical area are also examined to explore their influence on the buckling strength.

5.4.2 Parametric Studies

The cylindrical barrels of practical silos are generally thin shells with radius-to-thickness ratios ranging between 200 and 1000, support-width-to-radius ratios between 0.05 and 0.3, and shell height-to-radius ratios between 0 and 20. The parametric study in this section is intended to explore the buckling behaviour and buckling strength of discretely supported perfect cylinders of various geometries, characterised by R/t, d/R and H/R, which are varied within the above ranges. Throughout the study, four discrete rigid supports are used to support the cylinder.

The dimensionless mean meridional membrane stresses above the support at linear bifurcation buckling are listed in Tables 5-2 and 5-3 and plotted in Figs 5-7 and 5-8, for the cases where the cylinder has a higher aspect ratio (H/R=2.0) and a lower aspect ratio (H/R=0.2) respectively. In both cases, the radius-to-thickness ratios were chosen as 200, 500 and 1000 and the support-width-to-radius ratios as 0.05, 0.2 and 0.3.

From the bifurcation analyses, it was discovered that the dimensionless buckling strength generally varies inversely with both the radius-to-thickness ratio R/t and the support-width-to-radius ratio d/R (Figs 5-7 and 5-8). For each set of R/t, d/R and H/R, the roof load case always produces the lowest buckling load, wall friction leads to a slightly higher buckling load, and the hopper load case produces the highest strength. All the buckling deformations are found to occur in the highly stressed local area immediately above the support.

When the parameter R/t changes, the total load at buckling and the normalised mean buckling stress above the support both reduce with an increase in R/t. Changes in the corresponding

buckling modes can be seen in Fig. 5-9. It is noted that more meridional buckling waves occur in the buckle area for thinner cylinders but the waves get smaller in size with increasing R/t. When the three loading cases are compared, the differences in strength between the wall friction, hopper load and roof load are found to decline as R/t increases (Figs 5-7 and 5-8).

Variations in the support width, represented by the parameter d/R, induce notable changes in both the strength and buckling deformation. As the support becomes narrower, the total buckling load of the cylinder becomes smaller. When this is converted into the dimensionless mean buckling stress above the support (using the Equation (1.5) or (1.6) of Chapter 1), the mean buckling stress is found to increase as the parameter d/R becomes smaller. As shown in the stress analysis of Section 5.3, the large strength variation reflects the changes in the pre-buckling stresses above the support termination. On the other hand, it is discovered that when the support is very narrow with d/R=0.05 or very wide with d/R=0.3, the strength differences between the wall friction or hopper load cases and the roof load are much larger than the differences for the situation where the support has an intermediate width with d/R=0.2. The buckling modes for roof-loaded cylinders with d/R at 0.05, 0.2 and 0.3 and other parameters R/t and H/R remaining at 200 and 2.0 respectively are shown in Fig. 5-10. The buckling deformations are much more localised for narrow supports than for wide supports.

The effect of the height of the shell is found to be significant on both the buckling strength and the buckling mode. Table 5-3 shows the same results as Table 5-2, but for a squat cylinder (H/R=0.2). The low aspect ratio changes the buckling strength very much and irregularly (Fig. 5-8), so that it is difficult to draw a general conclusion. Buckling modes under various loading cases were examined and in general they illustrate similar patterns. For the roof load case, buckling modes for various values of d/R and R/t are shown in Figs. 5-11 and 5-12 respectively. The different load cases are compared in Fig. 5-13, for a cylinder with R/t=500, d/R=0.2 and H/R=0.2. For the wall friction and hopper load cases, the centre of the buckle area occurs near the middle of the cylinder, because the cylinder is so short that the entire wall participates in the buckling mode. However, for the roof load case, the centre of the buckle moves towards the top edge, indicating that the reduced restraint at this edge (no restraint against warping at all) attracts the buckle, whilst the rigid support at the bottom edge restrains it.

5.5 SUMMARY AND CONCLUSIONS

Linear elastic pre-buckling stress analyses and bifurcation buckling analyses were conducted for perfect cylinders which are rigidly supported on discrete supports. Only axial compression

forces applied to the cylinder were considered. The results were obtained by using the finite element program ABAQUS. Three types of axial loading: roof, wall friction and hopper load were applied to the shell. The effects of the position of the applied axial load on the meridional membrane stress distribution above the support centreline and on the bifurcation buckling strength were examined. Under the three loading cases, the geometric parameters which characterise the cylinder (R/t, d/R, H/R and n) were found to strongly affect the stress dispersal and buckling strength.

In the pre-buckling stress analysis, it was found that the meridional membrane stress distribution in the cylinder is very sensitive to the position of the applied loading, especially in the vicinity of the supports where the highest stresses arise. In general, a load applied at the top boundary induces the highest stress profile in the cylinder whilst one at the bottom boundary induces the lowest. The pattern of the stress dispersal above the support centreline does not change very much for cylinders with normal geometric parameters such as R/t varying from 200 to 1000, H/R larger than 1.0 and d/R larger than 0.1, except for very short cylinders on rather narrow supports.

Because of the influence of the position of the axial loading on the stress distribution in the cylinder, changes in the linear bifurcation load also occur. For a typical cylinder with R/t=500, d/R=0.2, H/R=2.0 and n=4, roof loading leads to a lower bifurcation load than wall friction loading and hopper loading by 1.6% and 25% respectively.

As the geometric parameters of the cylinder vary within practical bounds (such as R/t between 200 and 1000; d/R between 0.05 and 0.3; H/R less than 2.0), the bifurcation buckling load changes considerably. For example, the difference between the buckling strength of cylinders subject to hopper loading may reach a factor of 7.5 between thick tall cylinders on narrow supports and thin squat cylinders on wide supports.

The linear bifurcation analyses of discretely supported perfect cylinders performed in this chapter provide some insight into the effects of many parameters on the buckling strength. However, these analyses have the deficiency inherent in small deflection theories that they ignore the effects of the pre-buckling deflections and geometric imperfections, so that they cannot be used to assess accurately buckling strength of a practical silo. In order to probe the elastic stability of realistic silo structures, nonlinear analysis based upon large deflection theory is needed. Such analyses are presented in Chapter 6.

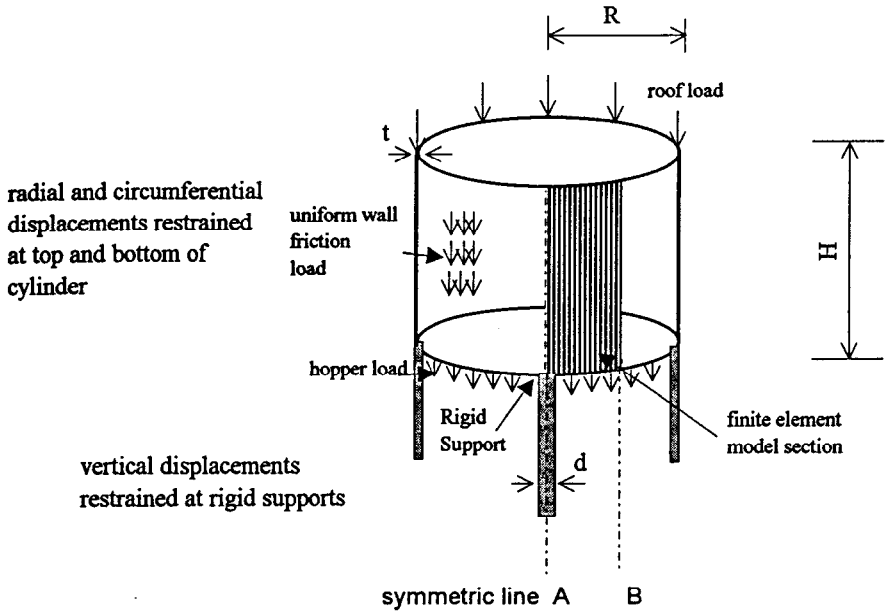

(a) Axially Compressed Cylinder on Discrete Supports

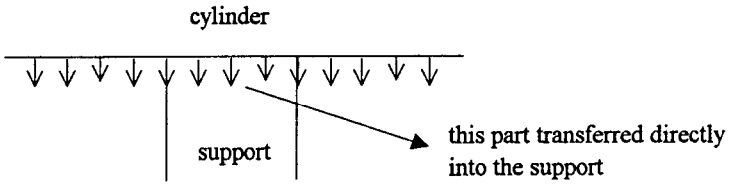

(b) Hopper Load Transference

Figure 5-1 Discretely Supported Cylinder Model

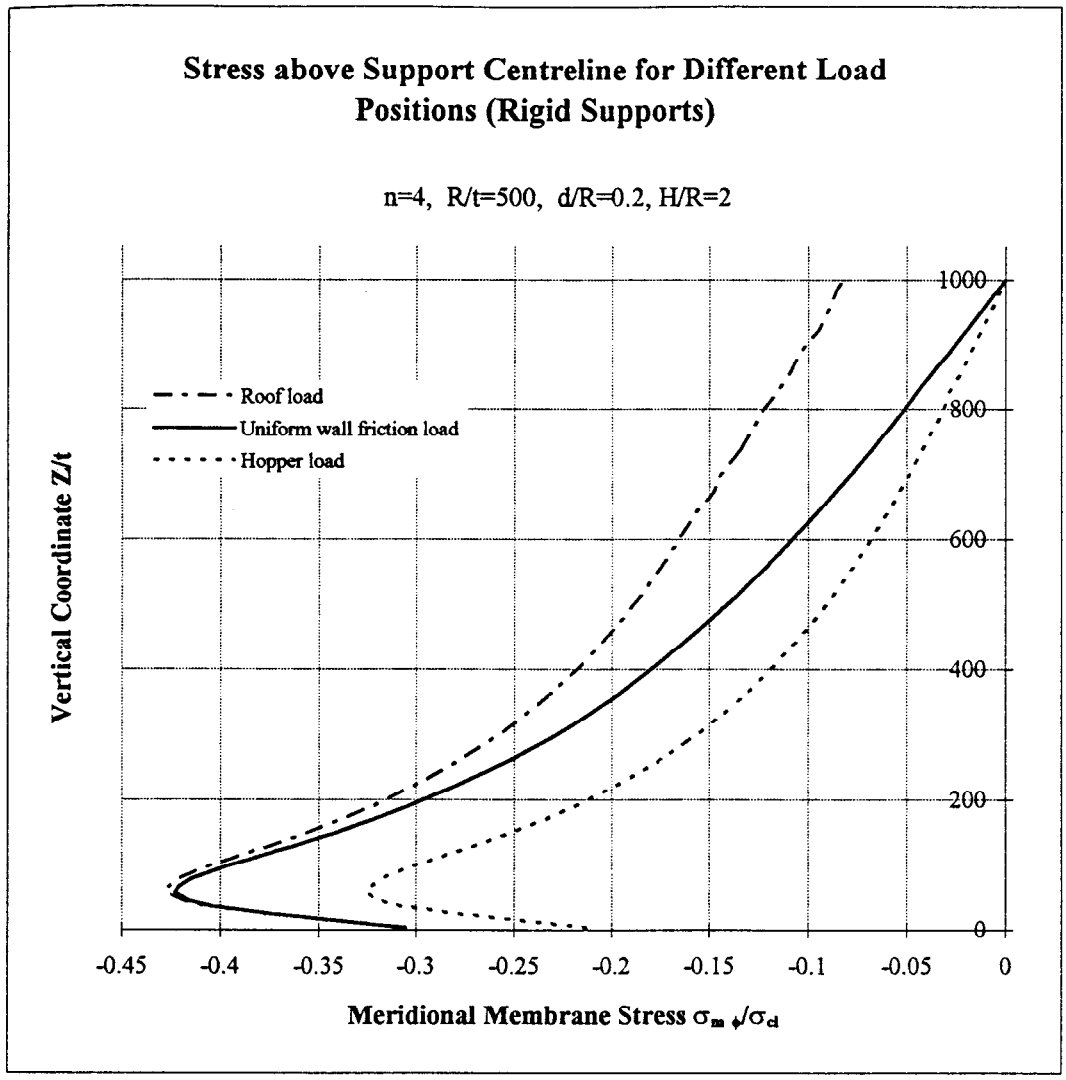

Figure 5-2

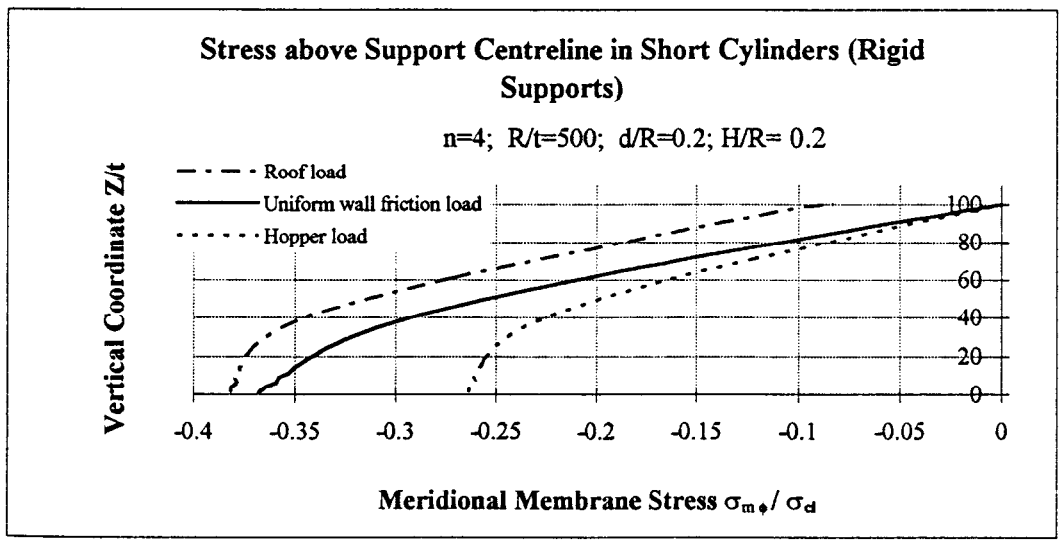

Figure 5-3

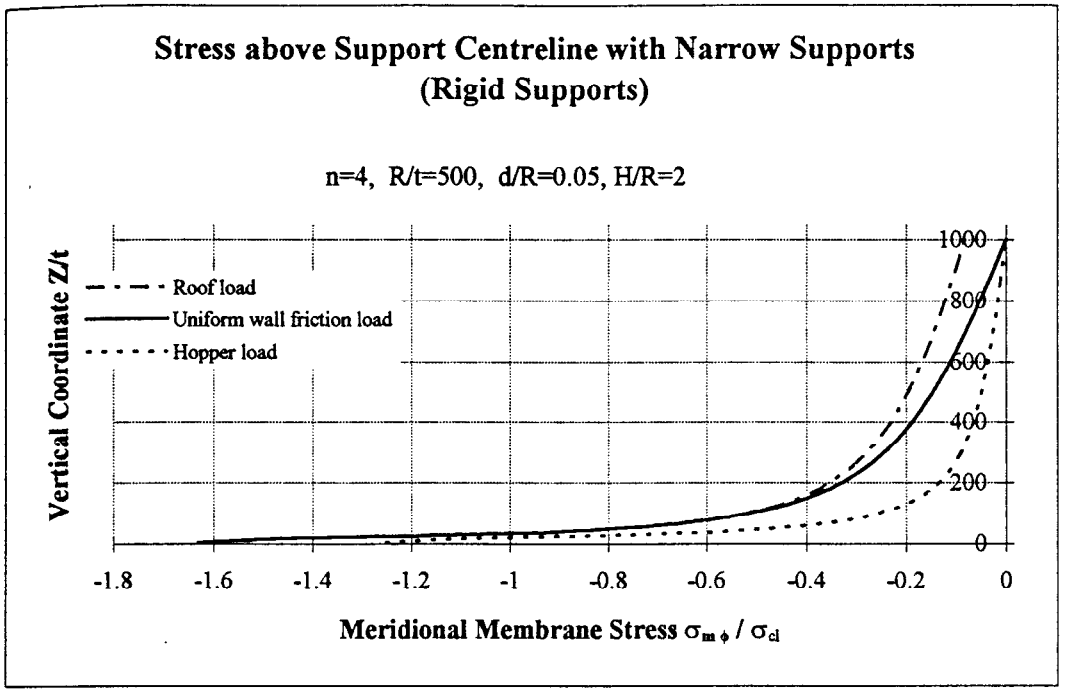

Figure 5-4

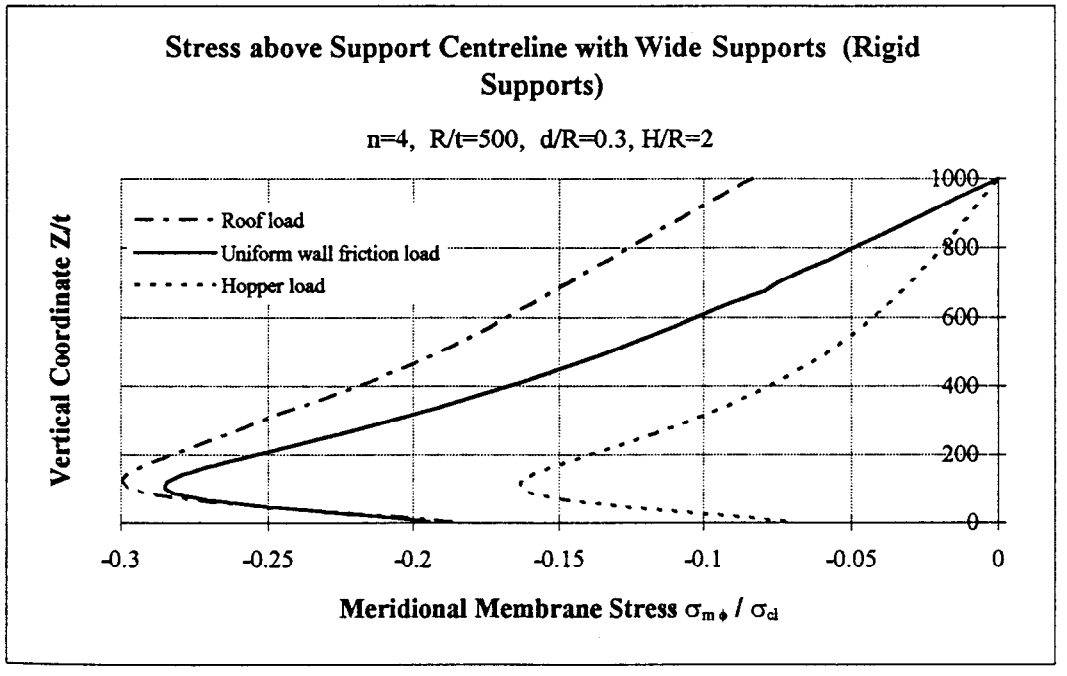

Figure 5-5

Bifurcation Buckling Mode for a Perfect Cylinder under Roof Load
n=4, R/t=500, d/R=0.2, H/R=2.0

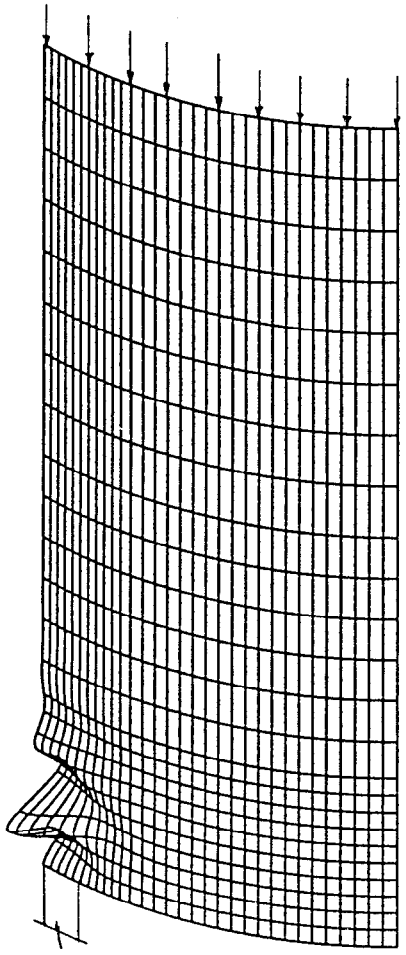

Figure 5-6

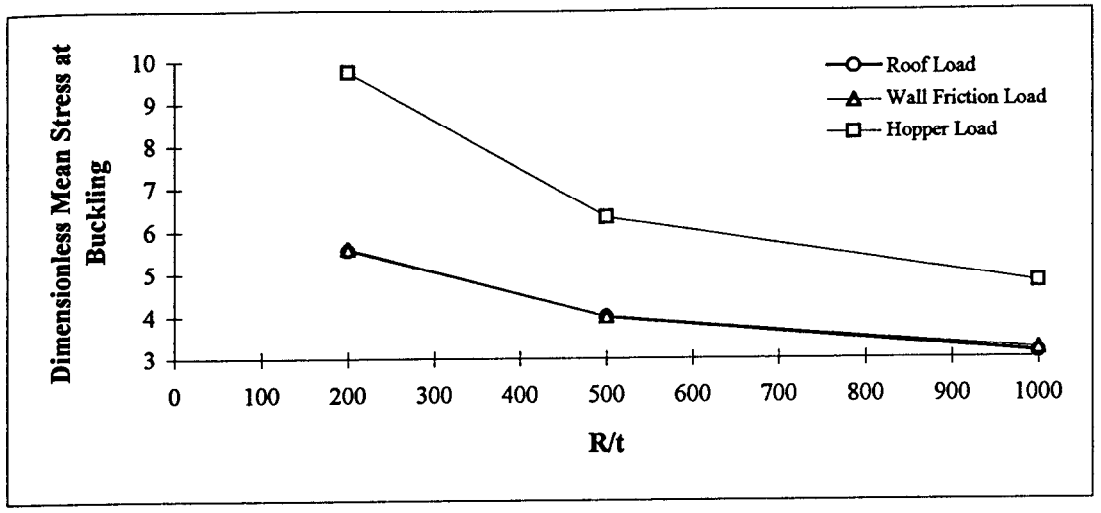

(a) d/R = 0.05

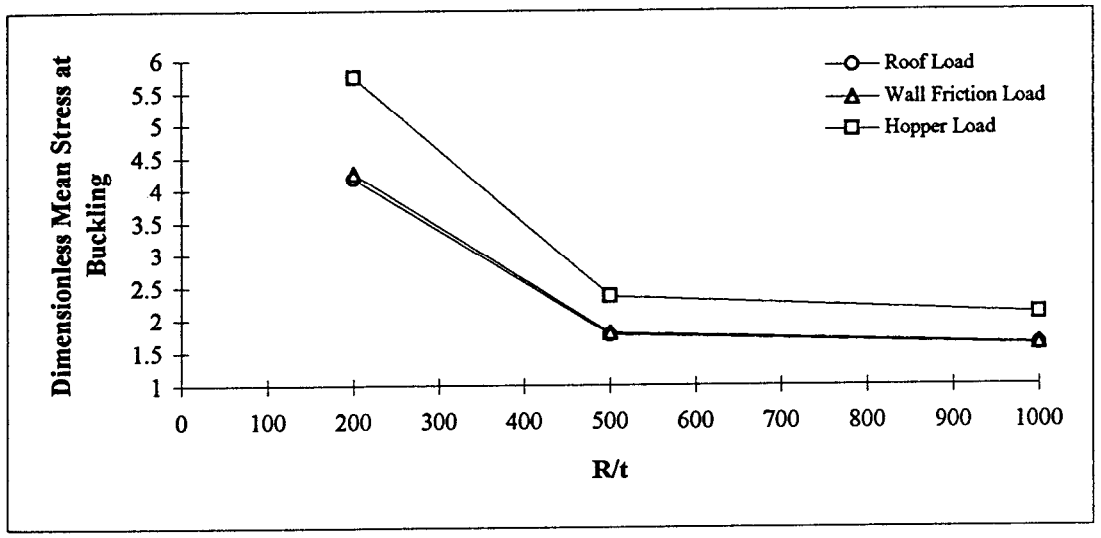

(b) d/R = 0.2

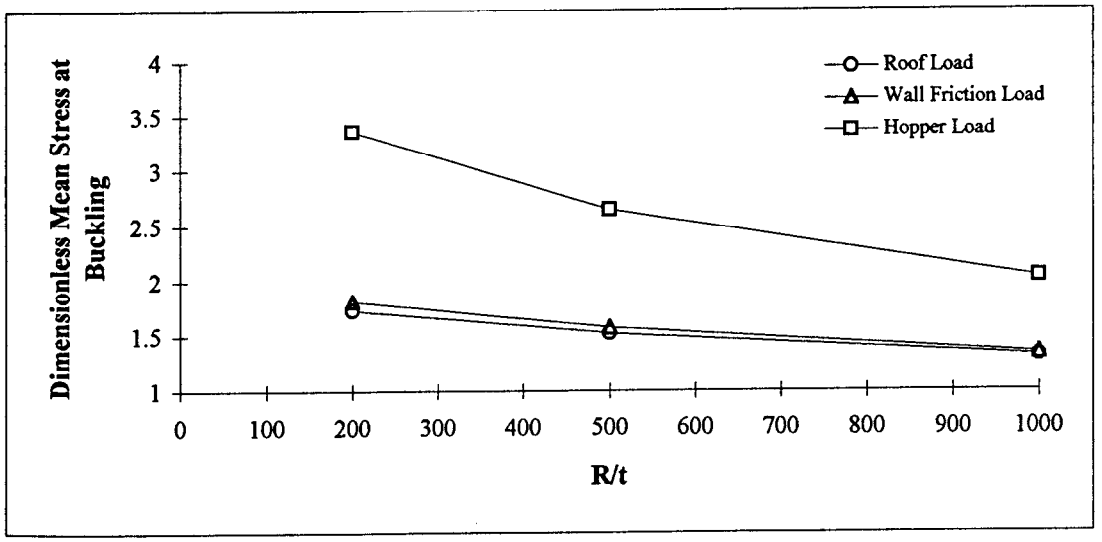

(c) d/R = 0.3

Figure 5-7 Bifurcation Buckling Strengths of Perfect Tall Cylinders under Three Loading Patterns (H/R=2.0, n=4)

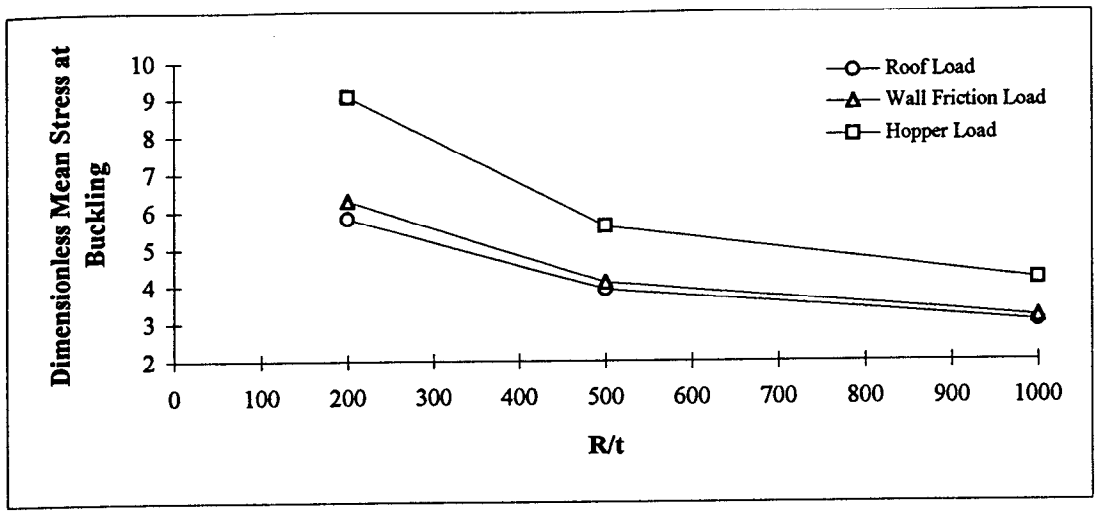

(a) d/R = 0.05

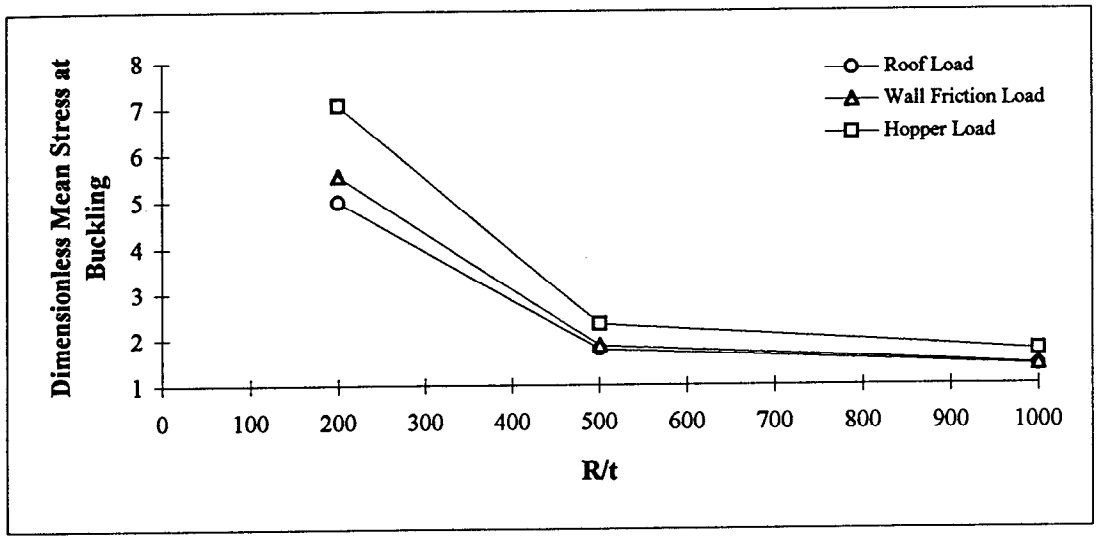

(b) d/R = 0.2

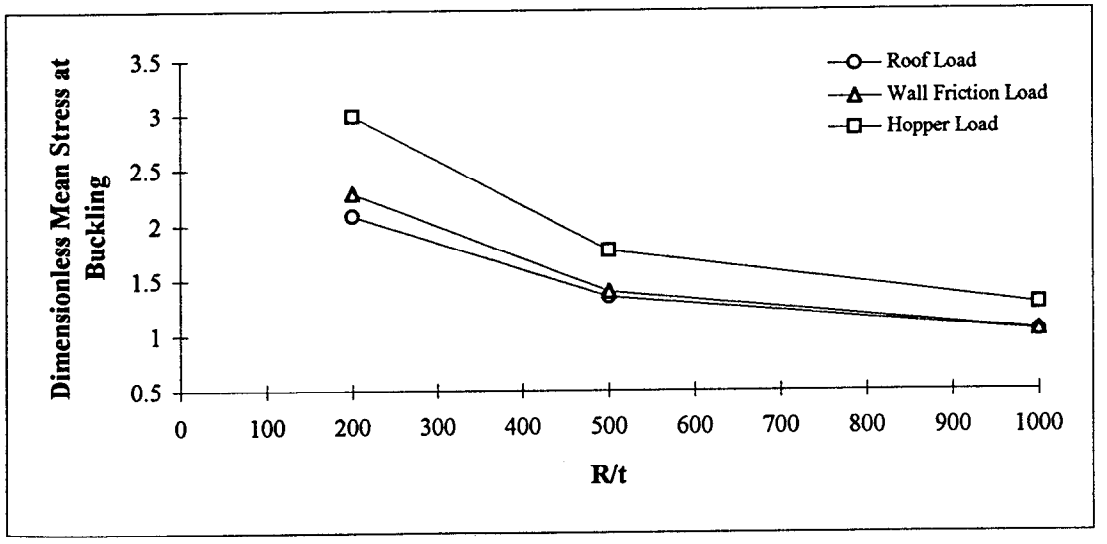

(c) d/R = 0.3

Figure 5-8 Bifurcation Buckling Strengths of Perfect Squat Cylinders under Three Loading Patterns (H/R=0.2, n=4)

Linear Bifurcation Buckling Modes for a Perfect Cylinder:
Changes with Cylinder Thickness t for a Tall Cylinder
d/R=0.2, H/R=2.0, n=4

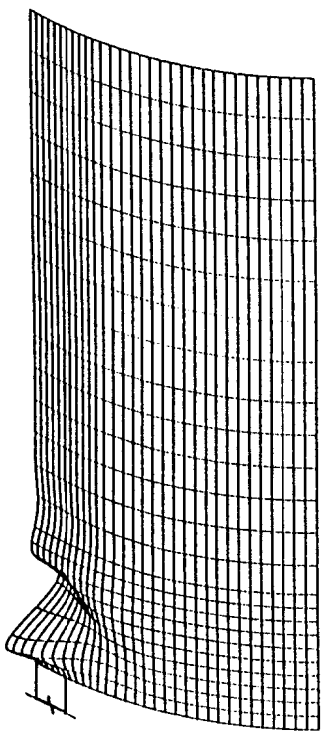

(a) R/t = 200
thick shell

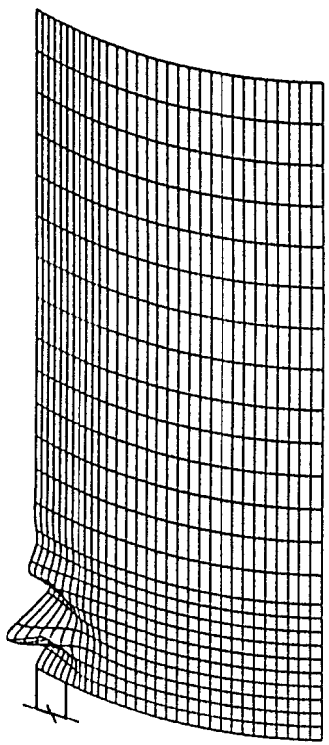

(b) R/t=500
intermediate shell

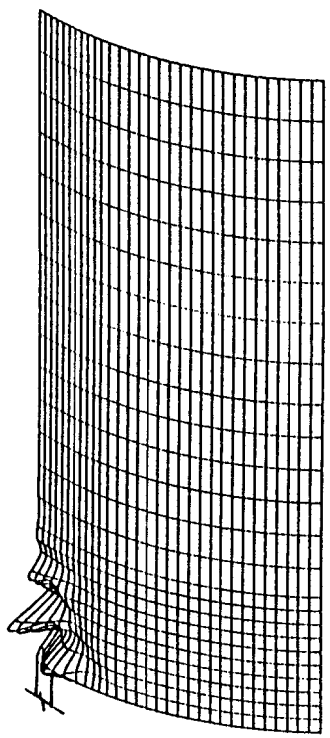

(c) R/t = 1000
thin shell

Figure 5-9

Linear Bifurcation Buckling Modes for a Perfect Cylinder:
Changes with Support Width d for a Tall Cylinder
R/t = 200, H/R = 2.0, n=4

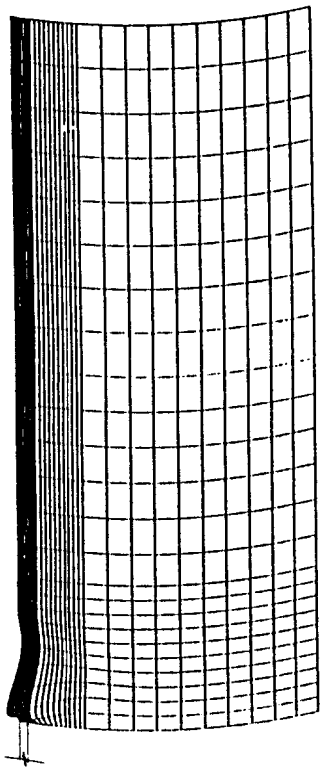

(a) d/R = 0.05
narrow support

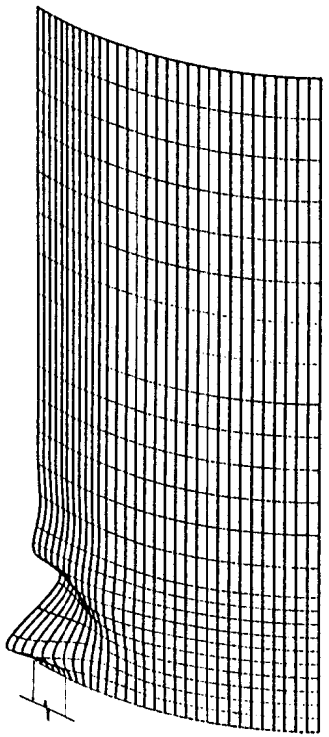

(b) d/R = 0.2
intermediate support

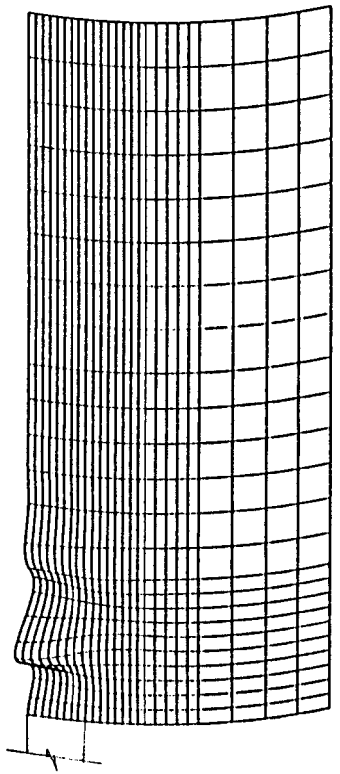

(c) d/R = 0.3
wide support

Figure 5-10

Linear Bifurcation Buckling Modes for a Perfect Cylinder :
Changes with Support Width d for a Squat Cylinder
R/t = 1000, H/R = 0.2, n=4

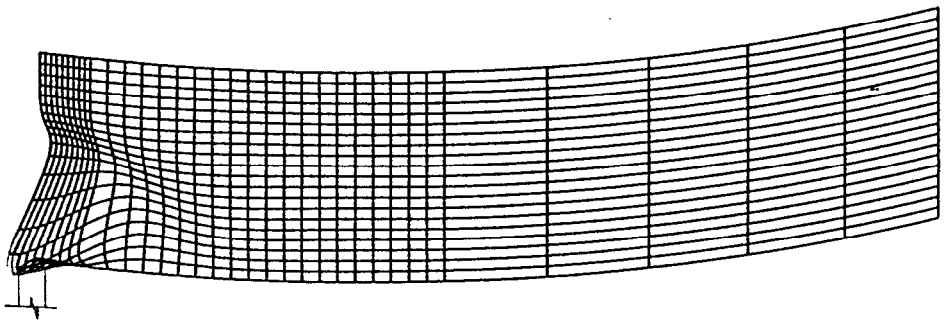

(a) d/ R = 0.05 : narrow support

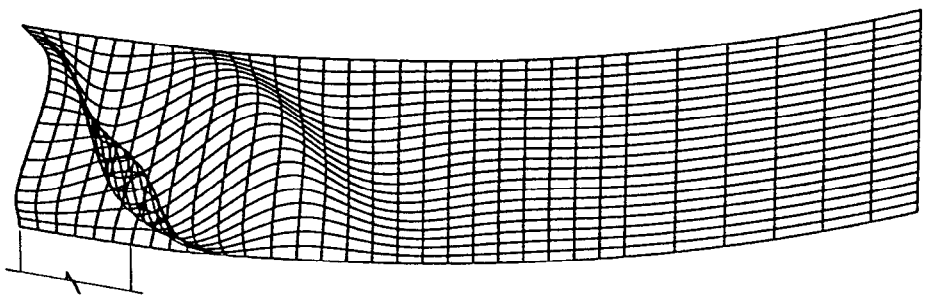

(b) d/R = 0.2 : intermediate support

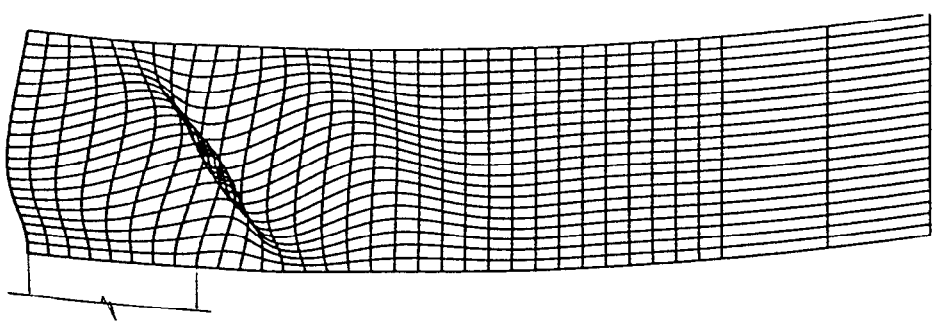

(c) d/R = 0.3 : wide support

Figure 5-11

Linear Bifurcation Buckling Modes for a Perfect Cylinder : Changes with Cylinder Thickness t for a Squat Cylinder
H/R = 0.2, d/R=0.3, n=4

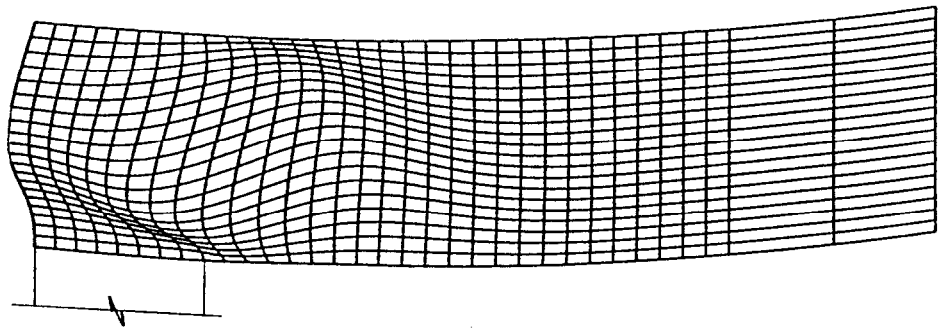

(a) R/t=200 : thick shell

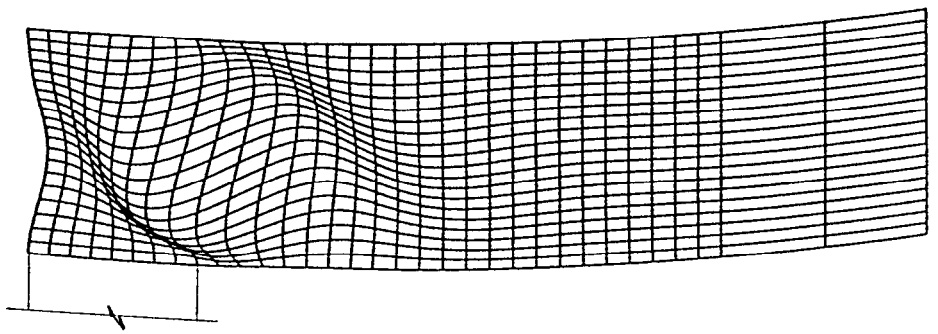

(b) R/t = 500 : intermediate shell

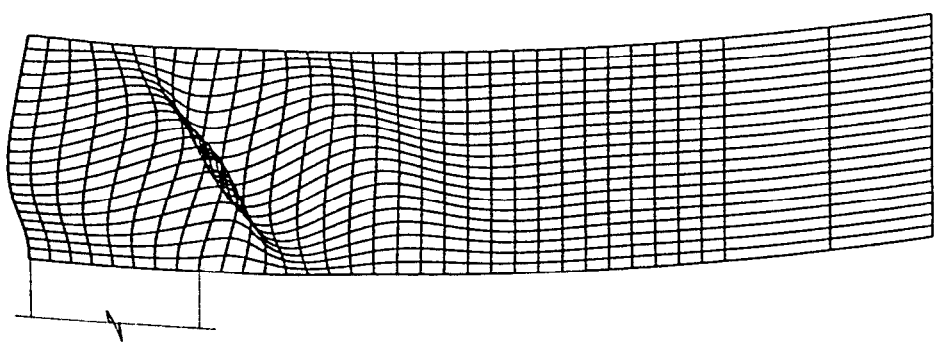

(c) R/t = 1000 : thin shell

Figure 5-12

Linear Bifurcation Buckling Modes for a Perfect Cylinder:
Changes with Load Case
R/t=500, H/R = 0.2, d/R = 0.2, n=4

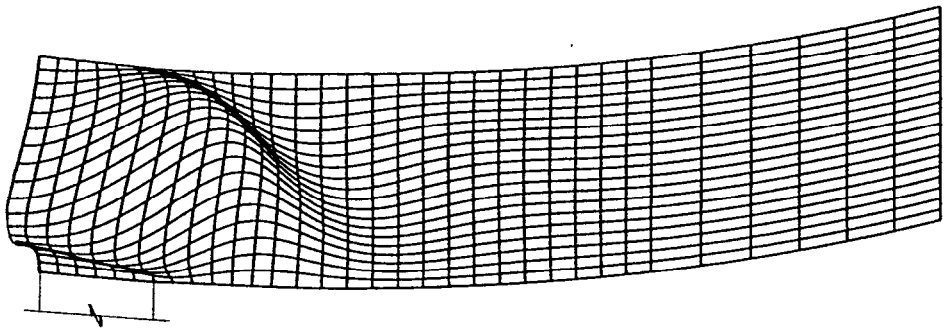

(a) Roof Load

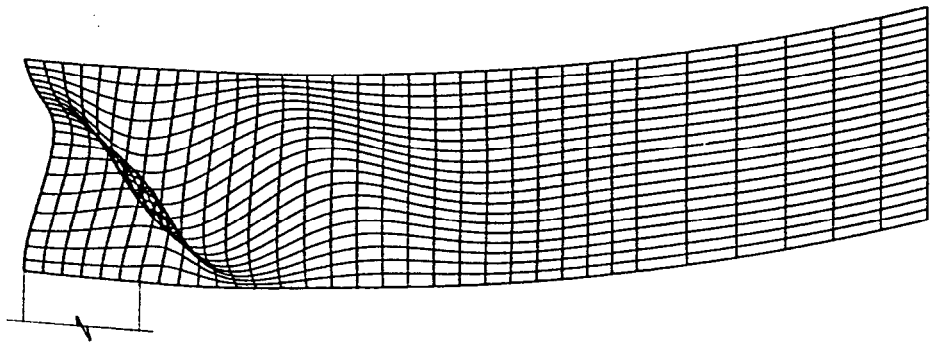

(b) Wall Friction Load

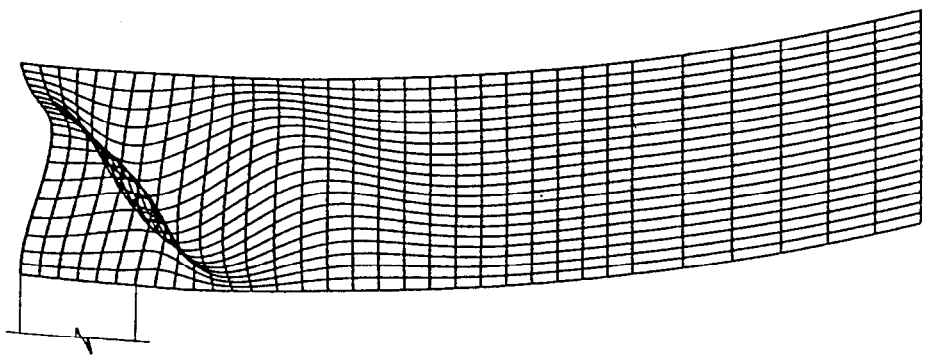

(c) Hopper Load

Figure 5-13

Bifurcation Buckling Analysis for a Perfect Cylinder

n=4, R/t=500, d/R=0.2, H/R=2.0

Load Pattern	Initial Load	Eigenvalue	Dimensionless Buckling Strength
Roof Load	0.04 N/mm	271.79	1.764
Wall Friction	0.0002 N/mm^2	276.18	1.793
Hopper Load	0.04 N/mm	363.43	2.359

Table 5-1

Bifurcation Buckling Strengths of Perfect Cylinders under Three Loading Patterns: Tall Cylinder (H/R=2.0)

Dimensionless Mean Axial Stress at Buckling σ_m / σ_{el}, (n=4, thickness t changes as R/t varies)

R/t \ d/R	0.05			0.2			0.3		
	Roof Load	Wall Friction	Hopper Load	Roof Load	Wall Friction	Hopper Load	Roof Load	Wall Friction	Hopper Load
200	5.554	5.596	9.742	4.177	4.255	5.741	1.733	1.815	3.36
500	3.98	3.997	6.326	1.764	1.793	2.359	1.524	1.576	2.646
1000	3.199	3.209	4.785	1.607	1.628	2.087	1.319	1.343	2.036

Table 5-2

Bifurcation Buckling Strengths of Perfect Cylinders under Three Loading Patterns: Squat Cylinder (H/R=0.2)

Dimensionless Mean Axial Stress at Buckling σ_m / σ_d, (n=4, thickness t changes as R/t varies)

R/t \ d/R	0.05			0.2			0.3		
	Roof Load	Wall Friction	Hopper Load	Roof Load	Wall Friction	Hopper Load	Roof Load	Wall Friction	Hopper Load
200	5.822	6.288	9.045	4.989	5.547	7.074	2.081	2.283	2.992
500	3.914	4.107	5.627	1.773	1.865	2.327	1.345	1.395	1.76
1000	3.035	3.151	4.171	1.403	1.424	1.748	1.028	1.041	1.277

Table 5-3

CHAPTER 6

NONLINEAR ELASTIC BUCKLING ANALYSIS OF DISCRETELY SUPPORTED CYLINDERS

6.1 INTRODUCTION

The linear bifurcation analysis of cylindrical shells discussed in the previous chapter was based upon small deflection theory and was only concerned with perfect cylinders under axial compression. However, a practical silo structure may have geometric imperfections and experience rather complex loadings. The results of the linear bifurcation analyses probably provide only an upper bound to the buckling strengths of cylinders, and therefore these results are of uncertain value for practical design. Precise prediction of the buckling strengths of cylinders requires a large deflection analysis which can take into account the possible geometric imperfections found in prototype structures.

Studies carried out by other researchers [Flügge, 1932; Koiter, 1945; Donnell and Wan, 1950; Budiansky, 1964; Hutchinson and Amazigo, 1967; Hutchinson et al, 1971; Narasimhan and Hoff, 1971; Arbocz and Sechler, 1974; Brush and Almroth, 1975; Singer et al, 1980; Yamaki, 1984; Rotter and Teng, 1989, 1990] have shown that the strengths of cylindrical shells are sensitive to the magnitude of initial imperfections in the shell surface. The size and shape of the most detrimental imperfection may be that of a depression extending around the circumference but over a short height. The buckling modes are relatively local and are directly associated with the critical imperfection.

Although the governing failure mode in practical silos is buckling under axial compression, many researchers [Weingarten et al, 1965; Lei and Cheng, 1969; Zyczkowski and Bucko,1971; Fischer, 1963, 1965; Almroth, 1966; Hutchinson, 1965; Esslinger and Geier, 1977; Tennyson et al., 1978, 1979; Kodama and Yamaki, 1983; Rotter and Teng, 1989] have discovered that the buckling strength of a cylindrical shell is significantly increased by internal pressure on the walls. When an axially compressed cylinder is internally pressurized, the tensile circumferential membrane stresses arising in the wall reduce the effects of the geometric imperfection and considerably enhance its buckling strength. To date, the study of this matter has been confined to cylinders under uniform axial compression with uniform support. Discrete supports were never considered.

It is widely accepted that the critical load for a silo cylinder is very dependent on the nature of the geometric imperfections in the wall, the loading conditions, and the boundary conditions. In order to reduce the discrepancies between the theoretical analysis and reality for these effects on silos, it is necessary to perform a geometrically nonlinear analysis.

This chapter presents some geometrically nonlinear elastic buckling analyses of perfect and imperfect thin cylinders on discrete supports (Fig. 6-1). The finite element computer program ABAQUS was used in the study. Studies of the effect of the axial loading position were not only performed on perfect cylinders (Fig. 6-1a) but also expanded to probe imperfect cylinders (Fig. 6-1b & 6-1c). For imperfect cylinders, two types of axisymmetric geometric imperfection (Fig. 6-1b & 6-1c) were assumed to model practical fabrication imperfections: one with an inward shape, the other with an outward shape. The form of the inward imperfection was chosen as the Type A shape used in previous studies [Rotter and Teng, 1989; Rotter and Zhang, 1990; Teng and Rotter, 1990, 1992; Rotter and She, 1993], modelling a type of circumferential welded joint depression in a full scale silo. The outward imperfection has an identical shape but the opposite amplitude. The location of the imperfections was taken as the critical position, producing the lowest critical load at buckling failure for a discretely supported cylinder with a local axisymmetric inward imperfection [Rotter and She, 1993; Rotter et al, 1993]. A loading pattern of a uniform internal pressure together with an applied axial load was used. The strengthening effect of the internal pressurization on the elastic buckling of perfect and imperfect cylinders were examined. The buckling behaviour, mode and strength of both unpressurized and pressurized cylinders under axial compression were thoroughly investigated.

6.2 FINITE ELEMENT MODELLING

The finite element results presented in this study were obtained by geometrically nonlinear elastic buckling analyses using the modified Riks method available in the ABAQUS finite element program. The 9-node doubly curved quadrilateral shell element type S9R5 which is recommended by the ABAQUS User's Guide [1991] for thin shell applications was again adopted.

In the study, the same geometric model of a cylinder which was used in the linear analysis of Chapter 5 (Fig. 5-1) was adopted and rigid discrete supports under the cylinder were again assumed. For cylinders under axial compression alone, the three loading patterns (Fig. 5-1) defined in Chapter 5 were again applied so that the structural behaviour could be compared with those found in the linear bifurcation investigation of Chapter 5. For the pressurized

cylinders, the axial compression was applied only as a line load at the top boundary; the internal pressure was assumed to be uniform on the wall (Fig. 6-2). This was studied in Chapter 5 and found to lead to lower collapse load predictions than the other two (Fig. 5-1). Hence it may be expected that the results obtained here under combined loads will provide a lower bound to the real buckling strength.

It has been noted that four dimensionless parameters can be used to characterise the geometry of a discretely supported perfect cylinder. These are the number of supports n, the radius-to-thickness ratio R/t, the height-to-radius ratio H/R and the support-width-to-radius ratio d/R. In the studies of imperfect cylinders, the imperfection was assumed to be both local and axisymmetric. As described in Chapter 3, two further parameters are used to define the local imperfection (Fig. 6-1c): the ratio δ_0/t of the imperfection amplitude δ_0 at the centre of the imperfection to the cylinder thickness t and the ratio Z_0/t of the distance Z_0 from the centre of the imperfection to the bottom edge of the cylinder to the cylinder thickness t. Both the inward and outward imperfection shapes (Figs 6-1b and 6-1c) are intended to represent local severe imperfections at a circumferential weld, which was assumed to resist flexural yielding completely during cooling (Type A weld) [Rotter and Teng, 1989, 1991]. The shape of the local imperfection was defined by Rotter and Teng [1989, 1991] and has been given in Chapter 3 as

$$\delta = \delta_0 \, e^{-\pi z/\lambda} \, [\, \sin(\pi z/\lambda) + \cos(\pi z/\lambda) \,]$$
$$z = |\, Z - Z_0 \,|$$

where δ is the local amplitude of the imperfection at height Z above the bottom edge and λ is the linear elastic meridional bending half wavelength of the cylinder ($\cong 2.44\,(Rt)^{1/2}$).

Throughout this study, a single geometry was used for the cylinder, defined by R/t=500, d/R=0.2, H/R=2 and n=4. The local imperfection amplitude was chosen as one wall thickness (ie. $\delta_0/t = 1$). The centre of the imperfection was located at the critical position proposed by Rotter and She [1993] in their recent nonlinear studies of cylinders (refer to Fig. 3-12 of Chapter 3). That is

$$Z_0/t = 0.02 \frac{[Rt]^{1/2}}{t} [R/t]^{7/8} = 103 \qquad (6.1)$$

Figure 6-1 illustrates the finite element models for the perfect and imperfect cylinders on four discrete supports respectively. Symmetry was again exploited so that only one eighth of the cylinder circumference was modelled.

The material of the cylinders was taken to be steel with a Young's modulus $E=2\times10^5$ MPa and Poisson's ratio $\nu=0.3$.

As previously indicated in Chapter 1, the strength of the perfect and imperfect cylinders was characterised by the mean meridional membrane stress above the support, σ_m, divided by the classical elastic critical stress for uniform axial compression σ_{cl}. The load versus deflection curve is examined throughout the loading history so that the bifurcation behaviour can be closely monitored. Here, the load is defined as the dimensionless mean meridional membrane stress above the support, whilst deflection is referred to u/t or w/t, where u represents the vertical displacement of the intersection point of the support centreline and the upper edge of the cylinder and w is the normal displacement of a point near the centre of the buckle above the support centreline for a perfect cylinder.

6.3 BEHAVIOUR OF PERFECT ELASTIC CYLINDERS

Various nonlinear analyses of perfect cylindrical shells have been carried out as described in Chapter 3, but some further critical aspects, such as the position of the applied load and the internal pressurization, have been ignored. Thus the research in this chapter begins by investigating the influence of these two aspects on perfect cylinders in order to obtain a comprehensive understanding of practical elevated silo structures.

6.3.1 The Effect of the Position of the Applied Axial Compression Load

A perfect cylinder, solely under axial compression, was first examined with R/t=500, d/R=0.2, H/R=2.0 and n=4. The three loading patterns previously described, roof, hopper and wall friction loads shown in Fig. 5-1, were again used. The bifurcation behaviour and the buckling mode and strength of a perfect cylinder under the three loading cases were studied.

Because the shell is a two dimensional surface, curved in the third dimension, the deflection of the shell may be characterised by many different measures. The measures chosen here are judged to be those which present the clearest picture of the behaviour: these are the vertical displacement of the top of the shell above the support centreline and the radial displacement of a point situated at the centre of the initial buckle. The latter is easily understood, but the vertical displacement at the top of the shell is sometimes far from the applied load, especially in the case of hopper loading. It was chosen because it is far from the local support, and its displacement effectively integrates the membrane strains and arc length changes through the complete buckle.

The load-deflection curves for these two displacements are shown in Fig. 6-3 and Fig. 6-4. It can be observed that both the vertical and radial displacements are very small until the load rises to the bifurcation point, when a single buckle occurs in a local zone above the support. Large displacements follow as the single buckle progressively grows. As expected, the three types of axial loading produce similar bifurcation behaviour but occur at different bifurcation loads. The hopper loading leads to the highest critical load, the roof loading the lowest and the wall friction loading a value between them. This exhibits the same feature as that discovered in the linear bifurcation analyses of Chapter 5. The values of these critical loads, which are listed in Table 6-1, are generally around 0.6 of the linear bifurcation load for the same geometry.

The buckling modes for the three loading patterns display a similar profile. Only one buckle appears above each support. This corresponds to a single bifurcation point on the load versus displacement curve. Figure 6-5 shows the deformed shape of the roof-loaded cylinder at the point A on the load deflection curve of Figs 6-3 and 6-4.

6.3.2 The Effect of Internal Pressurisation

A uniform internal pressure p was applied to an axially compressed cylinder. In the study, the dimensionless parameter p* was used. It has been defined in Chapter 1 as

$$p^* = \frac{pR}{t\sigma_{cl}}$$

where p is internal pressure, R the radius of the cylinder, t the thickness of the cylinder, and σ_{cl} the classical elastic critical stress for a perfect cylinder under uniform axial compression. For each value of p* (which was incremented from 0.1 to 1.5), the bifurcation behaviour and buckling modes of an axially compressed cylinder were carefully explored. The axial compression on the cylinder was represented by a uniformly distributed roof load.

The relationship between the normalised mean stress above the support and the dimensionless axial displacement at the top of the shell is shown in Figs. 6-6, 6-7 and 6-8 respectively, as the dimensionless internal pressure p* progressively increases from 0.0 to 1.5. When the structure is subjected to only small internal pressures ($0 \leq p^* \leq 0.2$) (Fig. 6-6), a sharp bifurcation and reversing axial displacements are found. The shape of the relevant load versus displacement curve does not change discernibly for low-pressurized cylinders ($0.0 < p^* \leq 0.2$), but the increase in strength is marked. As the internal pressure rises ($p^* \geq 0.4$) (Fig. 6-7), further increases in strength are found. No reversal of axial displacements is seen in the post-buckling zone and the shape of the load-displacement curve changes markedly, becoming flatter and smoother. At higher levels of pressurization ($p^* > 0.8$) (Fig. 6-8), no obvious bifurcation point is observed on the curve.

In Fig. 6-8, it is noticeable that the pre-buckling axial stiffness is much lower for a cylinder with no internal pressure than for cylinders with internal pressures in excess of $p^* = 0.4$. This changing pre-buckling stiffness, taken from the curves in Fig. 6-8 is plotted in Fig. 6-9. The reduced axial stiffness in unpressurised perfect cylinders in the pre-buckling phase appears to be caused by a non-linear geometric effect as the shell displaces inwardly just above the support. This explanation is reinforced by the observable curvature of the load-deflection curve and the significant change in stiffness from a load level of $\sigma_m/\sigma_{cl} = 0.2$ to $\sigma_m/\sigma_{cl} = 1.0$ (Fig.6-9).

A further interesting phenomenon may be observed in Fig. 6-10. The buckling strengths associated with internal pressurisation are depicted in this figure. The strengthening effect of internal pressurisation can be seen to cause a progressive increase in strength throughout the studied range $0 \leq p^* \leq 1.5$. For a uniformly compressed perfect cylinder, there is effectively no change in buckling strength as a result of internal pressurisation (Fig. 1-17) [Rotter and Teng, 1989]. The strength gains due to pressurisation relate entirely to a reduction in the imperfection-sensitivity of imperfect cylinders (Fig. 1-17). By contrast, for locally supported cylinders, even perfect cylinders display a strong increase in strength in the elastic range (Fig. 6-10). This is caused by the fact that the pre-buckling stress state for locally supported cylinders involves high local circumferential membrane stresses which cause strength reductions comparable with those of geometric imperfections. The internal pressure progressively reduces the circumferential compressions, leading to a considerable strength gain, with no obvious limit.

The deformed shapes of the cylinder at maximum load for several pressurized perfect cylinders are shown in Fig. 6-11 for the cases of $p^* = 0.1$, 0.6 and 1.5, respectively. These deformed shape are at the points indicated as A, B, and C on the corresponding load-displacement curves shown in Fig. 6-8. At very low internal pressures, the buckle occurs locally at a small distance above the base of the cylinder and its mode is similar to that for the unpressurized cylinder. This is consistent with the observation from the load-displacement curves shown in Fig. 6-6. As the internal pressure increases, these buckles become shorter in the axial direction and closer to the local support. By contrast, they extend in the circumferential direction. This change in the form of the buckles with internal pressurisation is identical to that observed experimentally in uniformly compressed cylinders subject to internal pressurisation. However, the prebuckling deformations which trigger the buckle in this instance are quite different in form from the geometric imperfections of the uniformly compressed cylinder, and this suggests that these buckle forms, ostensibly interchangeable with others on the Koiter circle, are in reality preferred buckle shapes.

At high internal pressures, the buckle is much more locally located in the zone of local bending immediately above the discrete support. In such a zone, the circumferential membrane and bending stresses are amplified by the axial compression and the restraint of the local support, and thus may induce local yield in the cylinder wall. Therefore, the buckling strength may be affected by local yielding, presenting a similar mode to an "elephant's foot" buckling mode which was discussed in Chapter 2. This problem is discussed again in the context of elastic-plastic behaviour in Chapter 7.

6.4 BEHAVIOUR OF IMPERFECT ELASTIC CYLINDERS WITH A LOCAL INWARD AXISYMMETRIC IMPERFECTION

Studies carried out by Teng and Rotter [1990, 1991] have indicated that circumferentially welded joint imperfections may play an important part in the imperfection-sensitivity of practical silo structures. A range of imperfection shapes was studied: the findings allow us to focus attention on imperfection forms which lead to low strengths whilst having a practical imperfection form. Thus it is possible to produce useful and reliable research results for practical engineering purposes.

In this section, an inward axisymmetric imperfection form, as shown in Fig. 6-1b, was examined, similar in form to those measured in full scale silos by Ding et al [1992]. An imperfect cylinder with an imperfection amplitude of one wall thickness ($\delta_0/t = 1$) placed in the critical location found by Rotter and She [1993] was studied here.

6.4.1 The Effect of the Position of the Applied Axial Compression Load

The load-displacement curves for the three axial compression load cases are illustrated in Fig. 6-12. These curves have a similar shape to one another but significantly differ from those of the perfect cylinder shown in Fig. 6-4. No bifurcation is observed. Before the load reaches the maximum value the vertical displacement of the studied point remains small. When the maximum load is exceeded, the displacement grows rapidly whilst the axial load decreases only slightly. This response is similar to that previously shown in Fig. 3-6 of Chapter 3 for cylinders under wall friction loading [Rotter and She, 1993]: the behaviour is not affected by the way in which the axial compression is introduced.

By comparison with the strengths in Table 6-1 for perfect cylinders, the introduction of a geometric imperfection is found to cause a significant reduction in the buckling strength. For this particular geometry, the reduction in the buckling strength may be as much as 44% for the cases of roof loading and wall friction loading and 33% for the case of hopper loading.

The deformed shapes for the three loading cases were very similar. The buckling mode of a cylinder subject to roof loading (point C in Fig. 6-12) is shown in Fig. 6-13. The buckle occurs in the zone where the inward imperfection has been introduced, leading to a substantial increase in the amplitude of the differences between the deformed and the perfect geometries.

6.4.2 The Effect of Internal Pressurisation

The strengthening effect of internal pressurization on the buckling strength was explored next. Internal pressure was applied first, and the axial compression then progressively applied to a cylinder with an inward local axisymmetric imperfection (Fig. 6-1b),

The relation between the axial load and the axial displacement at the top of the cylinder is shown in Fig. 6-14. For all the values of p^* studied, the shape of the curve is similar. No bifurcation points occur on the curves. The corresponding relationship between the maximum strength and the internal pressure is shown in Fig 6-15, where it can be compared with that for a perfect cylinder. The curve is particularly interesting when compared with the corresponding behaviour of uniformly compressed cylinders (Fig. 1-17). It was noted previously that internal pressure leads to increases in the buckling strength of perfect locally supported elastic cylinders (Fig. 6-10), though it does not significantly alter that of uniformly supported elastic cylinders. The strengths of both locally and uniformly supported cylinders are reduced by a local inward imperfection (Figs. 3-11 and 1-16), because the inward imperfection causes compressive circumferential membrane stresses. It is therefore reasonable to suppose that the effect of internal pressure on an imperfect elastic locally supported cylinder might be to increase its strength progressively until it approaches that of a perfect cylinder.

By contrast with the above speculation, it is found (Fig. 6-15) that, for locally supported cylinders, the strength of a pressurised elastic imperfect cylinder increases faster than that of a perfect cylinder, and higher strengths are attained by the imperfect than by the perfect cylinder when the pressurisation exceeds $p^* = pR/t\sigma_{cl} = 0.6$. This surprising condition deserves further investigation. The load-deflection curves of perfect and imperfect cylinders for the case of $p^*=0.6$ are compared in Fig. 6-16, where it may be seen that the maximum loads are very similar. It is evident that, although the calculated strengths are almost identical, the load-deflection curves are quite different, with a strong bifurcation and a weakening post-buckling path clearly visible in the perfect cylinder, whilst the imperfect cylinder displays a stable post-buckling response, and indeed reaches the maximum load at much larger displacements. It is clear that at high internal pressures, this is a problem in which the minimum of the post-buckling curve for a perfect cylinder is very different from the strength of an imperfect

cylinder. At very large amplitudes, the imperfection may function as a reinforcement ring or corrugation which resists rather than induces buckling.

The buckling modes at the indicated points A and B on the curves for $p^* = 0.6$ and 1.5 (Fig. 6-14) are shown in Fig. 6-17. Inspection of the buckling modes shows that, as the internal pressure increases, the buckle centring in the imperfect area above the support becomes shorter in the axial direction, wider in the circumferential direction and slightly closer to the support. At higher internal pressures, very large deformations in the zone adjacent to the support are seen. This demonstrates that the critical position for the imperfection is moving downwards. As discussed by Rotter [1991], the local yield may occur in that zone, affecting the buckling strength of the structure if the level of internal pressurization is high.

6.5 BEHAVIOUR OF IMPERFECT ELASTIC CYLINDERS WITH A LOCAL OUTWARD AXISYMMETRIC IMPERFECTION

Although outward local imperfections are less common than inward forms, outward imperfections do occur, and a study of their effect is valuable to assist with an understanding of the buckling behaviour. The following study is similar to that conducted in Section 6.4, but considers an imperfect cylinder (Fig. 6-1c) with the same imperfection magnitude and location as previously introduced but with an outward instead of an inward local defect. No previous study of an outward imperfection near a local support is known.

6.5.1 The Effect of the Position of the Applied Axial Compression Load

The load-axial shortening curves for the three different load cases of Fig. 5-1 are shown in Fig. 6-18, for axial loading without internal pressure. The three load-displacement curves show a very different response from those for cylinders with an inward imperfection (Fig. 6-12), but are similar to those for a perfect cylinder (Fig. 6-3). Bifurcation points appear on the curves with one bifurcation point on each curve. The values of the corresponding bifurcation loads are listed in Table 6-1 and shown in Fig. 6-19. These are larger than those for the inward imperfection cylinder by about 13 % for the cases of roof load and wall friction load and by about 5 % for the case of hopper load. They are smaller than those for the perfect cylinder by about 37 % for the cases of roof load and wall friction load and by about 30 % for the case of hopper load. It reveals that, apart from the magnitude and position of the imperfection, the imperfection form is a very influential factor which affects the structural behaviour and buckling strength of locally supported cylinders.

The buckling mode at Point A on the load-displacement curve shown in Fig. 6-18 is shown in Fig. 6-20 for a roof-loaded cylinder with an outward axisymmetric imperfection. The buckle is centred a short distance above the centre of the imperfection rather than effectively at the centre, as in the cylinder with an inward imperfection (Fig. 6-13). This mode reflects the changed state of stress caused by the outward imperfection around the area of imperfection. By contrast with the stresses associated with the inward imperfection (Fig. 2-2b), the outward imperfection gives rise to tensile circumferential stresses near the centre of imperfection and compressive circumferential stresses above and below the centre. In an axially compressed cylinder, a tensile circumferential stress in the buckle area helps to resist buckling, whilst a compressive circumferential stress helps to promote buckling [Calladine, 1983]. Based upon this principle, it may be supposed that buckling will occur in an imperfect cylinder at the point where detrimental compressive stresses in both the meridional and circumferential directions co-exist. For this cylinder with an outward axisymmetric imperfection, this area is found above the centre of the imperfection, as indicated by the contour of meridinal stress at buckling shown in Fig. 6-20b.

6.5.2 The Effect of Internal Pressurisation

The nonlinear elastic buckling behaviour of cylinders with local outward axisymmetric imperfections and subject to internal pressure together with axial compression load applied along the top edge of the cylinder was then analysed.

The load-deflection curves for cylinders with different levels of internal pressure are shown in Fig. 6-21. As soon as the internal pressure rises above zero, the behaviour is similar to that for the inward imperfection (Fig. 6-14). The buckling modes of pressurized cylinders display the same changes with internal pressure, as shown in Fig. 6-22a and 6.22b. The centre of the buckle moves to below the centre of imperfection in pressurised cylinders. As described in Section 6.5.1, the buckle occurs above the centre of the imperfection at $p^* = 0$ (Fig. 6-20), because circumferential compressions occurs above and below the imperfection, and above is the worst for $p^* = 0$. For the cases when $p^* > 0$, because of internal pressure, the worst position shifts to below the centre of the imperfection, thus the buckle occurs below the centre of the imperfection (Fig. 6-22c).

The load-deflection curves of Fig. 6-21 all show a more complex post-peak behaviour. The curve for the case of $p^*=0.4$ is separately drown in Fig. 6-23, and Figure 6-24 shows the corresponding deformed shapes at the different points A, B C and D marked on the curve of Fig. 6-23. The early part of the curve is almost linear, but deformations below the imperfection grow in a non-linear manner (Fig. 6-24), leading to a peak in the load-deflection curve at point B. Thereafter, the deflections in the buckle below the imperfection continue to

grow, but a bifurcation occurs above the imperfection, causing the load-axial shortening curve to reverse, with reducing loads and reducing deformations, similar to those in uniformly compressed perfect cylinders [Rotter and Teng, 1989], but more strongly marked. Following the bifurcation, the load stabilises and the displacements grow again (Point D).

The changes in the buckling strength with internal pressure are shown in Fig. 6-25, where they are compared with those for perfect cylinders and cylinders with an inward axisymmetric imperfection. The strength gains are generally smaller than those for an inward imperfection, and the strength is always lower than that of the perfect cylinder.

6.6 SUMMARY AND CONCLUSIONS

The nonlinear analyses carried out in this chapter concerned the elastic buckling of discretely supported thin cylindrical shells under axial compression. The study examined shells which were both geometrically perfect and imperfect, and both unpressurized and pressurized. The geometric parameters of the shells were kept constant at R/t=500, H/R=2.0, d/R=0.2 and n=4. A rigid discrete support for the cylinder was assumed. Two local axisymmetric imperfection forms, one with an inward shape and the other with an outward shape, were chosen and placed at a detrimental position on the basis of the studies described in Chapter 3. Three types of axial compression loading were studied to explore the sensitivity of the buckling behaviour, mode and strength to the position of the applied loading. The effect of internal pressurization on the nonlinear behaviour and elastic buckling of a discretely supported cylinder under axial compression was explored.

It was found that the position of the applied axial load has only a small effect on the buckling behaviour and buckling mode of a locally supported cylinder on discrete supports. However, the changes in buckling strength with load position are remarkable. The roof loading case leads to the lowest strengths. The difference between this and wall friction loading is generally around 2% and between roof loading and hopper loading is generally around 22% for perfect cylinders. This trend in the buckling loads is the same as that found in the linear bifurcation analyses of perfect cylinders described in Chapter 5.

The sensitivity of the buckling strength to the position of the applied load may or may not be as strong for an imperfect cylinder as that for a perfect cylinder, depending on the pattern of the imperfection form. For an outward imperfection, the increase in buckling strength over the value for roof loading is about 3% for wall friction loading and 44% for hopper loading. For an inward imperfection, the corresponding increases are about 3% and 55%. Thus, hopper

loading always produces very high strengths compared with other load cases, which are very similar.

The geometric imperfection, whether inward or outward, results in a notable reduction in the buckling strength. The imperfection form affects both the buckling strength and the buckling behaviour. With an imperfection of amplitude of one wall thickness ($\delta_0/t = 1$) placed at the critical height Z_0 for inward imperfections with wall friction loading, strength reductions relative to the value for a perfect cylinder of about 40% were found for the inward imperfection form and about 34% for the outward imperfection.

Previous studies of geometrically imperfect elastic axially compressed cylinders [Weingarten et al, 1965; Lei and Cheng, 1969; Zyczkowski and Bucko,1971; Fischer, 1963, 1965; Almroth, 1966; Hutchinson, 1965; Esslinger and Geier, 1977; Tennyson et al., 1978, 1979; Kodama and Yamaki, 1983; Rotter and Teng, 1989] showed that internal pressure reduces the imperfection-sensitivity and increases the buckling strength significantly. In this first-ever study of the effects of internal pressure in discretely supported cylinders, the same effect has been found, and has been shown to vary according to the form of the imperfection. However, contrary to the findings for uniformly compressed cylinders, the buckling strength of a perfect locally supported cylinder has also been found to be considerably increased by internal pressure.

For a perfect cylinder, the buckling behaviour and mode do not change significantly from the unpressurized case until the internal pressurization reaches a high level. For an imperfect cylinder with inward imperfections, the buckling behaviour remains similar as the internal pressure increases. However, for a cylinder with an outward local imperfection, the internal pressure seriously alters its behaviour and buckling mode from the case of axial compression alone. The buckling modes are very local in the zone immediately above the support. Only a single buckle has been found for the chosen cylinder geometry and relatively narrow supports used in the study.

Although the internal pressure can significantly enhance the buckling strength, the governing failure mode of a cylindrical silo is generally buckling under axial compression. From this study it is still difficult to produce a general proposal for estimating the strength gains due to internal pressurization. This is because high internal pressures give rise to severe local bending near the base of the cylinder and local yielding may then precipitate a buckling failure. Therefore, it is vital that the present study is extended to cover elastic-plastic behaviour before practical design proposals are formulated.

Perfect and Imperfect Discretely Supported Cylinder Models

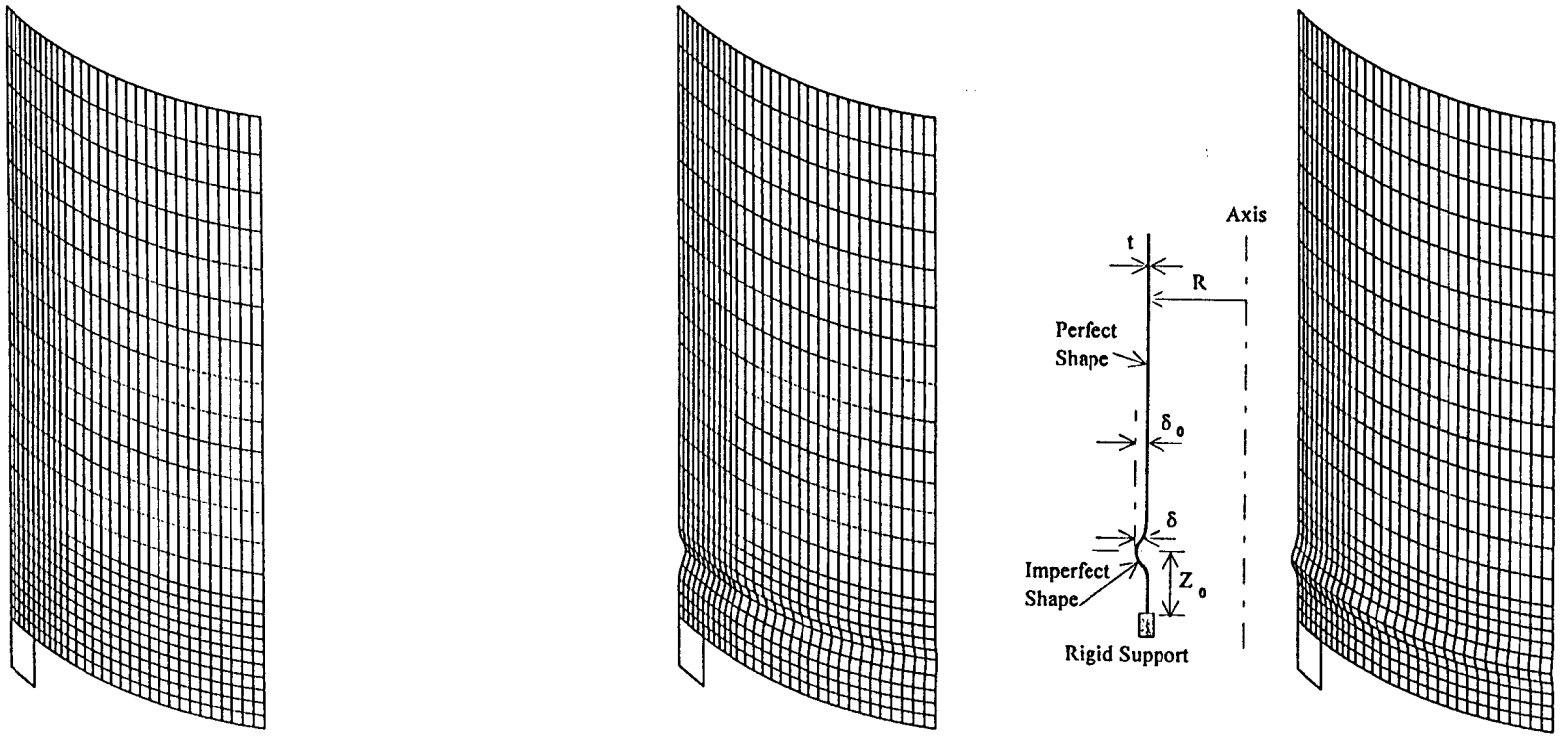

(a) Perfect Cylinder

(b) Imperfect Cylinder With An Inward Axisymmetric Imperfection

(c) Imperfect Cylinder With An Outward Axisymmetric Imperfection

Figure 6-1

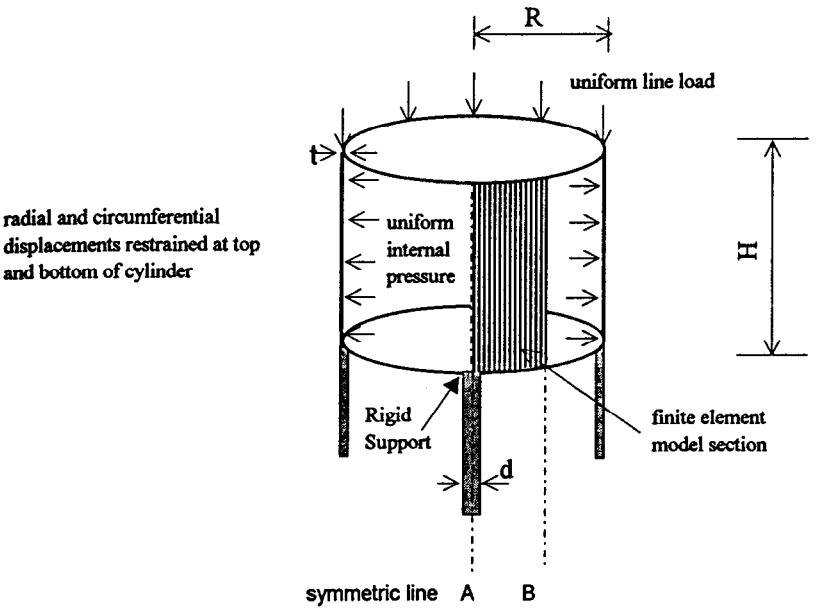

Axially Compressed Pressurized Cylinder on Rigid Supports

Figure 6-2

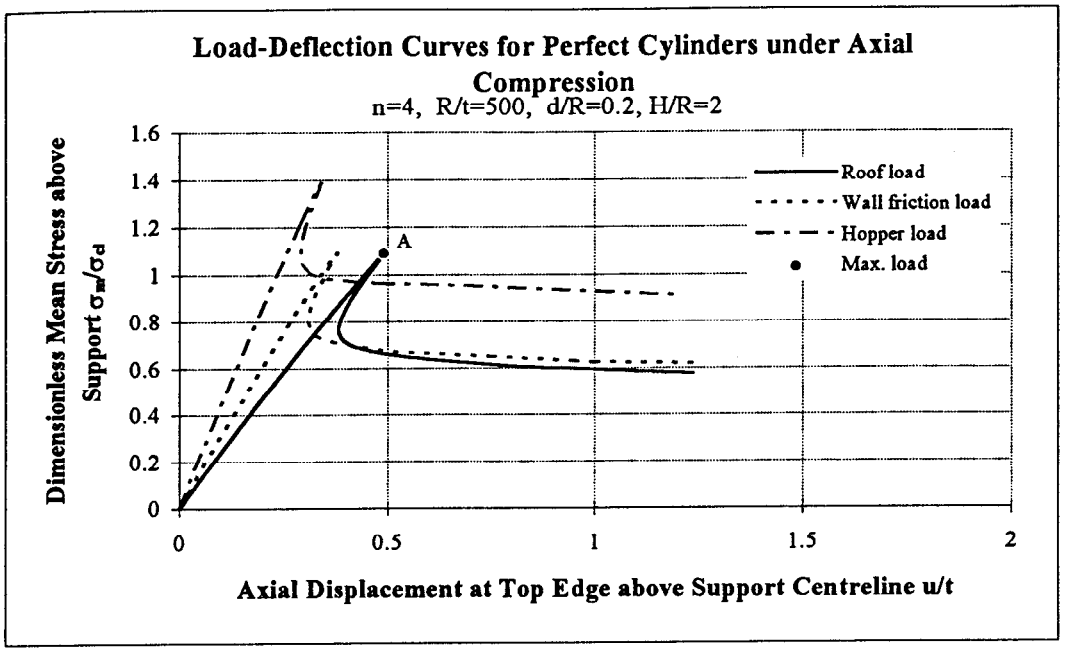

Figure 6-3

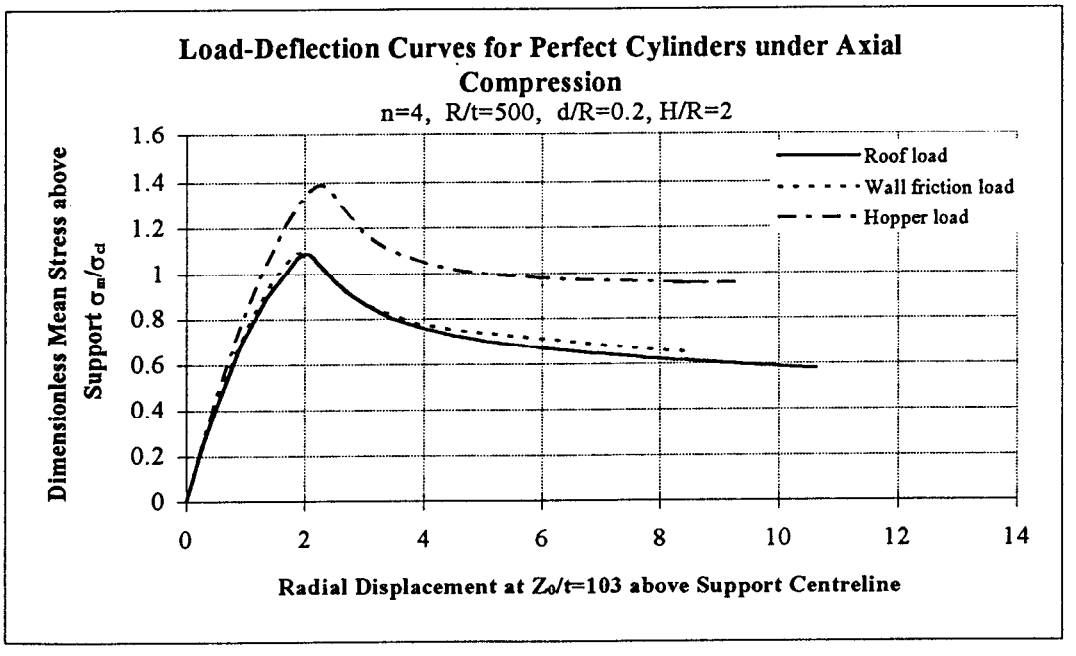

Figure 6-4

Buckling Mode for A Perfect Cylinder under Roof Load
n=4, R/t=500, d/R=0.2, H/R=2.0

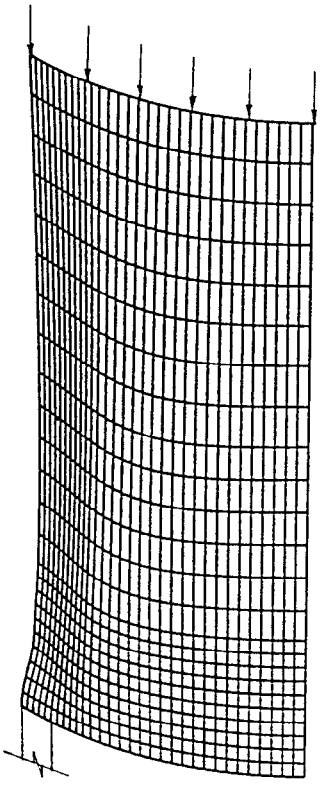

Figure 6-5

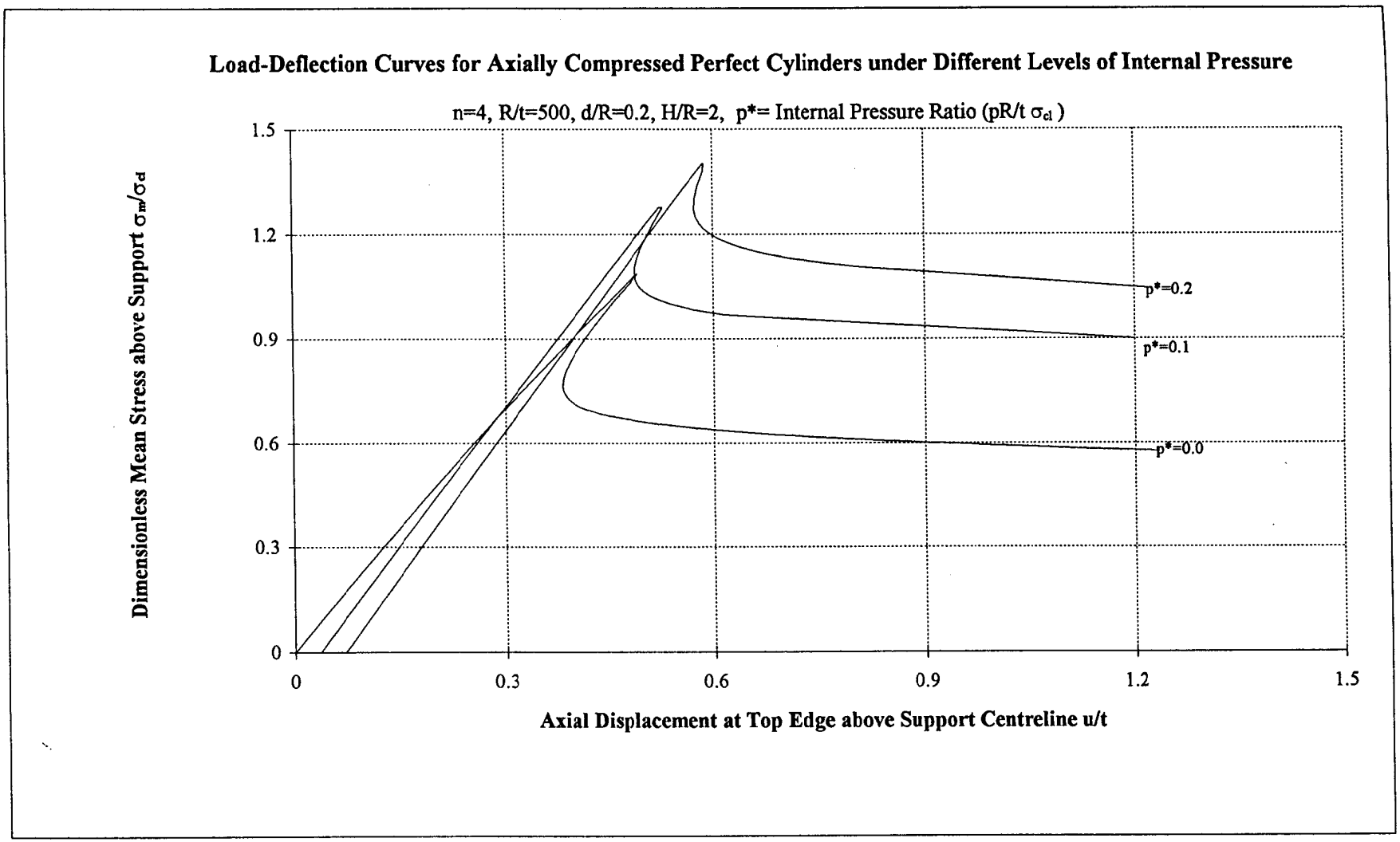
Load-Deflection Curves for Axially Compressed Perfect Cylinders under Different Levels of Internal Pressure
n=4, R/t=500, d/R=0.2, H/R=2, p*= Internal Pressure Ratio (pR/t σcl)
Dimensionless Mean Stress above Support σm/σd
1.5
1.2
0.9
0.6
0.3
0
p*=0.2
p*=0.1
p*=0.0
0
0.3
0.6
0.9
1.2
1.5
Axial Displacement at Top Edge above Support Centreline u/t

Figure 6-6

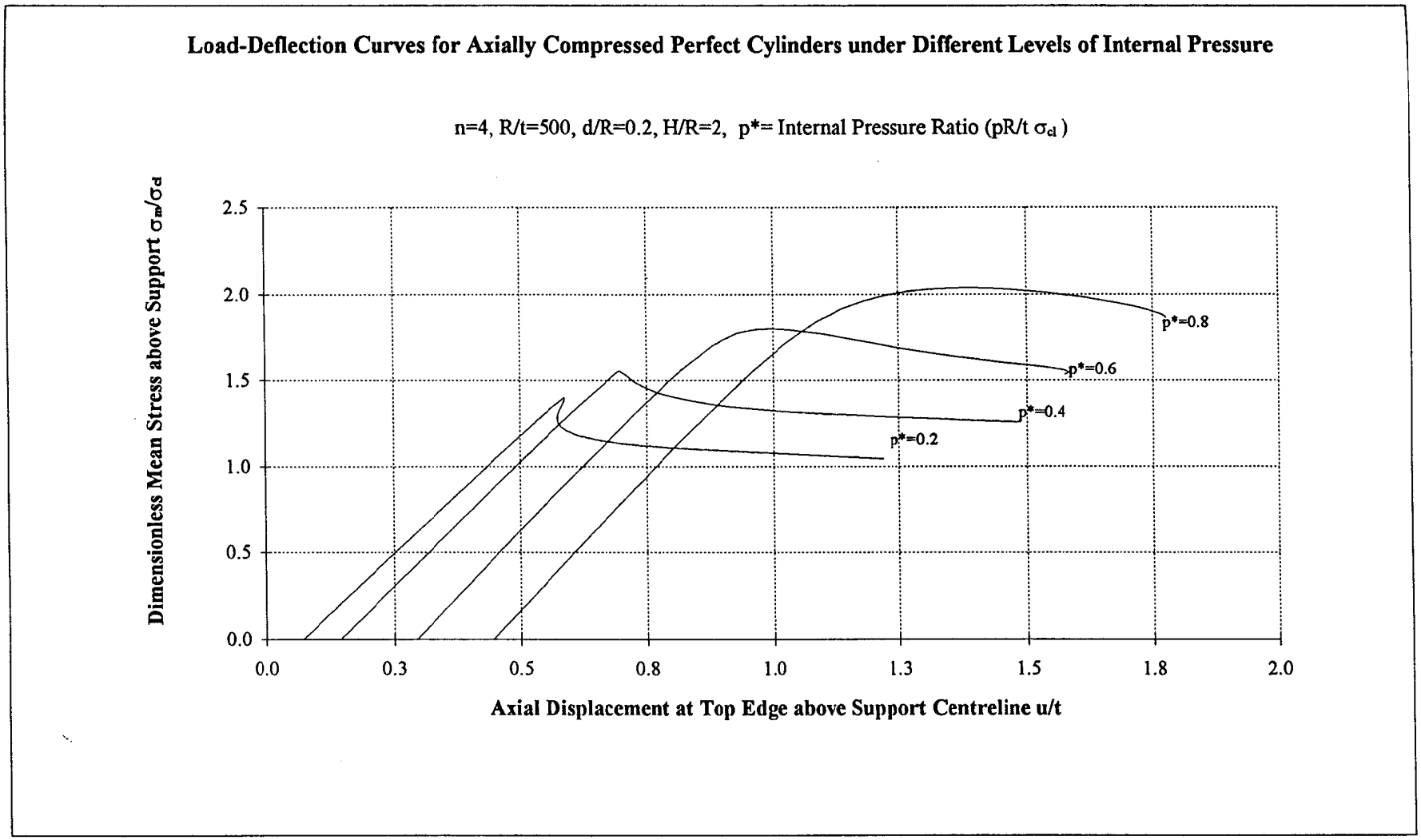
Load-Deflection Curves for Axially Compressed Perfect Cylinders under Different Levels of Internal Pressure
n=4, R/t=500, d/R=0.2, H/R=2, p*= Internal Pressure Ratio (pR/t σcl)
Dimensionless Mean Stress above Support σm/σd
2.5
2.0
1.5
1.0
0.5
0.0
0.0
0.3
0.5
0.8
1.0
1.3
1.5
1.8
2.0
p*=0.8
p*=0.6
p*=0.4
p*=0.2
Axial Displacement at Top Edge above Support Centreline u/t

Figure 6-7

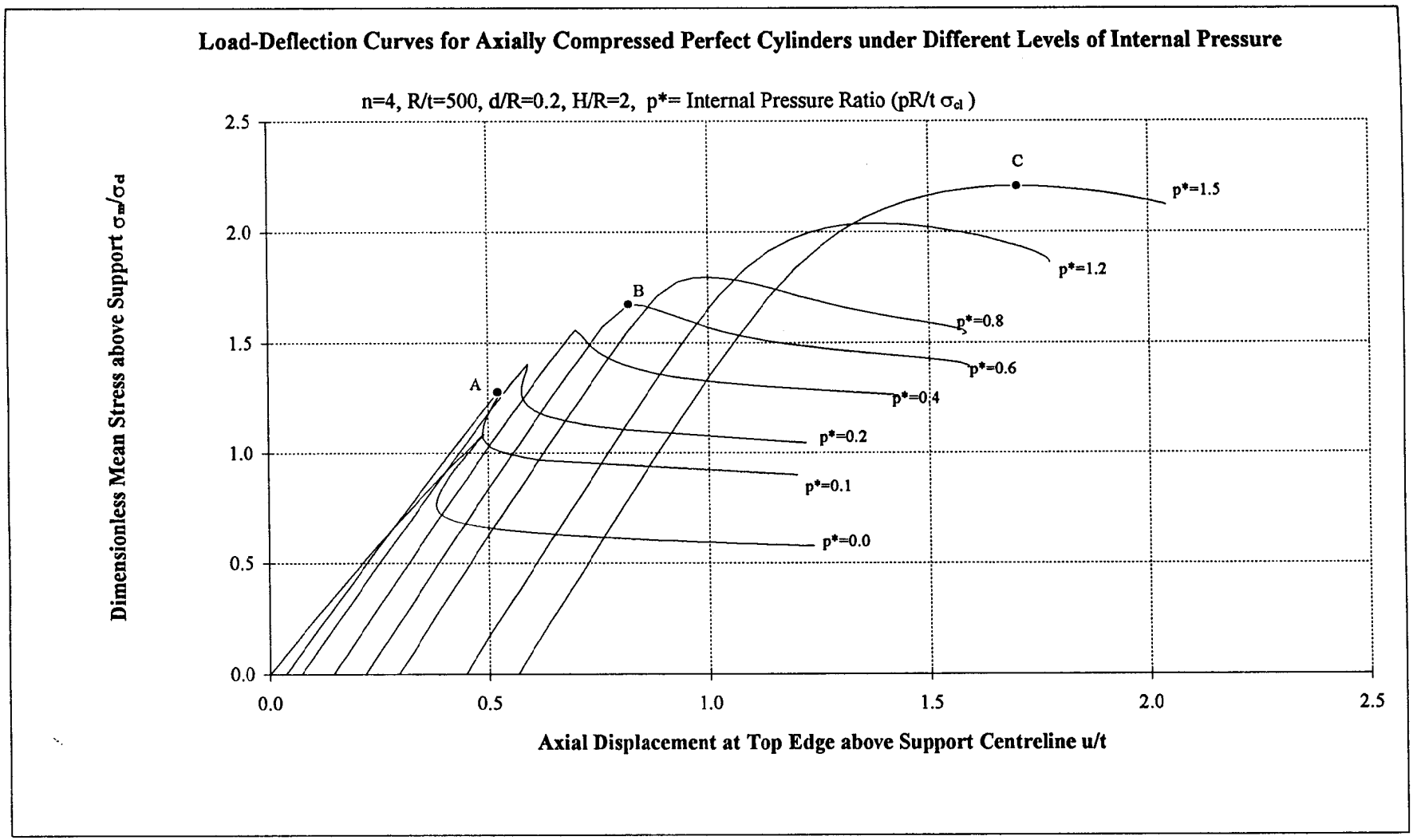
Load-Deflection Curves for Axially Compressed Perfect Cylinders under Different Levels of Internal Pressure
n=4, R/t=500, d/R=0.2, H/R=2, p*= Internal Pressure Ratio (pR/t σcl)
Dimensionless Mean Stress above Support σm/σd
Axial Displacement at Top Edge above Support Centreline u/t
0.0
0.5
1.0
1.5
2.0
2.5
A
B
C
p*=1.5
p*=1.2
p*=0.8
p*=0.6
p*=0.4
p*=0.2
p*=0.1
p*=0.0

Figure 6-8

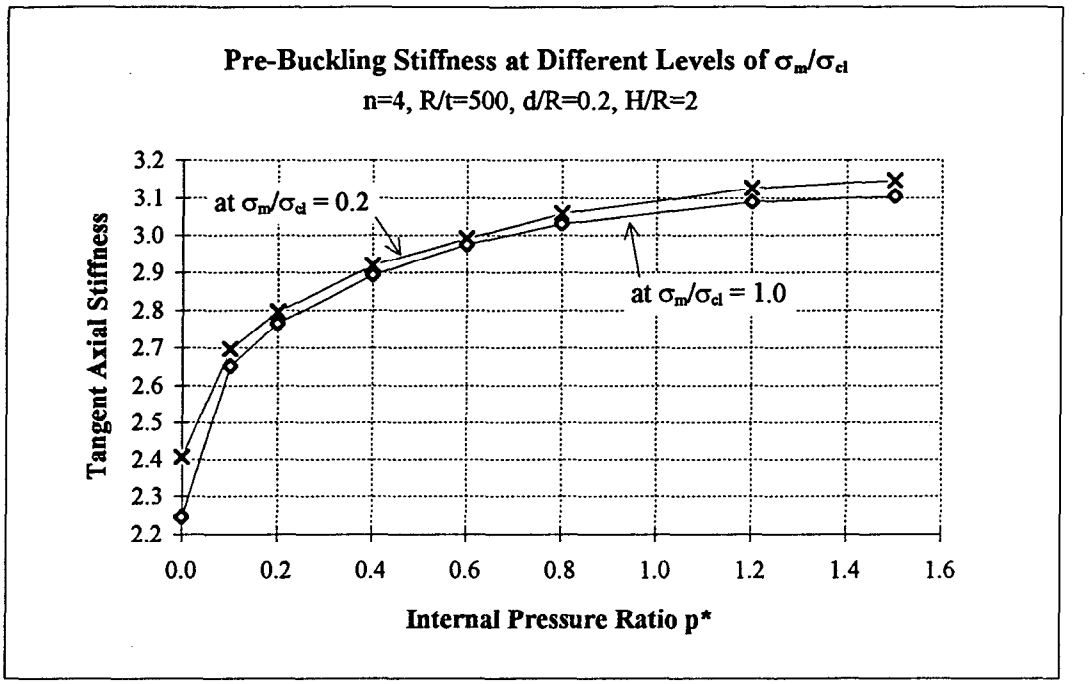

Figure 6-9

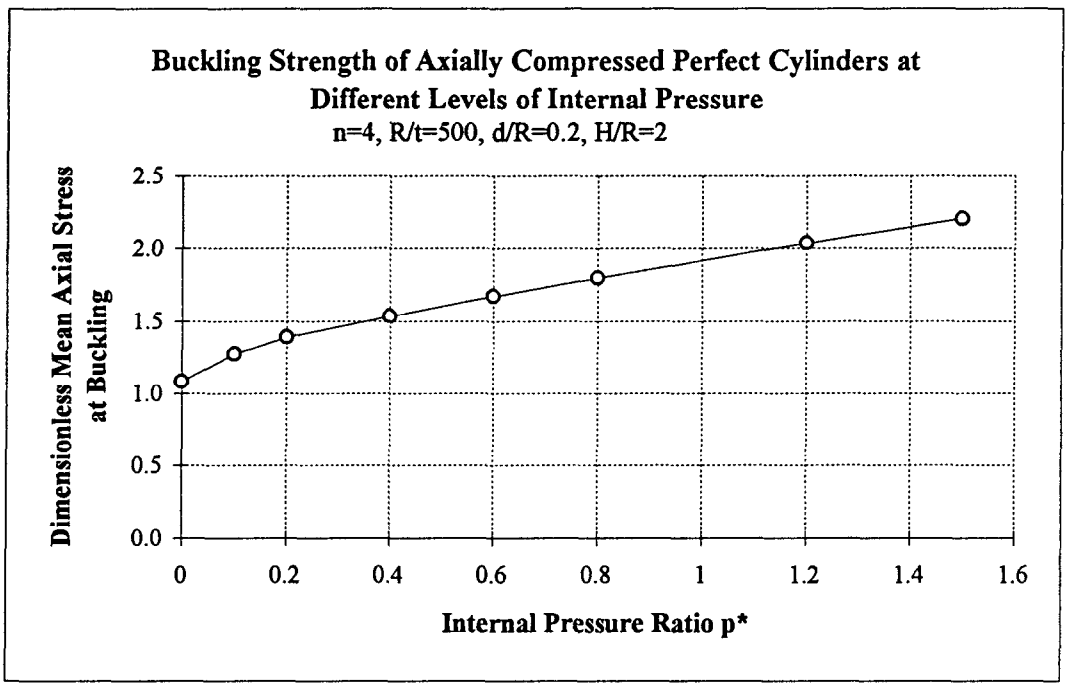

Figure 6-10

Buckling Modes for Elastic Perfect Cylinders under Axial Compression with Different Internal Pressure Levels
n=4, R/t=500, d/R=0.2, H/R=2.0

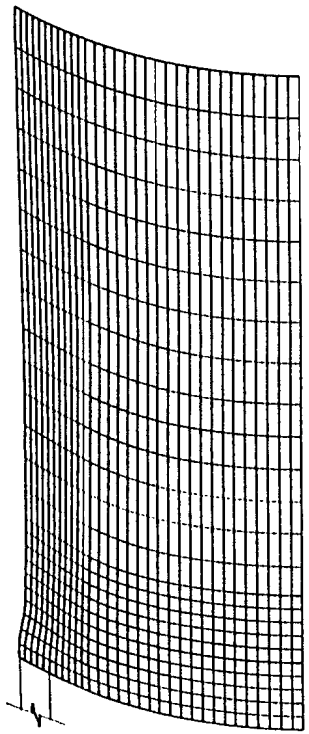

(a) p*=0.1
Low internal pressure: A

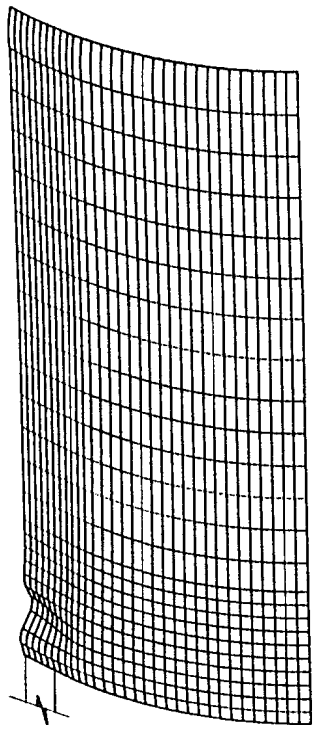

(b) p*=0.6
Moderate internal pressure: B

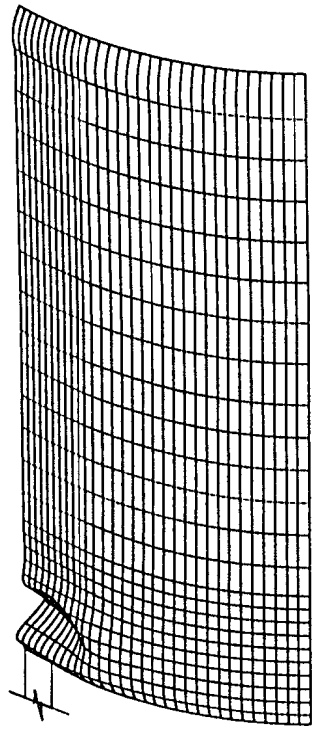

(c) p*=1.5
High internal pressure: C

Figure 6-11

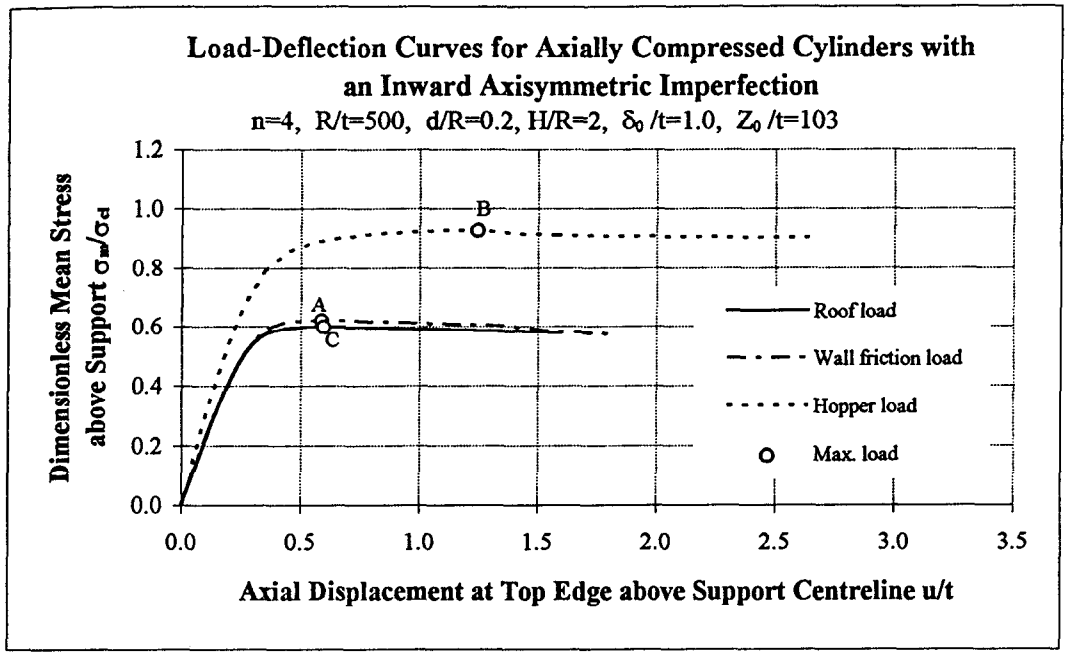
Load-Deflection Curves for Axially Compressed Cylinders with an Inward Axisymmetric Imperfection
n=4, R/t=500, d/R=0.2, H/R=2, δ0 /t=1.0, Z0 /t=103
Dimensionless Mean Stress above Support σw/σcl
1.2
1.0
0.8
0.6
0.4
0.2
0.0
0.0
0.5
1.0
1.5
2.0
2.5
3.0
3.5
A
B
C
Roof load
Wall friction load
Hopper load
Max. load
Axial Displacement at Top Edge above Support Centreline u/t

Figure 6-12

Buckling Mode for a Cylinder with an Inward Axisymmetric Imperfection under Axial Compression
n=4, R/t=500, d/R=0.2, H/R=2.0, δ_0 /t=1.0, Z_0 /t=103, Roof Load Case

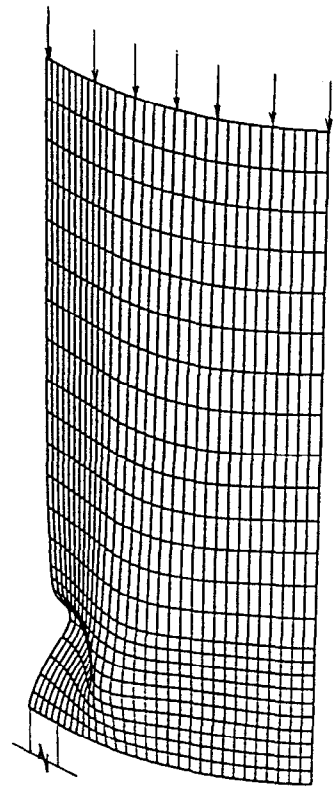

Figure 6-13

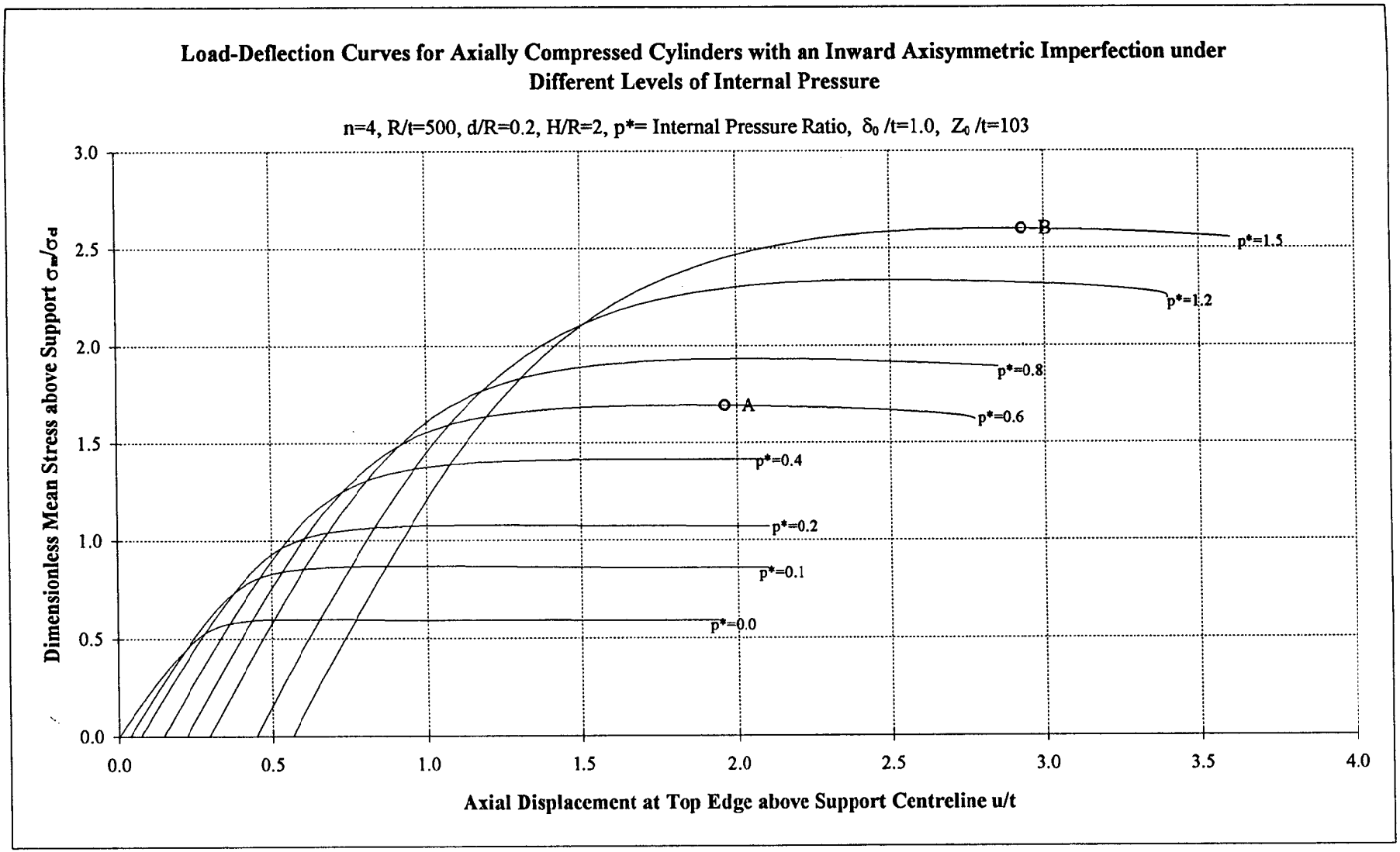
Load-Deflection Curves for Axially Compressed Cylinders with an Inward Axisymmetric Imperfection under Different Levels of Internal Pressure
n=4, R/t=500, d/R=0.2, H/R=2, p*= Internal Pressure Ratio, δ0 /t=1.0, Z0 /t=103
Dimensionless Mean Stress above Support σm/σd
Axial Displacement at Top Edge above Support Centreline u/t
0.0
0.5
1.0
1.5
2.0
2.5
3.0
3.5
4.0
A
B
p*=1.5
p*=1.2
p*=0.8
p*=0.6
p*=0.4
p*=0.2
p*=0.1
p*=0.0

Figure 6-14

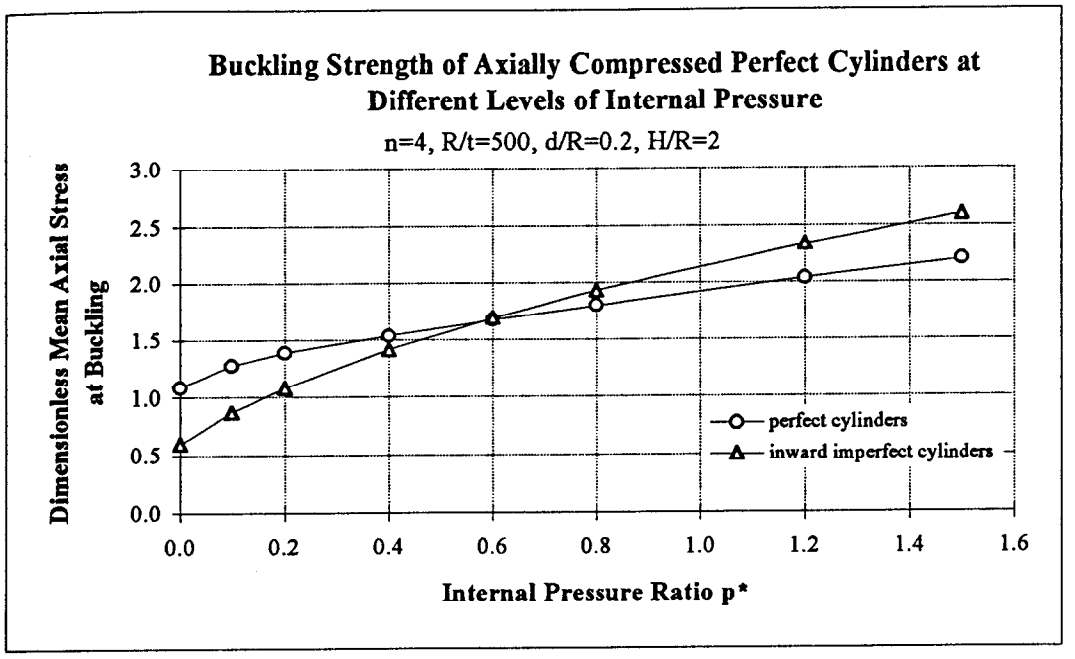

Figure 6-15

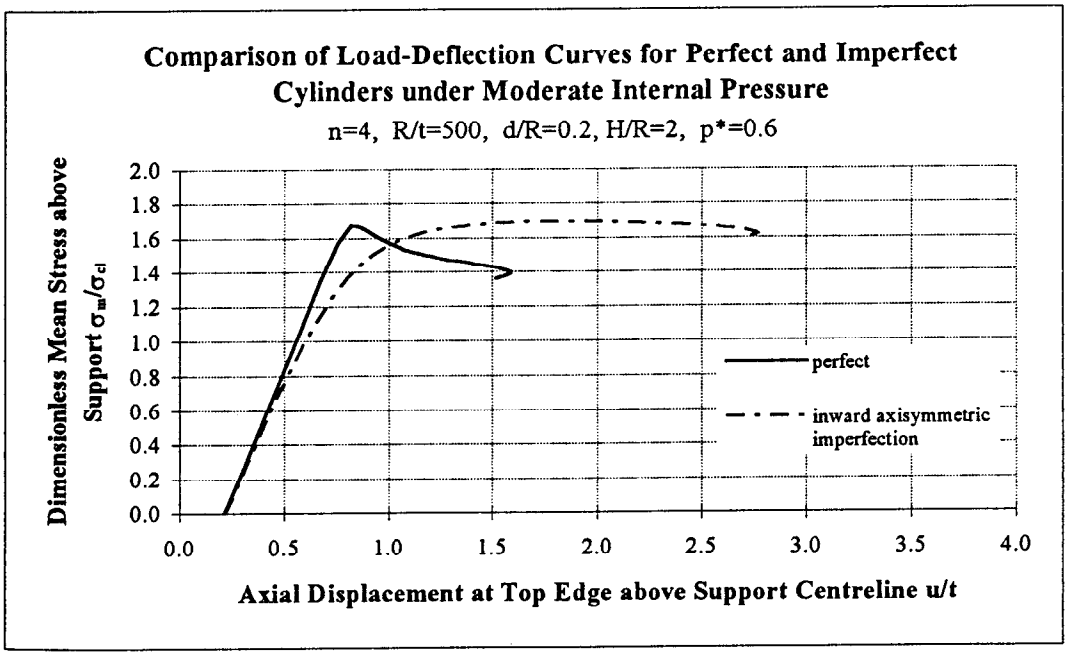

Figure 6-16

Buckling Modes for Axially Compressed Cylinders with an Inward Axisymmetric Imperfection under Different Internal Pressures

n=4, R/t=500, d/R=0.2, H/R=2.0, δ_0 /t=1.0, Z_0/t=103

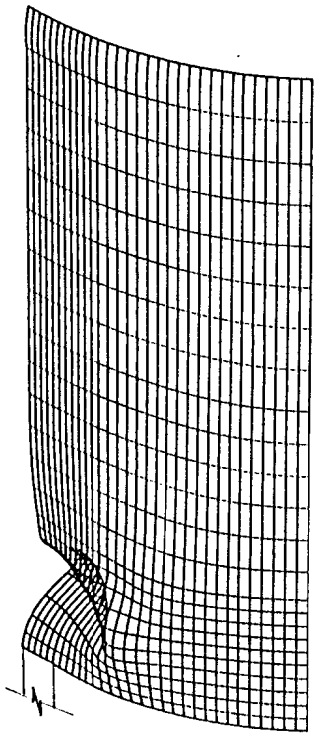

(a) p*=0.6
Moderate Internal Pressure: A

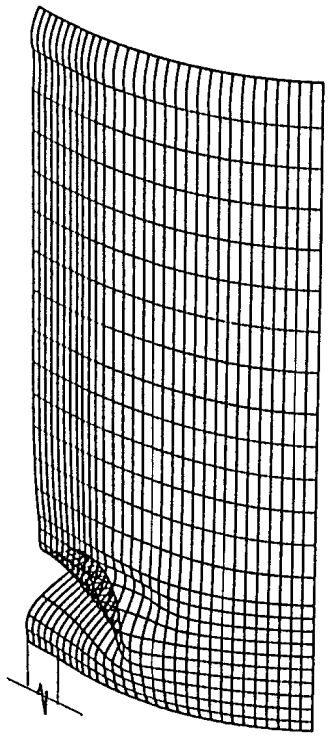

(b) p*=1.5
High Internal Pressure: B

Figure 6-17

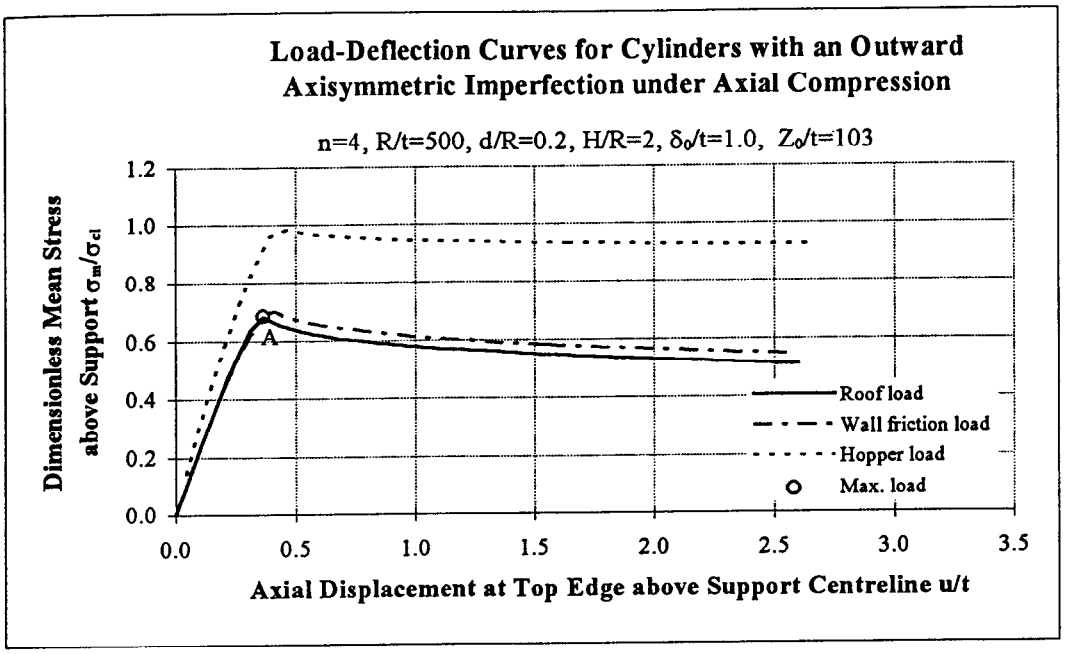

Figure 6-18

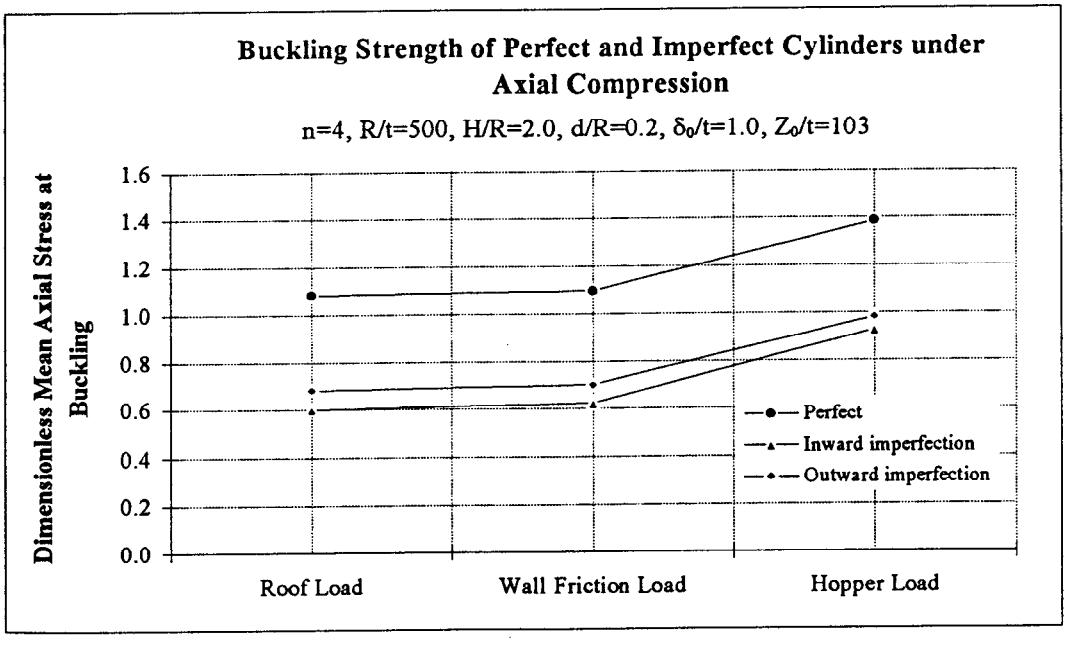

Figure 6-19

Buckling Mode for a Cylinder with an Outward Axisymmetric Imperfection under Axial Compression
n=4, R/t=500, d/R=0.2, H/R=2.0, δ_0/t=1.0, Z_0/t=103, Roof Load Case

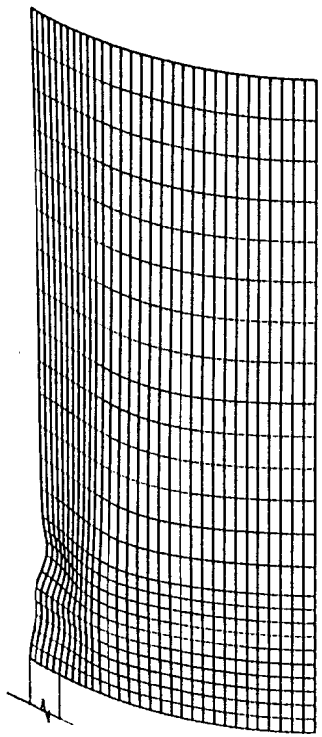

(a) Buckling mode

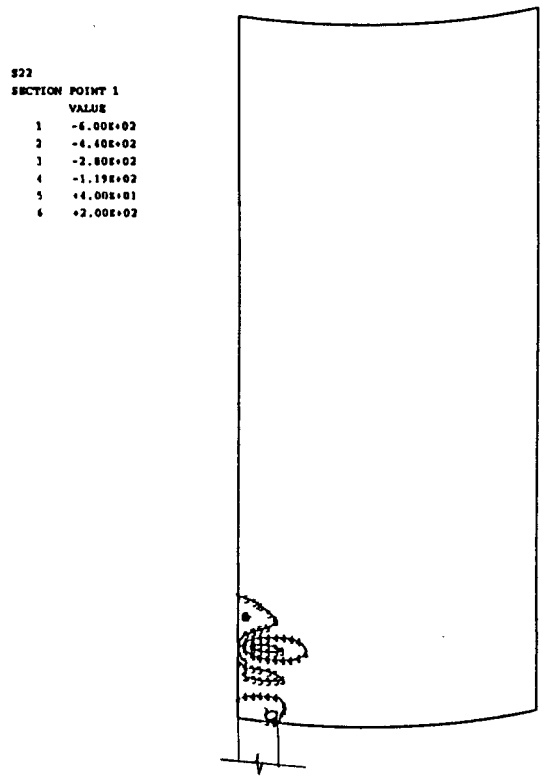

(b) Contour of meridional stress at buckling

Figure 6-20

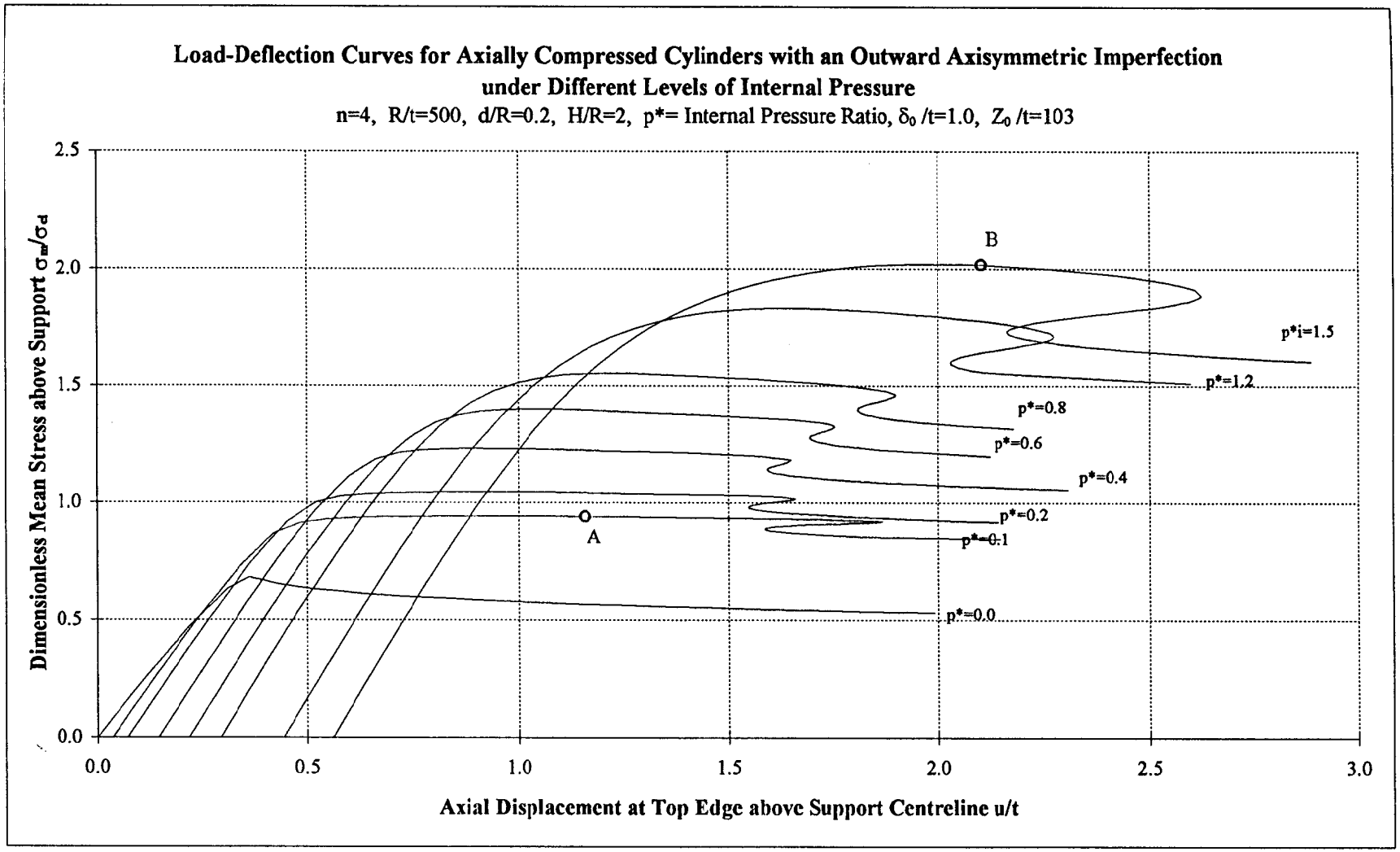
Load-Deflection Curves for Axially Compressed Cylinders with an Outward Axisymmetric Imperfection under Different Levels of Internal Pressure
n=4, R/t=500, d/R=0.2, H/R=2, p*= Internal Pressure Ratio, δ0 /t=1.0, Z0 /t=103
Dimensionless Mean Stress above Support σm/σd
Axial Displacement at Top Edge above Support Centreline u/t
0.0
0.5
1.0
1.5
2.0
2.5
3.0
A
B
p*i=1.5
p*=1.2
p*=0.8
p*=0.6
p*=0.4
p*=0.2
p*=0.1
p*=0.0

Figure 6-21

Buckling Modes for Axially Compressed Cylinders with an Outward Axisymmetric Imperfection under Different Internal Pressures

n=4, R/t=500, d/R=0.2, H/R=2.0, δ_0/t=1.0, Z_0/t=103

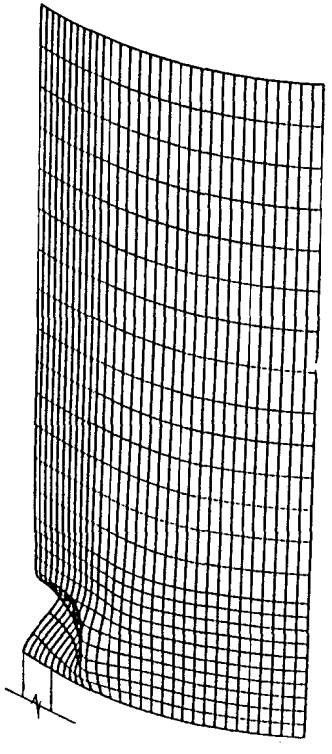

(a) p*=0.1
Low internal pressure: A

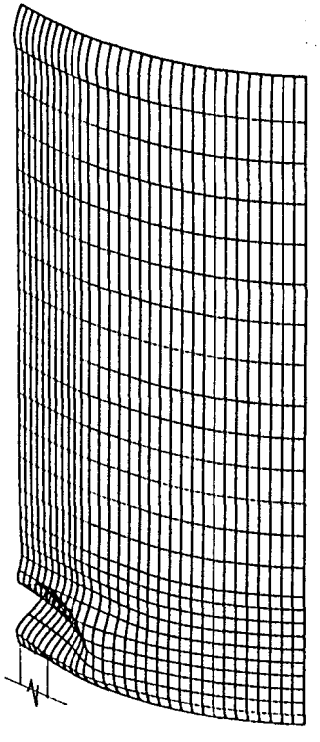

(b) p*=1.5
High internal pressure: B

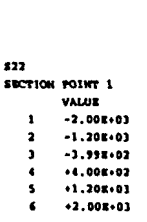

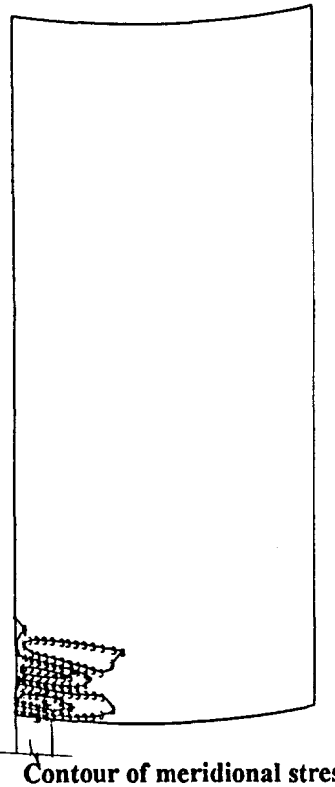

(c) Contour of meridional stress at buckling for the case of p*=1.5

Figure 6-22

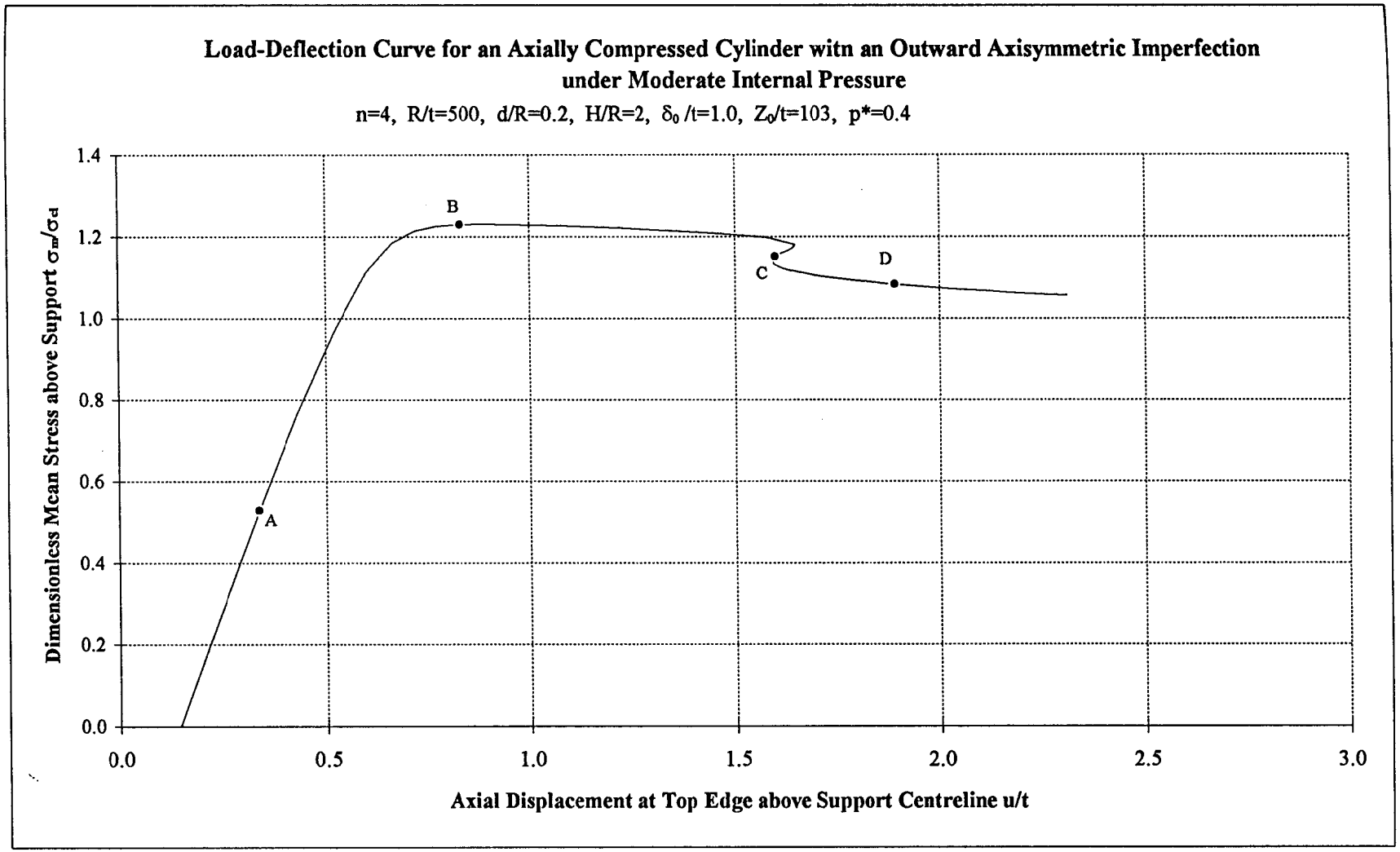
Load-Deflection Curve for an Axially Compressed Cylinder witn an Outward Axisymmetric Imperfection under Moderate Internal Pressure
n=4, R/t=500, d/R=0.2, H/R=2, δ0 /t=1.0, Z0/t=103, p*=0.4
Dimensionless Mean Stress above Support σm/σd
Axial Displacement at Top Edge above Support Centreline u/t
1.4
1.2
1.0
0.8
0.6
0.4
0.2
0.0
0.0
0.5
1.0
1.5
2.0
2.5
3.0
A
B
C
D

Figure 6-23

Deformed Shapes at Different Points on the Load-Deflection Curve of Fig. 6-23
n=4, R/t=500, d/R=0.2, H/R=2.0, δ_0/t=1.0, Z_0/t=103, p*=0.4

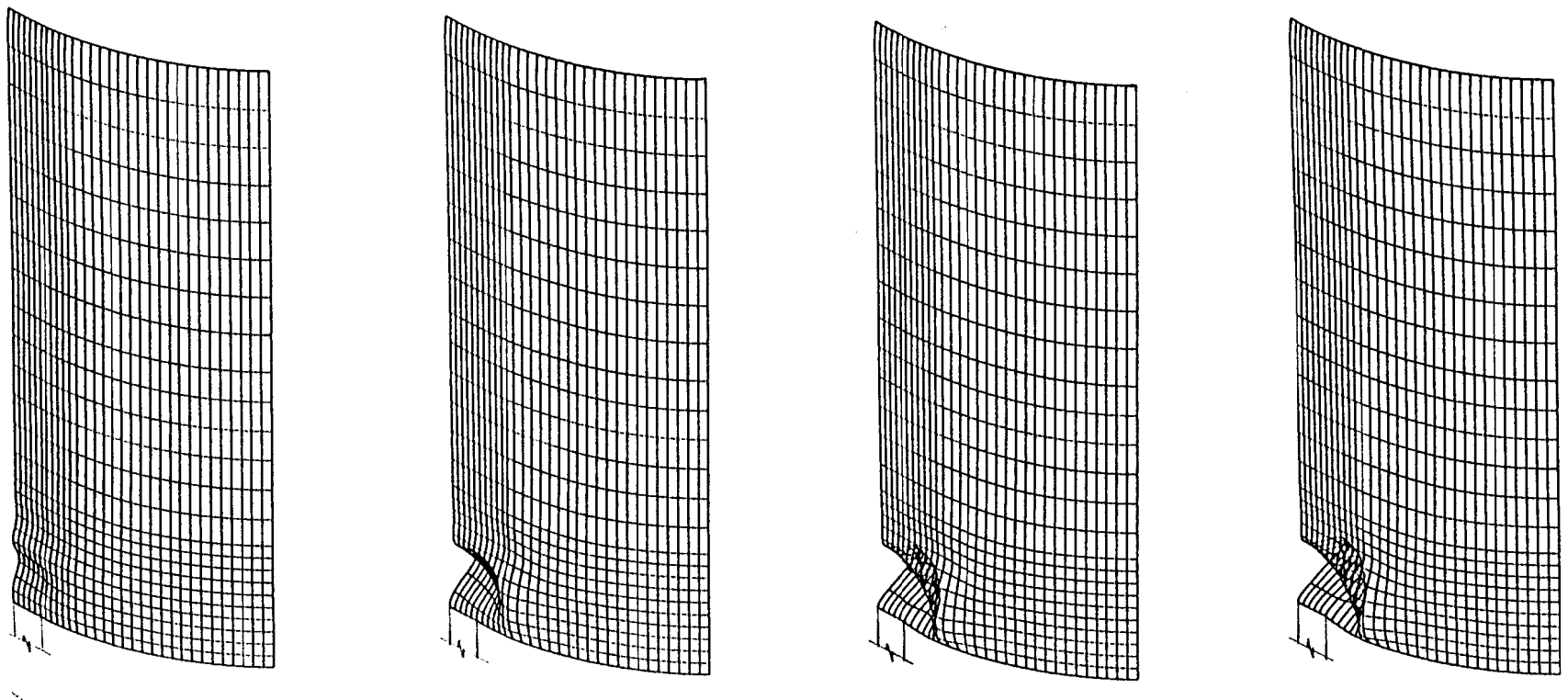

(a) Deformations at Point A (b) Deformations at Point B (c) Deformations at Point C (d) Deformations at Point D

Figure 6-24

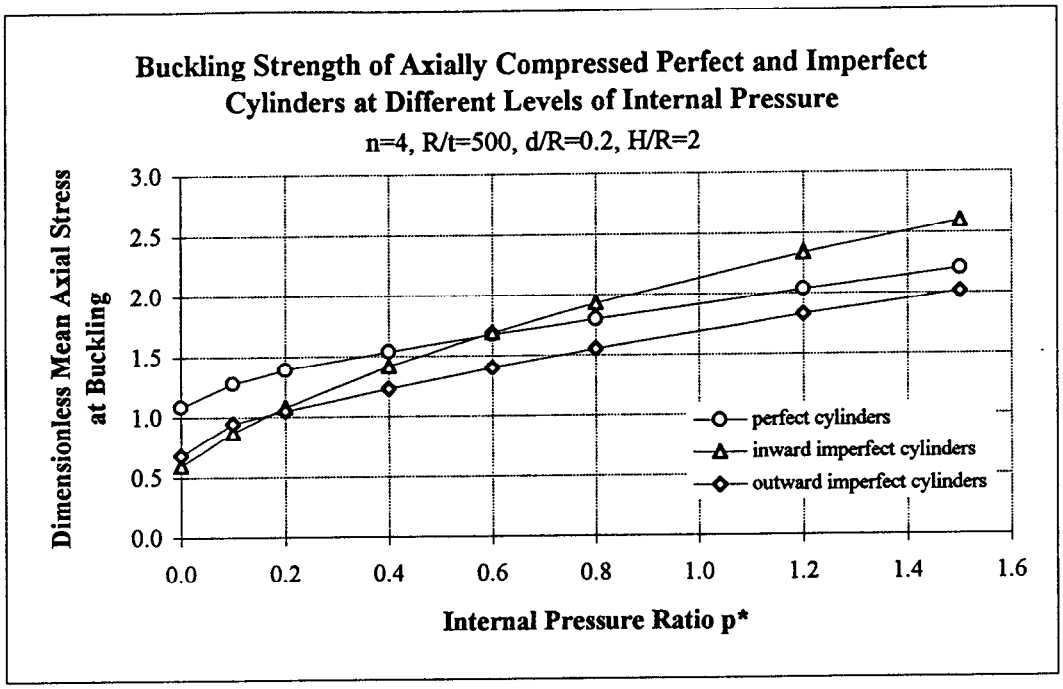
Buckling Strength of Axially Compressed Perfect and Imperfect Cylinders at Different Levels of Internal Pressure
n=4, R/t=500, d/R=0.2, H/R=2
Dimensionless Mean Axial Stress at Buckling
3.0
2.5
2.0
1.5
1.0
0.5
0.0
0.0
0.2
0.4
0.6
0.8
1.0
1.2
1.4
1.6
Internal Pressure Ratio p*
perfect cylinders
inward imperfect cylinders
outward imperfect cylinders

Figure 6-25

Buckling Strength of Discretely-Supported Cylinders under Axial Compression: Different Load Cases

n=4, R/t=500, d/R=0.2, H/R=2.0, δ_0 /t=1.0, Z_0 /t=103

This table shows values of the dimensionless mean stress above the support at buckling σ_m/σ_cl

Load Pattern	Perfect Cylinder	Inward Imperfect Cylinder	Outward Imperfect Cylinder
Roof Load	1.084	0.598	0.682
Body Load	1.095	0.620	0.698
Hopper Load	1.386	0.927	0.982

Table 6-1

CHAPTER 7

ELASTIC-PLASTIC STABILITY ANALYSIS OF DISCRETELY SUPPORTED CYLINDERS

7.1 INTRODUCTION

Studies in the preceding chapters have been entirely focused on the elastic behaviour of discretely supported cylinders. This chapter extends the study into the elastic-plastic range.

There are numerous practical situations in which thin-walled silo structures are loaded beyond the elastic limit of the material even when uniformly supported. For instance, when an axially compressed cylinder is subjected to high internal pressures on the wall, the pressures may induce severe local bending near the bottom edge of the shell. Local yielding may then precipitate a buckling failure, leading to a so-called "elephant's foot" buckle [Rotter, 1985, 1990]. Current knowledge of the elastic-plastic behaviour of practical silo structures is still fragmentary and extremely rare. Existing design rules for axially compressed cylinders [Johnston, 1976; Wozniak, 1979; AWWA, 1984; API, 1978; API, 1988; ESDU, 1974; ECCS, 1984; Gaylord and Gaylord, 1984] do not allow for local elastic-plastic failure near the boundary. In older design guides [Johnston, 1976; Wozniak, 1979; AWWA, 1979; API, 1978], no allowance is made for the beneficial effects of internal pressure, and the unpressurized cylinder buckling load dominates design for almost the entire range of internal pressures. The strengthening effects of internal pressure on the elastic buckling strength are included in some guides and codes [ESDU, 1974; Trahair et al, 1983; ECCS, 1984, 1988; Gaylord and Gaylord, 1984, AWWA, 1984; API, 1988], with the von Mises membrane yield criterion included as a test for plasticity in some cases. Local plastic collapse in these structures has only been recently investigated [Rotter, 1985, 1990; Teng and Rotter, 1989]. These investigations have only examined the local collapse of uniformly supported perfect cylinders. To date, only the limited study of Guggenberger [1991] has examined plasticity in discretely supported silos.

This chapter describes the elastic-plastic stability analysis of discretely supported cylinders. The aim is to explore the behaviour of such structures in the elastic-plastic region, and hence to draw preliminary guidance for practical design use.

The studies of this chapter are based upon both small displacement and large displacement theories and the von Mises yielding condition. Small displacement or limit analyses are first described, followed by geometrically nonlinear elastic-plastic collapse analyses. The finite element program ABAQUS was used to calculate the collapse loads of cylinders with a range of geometries, and to monitor the incremental load-displacement history and the relevant yielding modes. Prior to undertaking both of these analyses, a finite element mesh refinement study was executed to develop a mesh which is adequately fine to model the failure mode of the structure under this loading configuration. For both the limit analysis and the nonlinear elastic-plastic collapse analysis, parametric studies were conducted to examine the effects of some primary factors on the elastic-plastic stability of the cylinders. These factors involve the loading pattern, the material strength σ_y, the radius-to-thickness ratio of the cylinder R/t, the internal pressure p and the position of the imperfection in the cylinder wall Z_0 and the amplitude of the imperfection δ_0.

As a start in this new aspect of discretely supported cylinders, this chapter describes studies in the elastic-plastic region on the matters discussed in the previous elastic buckling analyses of Chapters 5 and 6. This is intended to provide a systematic picture of the behaviour of locally supported silo structures in the elastic-plastic domain.

7.2 FINITE ELEMENT MODELLING

The cylinders studied in this chapter were assumed to be directly supported on 4 discrete supports which were modelled as rigid supports, as described in Chapters 5 and 6. The finite element model of the cylinder was the same as that of Chapter 5 (Fig. 5-1). The height of the cylinder was fixed at H/R=2. Axial compression was applied to the cylinder in the same three loading patterns (Fig. 5-1). Throughout the studies of this chapter, the material of the cylinder was treated as isotropic and ideally elastic-plastic, obeying the von Mises yield criterion with a normal flow rule. The yield stress of the material, denoted by σ_y, was varied. The elastic modulus was taken as $E = 2 \times 10^5$ MPa and Poisson's ratio as $\upsilon = 0.3$.

A perfect cylinder was adopted as a reference structure, with the geometry defined by R/t=500, d/R=0.2, H/R=2.0 and n=4 and with a yield stress σ_y=250 MPa. In the parametric studies, when one of these parameters was chosen as a variable to be examined, the other parameters were retained at the values defined here.

For the study using small displacement or limit analysis, only perfect cylinders under axial compression (Fig. 5-1) were considered. The radius-to-thickness ratio R/t was varied between

200 and 1000, and three values of yield stress were studied: σ_y = 100, 250 and 500 MPa. For the study using nonlinear elastic-plastic collapse analysis, both perfect and imperfect cylinders were examined. Apart from the three loading cases (Fig. 5-1), a combination of a uniform internal pressure p together with an axial roof load (Fig. 6-2) was used to investigate the influence of internal pressurization on the nonlinear elastic-plastic collapse behaviour of the cylinders. In the study of imperfect cylinders, initial geometric imperfections with an axisymmetric pattern were again introduced in the walls, but only the detrimental inward imperfection (Fig. 6-1b) was explored. Four positions for the centre of the inward imperfection, Z_0/t, were selected to examine the effect of the imperfection location on the elastic-plastic collapse strength of the cylinder. With reference to the case when Z_0/t is equal to 103, which was described in Chapter 6, these positions may be specified as $(Z_0/t)/103$ = 0.25, 0.5, 1 and 1.25 respectively. Subsequently, the effect of varying the magnitude of the imperfection, δ_0/t, was investigated. Thus, a range of δ_0/t was particularly chosen as 0.1, 0.5, 1.0 and 2.0. The effect of internal pressure on the nonlinear elastic-plastic collapse behaviour was explored for an imperfect cylinder with a local axisymmetric imperfection with a amplitude of δ_0/t =1.0 and located at (Z_0/t)=103.

Two methods of describing the shell collapse strength are used in the studies of this chapter. Both are specified as the dimensionless mean stress above the support at collapse. In the first, the mean membrane stress above the support σ_m is normalised by the classical elastic critical stress σ_{cl} (ie. σ_m/σ_{cl}). In the other, it is normalised by the yield stress σ_y (ie. σ_m/σ_y). The description using σ_m/σ_{cl} is adopted to illustrate the loss of strength due to yielding, while the description using σ_m/σ_y is used more generally to express the collapse strength of the cylinder in the plastic region.

The 9-node quadrilateral shell element type S9R5 in ABAQUS was chosen again. To obtain reliable strength predictions, an appropriate mesh model of the cylinder must be devised before undertaking the main analyses of this chapter. This was achieved in the mesh refinement study which is described first.

7.3 MESH REFINEMENT STUDY

An inappropriate mesh would give rather inaccurate and unreliable results, producing a misleading understanding of the problem. A careful mesh refinement study is therefore essential. As shown in the elastic analyses of discretely supported cylinders of Chapters 5 and 6, large bending stresses and local deformations develop above the discrete support. Thus, a dense mesh arrangement is definitely required in that area. The mesh refinement study was

mostly undertaken using small displacement analyses, but the fine meshes were also analysed using large deflection theory. The following description relates to the small deflection theory study, unless otherwise specified.

For the mesh refinement study, the reference geometry introduced in Section 7.2 was considered. A uniformly distributed downward frictional load was imposed on the whole wall of the cylinder. The six shell element meshes shown in Fig. 7-1A and 7-1B were analysed to investigate the accuracy and convergence of the elastic-plastic collapse behaviour with respect to meshing. Details of these mesh arrangements and the corresponding plastic collapse strengths (σ_m/σ_y) are summarised in Table 7-1.

The collapse strength of the cylinder is very sensitive to the mesh arrangement. A coarse mesh such as *Mesh 1* or *Mesh 2* leads to a higher predicted stress at collapse. *Mesh 2* is much finer near the bottom edge of the cylinder than *Mesh 1*, whilst it retains the same refinement in the circumferential direction as *Mesh 1*. However, the normalised collapse strengths obtained with both meshes exceed the absolute theoretical limit of $\sigma_m=1.155\sigma_y$ which is the maximum of the von Mises yield interaction envelope of plane stress [Hodge, 1963; Save and Massonnet, 1972]. This verifies that coarse mesh arrangements in both the vertical and circumferential directions, especially in the small area above the support, are unable to present the structural behaviour accurately. Therefore, a very fine mesh is needed for elastic-plastic work.

In *Mesh 3* and *Mesh 4*, the mesh is refined above the support in the circumferential direction. The collapse loads obtained with them are lower than the theoretical limit of 1.155. The finer *Mesh 4* produces a lower strength prediction than *Mesh 3*. By investigating the yielding history of the structure, first-yield was found to occur at the intersection between the bottom edge of the cylinder and the support edge, where the membrane stresses in the cylinder reach their maximum value. At collapse, yielding is spread over only a small area immediately above the support. Thus, to adequately model such a yielding failure, a very fine mesh is needed in the critical area, especially at the bottom edge of the cylinder and near the edge of the support. *Meshes 5 and 6* were consequently designed after considering these characteristics of the discretely supported cylinder. In *Mesh 5*, the element size is reduced near both edges. *Mesh 6* has a similar arrangement to *Mesh 5*, but the element sizes are halved in the small area above the support in both directions.

When the small deflection theory results for *Mesh 5* and *Mesh 6* are compared, it is found that, although *Mesh 6* has much smaller elements than *Mesh 5* and the total number of elements in the former is double that of the latter, their collapse strengths differ by only 2%. However, the computing time for *Mesh 6* was approximately three times longer than that for *Mesh 5*. Table

7-1 also shows a comparison of the nonlinear elastic-plastic collapse strengths obtained with both meshes and shows that the difference between the strengths is only about 2%. Again, to achieve this collapse load, the job running time with *Mesh 6* was about four times as long as that of *Mesh 5*. Therefore, from these comparisons, it can be concluded that the mesh arrangement of *Mesh 5* is probably adequate for estimates of the structural strength within perhaps 3%, whilst still being cost effective. This mesh model was therefore adopted in the following studies.

The results listed in Table 7-1 also demonstrate that within the yielded area, a fine mesh arrangement either near the bottom edge of the cylinder or near the support edge alone cannot produce accurate estimates of the collapse strength, as are shown by *Mesh 3* and *Mesh 4*. Only finer meshes near both edges can give an acceptable and reliable result, regardless of the total number of elements used. For instance, the total number of elements in *Mesh 5* is less than that in *Mesh 4*, but the collapse prediction is evidently more accurate with *Mesh 5*.

The study of this section illustrates that, for discretely supported cylinders on rigid supports, there is a great sensitivity to local mesh refinement in plastic stability problems. This is much more severe than for elastic stability problems. When the nonlinear elastic buckling strengths were calculated using the above five mesh arrangements, the results obtained differed by no more than 12 % between *Mesh 1* and *Mesh 5*.

7.4 LIMIT ANALYSIS OF PERFECT CYLINDERS

At the time this study was undertaken, very little was known about the post-yield behaviour of locally supported cylinders. If an analogy is made with simple pin-ended supports, one might suppose that the strength of different support lengths can be characterised well by defining the Euler buckling stress and the plastic squash load, and then exploring the transition between these two for intermediate slendernesses [Rankine, 1857]. The elastic buckling strength has been well explored in Chapters 5 and 6, so it was natural to begin the elastic-plastic studies by trying to define the plastic limit load, which is the equivalent of a column's squash load. At the end of the study, it was apparent that this investigation of limit loads was not so useful, but the investigation is recorded here for the sake of completeness.

7.4.1 Study of the Three Loading Cases

The three axial loading cases discussed in Chapters 5 and 6 were applied to the example cylinder with R/t=500, H/R=2.0, d/R=0.2, n=4 and σ_y=250 MPa, with the aim of examining the influence of the position of the loading on the collapse strength of the discretely supported

cylinder. The calculated normalised mean collapse stress σ_m/σ_y above the support are shown in Table 7-2. The trend in the collapse strength for the three loading conditions was found to be different from that of the buckling strength. The hopper load case leads to the lowest strength among the three rather than the highest which was obtained from elastic buckling analysis. The strength calculated for the hopper load case is 34% lower than the strength under wall friction load, which is the highest of the three.

During the loading history, several common phenomena were observed regardless of the positions of the applied axial load. First yield occurred at the intersection of the bottom edge of the cylinder and the edge of the support. After first yield, the yielded zone gradually extended from that intersection point in towards the support centreline and upwards a certain distance above the lower boundary of the cylinder, until the maximum load condition was reached. At collapse, the yielded zone was localised immediately above the support termination. Comparing these with the results of the stress analysis of Chapter 5, it is known that the maximum membrane stresses caused by the local support occur precisely at the intersection point of the lower edge of the cylinder and the support edge, and that, above the support centreline, higher stresses develop in the area above the top of the support than are found at the support-shell contact point (Fig. 5-2). This stress pattern in the shell wall induces the yielding phenomena described above.

7.4.2 Parametric Studies

The effect of the thickness of the cylinder was first investigated. A range of radius-to-thickness ratios R/t = 200, 500, and 1000 was studied. The cylinder was subjected to a uniform wall friction load.

Collapse predictions (σ_m/σ_{cl}) for the range of R/t are shown in Fig. 7-2. For comparison, the relevant linear bifurcation buckling strengths obtained in Chapter 5 are also shown in this figure. The differences between the small displacement buckling strength and the small displacement plastic collapse strength are apparent from this comparison. For a thick cylinder with R/t=200, its plastic collapse strength is much lower than its elastic buckling strength, so plastic collapse occurs long before elastic buckling. By contrast, the governing failure mode of a thin cylinder with R/t=1000 is elastic buckling rather than plastic collapse since the buckling strength is low compared with the plastic collapse strength. For cylinders with R/t between 500 and 1000, the differences between the calculated strengths will be small. When R/t rises to a certain value, the two strengths will be equal. At low values of R/t, yielding dominates the failure of the structure, so the plastic collapse stress is important in design. At high values of R/t (ie. a thin cylinder), elastic buckling becomes the most significant failure mode, so the elastic buckling stress is critical in design.

The linear elastic-plastic (limit analysis) and nonlinear elastic-plastic collapse loads are compared in Fig. 7-3. The collapse loads obtained with R/t = 200, 500 and 1000 show the expected pattern. For relatively thick cylinders (R/t=200), the two loads are almost identical (1.5% different), indicating that nonlinear geometrical phenomena have little effect on the collapse load. By contrast, for thin cylinders (R/t=1000), the geometrical nonlinear collapse load falls far below the limit analysis load, as stability effects become important. In addition to the effect on nonlinear geometrical factors, it is also useful to examine the variation in the limit analysis collapse load with R/t. The thickest cylinder (R/t=200) is stronger than the thinnest cylinder (R/t=1000), but the difference is small (5.7%). Therefore, based upon small displacement limit analysis, the collapse strength of the discretely supported perfect cylinder may be considered to be independent of the thickness of the shell.

The effect of the material yield stress σ_y was examined next. Cylinders with a yield stress of 100, 250 and 500 MPa were analysed. The calculated collapse strengths are listed in Table 7-3. The effect of the yield stress σ_y on the dimensionless collapse strength above the support is insignificant and certainly within the error bounds for these calculations. The use of the yield stress to define the dimensionless collapse strength is therefore well justified.

7.4.3 Conclusions

Limit analysis is based on small deflection theory. In these limit analyses, the effects of varying the loading position, the radius-to-thickness ratio R/t and the material strength σ_y have been investigated.

It has been found that first-yield in the shell occurs at the intersection point of the bottom edge of the cylinder and the edge of the support. Under increasing axial compression, the yielded zone spreads and at collapse of the structure, the yielded zone reaches the support centreline. The position of the axial load has been found to have a marked effect on the dimensionless mean stress above the support at plastic collapse. The slenderness of the cylinder represented by the radius-to-thickness ratio R/t significantly affects the collapse strength ratio σ_m/σ_{cl}. However, the dimensionless collapse strength, σ_m/σ_y, may be considered to be independent of the radius-to-thickness ratio R/t as well as of the yield stress of the material σ_y.

It should be emphasised that these remarks apply only to small deflection limit analysis calculations. Nevertheless, these conclusions offer a useful insight into the plastic behaviour of locally supported silo structures. To understand the behaviour of a practical silo structure in depth, geometrical nonlinear phenomena and the post-yielding response must also be considered. In the following section, elastic-plastic stability analyses are described which

explore the nonlinear response of discretely supported cylinders using large displacement theory.

7.5 NONLINEAR ELASTIC-PLASTIC COLLAPSE ANALYSIS OF CYLINDERS

Geometrically nonlinear elastic-plastic stability analyses of discretely supported cylinders were next conducted. The mesh chosen in the previous limit analysis was also used here. Since the mesh convergence test (Table 7-1) demonstrated that the nonlinear elastic-plastic collapse strength obtained with this mesh (*Mesh 5*) was very close to that of the finer mesh (*Mesh 6*) (only 2% difference), the chosen mesh was judged to be adequate to model the nonlinear elastic-plastic collapse modes of discretely supported cylinders.

Both perfect and imperfect cylinders were studied. For consistency with all the preceding stability analyses using the ABAQUS program, the studies of this section used five integration points through the shell wall. This was found to be adequate to provide accurate modelling of the progress of yielding through the section of the thickness in all the cases analysed.

7.5.1 Study of Alternative Analysis Control Procedures

For geometrically nonlinear analysis, the finite element program ABAQUS provides two approaches - one for cases where the loading variations must follow a prescribed history, and another in which the loads are increased proportionally, so that the load factor is considered to be part of the solution. In ABAQUS, the loading history for which a structure's response is sought is defined by a sequence of steps. Each step is a period of response of a particular type such as the static loading used in the present studies.

In the cases where the loading variations during the step must follow a prescribed history, the entire load applied to the structure is usually divided into a number of increments during which loads are changed gradually. The automatic incrementation provided by this program has been used in most of this study. The automatic scheme for this procedure is based on the convergence of the iteration process at each increment. ABAQUS checks the convergence rate and estimates if convergence is likely to be achieved within the maximum number of iterations specified by a particular parameter. If so, one increment procedure finishes. If this results in a smaller increment than is specified as a minimum, the run is terminated. Using this approach to predict the nonlinear elastic-plastic collapse load of the discretely supported cylinder, the value of the last increment which is achieved within the given minimum load increment value can be considered to be an accurate estimate of the collapse load, so long as the minimum load

increment value is assigned to be small enough. A default value of 10^{-5} times the loading period of the step is assumed in ABAQUS.

The modified Riks method is provided for cases where load magnitude is considered to be part of the solution. This method of choosing increments is based on controlling the path length along the load-displacement response curve, and thus obtains a solution regardless of whether the response is stable or unstable. It should be noted that a solution at a predefined load or displacement value cannot be easily obtained using this method, because both are treated as unknowns - termination of the solution process occurs at the first solution that exceeds the load proportionality factor if the maximum value of it is specified, or at the end of the increment during which the maximum total displacement value assigned is crossed. Nevertheless, in structural buckling or collapse analysis, if the maximum and minimum values of the load increment are made small enough, then the solution when the load proportionality factor reaches the limiting value may be accepted as an adequate criterion to define the buckling or collapse load.

The example cylinder with R/t=500, d/R=0.2, H/R=2.0, n=4 and σ_y=250 MPa and subject to a uniform wall friction was used to study these two different calculation methods. The forestated two approaches were used: the corresponding nonlinear collapse strengths obtained are listed in Table 7-4. The time (loading) period, the minimum load increment and the maximum load increment values assigned in these ABAQUS runs are also noted in this table. Within the assumed limits shown in Table 7-4, the collapse strength achieved using the first approach can be treated as the accurate solution. Two cases were analysed using the modified Riks method. For *Case 1*, the analysis ends when convergence is deemed to be unlikely within the minimum load increment specified, so that no solution is gained. The problem encountered in *Case 1*, however, can be avoided by giving appropriate and efficient load increment limits, as in *Case 2*. For *Case 2*, the expected solution is achieved and agrees quite well with the accurate solution obtained using the first approach. The difference between the results using the two approaches is only about 0.5%. Such a close agreement illustrates that the modified Riks method can give accurate fast solutions provided that the minimum and maximum values of load increment are defined well. However, to achieve the collapse load of the cylinder, when the same initial load increment value is specified, the ABAQUS running-time required using the first approach is 5 times longer than using the modified Riks method. It is apparent that the modified Riks method is much more efficient. In addition to the achievement of the collapse load of the structure, the modified Riks method can also perform the post-yielding analysis, providing an incremental load-displacement response for this problem.

As a result of this study of alternative analysis procedures, the modified Riks method was adopted for the following nonlinear elastic-plastic collapse analyses of discretely supported cylinders. It was found that the value of the assigned load increment limits had a strong influence on the accuracy of the prediction of the collapse load of the cylinder. Thus, for all the cases studied in the following analyses, the time (loading) period value was fixed at 1.0; the default minimum load increment value of 10^{-5} was selected; and the maximum load increment value was specified as 0.1.

7.5.2 Behaviour of Perfect Cylinders

The example cylinder under axial compression was analysed first. The three axial loading conditions shown in Fig. 5-1 of Chapter 5 were again adopted. The nonlinear collapse strengths obtained under these three loading cases are compared in Table 7-2 with the previous small displacement limit analysis results. The collapse strengths show the same trend as was found in the elastic buckling analyses: the hopper load leads to the highest strength whilst the roof load gives the lowest. Again, the importance of large displacement effects is apparent when comparing the results of nonlinear elastic-plastic analysis and limit analysis.

When the loading history is examined, it is found that the nonlinear behaviour of the cylinder under the three loads is essentially similar. The load-displacement response for a typical cylinder under a uniform wall friction load is shown in Fig. 7-4. The axial displacements recorded in this figure are again those at the top edge of the cylinder above the support centreline. The axial displacements increase slowly until the load reaches the bifurcation point, which is also the point of maximum strength (point B). After this bifurcation point, the axial displacement first reduces under reducing load, and then increases rapidly as the load decays further. The pre-collapse, collapse and post-collapse deformed shapes, corresponding to the three points A, B and C on this curve, are illustrated in Fig. 7-6. First yield occurs at the intersection point of the lower edge of the cylinder and the edge of the support at the point indicated on this load-displacement path of Fig. 7-4. Yielding then gradually develops along the bottom edge of the cylinder back towards the support centreline and up the cylinder. At the bifurcation point, the yielded zone in the shell wall is localised immediately above the support, as shown in Fig. 7-7a. After this collapse condition, the cylinder enters into the post-collapse phase, when yielding develops more extensively in the shell (Fig. 7-7b).

Both the load-displacement curves obtained from the previous nonlinear elastic analysis and the present nonlinear elastic-plastic analysis are shown in Fig. 7-5 for this example perfect cylinder. In this figure, the load is represented by the calculated dimensionless mean stress above the support (σ_m/σ_{cl}). The influence of the yielding on the bifurcation loads and the deflections is apparent from this comparison.

The effect of varying the radius-to-thickness ratio R/t was examined next. Values of R/t were chosen at 200, 350, 500, 1000 and 2000 and the uniform wall friction load case adopted. Figure 7-3 compares the collapse strengths of the limit analysis and the nonlinear analysis for three cylinder slendernesses (R/t=200, 500 and 1000) to show the increasing influence of large displacement effects in thin cylinders. The nonlinear response is very different from the small displacement response, especially as the cylinder becomes thinner. For the thickest cylinder (R/t = 200), the large displacement theory collapse load was found to be lower than its small displacement theory value by only 1.3%, but at R/t = 500 and 1000, the difference increased to 21% and 29% respectively. Such large differences demonstrate that large displacement effects are much more significant and influential in thin cylinders than in thicker ones. Further, it is evident that the small displacement limit analysis cannot offer reliable solutions to this particular problem for very thin cylinders. The limit analysis always overestimates the actual collapse strength of a discretely supported cylinder.

The changes in the collapse strength with the cylinder slenderness (R/t) are shown in Fig. 7-8. Large deflection effects on the yielding for the cylinders of different thicknesses are clearly seen.

In practice, shells that are thick enough to yield before buckling under uniform axial compression alone are rarely found in silo structures. However, if a high level of internal pressurization is present in the cylinder, even very thin cylinders under uniform compression approach the yield condition. Previous investigations [Rotter, 1985, 1990] examined the geometrically nonlinear elastic-plastic collapse and the instability of perfect thin, internally pressurized cylinders under axial compression. These investigations revealed that first yield occurs in the zone of local bending adjacent to the shell boundary, where the circumferential membrane and the bending stresses are amplified by axial compression, leading to an "elephant's foot" buckling mode. The importance of elastic-plastic collapse as a failure mode is not dependent on the grade of steel used. Collapse loads are generally 10-20% higher than first-yield conditions, except for thin cylinders without internal pressurization, when elastic buckling occurs.

The influence of internal pressurization on the nonlinear elastic buckling strength of discretely supported cylinders was described in Chapter 6. The effect of yielding on changing these buckling predictions is investigated here.

The influence of internal pressurisation on the elastic-plastic collapse strength was explored, by considering the example perfect cylinder loaded by a combination of uniform roof load and

internal pressure p. One limiting condition is defined by uniform membrane circumferential yield, which occurs in internally pressurized cylinders without axial load when $pR/t = \sigma_y$. For the chosen $\sigma_y = 250$ MPa in the present study, membrane circumferential yield does not occur until p reaches to 0.5 MPa or the internal pressure ratio p* rises to 1.033. Therefore, 1.033 is the maximum possible value for p* in the study here. All the p* specified must be lower than this value.

A range of the internal pressure ratios p* = 0.1, 0.2, 0.4, 0.6, and 1.0 was analysed. Figure 7-9 shows the nonlinear elastic-plastic collapse strengths of these axially compressed pressurized cylinders together with the strength of a cylinder under a uniform roof load alone (p*=0.0). The weakening effect of internal pressurization (p* > 0.0) is evident on the yielding strength above the local support. In particular, higher levels of internal pressure lead to collapse of the cylinder at an axial load much smaller than the lower pressure levels. The strength declines markedly as p* increases. When p* rises to 1.0, the internal pressure induces wide scale yielding in the body of the cylinder, so that even a very small axial load is enough to cause collapse of the structure.

At low internal pressures, a uniformly supported imperfect cylinder experiences an increase in buckling strength with internal pressure, because the internal pressure reduces the effect of circumferential compressions which are implicated in the imperfection sensitivity [Calladine, 1983]. Here, the local bending effect of the discrete support serves in the role of the imperfection, as shown in Chapter 6, and the buckling strength rises with internal pressure. However, yielding effects soon interfere, and the strength begins to fall. For the geometry of this example cylinder, the range of pressure in which strength increases are found is very limited. When the internal pressure ratio p* is larger than around 0.1, as shown in Fig. 7-9, the strength reaches its maximum and then goes down continuously. Thus at most pressurisation levels, elastic-plastic collapse is the governing failure mode.

The load-deflection curves for cylinders undergone these different internal pressures are shown in Fig. 7-10. For all the cylinders pressurized below p* = 0.6, the load-deflection curve has a steadily changing form. At zero internal pressure, the sharp bifurcation and reversing axial displacements are found. As the internal pressure is raised, the sharpness of the bifurcation steadily declines, and by p* = 0.6 the curve demonstrates no reversal of axial displacements in the post-buckling zone. At higher internal pressures, the response becomes steadily more and more ductile. The deformed shapes at maximum load for the three levels of pressurisation p* = 0.1, 0.4 and 0.6 are shown in Fig. 7-11. These figures do not show the buckling mode or post-buckling pattern because they are drawn at the maximum load condition. Nevertheless, a local "elephant's foot" buckling mode can be identified just above the support at p* = 0.6.

7.5.3 Behaviour of Imperfect Cylinders

Attention was next directed to the imperfection-sensitivity of pressurised cylinders. A local axisymmetric imperfection with an inward shape, as shown in Fig. 6-1b of Chapter 6, was introduced in the cylinder wall.

Studies were first concentrated on the effect of the position of the imperfection, with a constant amplitude of δ_0/t =1.0. Four positions for the centre of the imperfection were chosen as $(Z_0/t)/103$ = 0.25, 0.5, 1.0 and 1.25. Figure 7-12 shows the collapse strength of the example cylinder with these three imperfection positions, together with the strength of a perfect cylinder discussed in Section 7.5.2. It is apparent that the collapse strengths of imperfect cylinders are considerably lower than that of the perfect cylinder. Among the four positions studied, the one specified as $(Z_0/t)/103$ = 1.0 leads to the lowest strength, a reduction of about 73% from the perfect cylinder strength. For elastic cylinders, the buckling strength reduction for an imperfect cylinder with Z_0/t = 103 was about 60% (see Chapter 6), so it appears that the imperfection-sensitivity is greater in this elastic-plastic domain than for the elastic buckling problem. It can be concluded from Fig. 7-12 that the position of the centre of the imperfection $(Z_0/t)/103$ at 1.0 is the worst for this cylinder with R/t=500. This conclusion is consistent with that drawn by Rotter and She [1993] in their studies of the nonlinear elastic buckling of discretely supported cylinders which were described in Chapter 3.

The load versus displacement response curves obtained for imperfect cylinders with an inward imperfection introduced at these different positions in the shell wall are found to be similar in form. Figure 7-13 shows the load-displacement curve of the imperfect cylinder with δ_0/t=1.0 and $(Z_0/t)/103$=1.0. The shape of this curve is clearly different from that of a perfect cylinder shown in Fig. 7-4. The behaviour is relatively ductile and no bifurcation point is observed on the curve. The magnitudes of the axial displacements are much larger than those for the perfect case. In particular, as the displacements develop after the maximum strength, the load declines only slightly. Because the initial imperfection was placed near the bottom edge of the cylinder, it is involved in the development of local yielding above the support and leads to early yielding of the shell wall.

The deformed shapes of the imperfect cylinder at the point of maximum strength are shown in Fig. 7-14 for the inward imperfection at three positions of $(Z_0/t)/103$ = 0.25, 1.0, and 1.25. It can be observed that the centre of the yielded zone occurs almost at the centre of the imperfection introduced in the shell wall, and among three modes, the one with the imperfection centred at $(Z_0/t)/103$ = 1.0 demonstrates the severest deformed configuration at collapse. Therefore, for this typical cylinder, an imperfection with its centre at $(Z_0/t)/103$ = 1.0 can be considered to be of the critical effect on the structural collapse.

Further calculations were performed to investigate the sensitivity of the collapse strength to the magnitude of the imperfection. The range of the imperfection magnitudes was specified as δ_0/t = 0.1, 0.5, 1.0 and 2.0. The collapse strengths obtained for this range of studied values are shown in Fig. 7-15. It is noteworthy that a large amplitude imperfection causes a gain in strength which is quite significant. An imperfection amplitude of only two wall thickness (δ_0/t=2.0) is found to produce a substantial strength increase over that for one thickness (δ_0/t=1.0).

The effect of the radius-to-thickness ratio R/t was also examined for imperfect cylinders with an inward axisymmetric imperfection with an amplitude of δ_0/t=1.0 and placed at $(Z_0/t)/103$=1.0. The same values of R/t as in the analysis of perfect cylinders were chosen at 200, 350, 500, 1000 and 2000. The uniform wall friction load case was adopted again. The changes in the collapse strength with the cylinder slenderness are shown in Fig. 7-16, where they are compared with those for perfect cylinders. It is evident from this comparison that the geometric imperfection results in a significant reduction in the collapse strength. In general, thin cylinders (R/t $\geq$ 500) induce greater reduction in the strength than thick ones. This indicates that the local yielding may play a more significant role in the buckling for thin cylinders than for thick shells.

The influence of internal pressure on the nonlinear elastic-plastic collapse strength was finally examined for discretely supported imperfect cylinders with δ_0/t=1.0 and $(Z_0/t)/103$ = 1.0 and under uniform roof load together with internal pressure p. The range of the internal pressure ratios p* = 0.1, 0.2, 0.4, 0.6 and 1.0 was analysed again. The calculated collapse strengths at different levels of internal pressure are shown in Fig. 7-17, where they are compared with those for axially compressed pressurised perfect cylinders. At low internal pressures, the collapse strength increases with internal pressure. The increase in the collapse strength corresponds to that the internal pressure reduces the imperfection-sensitivity. As the internal pressure is raised, yielding effects interfere, and the strength begins to fall. For this imperfect cylinder with this specified geometric imperfection, the range of pressure in which strength increases is longer than that for the perfect cylinder discussed in Section 7.5.2. Moreover, it can be seen that the trend of reduction in the strength for the imperfect cylinder is not as sharp as that for the perfect cylinder. By contrast, at high internal pressures (p*>0.8), the initial geometric imperfection resists the weakening effect of local yielding on the strength and induces higher strengths than the cases of the cylinder without geometric imperfection.

7.6 SUMMARY AND CONCLUSIONS

Plastic stability problems in discretely supported cylinders were studied in this chapter. Both small deflection limit analyses of perfect cylinders and geometrically nonlinear elastic-plastic collapse analyses of perfect and imperfect cylinders were performed using the finite element program ABAQUS. The von Mises yield criterion was used. In the limit analysis, the chief effort was exerted into investigating the effects of the load case, the geometric parameter R/t and the yield stress of the material. The nonlinear elastic-plastic collapse analyses were applied to a wide range of problems, covering the axial loading cases, the relative thickness of the shell (R/t), the level of internal pressurization and the magnitude and position of a detrimental axisymmetric inward imperfection in the wall of the cylinder. These parameters were chosen for study because they appeared to be the major influential factors on the behaviour of elastic-plastic cylinders.

For almost all the geometries, loadings and material strengths studied, the behaviour of the cylinders is generally similar. First yield occurs at the edge of the support on the lower edge of the cylinder. After first yield, the yielded zone grows progressively above the support with increasing displacements until a maximum load condition is attained when the cylinder collapses. After this collapse condition, found using the geometrically nonlinear analysis, the cylinder enters the post-collapse phase, when the displacements increase quickly.

The position of the applied axial load was found to alter the dimensionless mean stress above the support at plastic collapse significantly. The same trend in the collapse strengths as that of the buckling strength was obtained in the nonlinear elastic-plastic analysis. Varying the position of the axial loading from the upper edge to the lower edge of the cylinder may induce as much as 59% increase in strength. The limit analysis and the nonlinear analysis give completely different results for the effect of the variation of the thickness of the cylinder. In the limit analysis, the dimensionless collapse strength σ_m/σ_y alters only slightly as the radius-to-thickness ratio R/t varies, whilst a big change in the collapse strength is obtained from the nonlinear analysis. In particular, large displacement effects become very important as the cylinder gets thinner. The normalised collapse strength above the local support may be considered to be independent of the yield stress of the material if the normalisation is performed relative to the yield stress. Higher internal pressures may cause a significant decline in the collapse strength of the shell under axial compression.

A strong weakening effect of an inward imperfection near the bottom edge of the cylinder on the nonlinear collapse strength was revealed. This significant imperfection-sensitivity should receive particular attention in practical design, since about 73% strength reduction was found

for a typical inward imperfection with the amplitude of $\delta_0/t = 1.0$ and localised at the critical height of $Z_0/t = 103$. However, no further reduction in the collapse strength occurs once the imperfection amplitude exceeds a certain level. Higher internal pressures may induce the collapse strength of imperfect cylinders with a local inward axisymmetric imperfection slightly higher than that of axially compressed pressurised perfect cylinders.

A further investigation of the elastic stability response of a discretely supported complete silo structure is described in Chapter 8.

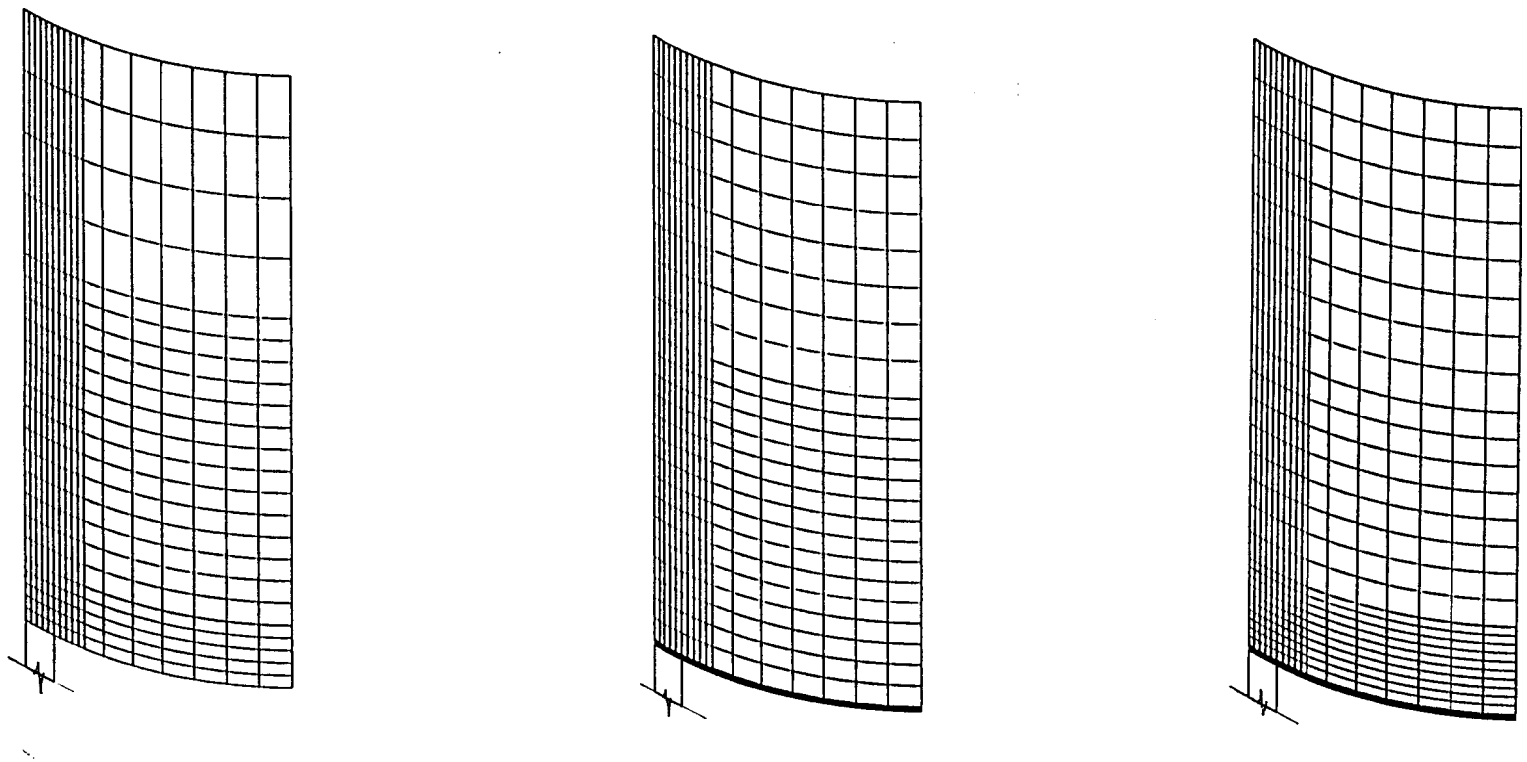

(a) Mesh 1 (b) Mesh 2 (c) Mesh 3

Figure 7-1A

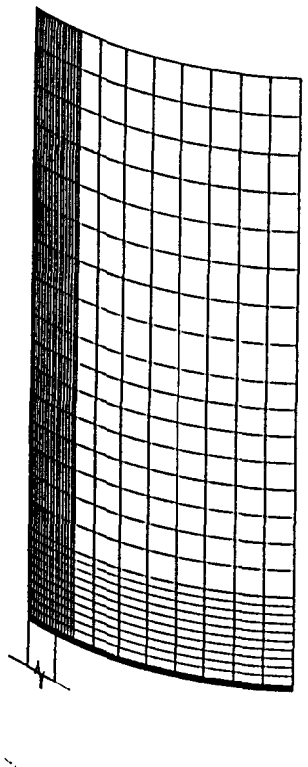

(d) Mesh 4

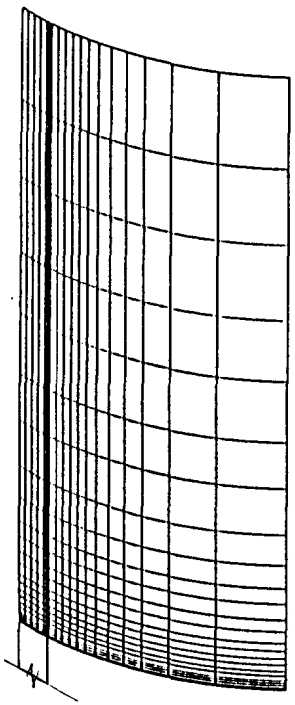

(e) Mesh 5

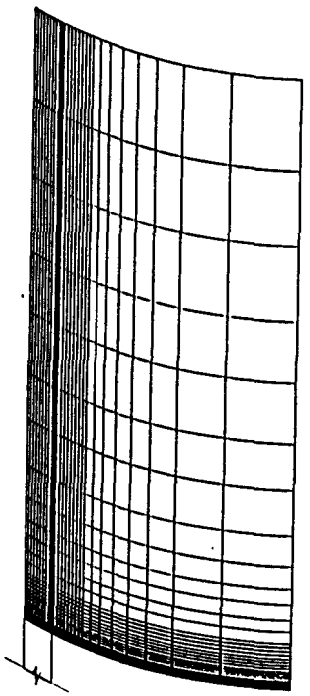

(f) Mesh 6

Figure 7-1B

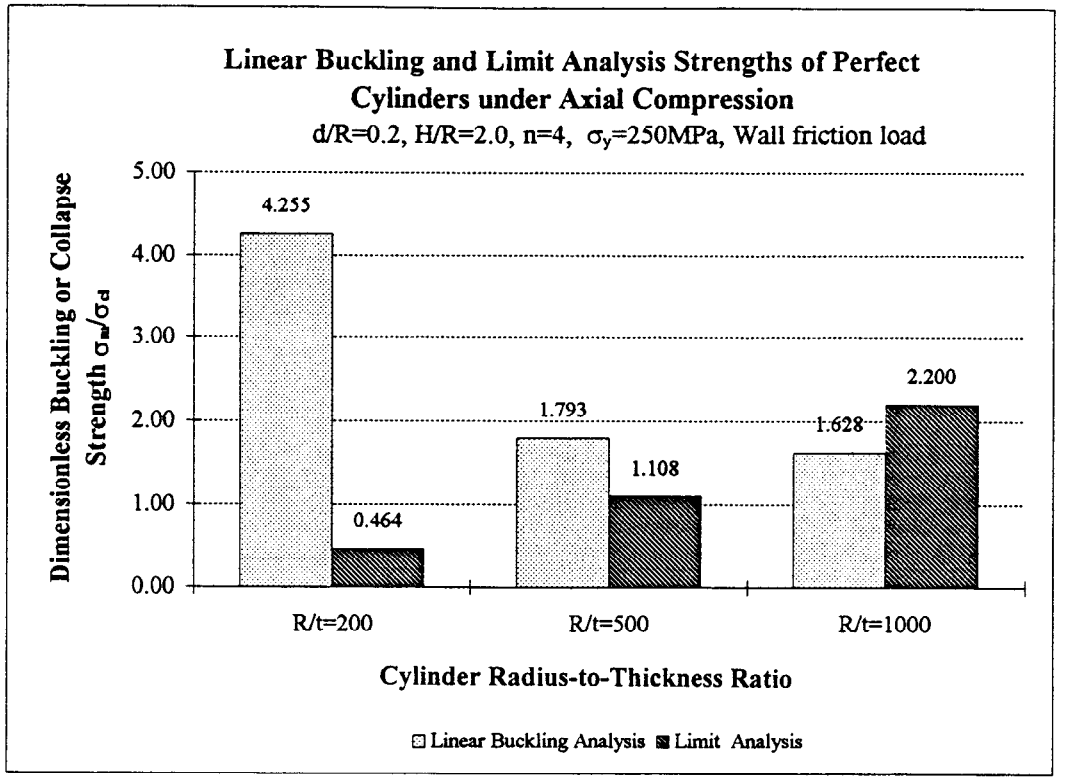

Figure 7-2

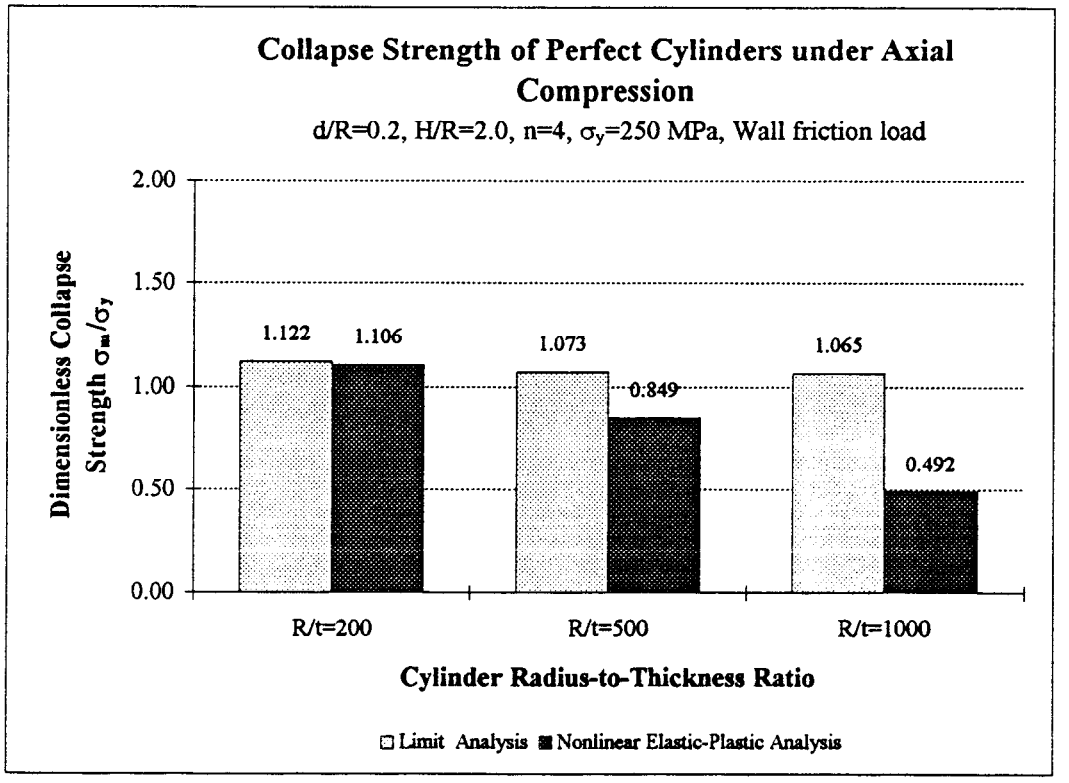

Figure 7-3

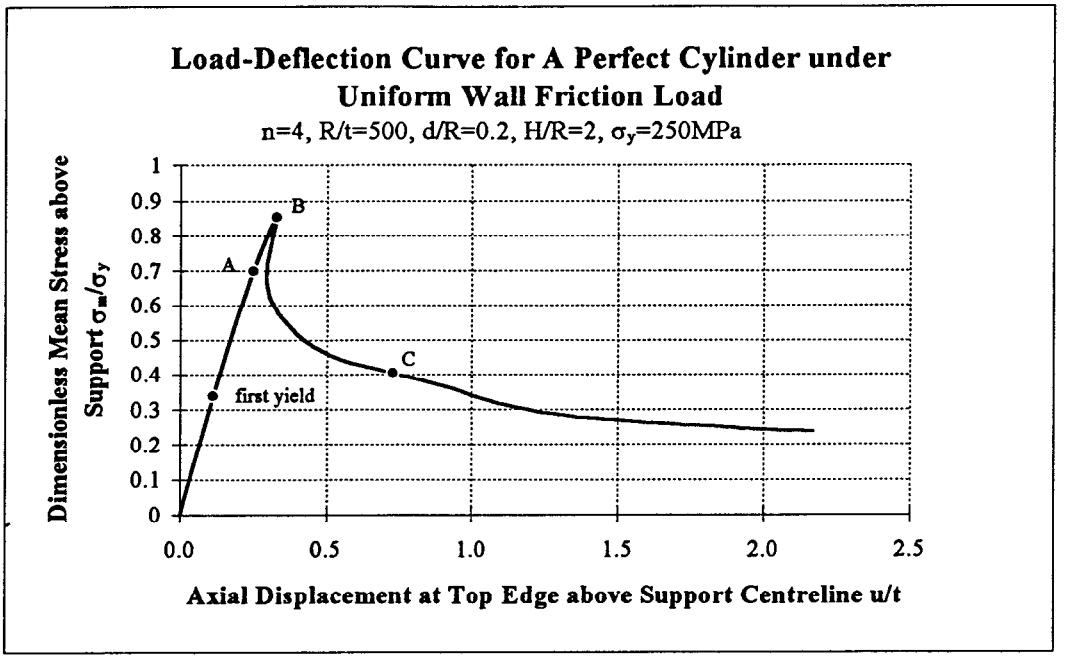

Figure 7-4

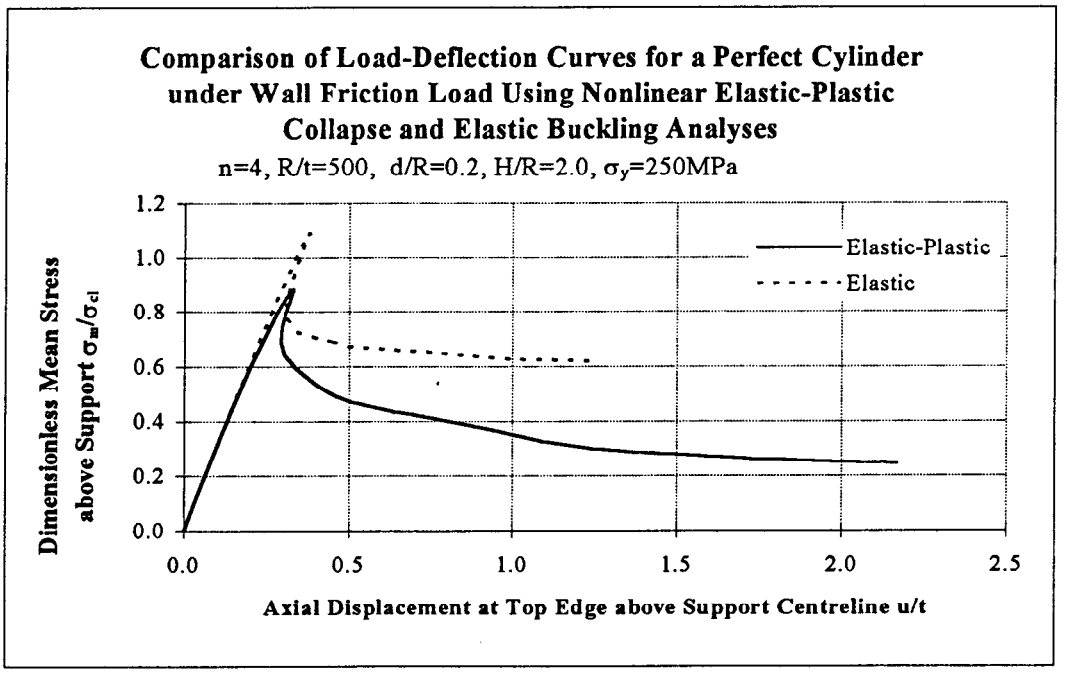

Figure 7-5

Deformed Shapes at the Points A, B and C on the Load-Deflection Curve of Figure 7-4
R/t=500, d/R=0.2, H/R=2.0, σ_y=250MPa, Wall Friction Load

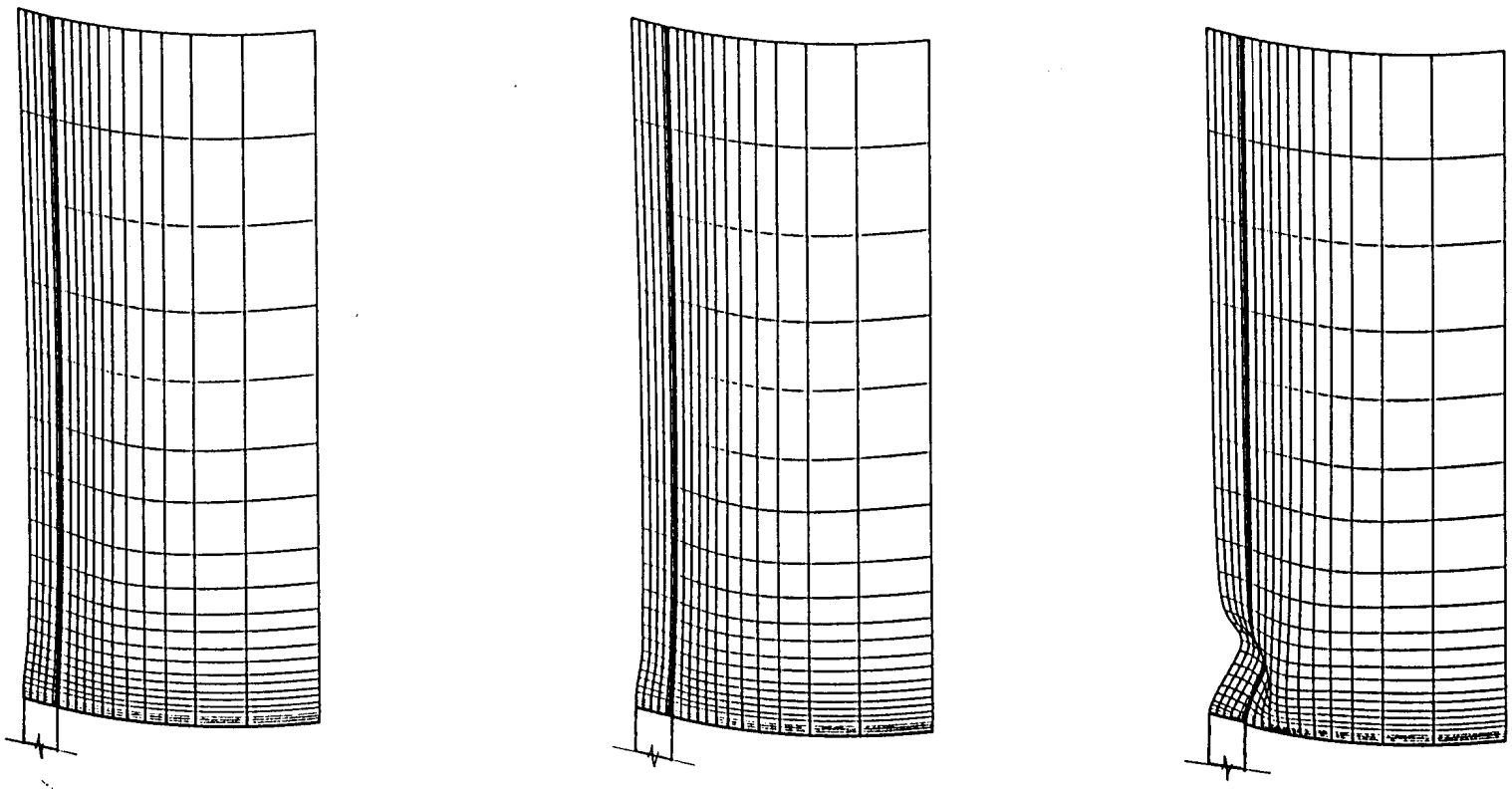

(a) Pre-buckling shape (A)

(b) Deformations at bifurcation (B)

(c) Deformations after bifurcation (C)

Figure 7-6

Contour of the Yielded Zone in the Cylinder Wall at the Points B and C on the Curve of Figure 7-4

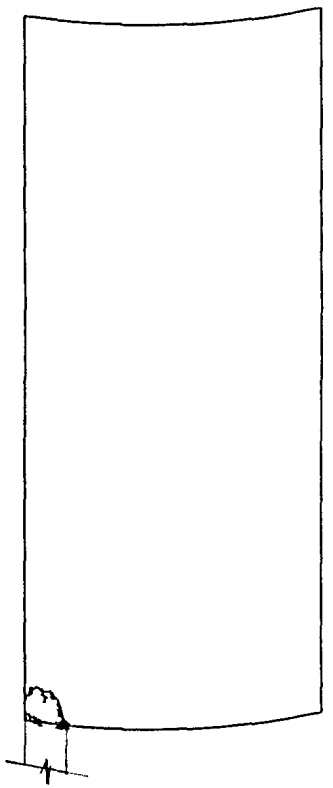

PEEQ
SECTION POINT 1
VALUE

1	+1.40E-08
2	+1.40E-02
3	+2.80E-02
4	+4.20E-02
5	+5.60E-02
6	+7.00E-02

(a) Yielded zone at bifurcation (B)

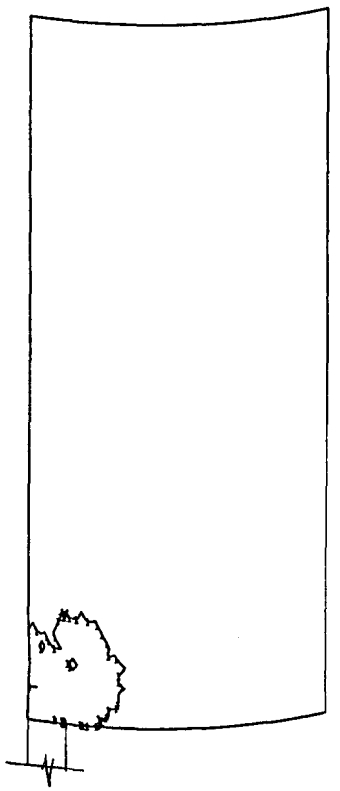

PEEQ
SECTION POINT 1
VALUE

1	+4.00E-08
2	+4.00E-02
3	+8.00E-02
4	+1.20E-01
5	+1.60E-01
6	+2.00E-01

(b) Yielded zone after bifurcation (C)

Figure 7-7

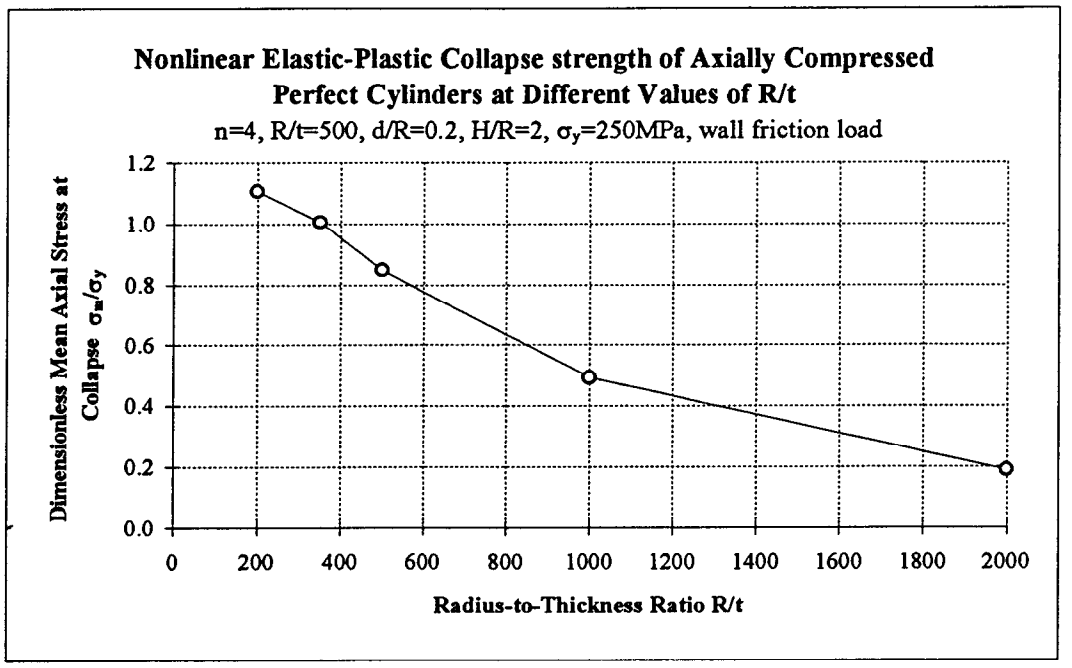

Figure 7-8

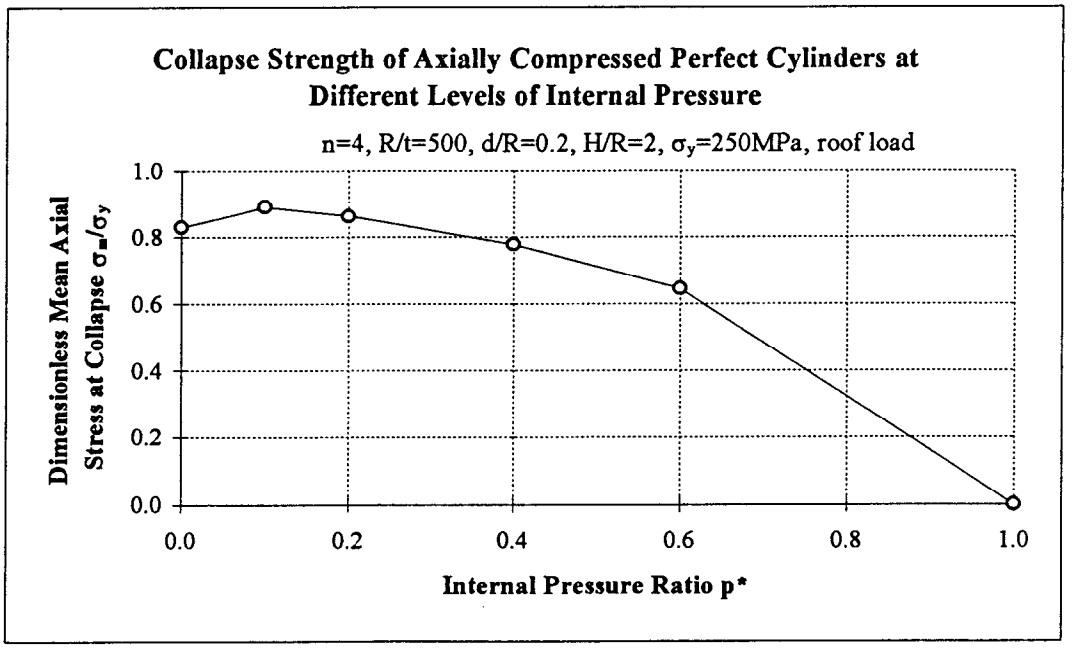

Figure 7-9

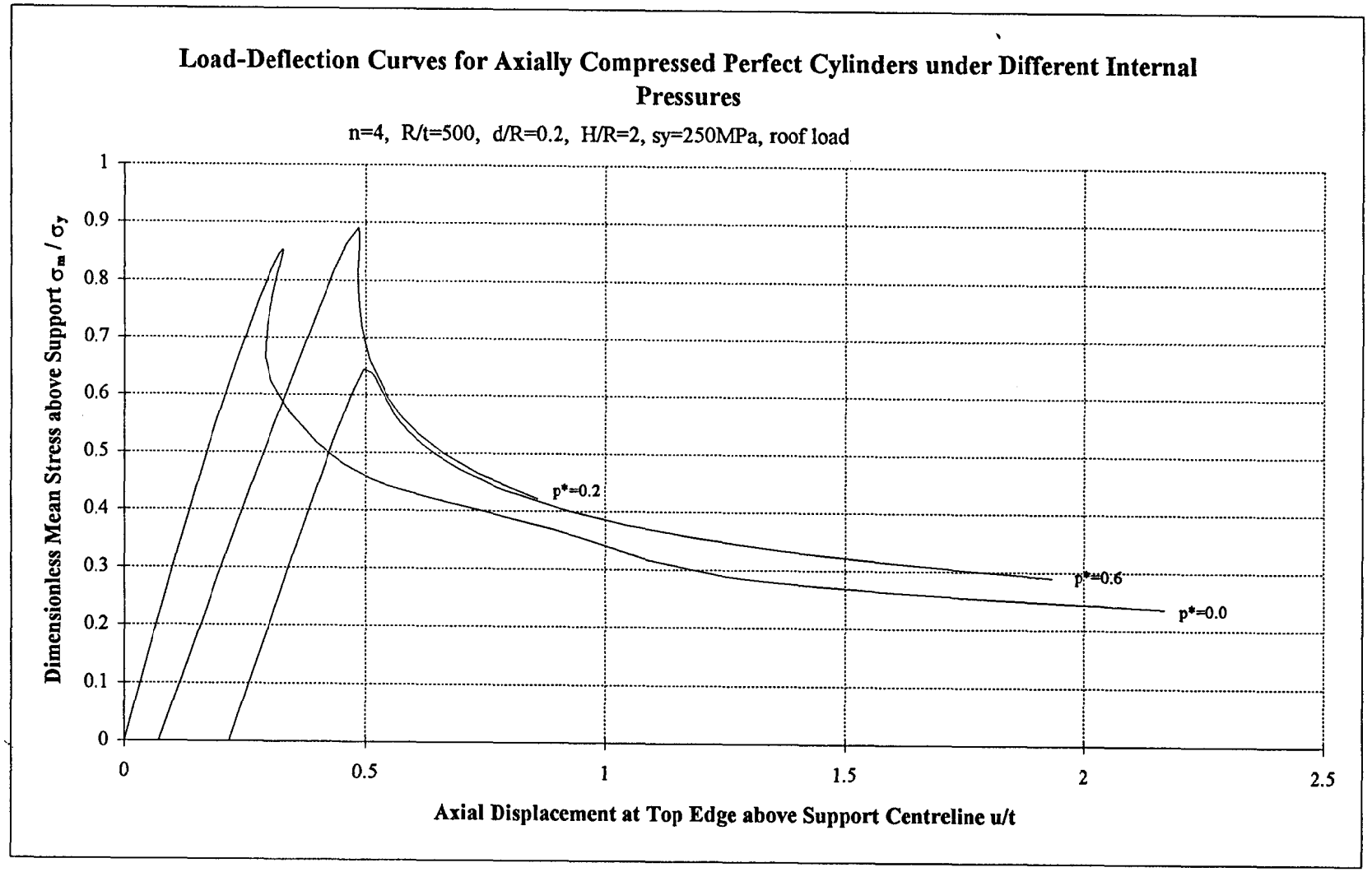
Load-Deflection Curves for Axially Compressed Perfect Cylinders under Different Internal Pressures
n=4, R/t=500, d/R=0.2, H/R=2, sy=250MPa, roof load
Dimensionless Mean Stress above Support σm / σy
Axial Displacement at Top Edge above Support Centreline u/t
p*=0.2
p*=0.6
p*=0.0
0
0.1
0.2
0.3
0.4
0.5
0.6
0.7
0.8
0.9
1
0
0.5
1
1.5
2
2.5

Figure 7-10

Deformed Shapes at Maximum Load for Axially Compressed Perfect Cylinders under Different Internal Pressures
R/t=500. d/R=0.2. H/R=2.0, σy=250MPa, Roof Load

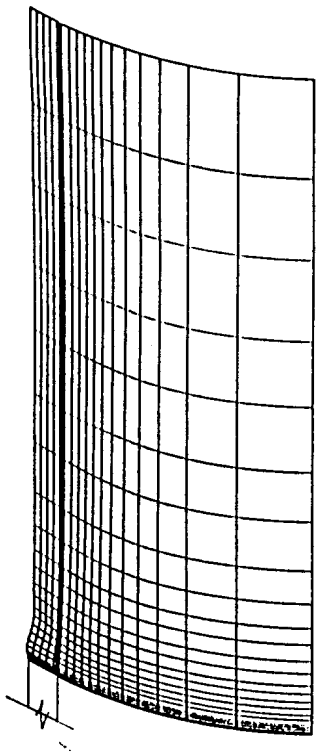

(a) p*=0.1

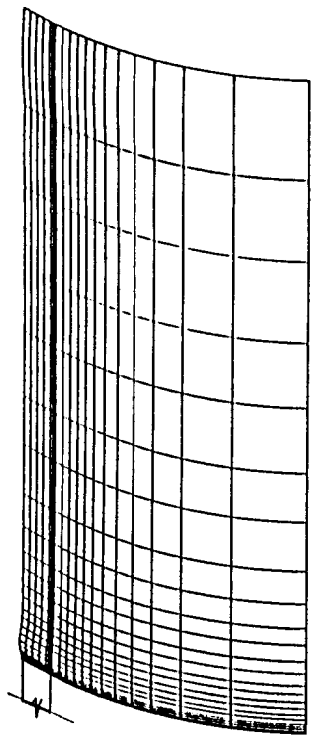

(b) p*=0.4

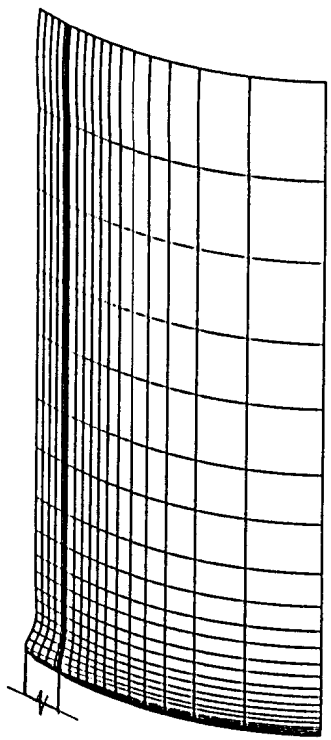

(c) p*=0.6

Figure 7-11

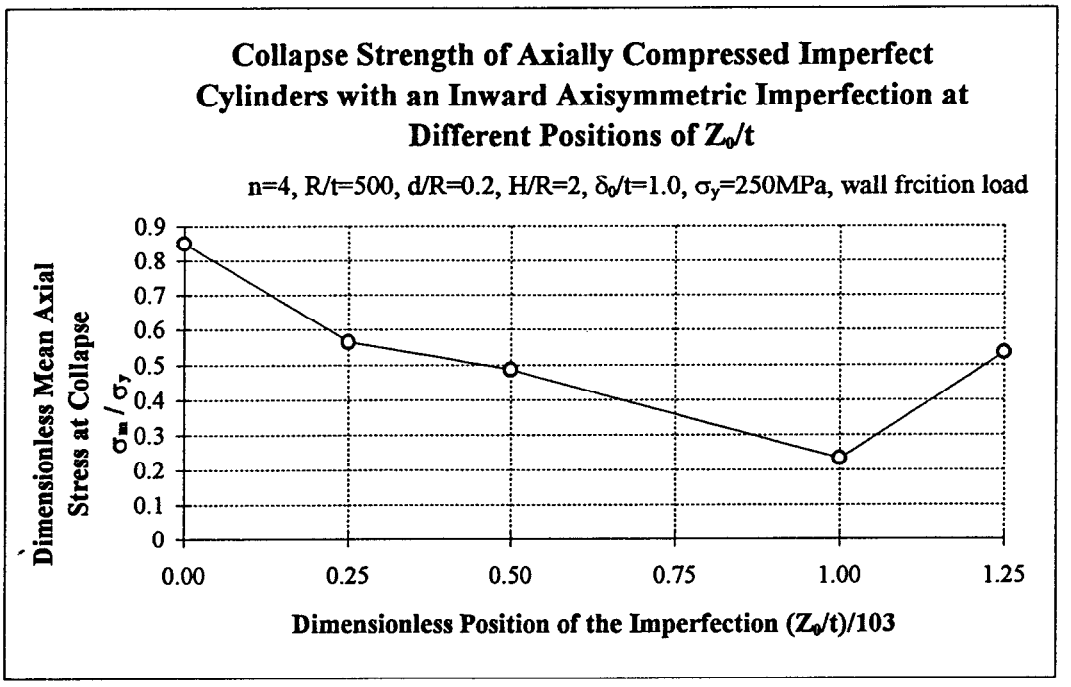

Figure 7-12

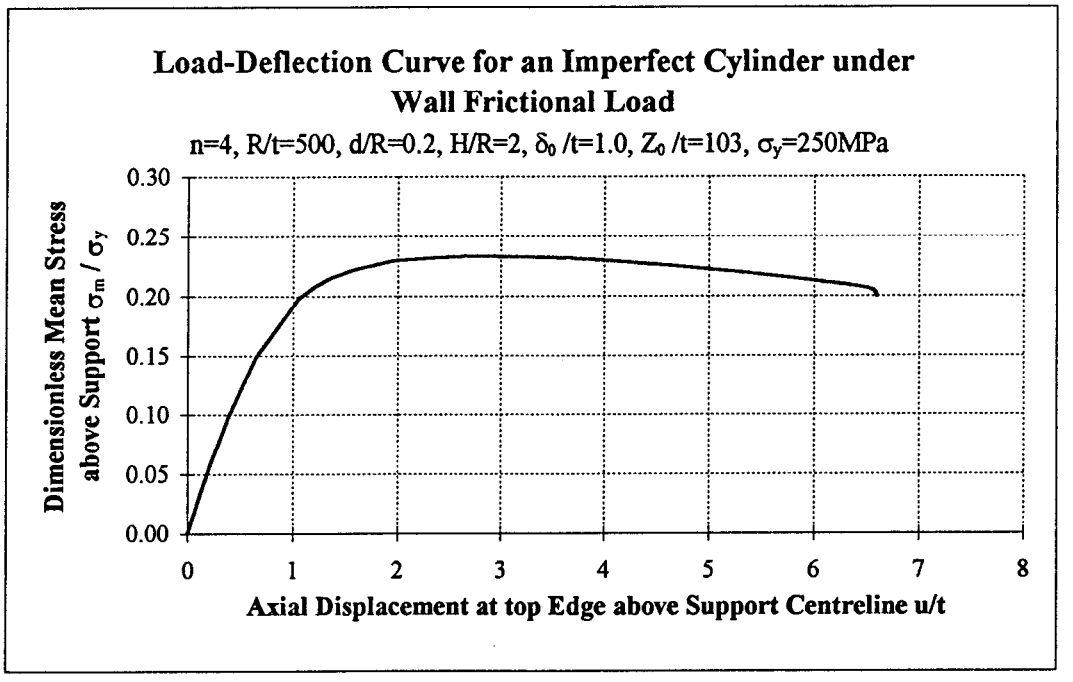

Figure 7-13

Deformed Shapes at Maximum Load for Imperfect Cylinders under Axially Compression
R/t=500, d/R=0.2, H/R=2.0, n=4, δ_0/t=1.0, σ_y=250MPa, Wall Friction Load

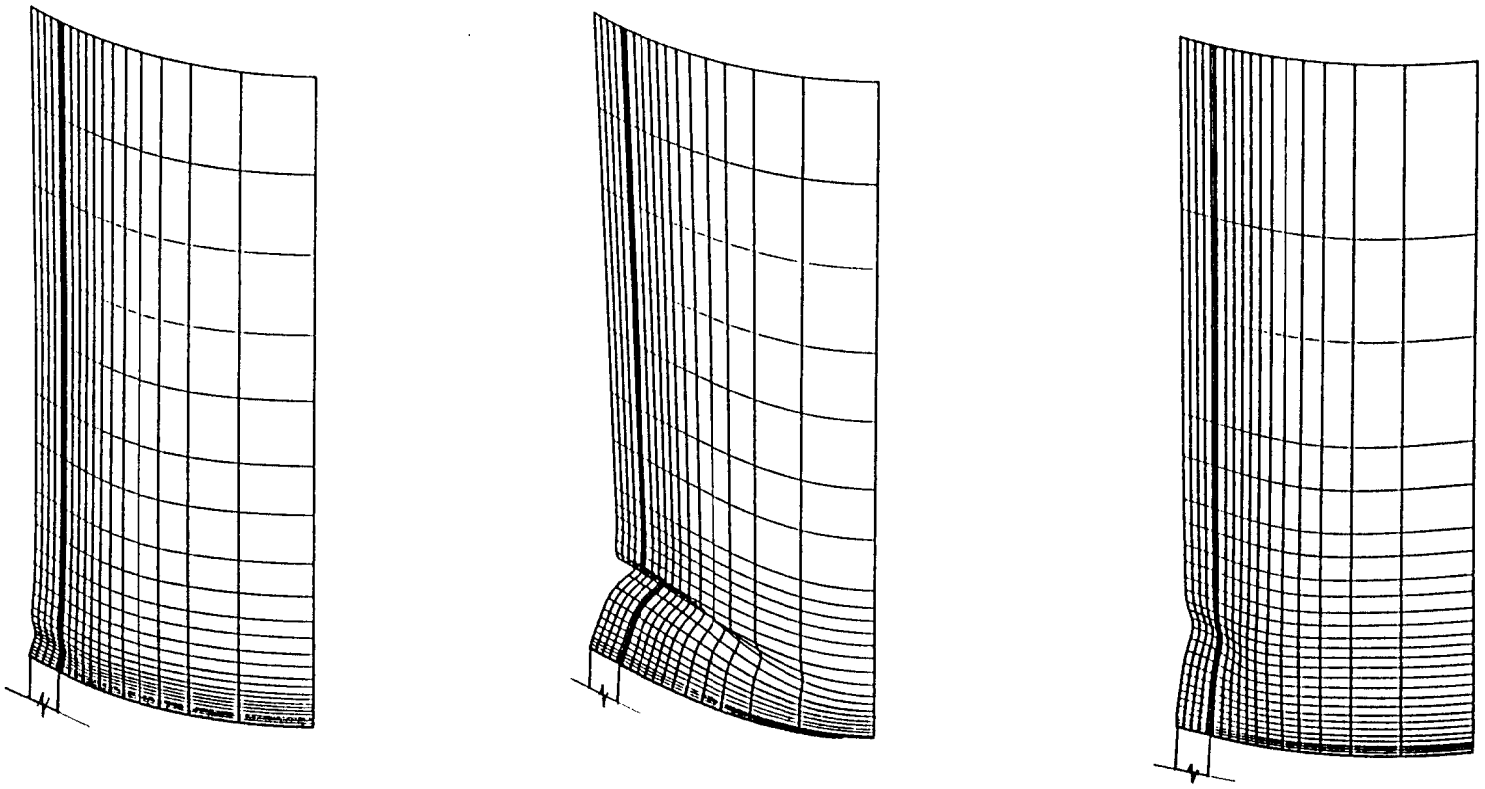

(a) $(Z_0/t)/103=0.25$ (b) $(Z_0/t)/103=1.0$ (c) $(Z_0/t)/103=1.25$

Figure 7-14

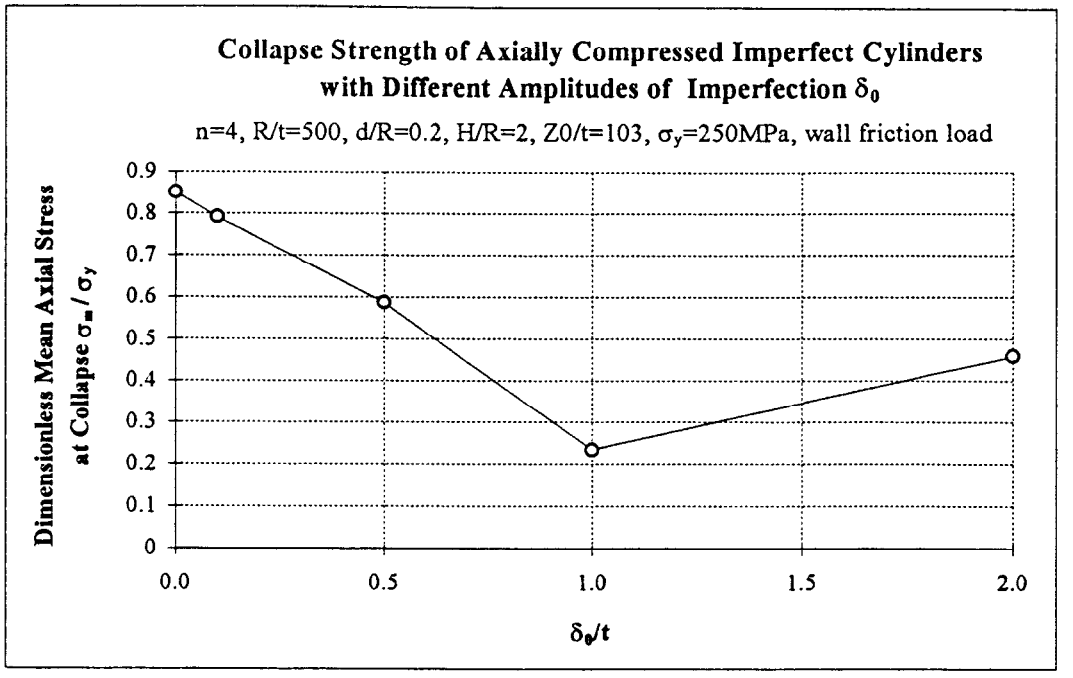

Figure 7-15

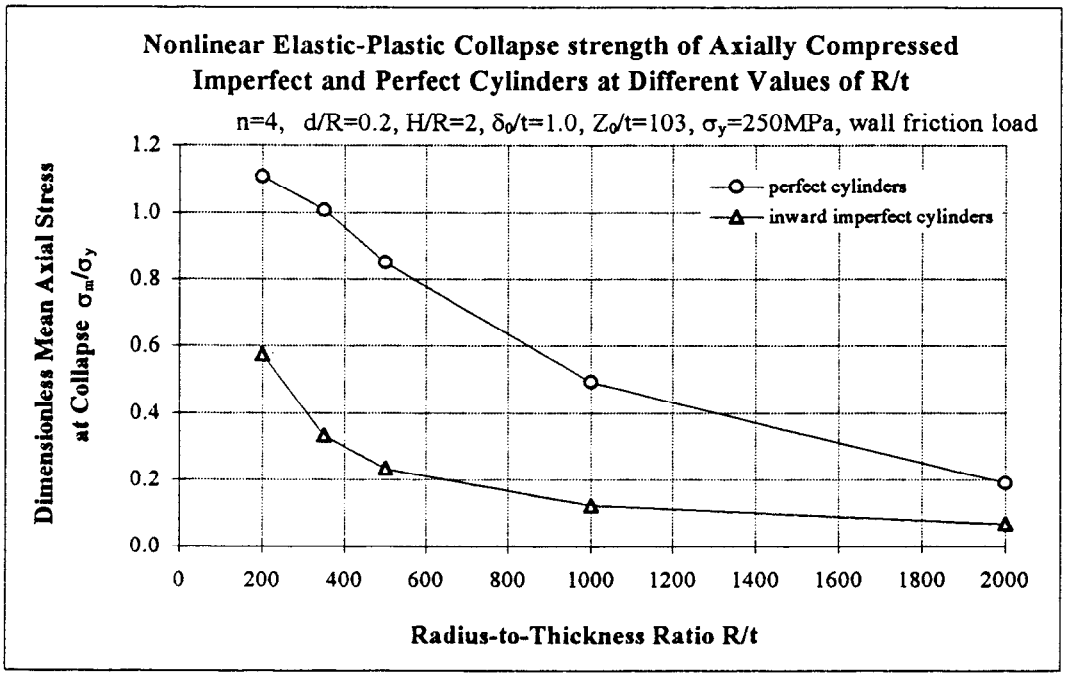

Figure 7-16

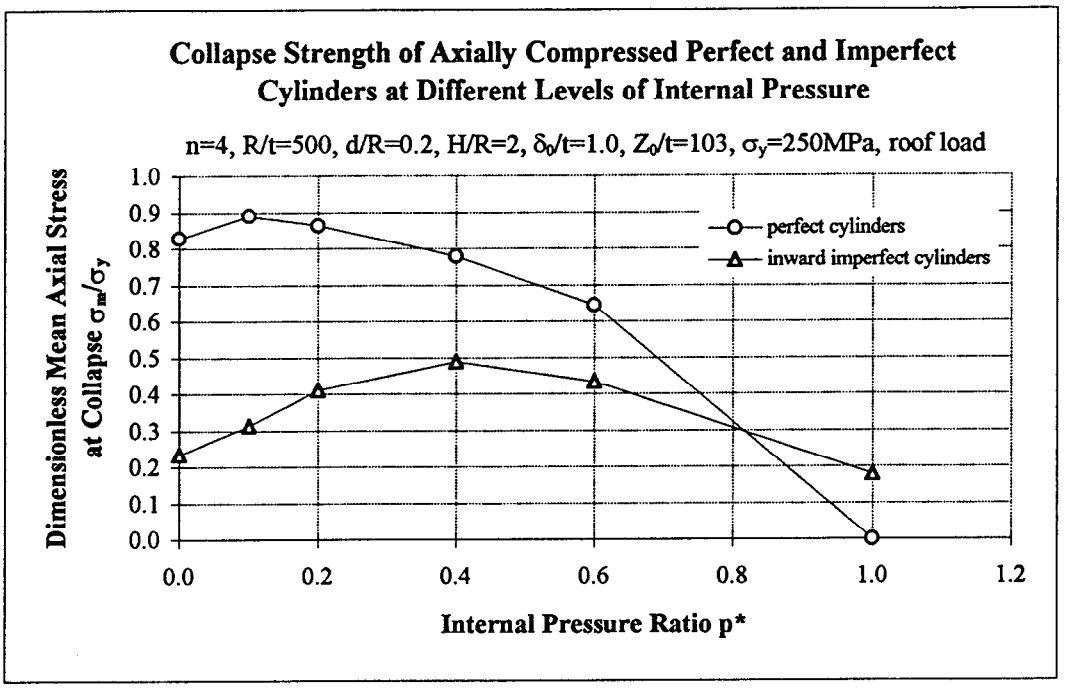
Collapse Strength of Axially Compressed Perfect and Imperfect Cylinders at Different Levels of Internal Pressure
n=4, R/t=500, d/R=0.2, H/R=2, δ0/t=1.0, Z0/t=103, σy=250MPa, roof load
Dimensionless Mean Axial Stress at Collapse σm/σy
1.0
0.9
0.8
0.7
0.6
0.5
0.4
0.3
0.2
0.1
0.0
0.0
0.2
0.4
0.6
0.8
1.0
1.2
Internal Pressure Ratio p*
perfect cylinders
inward imperfect cylinders

Figure 7-17

Perfect cylinder, R/t=500, d/R=0.2, H/R=2.0, n=4, σ_y=250MPa, wall friction load

	Mesh 1	Mesh 2	Mesh 3	Mesh 4	Mesh 5	Mesh 6
Number of Elements	17*23	17*28	17*31	24*31	21*24	34*35
Collapse Strength from Limit Analysis σ_m/σ_y	1.267	1.199	0.932	0.811	1.073	1.053
Collapse Strength from Non-linear Analysis σ_m/σ_y					0.849	0.833

Table 7-1: Mesh Information and Results

Perfect cylinder, R/t=500, d/R=0.2, H/R=2.0, n=4, σ_y=250MPa

Collapse Strength σ_m/σ_y	Roof Load	Wall Friction Load	Hopper Load
Limit Analysis	1.068	1.073	0.710
Non-linear Elastic-Plastic Analysis	0.829	0.849	1.320

Table 7-2

Perfect cylinder, R/t=500, d/R=0.2, H/R=2.0, n=4, wall friction load

Limit Analysis	Yield Stress σ_y (MPa)		
Collapse Strength	100	250	500
σ_m/σ_y	1.086	1.073	1.082

Table 7-3

Perfect cylinder, R/t=500, d/R=0.2, H/R=2.0, n=4, σ_y=250MPa, wall friction load

	Approach 1	Modified Riks Method	
		Case 1	Case 2
Time Period	1.0	1.0	1.0
Min. Load Increment	1.0E-5	0.01	1.0E-5
Max. Load Increment	0.1	0.2	0.1
Collapse Strength σ_m/σ_y	0.854	0.660	0.849

Table 7-4 Study of Alternative Nonlinear Analysis Control Procedure

CHAPTER 8

NONLINEAR ELASTIC BUCKLING ANALYSIS OF A DISCRETELY SUPPORTED SILO

8.1 INTRODUCTION

The failure of a discretely supported silo structure is an interesting problem of nonlinear structural response, and in this sense that discretely supported silos are different from ground supported silos. In a discretely supported thin-walled steel silo, the buckling failure under axial compression usually occurs in the cylinder. The cylinder buckles into a pattern of small, diamond shaped waves above the local supports. The peak axial stress is therefore a useful design parameter. In the preceding buckling analyses of Chapters 5 and 6, a discretely supported silo structure was simplified into a discretely supported cylinder, using the assumption that the buckling strength of this cylinder adequately represents the buckling strength of a complete silo structure. Accordingly, investigations of the linear bifurcation buckling behaviour and the nonlinear elastic buckling behaviour of discretely supported cylinders became the main objectives of those chapters.

Previous studies of the stability of silo structures have never addressed the relationship between buckling strength estimates for both a complete silo and an isolated cylinder. Such a investigation is carried out here to explore the validity of the simplified cylinder model as a substitute for a complete silo. This study will be beneficial to designers and to silo analysts who carry on further studies.

The limited time of this PhD research has meant that only a few analyses on this topic have been performed. In this chapter, the main focus is on a nonlinear elastic buckling analysis of an example complete practical silo on discrete supports, with the aim of providing a basis for further study of the subject. For this purpose, a discretely supported perfect silo has been modelled in the finite element analysis and the elastic buckling behaviour of the silo under axial compression examined.

8.2 FINITE ELEMENT MODELLING

The complete example silo used in the analysis of this chapter is shown in Fig. 8-1. It is a discretely-supported thin-walled silo which consists of a conical roof, a cylinder and a conical hopper. Discrete supports of a certain width were again assumed to terminate at the transition junction between the cylinder and the conical hopper. They were chosen to be equally spaced and to provide rigid supports. As in the previous buckling analyses of discretely supported cylinders, any 1/2n section of the silo (Fig. 8-1) can be modelled instead of the whole silo by taking the geometric and loading symmetries into consideration. The boundary conditions for the two vertical (meridional) edges of the modelled section were determined from symmetry considerations. Both the apices of the conical roof and hopper were assumed to move freely in the axial direction but to be fully restrained against displacements in other directions and all rotations. The axial compression developing in the silo wall was represented in terms of the three axial loading patterns shown in Fig. 8-1.

The finite element program ABAQUS was again used to perform all the numerical calculations of this chapter using the modified Riks method. Both shell element types STRI65 and S9R5 were used. The STRI65 triangular elements were assigned at the apices of the conical roof and hopper to fit the triangular mesh division there whilst the S9R5 elements were placed for all the other quadrilateral element meshes.

To define the geometry of a complete silo, two new geometric parameters were adopted in addition to the previous parameters R/t , d/R, H/R, n. The two parameters were defined in terms of the half angle of the conical roof and hopper, θ_1 and θ_2, respectively (Fig. 8-1).

Only an elastic perfect silo was examined in this study. The geometry of the example silo was specified by the geometric parameters R/t=500, d/R=0.2, H/R=2.0, n=4 (for the cylindrical shell of the silo), and θ_1 =60 deg. and θ_2 = 40 deg. (regarding the conical roof and hopper respectively).

This example silo was assumed to be made of steel with the same Young's modulus $E = 2\times10^5$ MPa and Poisson's ratio $\nu = 0.3$ as before. It is evident that the results obtained may also be applied to other materials by suitable dimensionless interpretation.

In this chapter, the results are presented in the dimensionless manner introduced in Chapter 1. The buckling behaviour, buckling strength and buckling mode of the example silo are described.

8.3 BEHAVIOUR OF AN ELASTIC PERFECT SILO ON DISCRETE SUPPORTS

In this study, the example elastic perfect silo defined in Section 8.2 was analysed. The behaviour of the silo under the three axial loading cases (Fig. 8-1) was investigated.

It was found that for the cases when the silo was subjected to a ring load at the upper edge of the cylindrical shell (roof load) or a uniform frictional load on the surface of the entire cylindrical wall (wall friction load), the ABAQUS program was not able to find a bifurcation point when the silo fails by elastic buckling. For both loading cases, the nonlinear incremental calculation terminated automatically at a certain load proportionality factor when convergence was judged unlikely above that load within the program's default minimum load increment of 10^{-5}. This might indicate a limitation in the ABAQUS program in analysing the particular silo structural model, or a load path which is very difficult to follow in the neighbourhood of this final load level.

A bifurcation point was obtained for the case when the silo is subjected to a ring load at the lower edge of the cylindrical shell (elsewhere termed hopper load). The relation between the axial load and the axial displacement of the point on the upper edge of the cylindrical shell above the support centreline is shown in Fig. 8-2. This load versus displacement curve exhibits a similar form to that of the curve obtained for an axially compressed perfect cylinder, which was shown in Fig. 6-3 of Chapter 6. The vertical displacements are very small until the load rises to the bifurcation point and then large displacements follow as the load decreases. Comparing the critical loads of the complete silo and the cylinder under the same hopper loading condition, it was found that the bifurcation load of the silo is higher than that of the cylinder by 17%. The buckling mode of the silo under the ring load at the lower edge of the cylinder is shown in Fig. 8-3. A single buckle occurs in a local zone in the cylindrical shell of the silo and presents a similar deformed configuration to that of an isolated cylinder at buckling as shown in Fig. 6-5 of Chapter 6.

The buckling strength of the silo under the hopper load, together with the available maximum converged strengths under the roof load and the wall friction load respectively, is listed in Table 8-1. Although the maximum load levels under the roof load and the wall friction cannot be assumed to be the strengths of the silo at buckling, it is certain that the buckling strengths for the silo under the roof load or the wall friction load are equal to or higher than the obtained values. Comparing with the results shown in Table 6-1 of Chapter 6, it can be seen that the buckling strength obtained for a complete silo is about 9 ~ 17% higher than that for a perfect cylinder of the same geometry.

The above analysis demonstrates that the simplification of modelling a silo as an isolated cylinder may give relatively conservative predictions for the buckling strength of a silo structure. The buckling behaviour and buckling mode found when using a discretely supported cylinder to model a discretely supported silo represent realistic models of the behaviour and buckling mode of a complete silo structure. Therefore it can be inferred that the results for the nonlinear elastic buckling analysis of discretely supported perfect cylinders are acceptable and conservative for the design of silo structures.

8.4 CONCLUSIONS

A complete practical silo structure was chosen and investigated. Studies were focused on the nonlinear elastic buckling of a discretely supported perfect silo with the same geometry of the cylindrical shell as that of a cylinder previously analysed in Chapter 6 and under the same axial loading conditions as described before. The buckling behaviour, buckling strength and buckling mode of the studied silo structure were examined.

From the results of this analysis, it is clear that the simplification of modelling a discretely supported silo into a discretely supported cylinder gives a conservative prediction of the practical buckling strength of the silo structure. Also, this simplification of using a discretely supported cylinder to model a complete silo represents the realistic behaviour and mode of a silo structure at buckling. Therefore it can be concluded that in practical design for a discretely supported thin-walled silo structure, using a cylinder to model a complete silo may not only simplify the calculation but also provide acceptable and conservative results for design use.

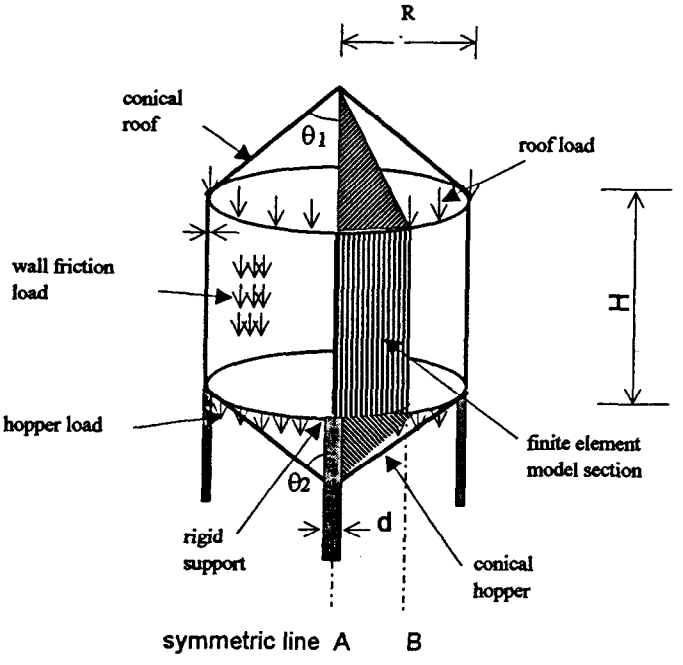

Discretely Supported Silo Model

Figure 8-1

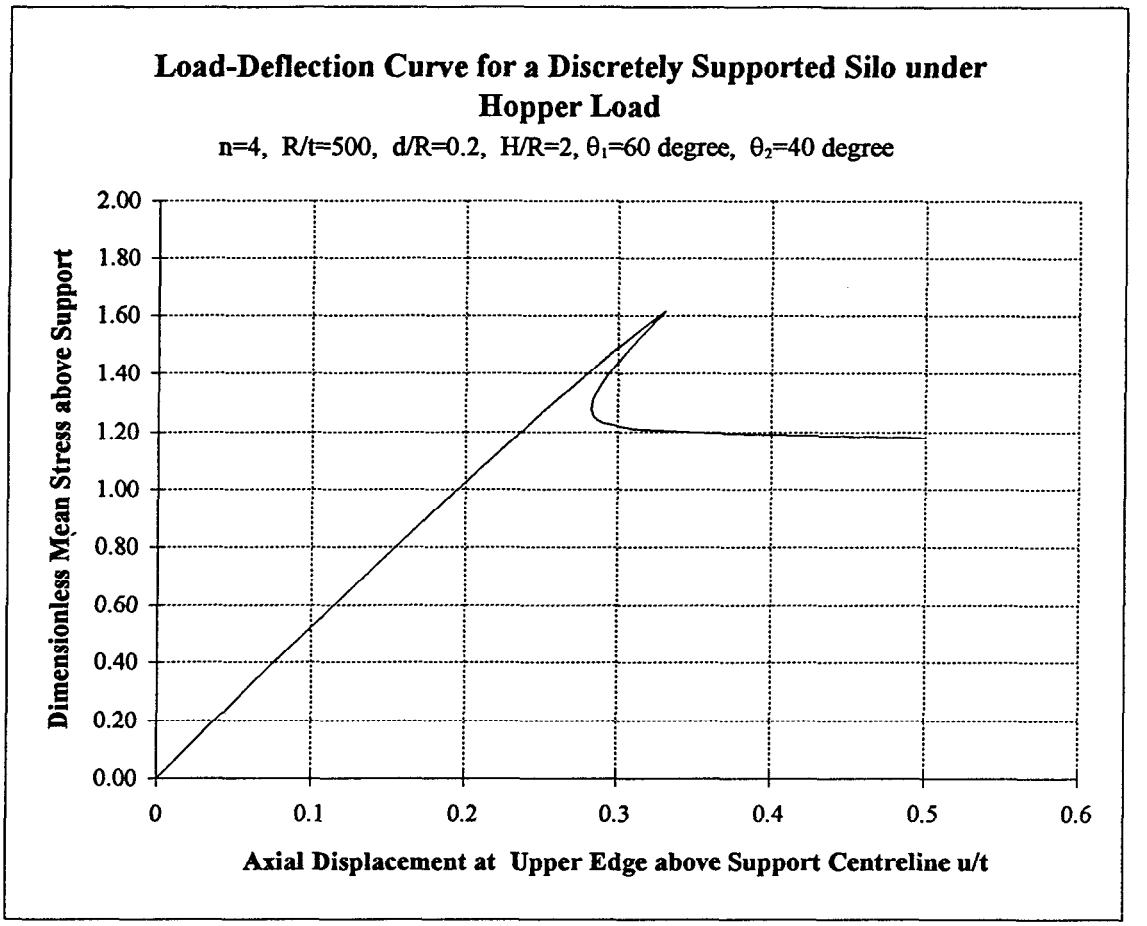
Load-Deflection Curve for a Discretely Supported Silo under Hopper Load
n=4, R/t=500, d/R=0.2, H/R=2, θ1=60 degree, θ2=40 degree
Dimensionless Mean Stress above Support
2.00
1.80
1.60
1.40
1.20
1.00
0.80
0.60
0.40
0.20
0.00
0
0.1
0.2
0.3
0.4
0.5
0.6
Axial Displacement at Upper Edge above Support Centreline u/t

Figure 8-2

Buckling Mode for a Discretely Supported Perfect Silo under Hopper Load
n=4, R/t=500, d/R=0.2, H/R=2.0, θ_1=60 degree, θ_2=40 degree

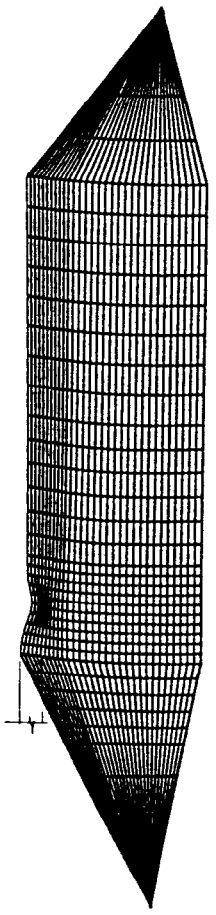

Figure 8-3

Nonlinear Elastic Buckling Analysis of A Discretely Supported Perfect Silo

R/t=500, d/R=0.2, H/R=2.0, n=4, θ_1 = 60 deg., θ_2 = 40 deg.

	Roof Load	Wall Friction Load	Hopper Load
Maximum Strength σ_m / σ_{cl}	1.186	1.240	1.616

Table 8-1

CHAPTER 9

CONCLUSIONS AND RECOMMENDATIONS

9.1 SUMMARY

Many analyses of steel silo structures on discrete supports have been carried out in this thesis. The studies performed in this thesis were concerned with linear elastic shell bending problems in cylindrical shells under local longitudinal loadings and stability (buckling and collapse) problems in isolated cylinders on discrete supports under a variety of geometric and loading conditions.

Before attacking the complex stability problems of elastic buckling and elastic-plastic collapse in locally supported silo structures using the finite element method, an analytical method was used to study elastic cylindrical shells under local loadings, with special attention to patches of longitudinal loading. A linear elastic algebraic solution of the shell bending equations was derived using double Fourier series. A computer program was developed to evaluate the expressions derived using this analytical method and the results were compared with those obtained from finite element analysis.

For the stability analyses, the discretely supported silo structure was first considerably simplified. It was modelled as a thin-walled cylinder directly supported on discrete rigid supports of a finite width at the lower edge. These rigid supports were assumed to fully restrained the vertical displacements at the lower edge of the cylinder. The finite element program ABAQUS was used to perform all the calculations. The geometry of the discretely supported perfect cylinder was characterised by four dimensionless parameters: the radius-to-thickness ratio R/t, the support-width-to-radius ratio d/R, the height-to-radius ratio H/R and the number of supports n. Two other parameters were used to define a local imperfection introduced in the cylinder wall: the ratio (δ_0/t) of the imperfection amplitude δ_0 at the centre of the imperfection to the cylinder thickness t and the ratio (Z_0/t) of the distance Z_0 between the centre of the imperfection and the bottom edge of the cylinder to the cylinder thickness t. The local imperfection was assumed to be axisymmetric and of either an inward or an outward shape, representing a local severe imperfection at a circumferential weld in the shell wall. Three types of axial loading: roof, wall friction and hopper load were assumed to model extreme cases of practical loadings on the silo walls from the stored bulk solids and were analysed in all the stability studies. A uniform internal pressure on the cylinder wall was assumed to represent the normal pressure imposed by the bulk solids stored in the shell and

was applied to the cylinder together with axial compression. The axial compression load applied to the cylinder wall was characterised by the ratio of the mean meridional (axial) stress above the support to the classical elastic critical stress for a cylindrical shell under uniform axial compression, σ_m/σ_{cl}, or to the yield stress, σ_m/σ_y. The strength of the cylinder at buckling or collapse was defined in terms of the maximum value of the dimensionless mean axial stress above support.

A typical perfect cylinder with R/t=500, d/R=0.2, H/R=2.0 and n=4 was most widely analysed as an example structure in the studies. An example imperfect cylinder was defined by introducing an inward axisymmetric imperfection with $\delta_0/t=1.0$ and $Z_0/t=103$ in the wall of the example perfect cylinder. The steel material of which the silos are made was assumed to be linear and isotropic with elastic modulus $E = 2\times10^5$ MPa and Poisson's ratio $\upsilon = 0.3$. The plastic response of the material was assumed to be ideally elastic-plastic, obeying the von Mises yield criterion with a normal flow rule. The yield stress of the material σ_y was mostly chosen as 250 MPa.

Linear elastic stability analyses of discretely supported perfect cylinders under axial compression were first carried out. The linear elastic stress analysis examined the pre-buckling meridional membrane stress distribution above the support centreline for perfect cylinders with various geometries and under different loading conditions. Next, linear bifurcation analyses investigated the linear bifurcation behaviour, mode and strength of these cylinders. Only axial compression forces applied to the cylinder were considered.

Taking large displacements in the cylinder into account, geometrically nonlinear elastic buckling analyses of discretely supported cylinders were performed next. Cylinders were studied which were both geometrically perfect and imperfect, and both unpressurized and pressurized. The effects of the position of the applied axial compression loading and internal pressurization on the nonlinear elastic buckling behaviour, mode and strength of discretely supported perfect and imperfect cylinders were examined.

Further, elastic-plastic stability problems in discretely supported cylinders were analysed. Both small deflection limit analyses of perfect cylinders and geometrically nonlinear elastic-plastic collapse analyses of both perfect and imperfect cylinders were performed. In the limit analysis, the chief effort was exerted on investigating the effects of the axial loading case, the geometric parameter R/t and the yield stress of the material. Nonlinear elastic-plastic collapse analyses were conducted on a wide range of problems, covering the different loading cases, the cylinder slenderness R/t, the level of internal pressurization and the magnitude and position of a detrimental axisymmetric inward imperfection in the wall of the cylinder.

Finally a complete practical silo structure was chosen and investigated. Studies were focused on the nonlinear elastic buckling of a discretely supported perfect silo with the same geometry of the cylindrical shell as that of the previously analysed cylinders in Chapter 6 and under the same axial loading conditions as described before. The buckling behaviour, buckling strength and buckling mode of the studied silo structure were examined.

9.2 CONCLUSIONS

9.2.1 Algebraic Analysis of Elastic Cylindrical Shells under Local Loadings

A linear elastic solution of the shell bending equations was presented for cylindrical shells under local loadings, with special attention to local longitudinal distributed patch loads. Algebraic expressions for the displacements and stresses induced by a patch of longitudinal load on a simply supported cylindrical shell were derived using double Fourier series. A satisfactory match has been found from the comparative studies between the predictions of stresses and displacements using these obtained expressions and the finite element results using the finite element program LEASH for a sample problem.

The method discussed in this chapter is of a general nature and therefore can be applied to many cases when cylindrical shells are subjected to local loadings in any direction and with different boundary conditions.

9.2.2 Linear Elastic Stress and Bifurcation Analyses of Discretely Supported Perfect Cylinders

Linear elastic pre-buckling stress analyses were used to explore the meridional membrane stress distribution in the cylinder. It was found that the distribution is very sensitive to the position of the applied loading, especially in the vicinity of the supports where the highest stresses arise. In general, a load applied at the top boundary induces the highest stress profile in the cylinder whilst one at the bottom boundary induces the lowest. The pattern of the stress dispersal above the support centreline does not change very much for cylinders with typical geometric parameters such as R/t varying from 200 to 1000, H/R larger than 1.0 and d/R larger than 0.1, except for very short cylinders on rather narrow supports.

Because of the influence of the position of the axial loading on the stress distribution in the cylinder, changes in the linear bifurcation load also occur. The magnitude of the buckling load varies with the magnitude of the maximum stress induced by a given loading pattern. A higher pre-buckling local stress generally leads to a smaller buckling load. It was found that the local high stress above the support is crucial to the formation of the buckle and strongly influences

the buckling strength of the cylinder. For the example perfect cylinder with R/t=500, d/R=0.2, H/R=2.0 and n=4, a ring load applied at the roof leads to a lower bifurcation load than wall friction loading or hopper loading by 1.6% and 25% respectively.

As the geometric parameters of the cylinder vary within practical bounds (such as R/t between 200 and 1000; d/R between 0.05 and 0.3; H/R less than 2.0), the bifurcation buckling load changes considerably. For example, the difference between the buckling strengths of cylinders subject to hopper loading may reach a factor of 7.5 between thick tall cylinders on narrow supports and thin squat cylinders on wide supports, even when expressed in the dimensionless terms used in this thesis, which substantially account for thickness effects.

The linear bifurcation analyses of discretely supported perfect cylinders have the deficiency inherent in small deflection theories that they ignore the effects of the pre-buckling deflections and geometric imperfections, so that these analyses cannot be used to accurately assess the buckling strength of a cylinder. In order to probe the elastic stability of cylinders, nonlinear analysis based upon large deflection theory is needed.

9.2.3 Nonlinear Elastic Buckling Analysis of Perfect and Imperfect Cylinders on Discrete Supports

Based upon large displacement theory, geometrically nonlinear elastic buckling analyses of cylinders under axial compression discovered that the position of the applied axial load has only a small effect on the buckling *behaviour* and buckling *mode* of a locally supported cylinder on discrete supports. However, the changes in buckling *strength* with load position are significant. The roof loading case leads to the lowest strengths. The difference between this and wall friction loading is generally around 2% and between roof loading and hopper loading is generally around 22% for perfect cylinders. This trend in the buckling loads is the same as that found in the preceding linear bifurcation analyses of perfect cylinders.

The sensitivity of the buckling strength to the position of the applied load may or may not be as strong for an imperfect cylinder as that for a perfect cylinder, depending on the pattern of the imperfection form. For an outward imperfection, the increase in buckling strength over the value for roof loading is about 3% for wall friction loading and 44% for hopper loading. For an inward imperfection, the corresponding increases are about 3% and 55%. Thus, hopper loading always produces very high strengths compared with other load cases, which are very similar.

The geometric imperfection, whether inward or outward, results in a major reduction in the buckling strength. The imperfection form affects both the buckling strength and the buckling

behaviour. With an imperfection amplitude of one wall thickness ($\delta_0/t = 1$) placed at the critical height Z_0 for inward imperfections with wall friction loading, strength reductions relative to the value for a perfect cylinder of about 40% were found for the inward imperfection form and about 34% for the outward imperfection.

Previous investigations of uniformly compressed and uniformly supported cylinders showed that internal pressure reduces the imperfection-sensitivity and increases the buckling strength significantly. In this first-ever study of the effects of internal pressure in discretely supported cylinders, the same effect was found, and was shown to vary according to the form of the imperfection. However, by contrast with the findings for uniformly axially compressed cylinders, the buckling strength of a *perfect* locally supported cylinder was also found to be considerably increased by internal pressure.

For a perfect cylinder, the buckling behaviour and mode do not change significantly from the unpressurized case until the internal pressurization reaches a high level. For an imperfect cylinder with inward imperfections, the buckling behaviour is similar as the internal pressure increases. However, for a cylinder with an outward local imperfection, the internal pressure seriously alters its behaviour and buckling mode from the case of axial compression alone. The buckling modes are very local in the zone immediately above the support. Only a single buckle was found for the chosen cylinder geometry and relatively narrow supports used in the study.

Although internal pressure can significantly enhance the buckling strength, the governing failure mode of a cylindrical silo is generally buckling under axial compression. From this study it is still difficult to produce a general proposal for estimating the strength gains due to internal pressurization. This is because high internal pressures give rise to severe local bending near the base of the cylinder and local yielding may then precipitate a buckling failure. Therefore, the study of this thesis was naturally extended to cover the elastic-plastic behaviour of discretely supported cylinders.

9.2.4 Elastic-Plastic Stability Analysis of Discretely Supported Cylinders

For almost all the geometries, loadings and material strengths studied, the behaviour of the cylinders in the elastic-plastic region was found to be generally similar, from both the small displacement limit analysis and the geometrically nonlinear elastic-plastic collapse analysis. First yield occurs at the edge of the support on the lower edge of the cylinder. After first yield, the yielded zone grows progressively above the support with increasing displacements until a maximum load condition is attained when the cylinder collapses. After this collapse condition,

found using the geometrically nonlinear analysis, the cylinder enters the post-collapse phase, when the displacements increase quickly.

The position of the applied axial load was found to alter the dimensionless mean stress above the column at plastic collapse significantly. The same trend in the collapse strengths as that of the buckling strength was obtained from nonlinear elastic-plastic analysis. Varying the position of the axial loading from the upper edge to the lower edge of the cylinder may induce an increase in strength by as much as 59%. The limit analysis and the nonlinear analysis give completely different results for the effect of the variation of the thickness of the cylinder. In the limit analysis, the dimensionless collapse strength (σ_m/σ_y) alters only slightly as the radius-to-thickness ratio R/t varies, whilst a big change in the collapse strength is obtained from the nonlinear analysis. In particular, large displacement effects become very important as the cylinder gets thinner. The normalised limit load strength above the local support may be considered to be independent of the yield stress of the material if the normalisation is performed relative to the yield stress. Higher internal pressures may cause a significant decline in the collapse strength of the shell under axial compression.

An inward imperfection near the bottom edge of the cylinder was found to have a significant weakening effect on the nonlinear collapse strength. This significant imperfection-sensitivity should receive particular attention in practical design, since about 73% strength reduction was found for a typical inward imperfection with the amplitude of $\delta_0/t = 1.0$ and localised at the critical height of $Z_0/t = 103$. However, no further reduction in the collapse strength occurs once the imperfection amplitude exceeds a certain level. Higher internal pressures may cause the collapse strength of an imperfect cylinder with a local inward axisymmetric imperfection to be slightly higher than that of an axially compressed pressurised perfect cylinder.

9.2.5 Nonlinear Elastic Buckling Analysis of a Discretely Supported Silo

This analysis has demonstrated that the simplification of modelling a discretely supported silo into a discretely supported cylinder gives a conservative prediction of the practical buckling strength of a silo structure. Also, this simplification of using a discretely supported cylinder to model a complete silo provides a satisfactory model of the behaviour and mode of a complete silo structure at buckling.

Therefore it can be concluded that in practical design for a discretely supported thin-walled silo structure, using a cylinder to model a complete silo may not only simplify the calculation but also provide acceptable and **conservative** results for design use.

9.3 RECOMMENDATIONS FOR FUTURE WORK

In this thesis, studies have been carried out on thin cylindrical shells under local loadings, with special reference to locally supported steel silo structures. Knowledge of the behaviour of practical silo structures has been extended through the theoretical analyses of this thesis. The conclusions drawn from this research may provide design guidance for practical silo design and construction. However, because of the time limitation of carrying out this PhD research, some parts of the work have not be conducted very comprehensively. To investigate the structural behaviour of realistic silo structures sufficiently for comprehensive design guidance to be developed, more extensive and probing work is needed. This section presents some recommendations for future work.

9.3.1 Algebraic Analysis of Elastic Cylindrical Shell under Local Loadings

In Chapter 4, a method of finding the loads and displacements, caused in cylindrical shells by local loadings, was described using double Fourier series. With this method, expressions were derived for the deflections, bending moments and membrane forces induced in a simply supported circular cylindrical shell subjected to local longitudinal distributed loadings. It is evident that these expressions are of special nature, only suitable for the shell with the assumed simply supported boundary condition and under a patch of load in the longitudinal direction. However, this method is general. Therefore, using this method and solving the general equilibrium equations for cylindrical shells under local loadings in three directions, defined by Equation (4.4) of Chapter 4, a general solution could be derived, and applied to cylindrical shells under local loadings in any direction and with different boundary conditions.

In addition, more computer calculations should be performed to predict the stresses and deflections in the shell caused by local loadings.

9.3.2 Nonlinear Stability Analysis of Locally Supported Silos

Analyses using large deflection theory lead to more accurate predictions of the buckling and collapse strengths of practical locally supported silos. In all the stability studies performed in this thesis, some assumptions concerning loading, material, support boundary conditions and the assumed geometric imperfections have been used to simplify the complex silo structures which exist in practice. In reality, failures and damage which occur to an elevated silo structure may be caused by more complex factors than those considered in this thesis. Therefore, the research in this thesis is basic and should be extended.

In this thesis, only rigid supports have been examined. However, in reality, a local support is neither completely rigid nor completely flexible, but lies between the two. In the case of

modelling the local supports as rigid, an upper bound on the strengths of practical locally supported silo structures has been derived. Assuming the discrete supports to be completely flexible is another limiting case which predicts the lower bound of the actual strength of silo structures. Therefore, it deserves further study, even though practical supports appear to be close to the rigid condition.

It is widely recognised that axial compression and internal pressure on the cylindrical wall of a silo during filling or flow are not as uniform as has been assumed in this thesis. As described in Chapters 1 and 2, they are actually rather complex and of a dynamic nature. Except for the loads from the bulk solids stored in the shell, other external loads, such as earthquake and wind loads may be applied to the structure. So far all the studies have been focused on simplified static loading conditions. Therefore more complex loading conditions should be taken into account in future studies of silo structures.

A locally supported silo in service is usually stiffened by the transition ring at the cylinder/hopper and the cylinder/roof transition junction or by the local supports engaging into the cylindrical shell for a short distance or extending to the eaves. Moreover, non-axisymmetric geometric imperfections and non-axisymmetric boundary conditions often arise in practical silo structures. These different structural forms may present different structural behaviours from those discovered in this thesis for the silo cylinders directly supported on discrete supports. Thus, analysis models should be generated to reflect these realistic structural forms and characters of silos. The nonlinear buckling and collapse analyses of practical silo structures using these advanced models will lead to more accurate and reliable results and findings for practical design use.

REFERENCES

ABAQUS Theory Manual, Users Manual, Version 4.8 (1989), Version 5.2 (1992), Hibbitt, Karlsson & Sorensen, Inc.

ACI 313-77 (1977) Recommended Practice for Design and Construction of Concrete Bins, Silos and Bunkers for Storing Granular Materials, with commentary, American Concrete Institute, Detroit, (Revised 1983).

API 620 (1978) Recommended Rules for the Design and Construction of Large Welded, Low-pressure Storage Tanks, American Petroleum Institute, 6th Edn, Washington, D.C..

Arbocz, J. (1974), "The Effect of Initial Imperfection on Shell Stability", in Thin Shell Structures, edited by Y.C. Fung and E.E. Sechler, Prentice Hall, pp 205-246.

Arbocz, J. (1983a), "The Imperfection Data Bank: A Means to Obtain Realistic Buckling Loads", in Buckling of Shells, edited by E. Ramm, Springer Verlag, Berlin 1982, pp 535-567.

Arbocz, J. and Babcock, C.D. (1969), "The effect of General Imperfection on the Buckling of Cylindrical Shells", Journal of Applied Mechanics, Vol. 36, pp 28-38.

Arbocz, J. and Sechler, E.E. (1974), "On the Buckling of Axially Compressed Imperfect Cylindrical Shells", Journal of Applied Mechanics, ASME, Vol. 41, No. 3, pp 737-743.

Arbocz, J. (1991), "Towards an Improved Design Procedure for Buckling Critical Structures", Buckling of Shell Structures, on Land, In the Sea and In the Air, Edited by J.F. Jullien, Elsevier Applied Science, 1991.

AWWA D100-79 (1979), Standard for Welded Steel Tanks for Water Storage, American Water Works Association, Denver, Colorado.

Baker, E.H., Kovalevsky, L. and Rish, F.L. (1972), Structural Analysis of Shells, McGraw-Hill.

Bavilacqua, L., Feijoo, R. and Valid, R. (1985), Inelastic Behaviour of Plates and Shells, IUTAM Symposium, Rio de Janeiro, Brazil, August 5-9, 1985, Springer-Verlag, Berlin Heidelberg New York London Paris Tokyo.

Bijlaard, P.P. (1954), "Stresses from Radial Loads in Cylindrical Pressure Vessels", Welding Journal (Supplement), Vol. 33, December 1954, pp 615-s - 623-s.

Bijlaard, P.P. (1955), "Stresses from Local Loadings in Cylindrical Pressure Vessels", Transactions of ASME, Vol. 77, August 1955, pp 805-816.

Bijlaard, P.P. (1955), "Stresses from Radial Loads and External Moments in Cylindrical Pressure Vessels", Welding Journal, Vol. 34, December 1955, pp 608-s - 617-s.

Blacker, M.J. (1988), "Buckling of Steel Silos under Wind Action", Proc. Int. Conf. 'Silos-Forschung und Praxis', Universitat Karlsruhe, October, pp 319-332.

Bornscheuer, F.W. and Häfner, L. (1983), "The Influence of an Imperfect Circumferential Weld on the Buckling Strength of Axially Loaded Circular Cylindrical Shells", 3rd International Colloquium on Stability of Metal Structures, Preliminary Report, Paris, November, 1983.

Briassoulis, D. and Curtis, J. (1985), "Design and Analysis of Silos for Friction Forces", Journal of Structural Engineering, Vol. 111, No. 6, June, 1985, pp 1377-1398.

Brush, D.O. and Almroth, B.O. (1975), Buckling of Bars, Plates and Shells, McGraw-Hill, New York.

Budiansky, B. (1976), Buckling of Structures, International Union of Theoretical and Applied Mechanics, Symposium Cambridge/USA 1974, Springer-Verlag Berlin Heidelberg N.Y..

Budiansky, B. and Radkowski, P.P. (1963), "Numerical Analysis of Unsymmetrical Bending of Shells of Revolution", AIAA Journal, Vol. 1, No.8, pp 1833-1842.

Budiansky, B. and Sanders, J.L. (1963), "On the Bset First-Order Linear Shell Theory", Progress in Applied Mechanics, The Prager Anniversary Volumn, Macmillan, pp 129-140.

Calladine, C.R. (1983), Theory of Shell Structures, Cambridge University Press.

Calladine, C.R. (1985), Plasticity for Engineers, Ellis Horwood, Chichester.

Clarke, M.J. and Rotter, J.M. (1988), "A Technique for the Measurement of Imperfections in Prototype Silos and Tanks", Research Report R565, School of Civil and Mining Engineering, University of Sydney, Australia.

Delpak, R. (1980), "Static Analysis of Thin Rotational Shells", Computers and Structures, Vol. 10, No. 4, pp 305-325.

DIN 1055 (1964) Design Loads for Buildings: Loads on Silos: B1.6, German Standards Institute, Berlin.

DIN 1055 (1986) Design Loads for Buildings: Loads on Silo Bins - Part 6, German Standards Institute, Berlin.

Donnell, L.H. (1933), "Stability of Thin-Walled Tubes under Torsion", NACA Technical Report, No. 479, pp 95-116.

Donnell, L.H. (1933), "A New Theory for the Buckling of Thin Cylinders under Axial Compression and Bending", ASME Transactions, Vol. 56, pp 795-806.

Drucker, D.C. and Shield, R.T. (1959), "Limit Analysis of Symmetrically Loaded Thin Shells of Revolution", Journal of Applied Mechanics, Vol. 26, March.

Dubas, P. and Gehri, E. (1986), Behaviour and Design of Steel Plated Structures, ECCS-CECM-EKS, Applied Statics and Steel Structures, Swiss Federal Institute of Technology Zurich, CH-8093 Zurich/Switzerland.

Flügge, W. (1973), Stress in Shells, 2nd edn, Springer-Verlag Berlin Heidelberg NewYork 1973.

Gaylord, E.H. and Gaylord, C.N. (1984), Design of Steel Bins for Storage of Bulk Solids, Prentice-Hall 1984.

Gould, P.L., Sen, S.K. (1974), "Column Moments in Eccentrically Supported Tanks", Journal of the Structural Division, Proc. of ASCE, Vol. 100(3), No. ST10, October, pp 2165-2169.

Gould, P.L., Sen, S.K., Wang, R.S.C., and Lowrey, D. (1976), "Column Supported Cylindrical-Conical Tanks", Journal of the Structural Division, ASCE, No. ST2, February, pp 429-447.

Greiner, R. (1991), "Elastic Plastic Buckling at Cone Cylinder Junctions of Silos", Buckling of Shell Structures, on Land, In the Sea and In the Air, Edited by J.F. Jullien, Elsevier Applied Science, 1991.

Guggenberger, W. (1991), "Buckling of Cylindrical Shells under Local Axial Loads", Buckling of Shell Structures, on Land, In the Sea and In the Air, Edited by J.F. Jullien, Elsevier Applied Science, 1991.

Guggenberger, W. (1991), Nichtlineares Beulverhalten von Kreiszylinderschalen unter Lokaler Axialbelastung, PhD Thesis, der Technischen Universität Graz.

Hill, R. (1950), Mathematical Theory of Plasticity, Oxford University Press.

Hodge, P.G. Jr. (1956), "Displacements in an Elastic-Plastic Cylindrical Shell", Journal of Applied Mechanics, Vol. 23, 1956.

Hodge, P.G. Jr. (1960), "Yield Conditions for Rotationally Symmetric Shells under Axisymmetric Loading", Journal of Applied Mechanics, Vol. 27, June.

Hodge, P.G. Jr. (1963), Limit Analysis of Rotationally Symmetric Plates and Shells, PRENTICE-HALL, INC., Englewood Cliffs, New Jersey.

Hodge, P.G. Jr. (1964), "Plastic Design of a Closed Cylindrical Structure", Journal of Mechanics and Physics of Solids, Vol. 12, pp 1-10.

Hodge, P.G. Jr. and Brooklyn, N.Y. (1954), "Rigid-Plastic Analysis of Symmetrically Loaded Cylindrical Shells", Journal of Applied Mechanics, Vol. 21, December.

Hodge, P.G. Jr. and Joseph Panarelli (1962), "Interaction Curves for Circular Cylindrical Shells According to the Mises or Tresca Yield Criterion", Journal of Applied Mechanics, Vol. 29, No. 2, June.

Hodge, P.G. Jr. and Nardo, S.V. (1958), "Carrying Capacity of an Elastic-Plastic Cylindrical Shell with Linear Strsin-hardening", Journal of Applied Mechanics, Vol. 25: Trans. ASME, Vol. 80, 1958.

Hoff, N.J. (1954), "Boundary-Value Problems of the Thin-Walled Circular Cylinder", Journal of Applied Mechanics, Trans. ASME, Vol. 76, 1954, pp. 343-350.

Hoff, N.J. and Rehfield, W. (1965), "Buckling of Axially Compressed Cylindrical Shells at Stresses Smaller Than the Classical Critical Value", Journal of Applied Mechanics, ASME, Vol. 32, pp 542-546.

Hoff, N.J. and Soong, T.C. (1965), "Buckling of Circular Cylindrical Shells in Axial Compression", International Journal of Mechanical Sciences, Vol. 7, pp 489-520.

Hoff, N.J. and Soong, T.C. (1967), "Buckling of Axially Compressed Cylindrical Shells with Non-Uniform Boundary Conditions", Proceedings, Symposium on Thin Walled Steel Structures, University College, Swansea, pp 61-80.

Hutchinson, J.W. (1965), "Axial Buckling of Pressurized Imperfect Cylindrical Shells", AIAA Journal, Vol. 3, pp 1461-1466.

Hutchinson, J.W. (1967), "Imperfection-Sensitivity of Externally Pressurized Spherical Shells", Journal of Applied Mechanics, ASME, Vol. 34, pp 49-55.

Hutchinson, J.W. (1974), "Plastic Buckling", Advances in Applied Mechanics, ed. C.S. Yih, Vol. 14, Academic Press, Ontario, pp 85-197.

Hutchinson, J.W. and Koiter, W.T. (1970), "Postbuckling Theory", Applied Mechanics Reviews, Vol. 23, pp 1353-1366.

Hutchinson, J.W. and Tennyson, R.C. and Muggeridge, D.B. (1971), "Effect of a Local Imperfection on the Buckling Behaviour of a Circular Cylindrical Shell under Axial Compression", AIAA Journal, Vol. 9, No. 1, pp 48-53.

Ignatenko, V.M. (1978), "Failure of Structural Steel Bins and Critical Design Considerations", Proceedings, Metal Structures Conference, Institute of Engineers, Australia, Perth.

Irons, B.M. (1976), "The Semi-Loof Shell Element", in Finite Elements for Thin Shells and Curved Members, eds. Ashwell and Gallagher, Wiley.

Irons, B.M. and Zienkiewicz, O.C. (1970), "Analysis of Thick and Thin Shell Structures by Curved Finite Elements", Int. Jnl for Numerical Methods in Engineering, Vol. 2, pp 419-451.

Jaky, J. (1948), "Pressure in Silos", Proceedings, 2nd International Conference on Soil Mechanics and Foundation Engineering, Rotterdam, June, Vol. 1, pp 103-107.

Janssen, H.A. (1895), "Versuche uber Getreidedruck in Silozellen", Zeitschrift des vareines Deutscher Ingenieure, Vol. 29, No. 35, pp 1045-1049.

Javaherian, H. and Dowling, P.J. (1985), "Large Deflection Elastic-Plastic Analysis of Thin Shells", Engineer Structures, Vol. 7, pp 154-162.

Jenkyn, R.T. and Goodwill, D.J. (1987), "Silo Failures: Lessons to be Learned", Engineering Digest, September, 1987, pp 19-22.

Jones, R.E. and Strome, D.R. (1966), "Direct Stiffness Method of Analysis of Shells of Revolution Utilizing Curved Elements", AIAA Journal, Vol. 4, No. 9, pp 1519-1525.

Jumikis, P.T. (1987), Stability Problems in Silo Structures, PhD Thesis, School of Civil and Mining Engineering, University of Sydney, N.S.W., Australia.

Kempner, J. (1955), "Remarks on Donnell's Equations", Journal of Applied Mechanics, ASME, march, 1955, pp 117-118.

Kildegaard, A. (1967), "Bending of a Cylindrical Shell Subject to Axial Loading", 2nd Symposium on Theory of Thin Shells, IUTAM, Copenhagen, September 1967, pp 301-315, Springer 1969.

Koiter, W.T. (1963), "The Effect of Axisymmetric Imperfection on the Buckling of Cylindrical Shells under Axial Compression", Proceedings, Kon. Ned. Akad. Wet., Proceedings Ser. B66, pp 265-279. (See also Applied Mechanics Reviews, Vol. 18, Review 3387, 1965).

Koiter, W.T. and Mikhailov, G.K. (eds) (1980) Theory of Shells, Proceedings, 3rd IUTAM Symposium on Shell Theory, 1978, North-Holland, Amsterdam.

Libai, A. and Durban, D. (1973), "A Method for Approximate Stability Analysis and its Application to Circular Cylindrical Shells under Circumferentially Varying Edge Loads", Journal of Applied Mechanics, December, pp 971-976.

Libai, A. and Durban, D. (1973), "Buckling of Cylindrical Shells Subjected to Nonuniform Axial Loads", Journal of Applied Mechanics, ASME, Vol. 44, December, pp 714-720.

Lukasiewicz, S. (1979), Local Loads in Plates and Shells, Sijthoff & Noordhoff, PWN-Polish Scientific Publishers, Warszawa.

Maeda, Y. and Ishizaki, S. (1979), "Analysis of Cylindrical Shells for Design of Steel Silos", Journal of Civil Engineering Design, Vol. 1, No. 4, pp 325-354.

Marcal, P.V. (1970), "Large Deflection Analysis of Elastic-Plastic Shells od Revolution", AIAA Journal, Vol. 8, No. 9, pp 1627-1633.

Meck, H.R. (1961), "Bending of a Thin Cylindrical Shell Subjected to a Line Load around a Circumference", Journal of Applied Mechanics, September, 1961, pp 427-433.

Navaratna, D.R., Pian, T.H.H. and Witmer, E.A. (1968), "Stability Analysis of Shells of Revolution by the Finite Element Method", AIAA Journal, Vol. 6, No. 2, pp 355-361.

Onat, E.T. (1955), "Plastic Collapse of Cylindrical Shells under Axially Symmetric Loading", Quarterly of Applied Mathematics, Vol. 13, pp 63-72.

Ooi, J.Y. and Rotter, J.M. (1986), "Wall Pressures in Squat Styeel Silos from Simple Finite Element Analysis", Research Report R538, School of Civil and Mining Engineering, University of Sydney, Australia.

Ooi, J.Y. and Rotter, J.M. (1987), "Elastic Predictions of Pressure in Conical Silo Hoppers" Research Report 555, School of Civil and Mining Engineering, University of Sydney, Australia.

Ory, H. and Reimerdes, H.G. (1987), "Stresses in and Stability of Thin Walled Shells under Non-Ideal Load Distribution", Proc. Int. Colloquium on the Stability of Plate and Shell Structures, Gent, Belgium, April, ECCS, pp 555-561.

Paul, B, and Hodge, P.G. Jr, (1958), "Carrying Capacity of Elastic-Plastic Shells under Hydrostatic Pressure", Proc. 3rd U.S. Cong. Appl. Mech., pp 631-640, 1958.

Pederson, P.T. (1974), "On the Collapse Load of Cylindrical Shells", in Buckling of Structures, edited by B. Budiansky, Springer, New York.

Ramm, E. and Buechter, N. (1991) "Buckling of Cylindrical and Conical Shells under Concentrated Loading", International Colloquium on Buckling of Shell Structures on Land, in the Sea and in the Air, Villeurbanne, Lyon, France, 17-19 Sept 1991, pp 313-322.

Rekach, V.G. (1978), Static Theory of Thin-Walled Space Structures, Translated from the Russian by A. Petrosyan, Mir Publishers · Moscow.

Resinger, F. and Greiner, R. (1982), Buckling of Wind-Loaded Cylindrical Shells: Application to Unstiffened and Ring-Stiffened Tanks, in Buckling of Shells, ed. E. Ramm, Springer-Verlag, Berlin, pp 305-332.

Riks, E. (1979), "An Incremental Approach to the Solution of Snapping and Buckling Problems", International Journal of Solids and Structures, Vol. 15, pp 529-551.

Rotter, J.M. (1981), "Axisymmetric Shells under General Loading", in Structural Aspects of Steel Silos and Tanks, School of Civil and Mining Engineering, University of Sydney, Australia, August, pp 6.1-6.39.

Rotter, J.M. (1982), "Analysis of Ringbeams in Column-Supported Bins", Proc., 8th Australian Conference on the Mechanics of Structures and Materials, University of Newcastle, Aug., pp 33.1-33.6.

Rotter, J.M. (1983a), "Structural Effects of Eccentric Loading in Shallow Steel Bins", Proc., 2nd Int. Conf. Design of Silos for Strength and Flow, pp 446-463.

Rotter, J.M. (1983b), "The Effect of Increasing Moisture Content on the Stresses in Silo Walls", Investigation Report S444, School of Civil and Mining Engineering, University of Sydney, Australia.

Rotter, J.M. (1983c), "Stress Amplification in Unstiffened Steel Silos and Tanks", Research Report R347, School of Civil and Mining Engineering, University of Sydney, Australia.

Rotter, J.M. (1985a), "Membrane Theory of Shells for Bins and Silos", Design of Steel Bins for the Storage of Bulk Solids, School of Civil and Mining Engineering, University of Sydney, pp 58-70.

Rotter, J.M.(1985b), "Bending Theory of Shells for Bins and Silos", Design of Steel Bins for the Storage of Bulk Solids, School of Civil and Mining Engineering, University of Sydney, pp 71-81.

Rotter, J.M.(1985c), "Buckling under Axial Compression", Design of Steel Bins for the Storage of Bulk Solids, School of Civil and Mining Engineering, University of Sydney, pp 122-137.

Rotter, J.M.(1985d), "Analysis and Design of Ringbeams", Design of Steel Bins for the Storage of Bulk Solids, School of Civil and Mining Engineering, University of Sydney, pp 164-183.

Rotter, J.M. (ed.) (1985e), Design of Steel Bins for the Storage of Bulk Solids, School of Civil and Mining Engineering, University of Sydney, Australia.

Rotter, J.M. (1986a), "The Analysis of Steel Bins Subject to Eccentric Discharge", Proceedings, Second International Conference on Bulk Materials Storage, Handing and Transportation, Institution of Engineers, Australia, Wollongong, July, pp 264-271.

Rotter, J.M. (1986b), "On the Significance of Switch Pressures at the Transition in Elevated Steel Bins", Proceedings, Second International Conference on Bulk Materials Storage, Handing and Transportation, Institution of Engineers Australia, Wollongong, July, pp 82-88.

Rotter, J.M. (1987), "The Buckling and Plastic Collapse of Ring Stiffeners at Cone/Cylinder Junctions", Proceedings, International Colloquim on Stability of Plate and Shell Structures, Gent, Belgium, April, pp 449-456.

Rotter, J.M. (1988a), "The Structural Design of Light Gauge Silo Hoppers", Research Report R571, School of Civil and Mining Engineering, University of Sydney.

Rotter, J.M. (1988b), "The Structural Design of Steel Silos for Agricultural Applications", Proceedings, Conference on Agricultural Engineering 1988, Institution of Engineers, Australia, Sydney, pp 333-345.

Rotter, J.M. (1988c), "Recent Research on the Strength of Circular Steel Silos", Proceedings, International Conference, October, pp 265-284.

Rotter, J.M. (1989a), "The FELASH Suite of Computer Programs for the Analysis of Axisymmetric Shells", Proceedings, 4th International Conference on Civil and Structural Engineeirng Computing, Vol. 1, pp 323-328.

Rotter, J.M. (1989b), "Stress Amplification in Unstiffened Cylindrical Steel Silos and Tanks", Civil Engineering Transactions, Institution of Engineers, Australia.

Rotter, J.M. (1990a), "Local Collapse of Axially Compressed Pressurized Thin Steel Cylinders", Journal of Structural Engineering, ASCE, Vol. 116, No. 7, July, pp 1955-1970.

Rotter, J.M. (1990b), "Structural Design of Light-Gauge Silo Hoppers", Journal of Structural Engineeing, ASCE, Vol. 116, No. 7, July, pp 1907-1922.

Rotter, J.M. (1990c), "Critical Design Features of Steel Industrical Storage Structures", in Developments in Structural Engineeirng, Proceedings of the 4th Bridge Century Conference, ed. B.H.V. topping, London, pp 909-928.

Rotter, J.M. and Hull, T.S. (1985), "Wall Loads in Squat Steel Silos during Earthquake", Research Report R509, School of Civil and Mining Engineering, University of Sydney, Australia.

Rotter, J.M. and Hull, T.S. (1989), "Wall Loads in Squat Steel Silos during Earthquake", Engineering Structures, Vol. 11, No. 3, pp 139-147.

Rotter, J.M. and Jumikis, P.T. (1985), "Elastic Buckling of Stiffened Ringbeams for Large Elevated Bins", Proceedings, Metal Structures Conference, Institution of Engineers, Australia, Melbourne, May, pp 104-111.

Rotter, J.M. and Jumikis, P.T. (1988), "Non-Linear Strain-Displacement Relations for Thin Shells of Revolution", Research Report R563, School of Civil and Mining Engineering, University of Sydney, Australia.

Rotter, J.M. and Seide, P. (1987), "On the Design of Unstiffened Cylindrical Shells Subject to Axial Load and Internal Pressure", Proceedings, International Colloquim on Stability of Plate and Shell Structures, Gent, Belgium, April, pp 539-548.

Rotter, J.M. and Teng, J.G. (1989), "Elastic Stability of Cylindrical Shells with Weld Depressions", Journal of Structural Engineering, ASCE. 115(5), 1989, pp 1244-1263.

Rotter, J.M. and Teng, J.G. and Li, H.Y. (1991), "Buckling in Thin Elastic Cylinders on Column Supports", in Buckling of Shell Structures, on Land, in the Sea and in the Air, edt. J.F. Jullien, Elsevier Applied Science, London and New York.

Rotter, J.M., Greiner, R., Guggenberger, W., Li, H.Y., and She, K.M. (1993), "Proposed Design Rule for Buckling Strength Assessment of Cylindrical Shells under Local Axial Loads", Submission to ECCS TWG8.4 Buckling of Shells, Edinburgh Meeting, September 1993.

Rotter, J.M., Trahair, N.S. and Ansourian, P. (1980), "Stability of Plate Structures", Proceedings, Symposium on Steel Bins for Bulk Solids, Australian Institute of Steel Construction and the Australian Welding Research Association, Melbourne, September, pp 36-42.

Sanders, J.L. (1963), "Nonlinear Theories for Thin Shells", Quarterly of Appled Mathematics, Vol. 20, No. 1, pp 21-36.

Save, M.A. (1985), "Limit Analysis of Plates and Shells: Research over Two Decades", Journal of Structural Mechanics, Vol. 13, Nos 3 & 4, pp 343-370.

Save, M.A. and Massonnet, C.E. (1972), Plastic Analysis and Design of Plates, Shells and Disks, North-Holland Publishing Company-Amsterdam · London.

Sanders, J.L. (1963), "Nonlinear Theories for Thin Shells", Quarterly of Applied Mathematics, Vol. 20, No. 1, pp 21-36.

Samuelson, L.A. (1987), "Design of Cylindrical Shells Subjected to Local Loads in Combination with Axial or Radial Pressure", Proc. Int. Colloquium on the Stability of Plate and Shell Structures, Gent, Belgium, April, ECCS, pp 589-596.

Sukhvarsh, J. and Arthur, P.B. (1979), "Stress Analysis of Bins by Shell Bending Theory", Journal of the Structural Division, Vol. 105, No. ST6, ASCE, June, 1979, pp 1069-1087.

Teng, J.G. (1990), Buckling and Collapse of Shells and Rings for Steel Silos, Ph.D Thesis, University of Sydney, Australia.

Teng, J.G. and Rotter, J.M. (1988), "Plastic Collapse of Steel Silo Hoppers", Research Report R568, School of Civil and Mining Engineering, University of Sydney, Australia.

Teng, J.G. and Rotter, J.M. (1990), "A Study of Buckling in Column-Supported Cylinders", Proceedings, International Union for Theoretical and Applied Mechanics, Symposium on Contact Loading and Local Effects in Thin-Walled Plated and Shell Structures, Prague, August, 1990, Preliminary Report, Springer, Berlin, pp 39-48.

Teng, J.G. and Rotter, J.M. (1991a), "Linear Bifurcation of Perfect Cylinders on Column Supports", Research Report No. 91.02, Department of Civil Engineering and Building Science, University of Edinburgh.

Teng, J.G. and Rotter, J.M. (1991b), "Linear Bifurcation of Column-Supported Perfect Cylinders: Support Modelling and Boundary Conditions", Research Report No. 91.03, Department of Civil Engineering and Building Science, University of Edinburgh.

Timoshenko, S.P. (1940), Theory of Plates and Shells, McGraw-Hill Book Company, Inc., New York and London.

Trahair, N.S., et al. (1983), Structural Design of Steel Bins for Bulk Solids, Australian Institution of Steel Construction, Sydney, Australia.

Walker, D.M. (1966), "An Approximate Theory for Pressure and Arching in Hoppers", Chem. Engrg. Sci., Vol. 21, pp 975-997.

Wang, Robert S.C. and Gould, Phillip L. (1974), "Continuously Supported Cylindrical-Conical Tanks", Proc. of ASCE, Jrnl. Struct. Div., Vol. 100(3), No. ST10, October, pp 2037-2052.

Weingarten, V.I. (1962), "The Buckling of Cylindrical Shells under Longitudinally Varying Loads", Journal of Applied Mechanics, Vol. 9, No. 1, March.

Yamaki, N. (1984), Elastic Stability of Circular Cylindrical Shells, North-Holland, Amsterdam, The Netherlands.

Zienkiewicz, O.C. and Taylor, R.L. (1989), The Finite Element Method, Fourth Edition, Vol. 1, Basic Formulation and Linear Problems, McGraw-Hill, New York.